# The regulation of trafficking and function of KCNQ1 potassium channels by phosphatidylinositol-4,5-bisphosphate

Alice Royal

Submitted in partial fulfilment of the requirements of the Degree of Doctor of Philosophy

This work was supported by the British Heart Foundation [FS/12/21/29482]

I, Alice Royal, confirm that the research included within this thesis is my own work or that where it has been carried out in collaboration with, or supported by others, that this is duly acknowledged below and my contribution indicated. Previously published material is also acknowledged below.

I attest that I have exercised reasonable care to ensure that the work is original, and does not to the best of my knowledge break any UK law, infringe any third party's copyright or other Intellectual Property Right, or contain any confidential material.

I accept that the College has the right to use plagiarism detection software to check the electronic version of the thesis.

I confirm that this thesis has not been previously submitted for the award of a degree by this or any other university.



Signature:

Date:

Details of collaboration and publications:

N/A

**Abstract**

The $I_{Ks}$ current constitutes part of the repolarisation reserve in the human myocardium, and whilst it does not play a major role at resting heart rates, it becomes a crucial component of repolarisation in the setting of increased sympathetic tone and high heart rates. The formation of the $I_{Ks}$ current requires the KCNQ1 α-subunit and the KCNE1 β-subunit. Mutations in either of these subunits can lead to long QT syndrome types 1 and 5, respectively. Loss-of-function mutations in the $I_{Ks}$ channel can reduce the repolarisation reserve and lead to action potential prolongation, predisposing to lethal cardiac arrhythmias such as torsades de pointes and ventricular fibrillation.

It is widely recognised that the $I_{Ks}$ channel requires the minor membrane phospholipid $PIP_2$ for its function, and previous work in this laboratory found that mutations in a $PIP_2$-binding region in KCNQ1 led to retention of the channel in the endoplasmic reticulum, suggesting that $PIP_2$ may play a role in anterograde trafficking.

Here, the rapamycin-inducible dimerisation system was used to manipulate levels of $PIP_2$ and/or PI4P at the plasma membrane or Golgi, and the effect of this on $I_{Ks}$ channel trafficking and function was investigated using molecular biology, confocal microscopy and electrophysiology.

Despite difficulties with optimising the rapamycin-induced dimerisation system, it was observed that the $I_{Ks}$ channel does not require $PIP_2$ for anterograde trafficking, but is heavily reliant on $PIP_2$ for channel opening. In addition, activation of the β1-adrenergic receptor (β 1-AR) led to an increase in the $I_{Ks}$ current amplitude. The potential interplay between β1-AR and $PIP_2$ signalling was also explored by depleting $PIP_2$ during β1-AR stimulation. $PIP_2$ depletion was less effective at inhibiting the $I_{Ks}$ current during β1-AR stimulation, but this requires further investigation.

In conclusion, the results suggest that the $I_{Ks}$ channel is reliant on $PIP_2$ for function, but not anterograde trafficking.

**Acknowledgements**

Firstly, I would like to express my sincere gratitude to Professor Andrew Tinker for obtaining funding for my Ph.D., as without this my research would not have been possible. I also thank him for his guidance on the direction of my Ph.D., and for his unrivalled knowledge on anything I ever asked him.

An incredibly huge thank you to Steve Harmer for all his help throughout my PhD (and while writing my thesis) – I definitely would't have made it to the end without him!

A humongous thank you to Grant Carruthers for all the support he gave me while writing my thesis – it may have taken me another 3 years or so without him ☺

I would also like to thank the following people (in no particular order) for the laughs, chats, drinks, technical help, guidance and motivation (whichever one applies!):

My mum
My dad
Qadeer Aziz
Naomi Anderson
Rob Grange
James Cartwright
Grace Salsbury
Malcolm Finlay
Mark Specterman
Sally Fletcher
Alison Thomas
Muriel Noble
Madhav Kishore
Robert Haas
Paul Chapple
Leo Guasti
Lucie Clapp
Robert Carruthers
Kayelene Carruthers

Cheers everyone!

## Table of Contents

## List of Figures

## List of Tables

**List of abbreviations**

| | |
|---|---|
| Ab | antibody |
| AC | adenylyl cyclase |
| ACE | angiotensin-converting enzyme |
| ADP | adenosine diphosphate |
| AF | atrial fibrillation |
| Ag-Cl | silver-chloride |
| AKAP | A-kinase anchoring protein |
| aLQTS | acquired long QT syndrome |
| AM | acetoxymethyl |
| ANOVA | one-way analysis of variance |
| AnP | antarctic phosphatase |
| AP | adapter protein |
| APD | action potential duration |
| AR | adrenergic receptor |
| ARF | ADP-ribosylation factor |
| AT | angiotensin |
| ATP | adenosine triphosphate |
| AVN | atrioventricular node |
| BK | bradykinin |
| bpm | beats per minute |
| BrfA | brefeldin A |
| $Ca^{2+}$ | calcium ions |
| CaM | calmodulin |
| cAMP | cyclic adenosine monophosphate |
| CCP | clathrin-coated pit |
| CCV | clathrin-coated vesicles |
| CD | current density |
| CF | cystic fibrosis |
| CFP | cyan fluorescent protein |

| | |
|---|---|
| CHO | chinese hamster ovary |
| CID | chemically induced dimerisation |
| CIP | calf-intestinal alkaline phosphatase |
| Ci-VSP | voltage-sensitive phosphatase from *Ciona intestinalis* |
| $Cl^-$ | chloride ions |
| cLQTS | congenital long QT syndrome |
| CM | confocal microscopy |
| CME | clathrin-mediated endocytosis |
| CoA | coenzyme A |
| CPD | cytidine-diphosphate |
| DAD | delayed afterdepolarisation |
| DAG | diacylglycerol |
| DN | dominant negative |
| dNTP | deoxynucleotide triphosphate |
| Dr-VSP | voltage-sensitive phosphatase from *Danio rerio* |
| dsDNA | double-stranded DNA |
| EAD | early afterdepolarisation |
| ECG | electrocardiogram |
| EEA | early endosomal antigen |
| $E_K$ | equilibrium potential |
| ER | endoplasmic reticulum |
| ERM | ezrin/radixin/moesin |
| ET | endothelin |
| FAPP | four phosphate adapter protein |
| FBS | foetal bovine serum |
| FPr | forward primer |
| FRB | FKB-rapamycin binding |
| GΩ | giga-ohm |
| GA | gibberellic acid |
| GAP | GTPase activating proteins |

| | |
|---|---|
| GDP | guanosine diphosphate |
| GFP | green fluorescent protein |
| GID1 | gibberellic acid insensitive dwarf 1 |
| GPCR | G protein-coupled receptor |
| GTP | guanosine triphosphate |
| HEK | human embryonic kidney |
| hERG | human ether-a-go-go-related gene |
| HR | heart rate |
| HTS | high-throughput screening |
| I | current |
| IC50 | half-maximal inhibitory concentration |
| $I_{Ca,L}$ | L-type $Ca^{2+}$ current |
| ICD | implantable cardioverter defibrillator |
| $I_K$ | delayed-rectifier potassium current |
| $I_{Kr}$ | rapid delayed-rectifier potassium current |
| $I_{Ks}$ | slow delayed-rectifier potassium current |
| $I_{Kur}$ | ultra-rapid delayed-rectifier potassium current |
| Ins3PR | inositol-3-phosphate receptor |
| $IP_3$ | inositol-3,4,5-trisphosphate |
| iPSC | induced pluripotent stem cell |
| ISO | isoproterenol |
| $I_{to}$ | transient outward potassium current |
| JLNS | Jervell and Lange-Nielsen Syndrome |
| $K^+$ | potassium ions |
| K2P | tandem-pore potassium channel |
| $K_{ir}$ | inwardly-rectifying potassium |
| $K_v$ | voltage-gated potassium |
| $K_v7.1$ | homomeric KCNQ1 channel |
| LC | long-chain |
| ln | natural log |

| | |
|---|---|
| LQTS | long QT syndrome |
| LSCM | laser-scanning confocal microscopy |
| LZ | leucine zipper |
| M1 | muscarinic acetylcholine type M1 |
| MEM | minimum essential media |
| ms | milliseconds |
| mTOR | mammalian target of rapamycin |
| $Na^+$ | sodium ions |
| NLS | nuclear localisation signal |
| NS | not significant |
| NT | non-targeting |
| PBS | phosphate buffer saline |
| PCR | polymerase chain reaction |
| PD | pore domain |
| PDE | phosphodiesterase |
| PDK | phosphoinositide-dependent kinase |
| PH | pleckstrin homology |
| $PH_{OSH2\times2}$ | oxysterol-binding protein homolog 2 |
| PI | phosphoinositide |
| $PI(3,5)P_2$ | phosphatidylinositol-3,5-bisphosphate |
| PI3K | phosphatidylinositol 3-kinase |
| PI3P | phosphatidylinositol-3-phosphate |
| PI4K | phosphatidylinositol 4-kinase |
| PI4P | phosphatidylinositol-4-phosphate |
| PI5P | phosphatidylinositol-5-phosphate |
| $PIP_2$ | phosphatidylinositol-4,5-bisphosphate |
| $PIP_3$ | phosphatidylinositol-3,4,5-trisphosphate |
| PITP | phosphatidylinositol-transfer protein |
| PJ | pseudojanin |
| PKA | protein kinase A |

| | |
|---|---|
| PLC | phospholipase C |
| PM | plasma membrane |
| PP | protein phosphatase |
| PP2B | protein phosphatase 2B |
| PPI | polyphosphoinositides |
| PtdIns | phosphatidylinositol |
| PTEN | phosphatase and tensin homologue |
| PTCD | peak tail current density |
| PVC | premature ventricular complex |
| P-WCPC | perforated whole-cell patch clamp |
| QTc | corrected QT interval |
| R | resistance |
| Rap | rapamycin |
| $R_e$ | electrode resistance |
| $R_f$ | feedback resistor |
| RFP | red fluorescent protein |
| RhoGEF | RhoGTPase nucleotide exchange factors |
| RISC | RNA-induced silencing complex |
| RGS | regulators of G protein signalling |
| $R_m$ | resting membrane potential |
| RNAi | RNA interference |
| RPr | reverse primer |
| $R_{series}$ | series resistance |
| RT | room temperature |
| RTK | receptor tyrosine kinase |
| RWS | Romano Ward Syndrome |
| siRNA | small interfering RNA |
| SR | sarcoplasmic reticulum |
| SAN | sinoatrial node |
| SDM | site-directed mutagenesis |

| | |
|---|---|
| SGK1 | serum- and glucocorticoid-inducible kinase 1 |
| SNARE | soluble *N*-ethylmaleimide-sensitive factor attachment protein receptor |
| SR | sarcoplasmic reticulum |
| SS | sum of squares |
| ssDNA | single-stranded DNA |
| SSA | steady state of activation |
| SUR | sulphonylurea receptor |
| T | time course |
| Taq | *Thermus aquaticus* |
| TdP | torsades de pointes |
| TGN | trans-Golgi network |
| TM | transmembrane |
| TT | top10 competent *Escherichia coli* |
| UVRAG | UV radiation resistance-associated gene protein |
| V | voltage |
| $V_{0.5}$ | half-maximal activation |
| $V_{cmd}$ | command voltage |
| $V_m$ | transmembrane potential |
| $V_p$ | pipette voltage |
| VSP | voltage-sensitive phosphatase |
| WCPC | whole-cell patch clamp |
| WTM | wortmannin |
| YFP | yellow fluorescent protein |

## Glossary of constructs used for PI manipulation

**Components of the rapamycin-dimerisation system**

**Pseudojanin** – contains the FKBP domain allowing dimerisation with FRB using rapamycin, and the SAC1 and INPP5E lipid-depleting domains for dephosphorylation of PI4P and $PIP_2$, respectively. (Tagged with RFP)

**PJ-INPP5E** – contains the FKBP domain allowing dimerisation with FRB using rapamycin, and the SAC1 and INPP5E lipid-depleting domains. The SAC1 domain contains an inactivating mutation, so PJ-INPP5E dephosphorylates only $PIP_2$. (Tagged with RFP)

**PJ-SAC** – contains the FKBP domain allowing dimerisation with FRB using rapamycin, and the SAC1 and INPP5E lipid-depleting domains. The INPP5E domain contains an inactivating mutation, so PJ-SAC dephosphorylates only PI4P. (Tagged with RFP)

**PJ-DEAD** – contains the FKBP domain allowing dimerisation with FRB using rapamycin, and the SAC1 and INPP5E lipid-depleting domains. Both the SAC1 and INPP5E domains contains an inactivating mutation, so PJ-DEAD does not dephosphorylate any PIs and is used as a control construct. (Tagged with RFP)

**CF-PIPK** – contains the FKBP domain allowing dimerisation with FRB using rapamycin, and the PIPK domain for PI4P phosphorylation to $PIP_2$. (Tagged with RFP)

**LYN11-FRB-CFP** – contains the FRB domain for dimerisation with FKBP using rapamycin, and the LYN11 sequence for PM tethering. (Tagged with CFP)

**LYN11-FRB-mCherry** – contains the FRB domain for dimerisation with FKBP using rapamycin, and the LYN11 sequence for PM tethering. (Tagged with mCherry)

**LYN11-targeted-FRB –** contains the FRB domain for dimerisation with FKBP using rapamycin, and the LYN11 sequence for PM tethering. (Untagged)

**Tgn38-FRB –** contains the FRB domain for dimerisation with FKBP using rapamycin, and the Tgn38 sequence for trans-Golgi membrane tethering. (Tagged with mCherry)

**Components of the gibberellin-induced dimerisation system**

**YFP-GID1** – contains the GID1 domain for dimerisation with LYN-CFP-GAI(1–92) using GA3-AM. (Tagged with YFP)

**PJ-GID1** – contains the GID1 domains for dimerisation with LYN-CFP-GAI(1–92) using GA3-AM, and the SAC1 and INPP5E domains for dephosphorylation of PI4P and $PIP_2$, respectively. (Tagged with RFP)

**LYN-CFP-GAI(1–92)** – conatins the GAI domain (residues 1–92) for dimerisation with GID1 using GA3-AM, and the LYN11 sequence for PM targeting. (Tagged with CFP)

# CHAPTER 1: Introduction

## 1.1 The Cardiac Conduction System

### 1.1.1 Normal electrical conduction in the heart

The heart is responsible for the pumping of blood containing oxygen and nutrients to the lungs via the pulmonary arteries and the rest of the body via the aorta (figure 1). To do this efficiently, a complex conduction system is in place to ensure the coordination of myocyte contraction. Initiating this is the sinoatrial node (SAN), the small but specialised area of tissue in the right atrium, first discovered by Keith and Flack (1907). Approximately 70 years later, the function of the SAN was established by Taylor and co-workers (1978). Action potentials are generated by the SAN at a rate of around 100 per minute, which is slowed at rest to approximately 60 per minute due to the domination of the parasympathetic nervous system over the sympathetic nervous system (SNS). The regular firing of action potentials that leads to the normal contraction of the heart, which the SAN is responsible for, is known as sinus rhythm.

Action potentials from the SAN travel through the atria via cell-to-cell conduction. Myocytes are coupled to adjacent cells through gap junctions at the intercalated disc, which provide a low-resistance pathway for the passage of ions between cells and allow the rapid depolarisation required to propagate the action potential (Lo *et al.*, 2000; Rohr, 2004). As the action potential travels through the atria, myocyte contraction follows, and this is responsible for forcing blood into the ventricles. The term 'excitation-contraction coupling' was coined by Sandow in 1952 to describe this process. The influx of calcium ions ($Ca^{2+}$) through L-type $Ca^{2+}$ channels in the plasma membrane (PM) causes release of $Ca^{2+}$ stores from the sarcoplasmic reticulum (SR). This process, termed calcium-induced calcium release, causes large increases in local [$Ca^{2+}$]. The free $Ca^{2+}$ binds to troponin C, part of the regulatory protein complex, and causes a conformational change in the complex to occur. This change causes troponin-I to expose the myosin-ATPase (found on the myosin head) binding site on the actin filament. The ATP hydrolysis that occurs due to the action of the ATPase provides the energy required for the myosin head to pull the actin filament towards the centre of the sarcomere, shortening the sarcomere and consequently contracting the myocyte (Bers, 2002).

Once the electrical signals have travelled the length of the atria they reach the physical barrier between the atria and ventricles, which they traverse via the atrioventricular node (AVN). The conduction is slower here owing to a lower density of high-conductance gap junctions, which allows for complete emptying of the atria before ventricular contraction starts (Temple *et al.*, 2013).

The electrical impulses travel down the His bundle and the left and right bundle branches to the ventricles via a large network of Purkinje fibres. A rapid depolarisation of the ventricles follows, and contraction is initiated by excitation-contraction coupling in the same manner as atrial contraction. Across the ventricle wall, excitation propagates from the endocardium (the inner layer of the ventricle wall) through to the epicardium (the outer layer of the ventricle wall). The action potential duration (APD) of cells in the epicardium is shorter than in the endocardium, and so the termination of action potential propagation occurs from epi- to endocardium. During contraction, blood is forced out of the left ventricle into the aorta, and from the right ventricle into the pulmonary artery.

The electrical activity associated with atrial and ventricular contraction can be seen on an electrocardiogram (ECG), and figure 2 shows how cellular depolarisation in different areas of the heart corresponds to characteristic inflections on the ECG.

### 1.1.2 The Electrocardiogram

The ECG trace corresponds to the electrical activity in the heart as it changes over time. Figure 3 shows a representative ECG trace, containing a complete cycle of atrial depolarisation through to ventricular repolarisation. Various parameters of the ECG are measured to indicate whether an individual is in sinus rhythm or not.

The P wave on the ECG represents the contraction of the right, then left atrium. The QRS complex, which is a combination of the three waves, corresponds to contraction of both ventricles. The QRS complex also masks the repolarisation of the atria on the ECG. The T wave shows ventricular repolarisation, which must occur before the next cycle commences (Hurst, 1998).

The U wave shown in figure 2 and 3 is only sometimes present on a real ECG. It has been suggested that the U wave arises from repolarisation of the Purkinje cells or the midmyocardial (M) cells, as these have longer than average APDs. Although the true origin of the U wave is unknown, repolarisation of the whole ventricular myocardium corresponds with the end of the U wave and, therefore, the T and U wave are resultant of the same process (ventricular repolarisation) (Ritsema van Eck *et al.*, 2005).

The intervals in figure 2 measure the time between certain points of the ECG. The PR interval runs from the start of the P wave to the start of the QRS complex. The PR interval can give an indication of AV node function, as it measures the time taken for electrical signals to travel from the SA node to the ventricles. The QRS complex, which is measured from the start of the Q wave to the end of the S wave, measures the time taken for the ventricles to depolarise. The QT interval is measured from the

start of the Q wave to the end of the T wave, and encompasses ventricular depolarisation and repolarisation. The J point is described as being the point where the QRS complex ends and the ST segment begins (Brownfield & Herbert, 2008), and should lie on the isoelectric line. Deviation from this (elevation or depression) can indicate cardiac problems that manifest with ST segment abnormalities. The ST segment runs from the end of the QRS complex to the start of the T wave.

The RR interval, which starts at the peak of one QRS wave and ends at the peak of the next, is used to assess ventricular rate.

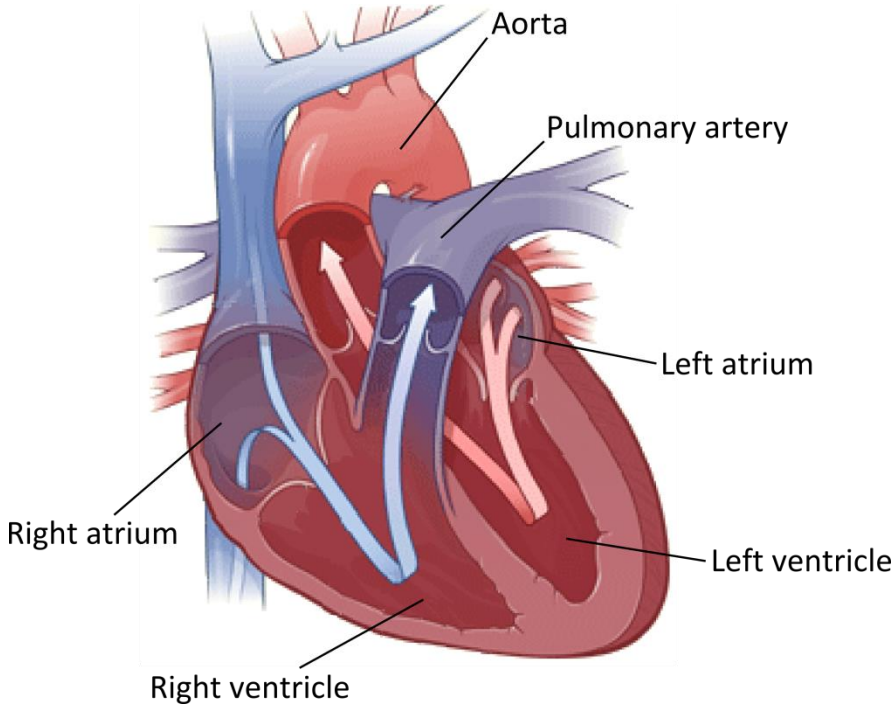


**Figure 1. Anatomy of the heart.** A schematic diagram of the heart showing both atria and ventricles, and the pulmonary artery and aorta. Blue and red arrows show the direction of blood flow. Adapted from the National Heart, Lung and Blood Institute (http://www.nhlbi.nih.gov).

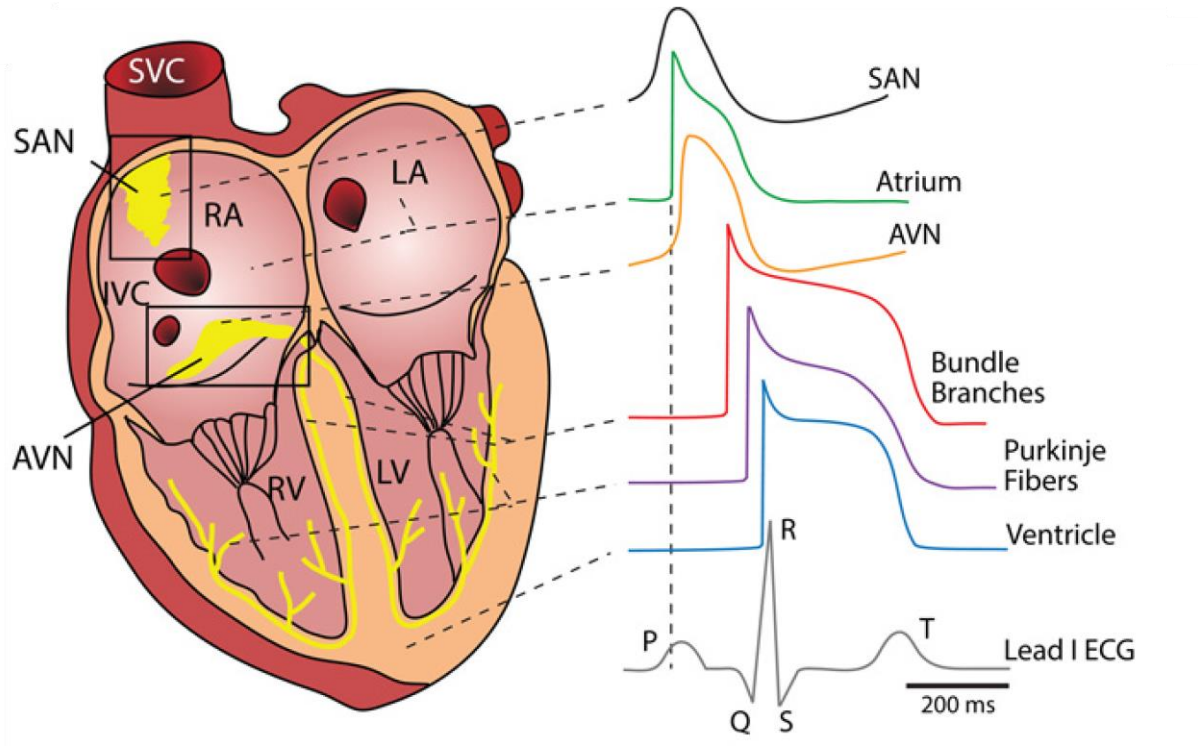


**Figure 2. Electrophysiology of the heart and the corresponding ECG.** The waveforms for each of the specialised cells are shown on the right, and their locations in the heart on the left. The ECG trace below show how these waveforms shape the ECG. Image adapted from Bartos *et al.* (2015).

### 1.1.3 Cardiomyocyte excitability and the action potential

Cardiac cells, along with other cells such as those found in the nervous system, possess the ability to be electrically excited. This excitation causes a transient depolarisation of the membrane from the resting membrane potential ($R_m$).

The potential difference across the membrane of an un-excited cell is the $R_m$, and describes the intracellular potential relative to the extracellular potential (Hoffman, 1959). The distribution of the main ionic species present in a cell at rest is tightly regulated. There is a large difference between the intra- and extracellular distribution of ions, the most notable being potassium ($K^+$), sodium ($Na^+$) and calcium ($Ca^{2+}$) ions. These large differences create concentration gradients for each respective ion, to which the plasma membrane (PM) confers a level of permeability through the activity of ion channels, transporters and pumps. The resting membrane of a cardiomyocyte is more permeable to potassium ($K^+$) ions than to other ions such as sodium ($Na^+$) or chloride ($Cl^-$), and therefore the $R_m$ is closer to the $K^+$ equilibrium potential. The equilibrium potential, or reversal potential, of an ion is the

voltage at which there is no net movement of that ion across the membrane, i.e. the distribution of ions means there is no gradient that causes a driving force for the ion to cross the membrane.

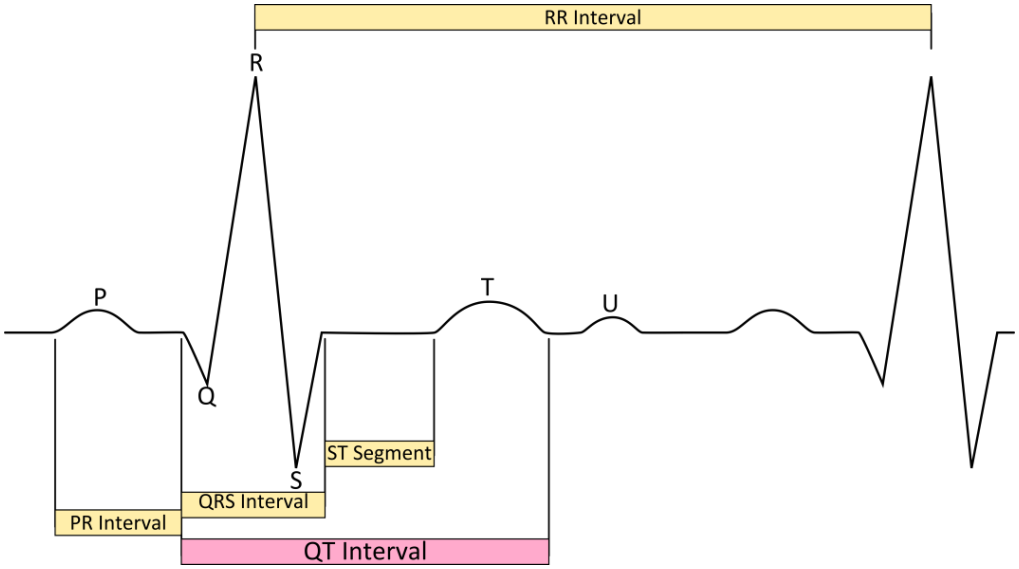


**Figure 3. The cardiac ECG and standard measurements.** A schematic diagram of an ECG trace showing the three waves (P, QRS and T) and the occasionally present U wave. The various measurable intervals can also be seen (PR, QRS, QT, ST and RR). ECG adapted from Ryan, S., accessed at: www.a-fib.com.

The equilibrium potential (reversal potential) of a single ion (e.g. $K^+$) can be calculated using the Nernst equation:

$$E = \frac{RT}{zF} \ln\left(\frac{[ion]_o}{[ion]_i}\right) \qquad \text{Equation 1.1}$$

By substituting the natural log (ln) for $\log_{10}$ using the conversion factor 2.303, the equation becomes:

$$E = 2.303 \frac{RT}{zF} log_{10}\left(\frac{[ion]_o}{[ion]_i}\right) \qquad \text{Equation 1.2}$$

Where E denotes the membrane potential (volts), R is the ideal gas constant (Joules per Kelvin per mole), T the temperature (Kelvin), F is the Faraday constant (Coulombs per mole), and z is the valency of the ion. $[Ion]_{in}$ and $[ion]_{out}$ are the concentration of the given ion inside and outside of the cell, respectively.

R (8.314 $J.K^{-1}mol^{-1}$) and F (96,485.33 $C.mol^{-1}$) are constant values. T can be thought of as a constant, and at body temperate this is 37 °C (310 K). For the $K^+$ ion, z=1, therefore 2.303 x (RT/zF) can be substituted to give:

$$E = 0.0614\, log_{10}\left(\frac{[ion]_o}{[ion]_i}\right) \qquad \text{Equation 1.3}$$

Calculating the remaining equation using a physiological intracellular and extracellular concentration of $K^+$ (150 mM and 4 mM, respectively) gives a $K^+$ equilibrium potential ($E_K$) of -96 mV.

However, the PM is not solely permeable to $K^+$, and the permeability to other ions contributes to the overall $R_m$. The Goldman-Hodgkin-Katz equation (Hodgkin & Katz, 1949), commonly known as the Goldman equation, is used to calculate the transmembrane (TM) potential ($V_m$) while considering the permeability of all ions across the membrane:

$$V_m = \frac{RT}{F}\ln\left(\frac{p_K[K^+]_o + p_K[Na^+]_o + p_K\,[Cl^-]_i}{p_K[K^+]_i + p_K[Na^+]_i + p_K\,[Cl^-]_o}\right) \qquad \text{Equation 1.4}$$

Where $V_m$ is the membrane potential, and $p_K$, $p_{Na}$ and $p_{Cl}$ are the relative membrane permeabilities of $K^+$, $Na^+$ and $Cl^-$ ions, respectively. $[K^+]_o$, $[Na^+]_o$ and $[Cl^-]_o$ are the extracellular concentrations of the named ions, and $[K^+]_i$, $[Na^+]_i$ and $[Cl^-]_i$ are the intracellular concentrations of the named ions.

As the cardiomyocyte $R_m$ does not lie at the reversal potential for any particular ion, an electrochemical gradient is created for each ion. Using $K^+$ ions as an example, the further $R_m$ is from $E_K$, then the higher the driving force across the membrane for $K^+$. This driving force is a major contributor to the ion flux during an action potential.

Despite an electrochemical gradient existing at rest for $Na^+$ and $K^+$ ions, and therefore movement of $Na^+$ into and $K^+$ out of the cell, the $R_m$ is maintained due to the action of a number of adenosine triphosphate (ATP)-dependent ion pumps and transporters. To preserve $R_m$, the $Na^+/K^+$-ATPase, which uses the energy provided from the conversion of ATP to adenosine diphosphate (ADP), pumps 3 $Na^+$ out of the cell and 2 $K^+$ into the cell (against their concentration gradients). This pump is described as being electrogenic due to the imbalance of charge being passed across the membrane, which is partly responsible for the negative $R_m$. Another contributor to the value of $R_m$ is the high $K^+$

conductance in comparison to other ions in a resting cell. This background $K^+$ current is conducted through the leak $K^+$ channels, which facilitate the diffusion of $K^+$ ions down their concentration gradient and out of the cell (Enyedi & Czirják, 2010).

*Ionic flux during the action potential*

Upon depolarisation of the cell membrane, the permeability of ions change, and an action potential can be fired. Action potential form differs depending on the cellular origin (figure 2) due to the differential expression of ion channels in each cell type. However, most cardiac atrial and ventricular action potentials consist of the same basic structure (figure 4) (Hoffman, 1959; Grant, 2009):

**Phase 0**: The rapid upstroke of the action potential caused by depolarisation of the $V_m$, which reaches +20 –30 mV during phase 0.

**Phase 1**: A rapid repolarisation to approximately 0 mV occurs.

**Phase 2**: The plateau phase follows. In ventricular myocytes this is more prolonged than in atrial myocytes.

**Phase 3**: A fairly rapid repolarisation occurs that brings $V_m$ back to $R_m$.

**Phase 4**: The resting potential is restored (around $E_k$, approximately -90 mV).

During phase 0, $Na^+$ channels open and pNa increases allowing influx of $Na^+$ ions down their electrochemical gradient. This causes membrane depolarisation. This, in turn, results in the opening of a vast number of $Na^+$ channels, and $V_m$ quickly reaches the threshold potential, causing the rapid upstroke of the action potential. These $Na^+$ channels inactivate at positive potentials and give way to the repolarising currents.

The repolarising phases that follow occur in different stages and are the result of a fine balance of inward $Ca^{2+}$ and outward $K^+$ currents. The rapid repolarisation in phase 1 is due to the fast activation of the voltage-gated transient outward $K^+$ current ($I_{to}$). During the plateau phase (phase 2) there is a vast reduction in the net current flow as the L-type $Ca^{2+}$ channel and the various $K^+$ channels (depending on the cardiac cell type; figure 4) open and allow opposing ionic currents to cross the PM. Upon (voltage- and calcium-dependent) inactivation of the L-type $Ca^{2+}$ channel and the release from inactivation of the rapid delayed rectifier $K^+$ channel ($I_{Kr}$), the repolarising outward $K^+$ currents prevail, and $V_m$ is brought back down to approximately -90mV.

The cardiac action potential is tightly regulated through activation kinetics and gating of each ion channel species, $Ca^{2+}$ signalling and feedback mechanisms that occur during each action potential and the inactivation/deactivation mechanisms of ion channels that govern the effective and relative refractory period, in which another action potential cannot yet be fired. Alteration of any of these processes, by genetic or acquired causes, can lead to discrepancies in the action potential form.

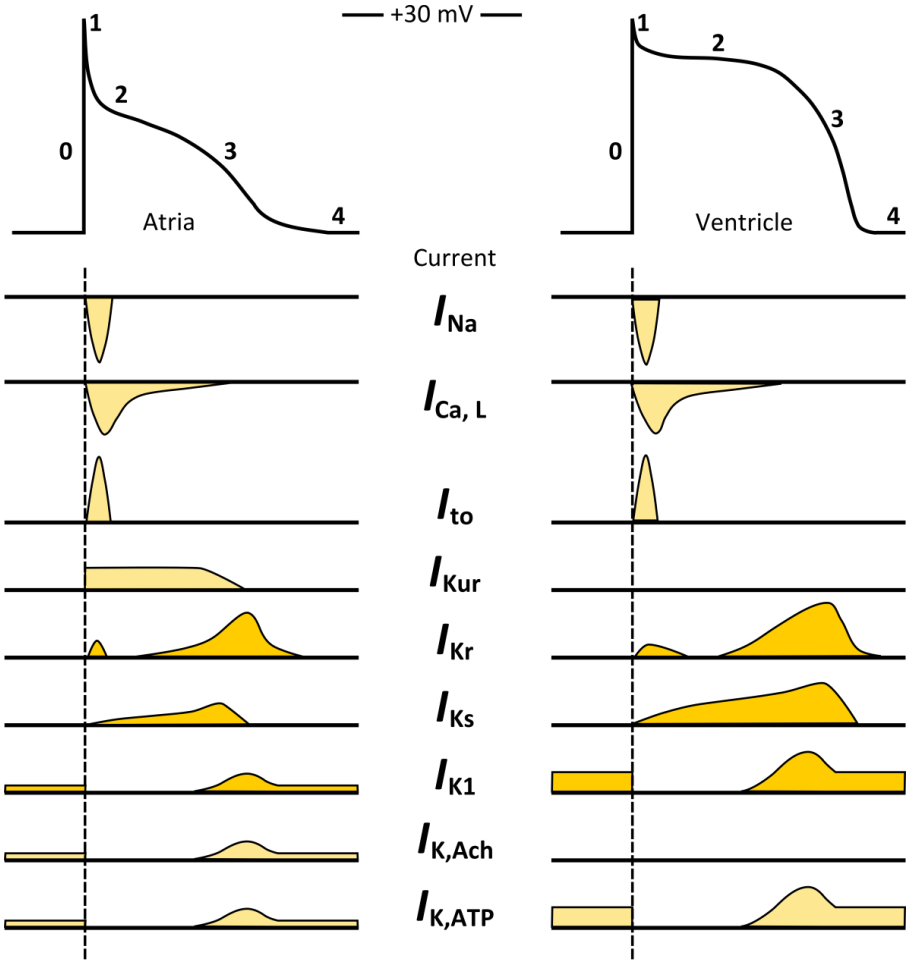


**Figure 4. Action potentials in the human myocardium**. A schematic diagram showing action potentials for (left) atrial and (right) ventricular cells, and the inward (downward deflection) and outward (upward deflection) currents that contribute to each. $Na^+$ and $Ca^{2+}$ currents flow into the cell, and $K^+$ currents flow out of the cell. Darker yellow currents indicate those studied in this project. 'Action potentials' adapted from Ravens & Cerbai (2008).

## 1.2 Ion Channels

### 1.2.1 An Overview of Ion Channel Structure and Function

Ion channels are a subset of proteins that form TM pores in cell membranes to facilitate the diffusion of ions across that membrane. There are over 300 different ion channels, which are collectively

involved in a multitude of cellular processes. Ion channels constitute a crucial element of the cardiac conduction system where, as previously mentioned, any alteration in their function can have deleterious consequences.

The structure of each species of ion channel is key to their specialised function, but the common structure to all ion channels is that they contain a number of TM domains that arrange to form a pore and a gating mechanism. Ion channels are commonly selective for one ionic species, and are classified into broad groups based on this selectivity, i.e. $K^+$, $Na^+$, $Ca^{2+}$ and $Cl^-$ channels.

Ion channels may have multiple 'open' or 'closed' states, and some also pass through an 'inactivated' state between the open and closed states. The open state of an ion channel corresponds with the conducting state, and the closed with the non-conducting state. A channel in the inactivated state has an open gate but a blocked pore, and, as a result, ions cannot flow through. Depending on the type of channel, the gate may be opened by either chemical, temperature, electrical or mechanical stimulus (Tabassum & Feroz , 2011). In addition to being classified based on the ion that the channel is selective for, an ion channel is further classified based on the gating mechanism it employs. For example, a $K^+$ channel that opens in response to a change in TM voltage is termed a voltage-gated $K^+$ ($K_v$) channel.

Once in a conducting state, the ion channel can facilitate the passage of ions from one side of the membrane to the other. At the narrowest point of the pore lies the selectivity filter, which controls the type of ionic species that can pass through. The x-ray structure of the $K^+$ channel from *Streptomyces lividans* (KcsA $K^+$ channel), which is similar to a number of vertebrate $K^+$ channels, allowed a detailed insight into the pore environment (Doyle et al., 1998). The selectivity filter of the KcsA $K^+$ channel was found to be in an optimal position to allow dehydrated $K^+$ ions to enter (figure 5C). Usually, $K^+$ ions are surrounded by eight water molecules, and so the pore mimics this environment with eight carbonyl oxygen atoms from residues that line the pore. This provides the perfect environment for $K^+$ to transfer stably between the intra- or extracellular solution and the ion channel pore. $Na^+$ ions, despite being smaller than $K^+$ ions, cannot pass through the $K^+$ channel pore. Doyle *et al* (1998) found that $Na^+$ ions were unable to make stable interactions with the backbone carbonyl oxygens that line the selectivity filter due to the smaller size of the $Na^+$ ions.

### 1.2.2 Potassium Channels

$K^+$ channels selectively allow the flow of $K^+$ ions from one side of a membrane to the other. They contain a conserved sequence that confers this selectivity (TXXTXGYG), which was identified based on the Shaker channel sequence (TMTTVGYG) and is referred to as the signature sequence (Heginbotham *et al.*, 1994).

This selectivity for $K^+$ ions allows K+ channels to perform a variety of functions throughout the human body, including controlling and limiting cardiac excitability (Snyders, 1999).

*Voltage-gated $K^+$ channels*

The members of this large subset of $K^+$ channels are dependent upon the membrane potential for opening and closing. The first cloned $K_v$ channel, the Shaker channel, allowed analysis of the primary protein sequence of a $K_v$ channel (Tempel *et al*., 1987). This sequence uncovered similarities with voltage-gated channels selective to other ions, namely the $Na^+$ and $Ca^{2+}$ voltage-gated channels.

The $K_v$ channel α-subunit contains the pore and gating mechanism, and it may interact with one or more β-subunits to modulate its function. $K_v$ channel nomenclature begins with the family $K_v1$ and continues through to $K_v12$, with members of each family called, for example, $K_v1.x$, where x denotes a number starting at 1, which increases throughout the family.

A single $K_v$ channel gene codes for one of the four α-subunits that a channel complex consists of. One subunit contains 6 TM domains and an intracellular N- and C-terminus. The TM domains are named S1–S6, with S1–S4 of each of the 4 subunits comprising the voltage-sensing domain, and the S5–S6 domains from each of the 4 subunits forming the pore domain (PD) (figure 5A & 5B). The S4 domain in $K_v$ channels contains a number of positively-charged lysine (Lys) or arginine (Arg) residues, each separated by two hydrophobic residues (Bezanilla, 2000). Upon membrane depolarisation, the S4 domain of each subunit moves outwards in the membrane in response to a change in the membrane potential, and the interaction of this with the positive charges in the S4 domain. This movement causes the channel to alter its conformation to one that favours the open state. S4 movement is thought to be coupled to channel pore opening via the S4–S5 linker (Ferrer *et al*., 2006).

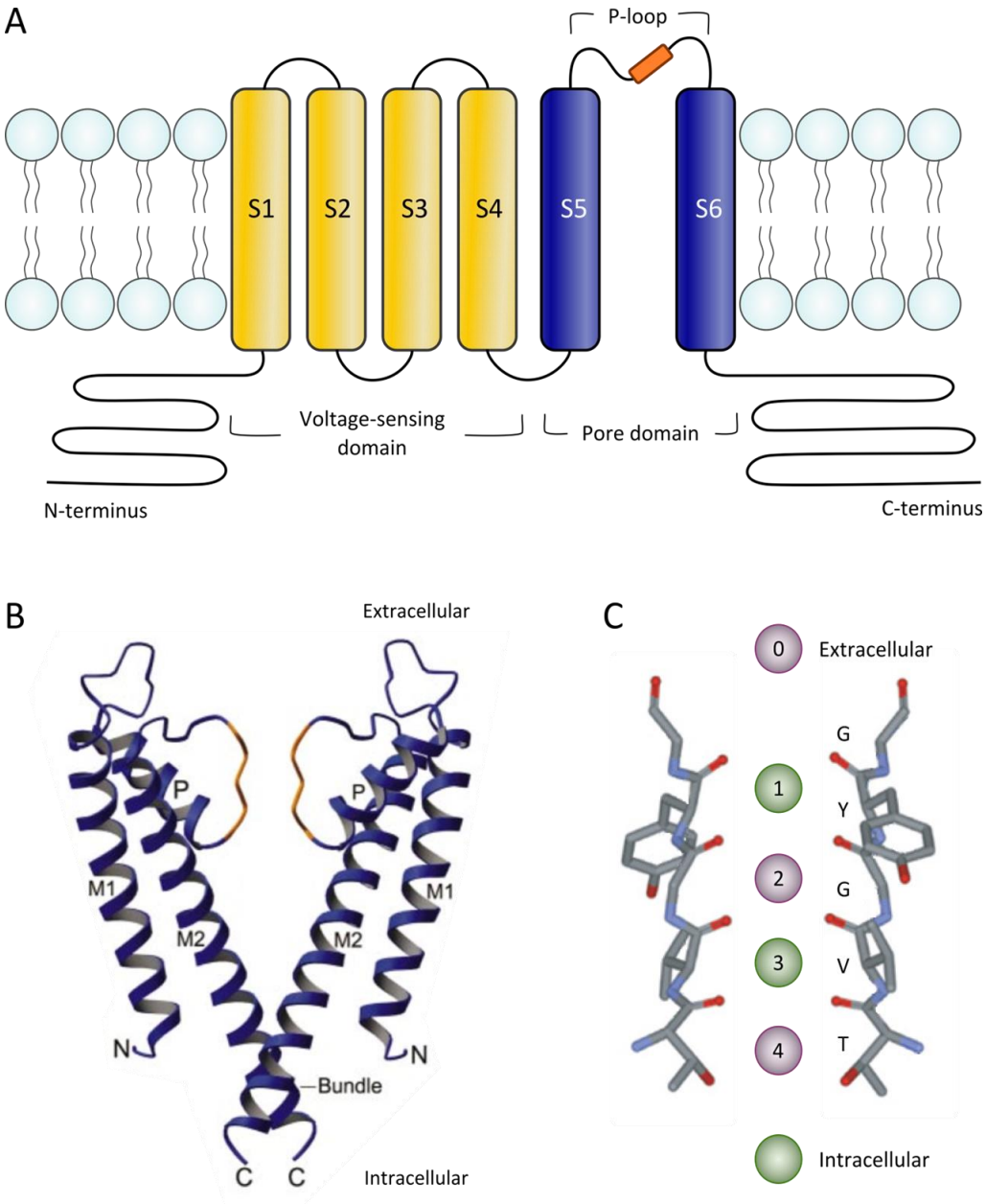


**Figure 5. The structure of a voltage-gated potassium channel. A –** A schematic diagram of the structure of a $K_v$ channel subunit. S1–4 form the voltage-sensing domain, while S5–6 form the pore domain. Four pore domains from each of the 4 subunits come together to form a single, central ion-conducting pore. The P-loop that lies in between S5 and S6 contains the selectivity filter sequence. **B –** A Ribbon diagram of two subunits of the KcsA $K^+$ channel. Each subunit comprises of M1 and M2, which are analogous to the S5 and S6 of $K_v$ channels, and a P-loop (P). The selectivity filter is shown in orange. The inner helix bundle forms the ion channel gate (adapted from Jiang et al., 2002). **C –** Selectivity filter from two subunits of the KcsA $K^+$ channel, with the TVGYG signature sequence labelled. Two $K^+$ ions can occupy the selectivity filter at any one time, at positions 2 and 4, or 1 and 3, before exiting via position 0 (adapted from Bichet et al., 2003).

The 4 $K_v$ channel subunits can assemble in a homotetrameric or heterotetrameric fashion. Homotetramers consist of 4 identical subunits, whereas heterotetramers contain different subunits, which can arrange in a number of configurations. Heterotetrameric channels can contain subunits

from the same class of $K_v$ channel (Brown & Passmore, 2009), but interclass heterotetrameric channels also form (Bocksteins *et al.*, 2012).

*Inwardly-rectifying $K^+$ channels*

The inwardly-rectifying $K^+$ ($K_{ir}$) channels are named due to the fact that they conduct a larger current in the inward direction at potentials negative to $E_K$, rather than the typical outward direction at potentials positive to $E_K$, as is the case for other $K^+$ channels. At membrane potentials positive to $E_K$, these channels are subject to open-channel block by intracellular $Mg^{2+}$ and other molecules such as polyamines (Matsuda *et al.*, 1987; Lopatin *et al.*, 1994), which limits the current that can be conducted through the channel pore. Physiologically, $K_{ir}$ channels do not conduct this large inward current that they are capable of. The $K_{ir}$ channels are named due to the characteristics identified in experimental systems, which are able to force the membrane potential to negative voltages that would not occur in a physiological environment.

The structure of $K_{ir}$ channels is different to that of $K_v$ channels. $K_{ir}$ channels consist of 4 domains, but these domains are only made of 2 TM domains, as opposed to 6 in $K_v$ channels. This was discovered by cloning the ROMK1/$K_{ir}$1.1 (Ho *et al.*, 1993) and IRK1/$K_{ir}$2.1 (Kubo *et* al., 1993) from rat and mouse, respectively. Between the 2 TM domains, termed M1 and M2, lies the H5 region. This is responsible for $K^+$ ion selectivity. Members of the $K_{ir}$ channel family do not contain an S4 segment, which serves as the voltage sensor in $K_v$ channels, and as a result $K_{ir}$ channels lack voltage sensitivity. These channels therefore use other gating mechanisms to regulate the passage of ions through the pore.

This group of channels possess a diverse range of activation mechanisms between them. For example, $K_{ir}$3.x are activated by a G protein-coupled receptor (GPCR) (Kurachi *et al.*, 1986), and are also classed as ligand-gated channels. The $K_{ir}$6.x channels and $K_{ir}$2.x channels are both thought of as constitutively-active channels in the heart, but both show different degrees of inward rectification, and $K_{ir}$6.x channels are also sensitive to cellular ATP concentrations.

$K_{ir}$ channels show varying degrees of inward rectification between them. They can be grouped into strong ($K_{ir}$2.x and 3.x), intermediate ($K_{ir}$4.x) and weak ($K_{ir}$1.1 and 6.x) inward rectifiers. The level of inward rectification depends highly on Asp172 in TM2 (Wible *et al.*, 1994; Stanfield *et al.*, 1994) and Glu224 and Glu229 in the large cytoplasmic region (Yang *et al.*, 1995; Kubo & Murata, 2001) of each subunit. These negatively charged residues contribute to the strong inward rectification seen in some members of the $K_{ir}$ channel family, and it was found that $K_{ir}$1.1 contains a neutral residue at this position, which is responsible for the lower $Mg^{2+}$ affinity and consequent weak rectification.

However, the presence of these residues does not completely correlate with strength of rectification throughout the $K_{ir}$ channel family.

*Tandem two-pore domain channels*

The tandem-pore $K^+$ ($K_{2P}$) channels are characteristically composed of two subunits that form a dimer. Each subunit comprises 4 TM domains and 2 P loop domains (in contrast to $K^+$ channels made from 4 subunits, each of which contain 1 P loop), which together form the pore domain and selectivity filter consisting of 4 P loops (Enyedi & Czirjak, 2010).

The $K_{2P}$ channel family has 15 members, all of which conform to the tandem two-pore domain structure, but differ greatly in their protein structure (Lesege & Lazdunski, 2000).

The $K_{2P}$ channels are responsible for the background, or leak, currents that are present in, for example, the cardiomyocyte. These channels contribute to the negative resting membrane potential of excitable cells (Sepúlveda *et al*., 2015). A true leak channel would be voltage independent, meaning that the $P_0$ does not change with membrane potential, as with many other $K^+$ channels. These channels would also be 'time independent', in that they would not show activation, inactivation or deactivation kinetics. $K_{2P}$ channels, however, do show weak voltage dependence and rectification, but are widely considered to be leak channels (Enyedi & Czirjak, 2010).

### 1.2.3 Cardiac $K^+$ channels

At physiological membrane potentials, cardiac $K^+$ channels facilitate the outward flow of $K^+$ ions. These channels are involved in almost all phases of the cardiac action potential, and provide crucial repolarising currents that restore and maintain the $R_m$ between the firing of each action potential. Consequently, the activity of $K^+$ channels during the action potential prevents spontaneous action potential firing that could lead to ectopic beats – a substrate for arrhythmia.

The $K^+$ current that first contributes to action potential repolarisation after the rapid depolarisation in phase 0 is the transient outward $K^+$ current, $I_{to}$. This current can be divided into the fast, $I_{to,\,f}$ and slow, $I_{to,s}$ currents, which are conducted through channels consisting of $K_v4.2/4.3$ and $K_v1.4$ subunits, respectively (Niwa & Nerbonne, 2010). $K_v4.3$ channels interact with the auxiliary subunit KChIP2, which increases PM channel density and current amplitude, and decreases the time of recovery from inactivation and slows the rate of inactivation (Patel *et al*., 2002). It is thought that the expression of KChIP2 regulates the density of $I_{to}$, as the expression of $K_v4.3$ was found to be constant across the ventricular wall (Näbauer *et al.,* 1996) whilst $I_{to}$ density is higher in atrial, epicardial and

midmyocardial cells and Purkinje fibres compared to the endocardial cells (Roasti *et al*., 2001). The transient nature of this current coupled with the activation of the L-type $Ca^{2+}$ channel, and hence increase of the L-type $Ca^{2+}$ current ($I_{Ca,L}$) at potentials more positive than approximately -40 mV, prevents full repolarisation at this stage, so only a small repolarising notch is seen.

During phase 2, when $Ca^{2+}$ ions are still passing into the cell via the L-type $Ca^{2+}$ channel, further depolarisation is prevented by the activation of the delayed rectifier $K_v$ channels. The delayed rectifier current ($I_K$) can be split into three components: the ultrarapid ($I_{Kur}$), rapid ($I_{Kr}$) and slow ($I_{Ks}$). $I_{Kur}$ is conducted by the $K_v1.5$ channel, and has been recorded in human atrial cells, but not ventricular cells (Wang *et* al., 1993). The $K_v11.1$ α-subunit forms the human ether-a-go-go-related gene (hERG) channel, which is thought to interact with the KCNE2 β-subunit to form the channel that conducts the $I_{Kr}$ current in human atrial and ventricular cells (Wang *et al*., 1994; Li *et al*., 1996). The $I_{Kr}$ current rapidly activates at approximately -30 mV, and shows a strong inward rectification at positive potentials due to a rapid C-type inactivation. The remaining component of $I_K$, the $I_{Ks}$ current, also contributes to action potential repolarisation, but possesses much slower activation kinetics compared to $I_{Kr}$ and $I_{Kur}$. The $I_{Ks}$ channel in the heart corresponds to the channel formed by KCNQ1 ($K_v7.1$) α-subunits and KCNE1 β-subunits. The channel activates at approximately -30 mV, and does not undergo inactivation. The $I_{Ks}$ current was primarily thought to be present only in ventricular cells, but sporadic evidence has shown that this current may also contribute to atrial repolarisation (Hong *et al*., 2005; Wang *et al*., 1994)

Phase 3 of the action potential begins when $Ca^{2+}$-dependent inhibition of the L-type $Ca^{2+}$ channel occurs and the sustained outward $K_v$ currents cause a net outward flow of ions. In ventricular cells, the rapid and slow delayed-rectifier $K^+$ currents, $I_{Kr}$ and $I_{Ks}$, are responsible for the outward $K^+$ current. Upon repolarisation of the membrane to potentials of 0 mV and below, the $I_{Kr}$ channel becomes relieved from inactivation and an outward flow of $K^+$ ions occurs, increasing the rate of phase 3 repolarisation. The $I_{Kr}$ channel then slowly deactivates. The $I_{ks}$ current gradually increases over the course of phase 2 and 3, but the total current is usually less than that of $I_{Kr.}$

### 1.2.4 Cardiac repolarisation reserve

The term repolarisation reserve was coined by Roden in 1998, who described it as a 'mechanism to effect orderly and rapid repolarisation that runs essentially no risk of setting up re-entrant circuits or of generating EADs', and suggested the normal functioning of $I_{Kr}$ and $I_{Ks}$ was a major contributor to a stable repolarisation (Roden, 1998).

The repolarisation reserve is a mechanism of redundancy in cardiac cells to protect against unwanted disturbances in action potential duration that could lead to arrhythmia. Block of $I_{Ks}$ has been shown to produce no ill effect on APD in human ventricular tissue without sympathetic stimulation, suggesting that this current does not play a role in repolarisation in normal physiological conditions. When sympathetic stimulation was increased pharmacologically by Jost *et al*. (2005), however, block of the $I_{Ks}$ current increased the APD, supporting the hypothesis that $I_{Ks}$ becomes a significant repolarising current in times of increased sympathetic drive.

The availability of the repolarisation reserve can be reduced by pharmacological inhibition of the $I_{Kr}$ channel, but the $I_{Ks}$ current has been shown to compensate for the reduction in $I_{Kr}$ due to the increased length and voltage of the action potential plateau (Jost *et al*., 2005). This enables an increased number of $I_{Ks}$ channels, which are characteristically slow to activate, to move to the open and conducting state. This also allows a greater proportion of $I_{Ks}$ channels to adopt a conformation close to the conducting state so they are able to open more rapidly during the following action potential.

Mutations in the SCN5A gene, encoding the cardiac $Na_v$ channel, $Na_v1.5$, can affect repolarisation reserve. Even though the $Na_v1.5$ current undergoes characteristic rapid inactivation, a small fraction of the $Na^+$ current is slow to inactivate – this so-called persistent $Na^+$ current opposes the repolarising $K^+$ currents and delays repolarisation. When the $Na^+$ current becomes increased, for example in heart failure or in the presence of gain-of-function mutations in SCN5A, the capacity of the repolarisation reserve to overcome this can become compromised (Varró & Baczkó, 2011).

In addition to mutations in the cardiac $Na^+$ channel, mutations in the KCNQ1 and KCNH2 genes (which code for the $I_{Ks}$ and $I_{Kr}$ channel α-subunits, respectively) can profoundly influence action potential repolarisation by causing a reduction in repolarising $K^+$ currents resulting in APD prolongation. Precipitation of arrhythmia under these circumstances usually occurs during periods of stress or exercise, when increased sympathetic stimulation requires an enhancement of outward $K^+$ current to counteract the concomitant increase in $Ca^{2+}$ influx (Carmeliet, 2006).

## 1.3 Arrhythmia

### 1.3.1 A Background to Arrhythmia

A small aberration from the precisely-controlled cardiac electrical conduction can lead to life threatening cardiac conditions such as arrhythmias, which are characterised by heart rate and rhythm abnormalities. The understanding of arrhythmia began during the first observations and descriptions by William Harvey in the early 17$^{th}$ century, and the expansion of his ideas continued in the mid-18$^{th}$ century by Jean-Baptiste de Sénac.

At present day, atrial fibrillation (AF) is the most common and sustained cardiac arrhythmia. The prevalence reaches almost 9% at aged 80+, and it is likely that the total number of AF sufferers will continue to increase due to the aging population (Colilla, 2013).

Arrhythmias arising in the ventricles can manifest as torsades de pointes (TdP), ventricular tachycardia, ventricular bradycardia or ventricular fibrillation, and can be caused by a number of substrates, including long QT syndrome (LQTS).

Across the wide range of arrhythmias there are those associated with underlying cardiac disease that can be rapidly fatal, and others that manifest as relatively asymptomatic conditions. The heterogeneous phenotype of arrhythmias is due to the number of different mechanisms and origins that exist. Many arrhythmias can be inherited or acquired, and these two distinct categories can contain multiple mechanisms of arrhythmogenesis.

Tachyarrhythmia describes when the heart rate is faster than normal, and a bradyarrhythmia is described as being when the heart rate is slower than normal. Bradyarrhythmia can be caused by a slowing or blockage of conduction between, for example, the SAN and the atria or the AVN and the bundle of His. Other mechanisms include the alteration of gap junction expression at the intercalated disc, which affects cell-to-cell conductance, or decreased $Na_v$ channel activity, reducing the source of depolarisation (Dhein *et al*., 2014).

### 1.3.2 Mechanisms of Arrhythmia

In terms of action potential propagation from one cell to the next, the excited cell is known as the ‘source’, and the unexcited cell is known as the ‘sink’. The excited cell ‘offloads’ a charge to the unexcited cell via gap-junction channels, which provides a level of excitation from the source to the electric sink. If the extent of excitation depolarises the unexcited cell to the threshold potential, an

action potential will propagate and the original unexcited cell will now become the new source of charge for downstream cells (Kléber & Rudy, 2004).

Problems can arise in this source-sink relationship when the sink is larger than the source, i.e. when a small area of activated cells meets a large area of unexcited cells. In this situation, the unexcited cells would not likely depolarise to the threshold potential, and action potential propagation would terminate. This can occur at an ischemic area of tissue, which contains non-excitable cells (and therefore acts as an electric sink) that consequently causes conduction failure (Dhein *et al*., 2014).

The Purkinje system is thought to be a common source of ventricular arrhythmias. As this source of electrical excitation meets a relatively large ventricular myocardium, it is prone to conduction block, which can lead to delayed ventricular activation. This unidirectional conduction block can lead to re-entry circuits, which can lead to ventricular tachycardia and fibrillation.

*Afterdepolarisations and re-entry circuits*

Source-sink mismatch can be a protective measure against arrhythmia in well-coupled cardiac tissue; when an ectopic beat occurs (known as either an early afterdepolarisation (EAD) or delayed afterdepolarisation (DAD)) the small source (i.e. one action potential from one cell) cannot lead to action potential propagation because each cardiomyocyte is usually coupled to 4-6 other cells, which provides a large electrical sink.

Afterdepolarisations are described as oscillations in the membrane potential that occur during, or immediately following, an action potential (figure 6). An EAD is caused by increased net $Ca^{2+}$ conductance during phase 2 and 3 of the action potential, which occurs due to a loss of phase 2 and 3 $K^{+}$ conductance (for example, in the setting of acquired or congenital LQTS or heart failure). DADs are a result of intracellular $Ca^{2+}$ overload thought to be caused by spontaneous $Ca^{2+}$ release from the SR after termination of the preceding action potential (Gaztañaga *et al*., 2012; Volder *et al*., 2000).

Xie *et al* (2010) found that the number of contiguous myocytes required for an EAD or DAD to trigger a premature ventricular complex (PVC), an ectopic beat arising from within the ventricles, was extremely high in normal cardiac tissue. Only in the presence of gap junction, electrical and structural remodelling, such as in cardiac disease, was a much smaller number of cells required to stimulate propagating PVC (Xie *et al*., 2010).

If an ectopic depolarisation such as that caused by an EAD or DAD succeeds in propagation, the trigger for a re-entrant circuit may be created. There are two categories of re-entry:

classical/anatomical and functional. Anatomical re-entry occurs when a circular trajectory of activation reactivates the point of origin. This model of re-entry describes when the propagating impulse reaches, for example, a bifurcation or an obstacle, in which one path acts as a unidirectional block (figure 7). Activation of the tissue occurs down one path, and when reaching the distal end of the other it travels in a retrograde manner to the point of bifurcation. In the absence of unidirectional block, activation would occur down both paths and the circular re-entrant pathway would never be created. Maintenance of a re-entry circuit is dependent upon the length of the refractory periods in each pathway. The 'excitable gap', i.e. the period of time between the tail-end and the head-end of the re-entrant impulse wavefront, allows the re-entrant circuit to propagate. If there were no excitable gap because the tissue had not yet recovered from the previous action potential, the circuit would terminate (Kléber & Rudy, 2004). In contrast to anatomical re-entry, functional re-entry is facilitated by circuits that are not dependent on physical barriers, but on heterogeneities in neighbouring cells' excitability.

Unidirectional block is a prerequisite to re-entry. This can develop from local source-sink relationships that vary throughout the cardiac tissue, creating neighbouring areas with differing extents of refractoriness, or may be an inherent part of myocyte physiology; transmural differences in repolarisation between the three main cell types in the ventricular myocardium can also be a substrate for re-entry (Antzelevitch, 2005).

*Electrical remodelling*

Many types of cardiac abnormalities and cardiac disease lead to adaptive changes in the expression of ion channels, transporters and gap junctions. These changes are usually intended to counteract the initial dysfunction, but usually cause more damage due to the common induction of tachyarrhythmia (Nattel *et al*., 2007). Primary remodelling is a result of altered electrical activity, e.g. pacing. In contrast, secondary remodelling arises as a result of a structural insult to the cardiac tissue, as occurs in heart failure and myocardial infarction (Cutler *et al*, 2011).

APD prolongation is commonly seen in people with heart failure, and delayed repolarisation is a prime cause of EAD generation. A cause of this phenomenon in heart failure is the change in $K^+$ currents brought about by remodelling. Changes in $K^+$ currents seen in experimental models of congestive heart failure include a decrease in the $I_{Ks}$ and $I_{to}$ currents, which would give rise to a net increased in the inward $Ca^{2+}$ current. Decreased $K^+$ current at this phase of the action potential can give rise to EADs via two mechanisms: delayed repolarisation reserve, or a prolongation of the plateau phase long enough for reactivation of the L-type $Ca^{2+}$ channel (Viswanathan & Rudy, 1999).

Guo *et al*. (2012) found that chronic ischemia and reperfusion increased the incidence of ventricular arrhythmias in a rabbit model, and concluded that the downregulation of KCNQ1 may underlie this. Much of the ionic remodelling seen in heart failure mimics the effects of congenital ion channel abnormalities seen in LQTS (Nattel *et al*, 2007).

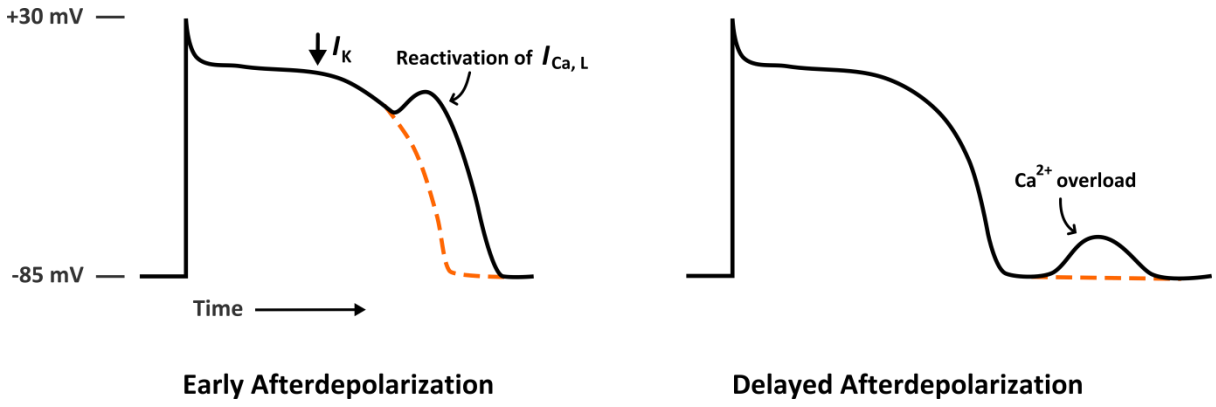


**Figure 6. Proposed mechanisms of afterdepolarisations in the heart.** Schematic representation of early (left) and delayed (right) afterdepolarisations in a ventricular action potential. EADs occur during phase 2 or 3, and DADs occur after action potential repolarisation, in phase 4. Orange dashed lines represent a normal action potential waveform; solid black lines represent the corresponding afterdepolarisation.

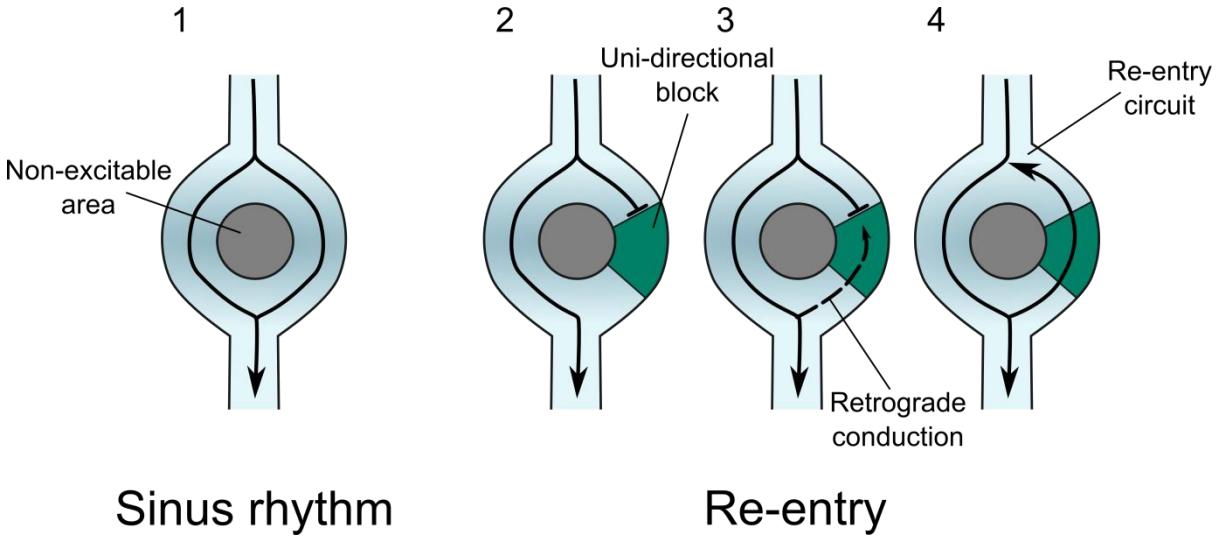


**Figure 7. Mechanism of re-entry circuit formation.** Re-entry circuits can be caused by unidirectional block at a bifurcation/obstacle, where retrograde conduction then occurs (Gaztañaga et al., 2012).

### 1.4 Long QT syndrome

LQTS is named after the characteristic prolonged QT interval on an ECG, which represents the time between ventricular depolarisation and ventricular repolarisation. In its congenital form, LQTS is one of the leading causes of death in the paediatric population. Prolongation of the QT interval predisposes an individual to the potentially lethal arrhythmia TdP, which can degenerate into VF (figure 8). TdP is characterised by a change in amplitude and a 'twisting' of the QRS complex around the isoelectric line. This change in morphology, however, may not be visible in all ECG leads. The

heart rate during periods of TdP can be between 160 and 240 bpm (but this is slower than during periods of VF). TdP often terminates spontaneously, but can progress to VF (Drew *et al.,* 2010). Symptoms of LQTS include palpitations, syncope, seizures and sudden death (Beher & Weindling, 2015).

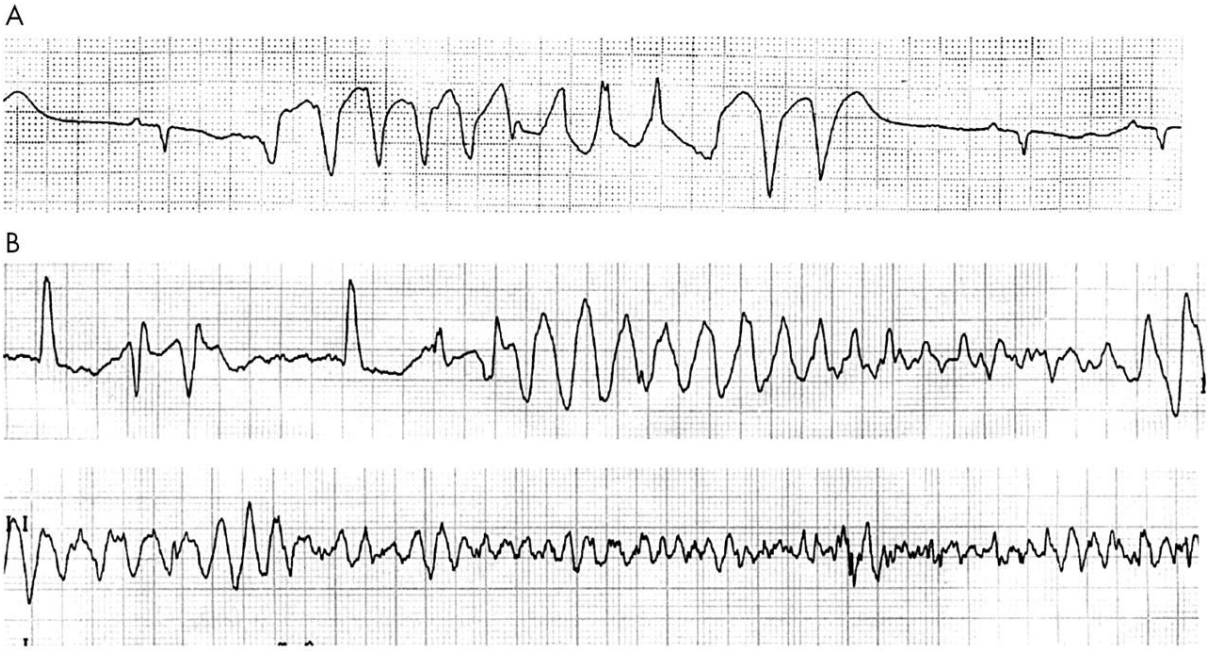


**Figure 8. Torsade de pointes and ventricular fibrillation.** A – an episode of self-limiting torsade de pointes. B – an episode of torsade de pointes, which degenerated into ventricular fibrillation. Figure taken from Yap & Cam (2003).

*Measuring the QT interval*

When determining the duration of the QT interval, heart rate is taken into consideration to give a 'corrected' QT interval (QTc), enabling the comparison of QT interval measurements taken at different heart rates. One of the earliest, but still the most common, ways of correcting the QT interval for HR was published in the 1920s by Bazett, and uses the formula $QTc = QT/RR^{1/2}$, where RR is determined from the previous RR interval. This formula, however, can lead to overcorrection and undercorrection of the QT interval at slower and faster heart rates, respectively (Postema & Wilde, 2014). The Fridericia method uses the formula $QTc = QT/RR^{1/3}$, and is considered to be more accurate at higher heart rates than the Bazett formula. Another formula used is the linear Framingham method, which uses the formula QTc = QT+0.154(1-RR) (Postema & Wilde, 2014).

The threshold beyond which QTc prolongation is diagnosed is 460 ms for females and 450 ms for males, in recognition that females have a higher resting heart rate than males. Table 1 details the boundaries that are used to determine the extent of QTc shortening/prolongation.

| **QTc (ms)** | **QT classification** |
|---|---|
| Females: <360; Males: < 350 | Short QT interval |
| Females: 360–460; Males: 350–450 | Normal range |
| Females: >460; Males: >450 | Prolonged QT interval |

**Table 1. QTc range and classification**. The length in milliseconds (ms) of QTc values in males and females, and how this is interpreted and classified into short, normal or prolonged QT interval categories. Values taken from Vincent (2002) and Patel et al. (2010).

Normal QTc values vary between individuals, between 350–460 ms, and as a result of this wide range, prolonged QTc values can lie anywhere from approximately 410 ms upwards. Values in the 440–460 ms range are seen in around 12% of congenital LQTS (cLQTS) cases. Further complicating diagnosis, 30% of LQTS-causing mutation carriers have a QTc between 410–460 ms whilst approximately 60% of the normal population have a QTc in this range (Vincent, 2002).

The diagnosis of LQTS poses particular difficulty because the measurement and calculation of the QTc value is prone to human error. In fact, Viskin *et al*. (2005) highlighted that many physicians, including cardiologists, cannot accurately measure QTc or identify a prolonged QT interval. Many physicians use clinical diagnostic assessment criteria to create a risk score to help in the diagnosis of LQTS. A significant portion of this score, however, relies heavily on the calculated QTc value for its result (Johnson & Ackerman, 2014).

### 1.4.1 Acquired long QT syndrome

Prolongation of the QT interval can occur upon exposure to environmental factors acting on the repolarising $K^+$ currents or depolarising $Na^+$ or $Ca^{2+}$ currents (Anzelevitch, 2007). The majority of acquired LQTS (aLQTS) cases are a result of pharmacological blockade of the hERG channel, but can also occur due to hypokalemia and hypomagnesemia. Cases of aLQTS revert back to normal upon removal of the environmental stressor.

*Drug-induced aLQTS*

In the case of drug-induced aLQTS, anti-arrhythmic medication is responsible for more cases than non-cardiac medication. Commonly-used anti-arrhythmic drugs that cause aLQTS include disopyramide, dofetilide and amiodarone (Roden & Viswanathan, 2005). The efficacy of anti-arrhythmic medication varies significantly, and can be between 30–60%. The choice of anti-arrhythmic drug in any given case is complicated by the fact that arrhythmias differ significantly in their aetiology. Nevertheless, these drugs are widely prescribed, but their success is often offset by their negative effects on mortality (Sanguinetti & Bennet, 2003).

The first incidences of QT prolongation as a direct result of anti-arrhythmic medication were identified in the 1960s (Selzer & Wray, 1964), where quinidine treatment resulted in the emergence of a prolonged QT interval and ventricular fibrillation in a number of patients. Prior to this study, mortality during quinidine treatment was assumed to be due to a phenomenon known as 'quinidine shock', caused by toxic effects on the central nervous system (Thompson, 1956).

The quintessential mechanism of drug-induced QT prolongation is blockade of the hERG ($I_{Kr}$) channel (Redfern *et al*., 2003; Sanguinetti *et al*., 1995). This channel's unique pore structure gives rise to the increased rate of drug-block compared to other ion channels. Unlike other channels, the hERG channel contains many aromatic residues in its pore region. Two of these possess inwardly-facing side chains (Tyr652 & Pro656), giving rise to a high-affinity binding site for a wide range of drugs (Mitcheson *et al*., 2000). In addition to this, the hERG channel lacks the two proline residues responsible for the kink in S6 usually present in $K_v$ channels. The absence of these residues causes a wider opening to the pore and consequently gives increased access to the binding site. Introduction of the 'missing' Pro-Val-Pro motif into the hERG channel reduces the channel's sensitivity to drug binding (Fernandez *et al*., 2003; Roden & Viswanathan, 2005).

Pharmacological inhibition of the hERG channel reduces the $K^+$ efflux from myocytes during phase 3 repolarisation, resulting in QT prolongation. This can lead to the generation of afterdepolarisations, and as detailed in section 1.3.2, and may contribute to the formation of re-entry circuits and increase the likelihood of arrhythmia.

As it is now known that the pharmacological promiscuity of the hERG channel puts a high proportion of drugs at risk of causing adverse cardiac side effects, even with non-cardiac medication, 'cardiac safety' screening now takes place early in the drug-discovery process.

*Risk factors for aLQTS*

Of those at risk of aLQTS, a small percentage (10–15 %) carry a mutation in one of the known LQTS-causing genes (which are detailed in table 2). These patients do not usually suffer symptoms as a result of these mutations as there is little or no change in normal protein function. These mutations are classed as being 'subclinical'. When control of the APD is challenged by hERG-blocking drugs, however, these underlying mutations increase the risk of aLQT. In individuals harbouring subclinical mutations that have been affected by drug-induced LQT, mutations have been found in the KCNQ1, KCNH2, KCNE1, KCNE2 and SCN5A genes (Yang *et al*., 2002; Paulussen *et al*., 2004).

It is not only mutations in LQTS-causing genes that influence the risk of aLQT, but those also found in proteins involved in a drug's metabolism. Mutations in certain drug-metabolising enzymes can increase the risk of aLQT by slowing down the metabolism of the active form of the drug, resulting in increased drug plasma concentration (Paulussen *et al.*, 2004). In the past, high-profile drugs have been withdrawn from the market after it was discovered that their use was linked to sudden cardiac death. Notable examples include the antihistamine terfenadine (Woosley et al., 1993), and the gastroprokinetic agent cisapride (Rampe et al., 1997), both of which are metabolised by the CYP3A family of cytochrome P450 enzymes. These two drugs are rapidly metabolised into entities that do not inhibit the hERG channel, and rates of TdP are usually considered rare. However, in patients with compromised metabolism via the CYP3A pathway (e.g. due to overdose, liver disease or administration of CYP3A inhibitors), toxicity and TdP can ensue as the active compounds remain in circulation (Roden & Viswanathan, 2005). Besides terfenadine and cisapride, an example of this occurrence is in the case of treatment with thioridazine, an antipsychotic medication. This drug is eliminated by the cytochrome P450, CYP2D6, and loss-of-function variants of this enzyme are found in approximately 7% of the population. Individuals harbouring these mutations consequently risk TdP as a result of thioridazine treatment (Roden & Viswanathan, 2005).

In addition to mutations in LQTS-causing genes and those involved in the metabolism of hERG-blocking drugs, uncontrollable factors also increase the risk of QT prolongation and TdP. These include gender, and it was found that women are 2–3 times more likely to develop aLQT than men (Makkar *et al*., 1993). This disparity between the sexes is likely to result from the shortening of the QT interval that occurs in males after puberty (Rautaharju *et al*., 1992).

Avoidable or controllable factors that can lead to aLQTS include high drug concentration, hypokalaemia and severe hypomagnesemia (Kallergis *et al*., 2012).

*Electrolyte imbalance*

Divergence of electrolyte concentrations from their optimal range can lead to QT prolongation, and hence increases the risk of TdP generation.

The most common electrolyte imbalance associated with QT prolongation is hypokalaemia, which is a deficiency of $K^+$ in the bloodstream. This condition can result from a multitude of different situations, including gastrointestinal losses (i.e. diarrhoea and vomiting), hyperthyroidism, prolonged excess of caffeine, long-term inadequate intake and use of certain drugs (Widimsky, 2008).

It is thought that the sensitivity of the hERG channel to extracellular $K^+$ concentration provides the mechanistic link between hypokalaemia and QT prolongation. A study in guinea pig ventricular myocytes found that a reduction in extracellular $[K^+]$ reduced the $I_{Kr}$ current, despite the existence of an increased concentration gradient for $K^+$ (Sanguinetti & Jurkiewiez, 1992), and a study in rabbit hearts found that a reduction in extracellular $[K^+]$ lead to an increase in the rate of internalisation and degradation of hERG (Guo *et al*., 2009). Accordingly, an increase in serum $[K^+]$ corrected QT-interval abnormalities in patients with mutation(s) in KCNH2 (Compton *et al*., 1996).

In addition to causing prolongation of the QT interval itself, hypokalaemia may also influence the effect of hERG-blocking drugs. A study that investigated the $[K^+]$-dependent block of hERG by quinidine found that by lowering $[K^+]$ from 5 mmol/L to 2.5 mmol/L, quinidine inhibition was enhanced (Lin *et al*., 2005). Supporting these observations, Yang *et al*. (1996) found that inhibition of hERG by either quinidine or dofetilide was highly dependent on extracellular $[K^+]$.

Prolongation of the QT interval by hypokalaemia has also been reported to precipitate TdP in a patient with a subclinical KCNQ1 missense mutation (Arg259Cys) (Kubota *et al*., 2000).

Besides hypokalaemia, a severe deficiency in extracellular magnesium, known as hypomagnesemia, can result in QT prolongation. This condition can be caused by low $Mg^{2+}$ intake, poor intestinal absorption, excessive alcohol consumption or the use of diuretics (Efstradiadis *et al*., 2006). It has been shown *in vivo* that reduction of $Mg^+$ has very little effect on the action potential (Surawicz, 1989). However, $Mg^{2+}$ deficiency can lead to disrupted $Na^+/K^+$-ATPase activity, which results in an increase in intracellular $Na^+$ and a decrease in intracellular $K^+$. Shils (1964) observed that experimentally-induced hypomagnesemia caused hypokalaemia in patients. As maintenance of the $K^+$ gradient is disrupted in the setting of hypomagnesemia, inhibition of $K^+$-dependent processes is likely to be the cause of arrhythmia generation in patients with low serum $[Mg^{2+}]$. It has also been found by others that hypokalaemia cannot be corrected without first treating any underlying

magnesium deficiency (Huang & Kuo, 2007; Whang, 1997).

In order to successfully prevent aLQT episodes of any origin, it was emphasised by Digby *et al*. (2011) that awareness of drug interactions and the early identification of individuals with a predisposition to QT prolongation are both crucial, so exacerbation of their risk does not occur.

### 1.4.2 Congenital long QT syndrome

The inherited, or congenital, form of LQTS is a collection of genetic disorders that can independently give rise to QT prolongation. Mutations are more commonly found in the cardiac $K^+$ or $Na^+$ channels, but are also found in accessory, regulatory and anchoring proteins (Table 2).

The clinical manifestations of cLQTS were first identified in the late 1950s and early 1960s as two separate conditions: Jervell and Lange-Nielsen Syndrome (JLNS) and Romano Ward Syndrome (RWS) (Jervell & Lange-Nielsen, 1957; Romano *et al*., 1963; Ward, 1964). Once thought to be an extremely rare occurrence, the prevalence of cLQTS is now estimated at between 1:2000 and 1:2500 (Schwartz *et al*., 2009). The vast majority of cases are classified as RWS, and JLNS is an extremely rare condition that is accompanied by congenital deafness.

Mutations in the KCNQ1 (LQT1), KCNH2 (LQT2) and SCN5A (LQT3) genes are by far the most common in cLQTS (Kapplinger *et al*., 2009). Despite causing a potentially fatal cardiac arrhythmia, the propagation of cLQTS continues because a large proportion of patients do not exhibit symptoms (Priori *et al*., 2003). Autosomal dominant inheritance of mutations in RWS gives offspring a 50% likelihood of inheriting the LQTS-causing gene, but with only 1 copy of the allele the effects can be mild enough to allow a carrier to live an average lifespan and pass on the mutated gene to their own offspring. An unfortunate consequence of the varying penetrance of this disease is that many people do not realise they suffer QT prolongation and are at risk of fatal ventricular arrhythmias; approximately 5% of mutation-carrying individuals suffer cardiac death as the first manifestation of LQTS (Tester & Ackerman, 2012).

*Mechanisms of APD prolongation in cLQTS*

Mutations in KCNQ1 more commonly lead to arrhythmia when an individual is under emotional stress or physical exertion, but particularly whilst swimming or diving. The adrenergic drive and release of catecholamines (such as norepinephrine) that occurs during these situations normally causes an increase in $I_{Ca,L}$ amplitude to increase the force of myocyte contraction. This is accompanied by an increase in repolarising $K^+$ currents, such as $I_{Ks}$, to counter the increased

depolarising $Ca^{2+}$ current and shorten the APD. Individuals harbouring KCNQ1 mutations are less able to shorten their cardiac APD and are therefore prone to arrhythmia generation (Herbert *et al*., 2002).

KCNH2 mutations are the second most common cause of cLQTS, and cause a reduction of the characteristic resurgent $I_{Kr}$ current, which occurs after the channel becomes relieved from inactivation as the membrane potential repolarises. This reduced $I_{Kr}$ current can occur through a variety of mechanisms, from acceleration in channel deactivation (which reduces the time the channel remains in the open state after relief from inactivation (Chen *et al*., 1999)), to a leftward shift in the voltage-dependence of inactivation (causing a reduction in the available resurgent $I_{Kr}$ current (Nakajima *et al*., 1998)). A reduction in contribution of the $I_{Kr}$ current to the repolarising $K^+$ current in the heart may also arise due to mutations causing defective channel trafficking (Zhou et al., 1998).

Mutations in the SCN5A gene represent another major cause of LQTS (Wang *et al*., 1995), accounting for approximately 10% of cLQTS cases. Shortly after the first cLQTS-causing SCN5A mutation was described, it was discovered that the mechanism by which SCN5A mutations lead to APD prolongation was through a sustained inward $Na^+$ current through the cardiac $Na^+$ channel, $Na_v1.5$, causing prolonged depolarisation (Bennet *et al*., 1995).

Some of the less-common types of cLQTS affect the $I_{Ks}$, $I_{Kr}$ and $I_{Na}$ currents indirectly. For example, mutation of the β-subunits that are required by the pore-forming subunits for proper channel function can lead to LQTS. This occurs in LQT types 5, 6 and 10 (Table 2).

| LQT Type | Mutated gene | Encoded protein | Current/Function |
|---|---|---|---|
| 1 | KCNQ1 | $K_v7.1$ α-subunit | $I_{Ks}$ current in heart & $K^+$ current in inner ear (when complexed with KCNE1) |
| 2 | KCNH2 | $K_v11.1$ α-subunit | $I_{Kr}$ current in heart |
| 3 | SCN5A | $Na_v1.5$ α-subunit | $I_{Na}$ current in heart |
| 4 | ANK2 | Ankyrin-B | Involved in assembly of Na/Ca exchanger, Na/K ATPase and $InsP_3$ receptor |
| 5 | KCNE1 | $K_v7.1$ β-subunit | $I_{Ks}$ current in heart & $K^+$ current in inner ear (when complexed with KCNQ1) |
| 6 | KCNE2 | $K_v11.1$ β-subunit | $I_{Kr}$ current in heart |
| 7 | KCNJ2 | $K_{ir}2.1$ α-subunit | $I_{K1}$ current in heart, skeletal muscle, nervous system |
| 8 | CACNA1C | $Ca_v1.2$ α-subunit | L-type $Ca^{2+}$ current in heart, nervous system |
| 9 | CAV3 | Caveolin 3 | Scaffolding protein for caveolae-associated proteins in heart and muscle |
| 10 | SCN4B | $Na_v1.5$ β-subunit | $I_{Na}$ current in heart (when complexed with SCN5A) |
| 11 | AKAP9 | Yotiao | Anchor protein in $I_{Ks}$ signalling complex |
| 12 | SNTA1 | α1-Syntrophin | Membrane scaffold interacting with $Na_v1.5$ |
| 13 | KCNJ5 | $K_{ir}3.4$ α-subunit | $I_{KAch}$ current in heart (when complexed with KCNJ3 ($K_{ir}3.1$) |
| 14 | CALM1 | Calmodulin 1 | Involved in adrenergic receptor signalling cascade, and essential for $I_{Ks}$ gating and assembly |
| 15 | CALM2 | Calmodulin 2 | Involved in adrenergic receptor signalling cascade, and essential for $I_{Ks}$ gating and assembly |

**Table 2. Mutated genes involved in Long QT Syndrome types 1–15.** The 15 types of LQT, with corresponding mutated gene, encoded protein and the current conducted or normal role served. Mutations in ion channel α-subunits are responsible for 6 types of LQT, whilst ion channel β-subunit mutations account for 3 types. The remaining 6 types of LQT are caused by mutations in ion channel-associated proteins, involved in trafficking, or membrane or complex anchoring.

*Compound mutations*

As many carriers of single mutations show no (or mild) clinical symptoms, and therefore reach reproductive age with no indication they harbour a LQTS-associated mutation, the appearance of compound mutations can occur. This is estimated to occur in 4–11% of LQTS cases (Itoh *et al*., 2010). This usually arises when each parent passes on a single mutation to their child, who then possess two LQTS-causing mutations.

Recent work in this laboratory identified the molecular mechanisms behind the increased clinical severity of 6 compound mutations in KCNQ1. It was found that 3 of these compound mutations (Thr391Ile/Gln530X, Ala525Thr/Arg518X and Ala178Thr/Lys422fs39X) caused severe disruption to channel trafficking when in compound form, and an additional mutation (Val310Ile/Arg594Gln) had a moderate, but not compound, effect on channel trafficking (Harmer *et al*., 2014).

Compound mutations have been found in the same LQTS-causing gene or in different LQTS-causing genes. For example, Schwartz and colleagues identified 6 heterozygous carriers of LQTS mutations. Two of these probands carried 2 independent mutations in the KCNQ1 gene, two had mutations in KCNQ1/SCN5A, one had KCNQ1/hERG mutations and one had hERG/SCN5A mutations (Schwartz *et al*., 2002). The parents of these 6 probands were confirmed to have contributed one of the identified mutations each. Compound mutations can, however, be passed on by a single parent or appear *de novo*.

Schwartz *et al.* (2002) also highlighted that carriers of compound mutations experience a more severe phenotype than would be expected taking into account the symptoms of the respective single-mutation carriers. This was also noted by Itoh and colleagues, whose larger Japanese study involved 26 compound mutation carriers (8.4% of genotyped probands). This study also found that compound mutation carriers exhibited a longer QT interval when compared to single mutation carriers, and an earlier age of onset for cardiac events (Itoh *et al*., 2010).

### 1.4.3 KCNQ1 mutations

Mutations in the KCNQ1 gene are the leading cause of LQTS, accounting for approximately 40–55 % of cases. Missense mutations are the most common occurrence, followed by frameshift mutations (Splawski *et al.*, 2000). Most mutations reside in the intracellular and TM regions, and mutations within the TM regions, including S4, the pore domain and P-loop, lead to the highest number of cardiac events (Donger *et al.,* 1997).

The study of mutations that are identified in LQTS patients is made possible by the introduction of these mutations into the KCNQ1 gene, and expression of the mutant protein in heterologous cell systems or induced pluripotent stem cells (iPSCs) (Bellin *et al*., 2013). Cells expressing the mutant KCNQ1 protein can then be studied using electrophysiological techniques to investigate its function, by molecular biology techniques to assess its expression and by imaging techniques to visualise its expression and localisation.

Within the regions of high-risk mutations, those in the pore region were identified by Burgess *et al*. (2012) as particularly high risk in the onset of cardiac events in LQTS. The mutations studied by Burgess and colleagues (Thr322Met, Thr322Ala, and Gly325Arg) exhibited a DN effect over WT channel subunits, and hence generated non-functional channels. These mutations decreased the repulsion of $K^+$ ions in the selectivity filter, and as a result of this, decreased the permeation of $K^+$ through the pore.

Distinguished from typical loss-of-function mutations, some KCNQ1 mutations can cause a shift in the voltage-dependence of activation (Boulet *et al.,* 2006; Chouabe *et al*., 2000). When these mutations are expressed in heterologous cell lines and the membrane potential is depolarised to more positive potentials, the resulting current can reach a level comparable to WT. However, the activation is shifted to a more depolarised potential than the WT channel, and at physiological potentials (i.e. in a ventricular myocyte) the mutant channel would not produce a sufficient level of current required for repolarisation.

In addition to mutations leading to functional defects in the channel, a number of mutations studied are now found to cause trafficking abnormalities. The effect of trafficking mutations can vary in severity, and are commonly studied using confocal microscopy to enable colocalisation analysis of the channel subunit with a fluorescent protein-tagged ER marker (i.e. DsRed-ER). On the other hand, a number of mutations have been identified that result in both functional aberrations and trafficking deficiencies (Schmitt *et al.*, 2007).

As a result of the extensive research into the mechanisms of different LQTS-causing mutations, it is now recognised that the classically-described dominant inheritance of RWS mutations and recessive inheritance of JLNS mutations is not always true. Mutations that cause RWS have been identified (i.e. no hearing loss) that follow a recessive inheritance pattern (Priori *et al.,* 1998). The penetrance of different LQTS mutations is highly variable. Some individuals have life-threatening heterozygous mutations, and other have heterozygous mutations that only slightly increase their predisposition to cardiac events. Others have homozygous mutations that cause only cardiac effects, whereas some

individuals suffer from this and a loss of hearing (i.e. JLNS).

Regardless of whether the function or trafficking of the $I_{Ks}$ channel is affected, the outcome is the same. That is, the ability of the $I_{Ks}$ current to contribute to ventricular repolarisation is partly or completely diminished.

### 1.4.4 Treatment for long QT syndrome

The response of a patient to treatment for cLQTS is thought to differ based upon the location of their LQTS-associated mutation(s). The majority of evidence for or against this is in the setting of LQT1-3, as these are most commonly seen and treated clinically.

Some claim that the molecular substrate of cLQTS does not matter when it comes to prophylactic treatment strategies, and that administration of β-blockers can help reduce the chance of cardiac events in all types of LQTS. A recent study highlighted the effect of the β-blocker propranolol in preventing the induction of ventricular tachycardia and fibrillation in an established mouse model of LQT3 (Calvillo *et al*., 2014), and suggested that patients with LQT3 should also be placed on β-blocker therapy without hesitation. This is in contrast to previous findings by Moss and colleagues, who, in their study of 869 patients treated with β-blockers, found that the number of cardiac events in LQT1 and LQT2 patients was reduced, but there was no beneficial effect of β-blocker therapy in LQT3 patients (Moss *et al*., 2000).

It is commonly thought that the origin of LQTS should be taken into consideration when deciding the most effective prophylactic strategy. LQT1 and LQT2 patients, with mutations residing in the KCNQ1 and KCNH2 genes, respectively, have a reduced ability to provide sufficient repolarising current in phases 2 and 3 of the cardiac action potential. These patients are thought to be more responsive to β-blocker therapy because it removes the need of the repolarising $K^+$ currents to counter the increased $Ca^{2+}$ current normally induced by adrenergic stimulation (Moss *et al*., 2000).

A retrospective study of 216 LQT1 patients treated with β-blockers revealed that this strategy is highly effective in LQT1, and that non-compliance was responsible for almost all life-threatening cardiac events in this patient group (Vincent *et al*, 2009). Supporting the effectiveness of β-blocker therapy in LQT1 patients, Schwartz *et al*. (2001) reported that in 162 LQTS patients treated with β-blockers, patients with LQT2 and LQT3 had a higher rate of recurrence than LQT1 patients.

Many LQTS patients that have a high risk of VF have a permanent pacemaker or implantable cardioverter defibrillator (ICD). A pacemaker is a small device that is placed in the chest, which

controls abnormal cardiac rhythms. It can be particularly beneficial in patients with LQT3, who may be unresponsive to β-blocker therapy. In addition, pacing the heart can reduce the heightened risk of arrhythmia in these patients during periods of bradycardia (Viskin, 2000). A portion of patients may benefit from a combination of β-blockers and a pacemaker, either due to the increased protection from episodes of TdP or by reducing the symptoms of bradycardia resulting from by β-blocker therapy (Eldar *et al*., 1987).

An ICD is a device implanted inside the body that is able to perform cardioversion and defibrillation as well as pacing, and is hence able to abort life-threatening arrhythmias. In the past, the majority of LQTS patients receiving ICDs were aged >60. However, increased diagnosis of LQTS patients at earlier stages in their life has led to the implantation of ICDs into young patients also (Schwartz *et al*., 2010), as the first manifestation of LQTS can occasionally be sudden death.

There is no hard and fast rule regarding the treatment strategies employed for LQTS patients of any genetic origin, and the precise management is commonly at the discretion of the clinician. However, increased knowledge on the mechanisms underlying each type of LQTS will provide an increased understanding of an individual patient's disease, and enable clinicians to plan more effective treatment strategies accordingly.

## 1.5 KCNQ1

### 1.5.1 KCNQ1 structure and function

The KCNQ1 protein is the founding member of the KCNQ family, of which there are 5 members. The KCNQ2-5 subunits may form homomeric or heteromeric complexes throughout the body to perform a multitude of functions, but the KCNQ1 subunit does not associate with any other members of the family (Schroeder *et al.*, 2000a; Kubisch *et al.*, 1999).

The KCNQ1 homomeric channel, also called KvLQT1 or $K_v7.1$, follows the typical $K_v$ channel structure, and consists of 4 pore-forming KCNQ1 α-subunits that are each made from one stretch of protein assembled into 6 TM domains. It is thought that physiologically, the KCNQ1 channel associates with a number of single-TM-domain KCNE1 β-subunits (between 1 and 4 subunits) (Chen *et al.*, 2003; Murray *et al*., 2016; Plant *et al.*, 2014; Wang *et al.*, 1998) to form the $I_{Ks}$ channel in the heart and inner ear (Barhanin *et al*., 1996; Sanguinetti *et al.*, 1996). The KCNQ1 channel can also associate with other KCNE subunits, which play different roles throughout the body.

*KCNQ1 cytoplasmic domains*

The KCNQ1 subunit exists in a number of different splice variants, the two most common being isoform 1 and isoform 2. Each of the KCNQ1 isoform 1 subunits is 676 amino acids in length and possesses an intracellular N- and C-terminus, which are comprised of 122 and 322 residues, respectively. The C-terminus contains 4 helical domains that are conserved throughout the KCNQ family, named helix A, B, C and D, respectively. Isoform 2 is a truncated version of isoform 1, and consists of only 549 residues due to truncation of the N-terminus and the initial part of the first TM domain (Neyroud *et al*., 1999).

Helices A and B form the proximal portion of the C-terminus, and create a calmodulin (CaM) binding site (Yus-Najera *et al*., 2002). It is thought that KCNQ channels require CaM for their function (Kosenko & Hoshi, 2013). The binding of CaM to KCNQ1 is also said to relieve channel inactivation and contribute to channel folding (Ghosh *et al*., 2006), and mutation of the CaM binding site has been shown to cause abnormalities in these processes (Shamgar *et al*., 2006). Bai *et al*., (2005) observed that in guinea pig myocytes there was a $Ca^{2+}$-dependent increase in the $I_{Ks}$ current, which was inhibited by a CaM antagonist. This suggests that CaM not only aids the channel in folding and assembly, but also provides a means of $Ca^{2+}$-dependent modulation during the cardiac action potential. Further evidence supporting $Ca^{2+}$-CaM modulation of KCNQ channels came from studies involving the KCNQ2 channel. Alaimo and colleagues found that binding of CaM to the KCNQ2 channel was required for channel trafficking, and this was performed in a $Ca^{2+}$-dependent manner (Alaimo *et al*., 2015).

Also found in the proximal C-terminus of KCNQ1 is a cluster of basic residues that have been shown to bind a number of phospholipids, including phosphatidylinositol-4,5-bisphosphate ($PIP_2$), with the most important residues in this region being Lys358 and Arg360 (Thomas *et al.*, 2011). $PIP_2$ is known to be required for $I_{Ks}$ channel opening (Loussouarn *et al.*, 2003; Zaydman *et al.*, 2013).

The distal portion of the C-terminus contains the coiled-coil helices C and D, which constitute the assembly domain. The assembly, or 'A'-domain is responsible for the specific homomeric KCNQ1 assembly. Residues 589–620 show similarity to the tetramerization (T-1) domain in Shaker $K^+$ channels. It was found that a KCNQ1 mutation that disrupts part of the assembly domain led to the inability of KCNQ1 mutant subunits to assemble with each other, resulting in a reduction of $I_{Ks}$ channel cell-surface expression (Schmitt *et al*., 2000).

The distal C-terminus also contains a leucine zipper (LZ) motif, located within helix D, which is known to be required for the binding of the A-kinase anchoring protein (AKAP) 9, also named yotiao. Binding of yotiao enables $I_{Ks}$ channel regulation by β-adrenergic receptor activation (Marx *et al*., 2002).

The most distal portion of the C-terminus contains a PY domain, which is required for interaction of the channel with Nedd4-2 ubiquitin ligase. Nedd4-2 is involved in controlling the regulation of channel recycling and degradation, and therefore the density of the $I_{Ks}$ channel at the PM (Jespersen *et al*., 2007).

The N terminus of KCNQ1 contains residues that can be phosphorylated to modulate channel activity. Ser27 (Kurokawa *et al*., 2004) and Ser92 (Lopes *et al*., 2007) are phosphorylated by protein kinase A (PKA), which is brought into close proximity to the $I_{Ks}$ channel by binding to yotiao. Dahimène and colleagues suggested that the N-terminus could also play a role in channel trafficking, as they observed an increased ER retention of channels with N-terminal mutations (Tyr111Cys, Leu114Pro and Pro117Leu), and suggested that a juxtamembranous region of the KCNQ1 N-terminus is critical for channel surface expression (Dahimène *et al*., 2006).

*Gating and Electrophysiological properties*

Assembly of 4 KCNQ1 pore-forming subunits forms the $K_v7.1$ channel, which is gated by voltage due to the presence of the S4 TM α-helix in each subunit. The S4 domain contains multiple basic residues that occur at regular intervals, which allows the channel to be responsive to changes in membrane potential. The KCNQ1 subunit contains fewer basic residues in its S4 domain compared with other members of the $K_v$ family, and as such its voltage dependency and gating characteristics are more flexible than other channels and can be highly modified by accessory subunits. The KCNQ1 channel is therefore able to fill many different roles physiologically (Panaghie & Abbott, 2007).

The homomeric $K_v7.1$ channel and the $I_{Ks}$ channel possess different electrophysiological properties due to the presence of the KCNE1 subunit in the $I_{Ks}$ channel. The Kv7.1 channel activates rapidly at negative voltages and subsequently inactivates at positive voltages. The inactivation displayed by the $K_v7.1$ channel was studied by Pusch *et al.* (1998) by dropping the membrane voltage in oocytes to a negative value after a depolarising step, which revealed a transient increase in current that is indicative of a relief from inactivation. This inactivation is absent when the KCNE1 β-subunit is co-expressed with the KCNQ1 α-subunit (Pusch *et al*., 1998; Tristani-Firouzi & Sanguinetti, 1998). In addition to preventing inactivation, co-assembly with the KCNE1 subunit causes a slowing of the $I_{Ks}$

channel's activation kinetics, and depolarises the voltage-dependence of activation (Barhanin *et al*., 1996; Sanguinetti *et al*., 1996). The single-channel conductance of $I_{Ks}$ is also larger than that of the $K_v$7.1 channel (Sesti & Goldstein, 1998). Supporting the role of KCNE1 in modification of the KCNQ1 channel's electrophysiological properties, mutations in the S4 domain (Trp248Arg, Glu261Lys and Arg243Cys) were found to abrogate channel function and reduce KCNE1 binding, in the case of Glu261Lys, or slow activation and shift the voltage-dependence of activation and inactivation, in the case of Trp248Arg and Arg243Cys (Franqueza *et al*., 1999). These mutations are highly conserved throughout the KCNQ1 family, suggesting critical importance in this role.

Unlike other $K_v$ channels, the voltage dependence of $K_v$7.1 is drastically altered when the channel associates with other β-subunits. Co-assembly with KCNE2 or KCNE3 leads to the resulting channels taking on the characteristics of a leak channel, where the channel no longer responds to changes in membrane potential and is instead constitutively active (Schroeder *et al.*, 2000; Tinel *et al*., 2000), and co-assembly with KCNE4 or KCNE5 leads to a drastic inhibition of the KCNQ1 current (Angelo *et al*., 2002; Grunnet *et al*., 2002).

### 1.5.2 Regulation of KCNQ1

*Regulation by KCNE1*

The most studied KCNE subunit with regards to KCNQ1 regulation is KCNE1, as together they form the cardiac $I_{Ks}$ channel. The KCNE1 subunit is a single TM domain of 129 amino acids in length, and was originally thought to comprise a $K^+$-conducting channel itself because KCNE1 was cloned after recording a slow-activating voltage-dependent $K^+$ current in Xenopus oocytes (Takumi *et al*., 1988). It was later found that this current was formed from the association of the KCNE1 subunit with KCNQ1 channels, which are endogenously expressed in oocytes (Barhanin *et al*., 1996; Sanguinetti *et al*., 1996). Although the effects of KCNE1 on the KCNQ1 current characteristics are known, the mechanism by which KCNE1 exerts these effects is still under speculation.

Because KCNQ1 activation kinetics are drastically altered by KCNE1 it has been postulated that KCNE1 binds to the channel between the voltage-sensing domain (VSD) and the PD, as here it would be in a prime position to control voltage sensing and gating (Barro-Soria *et al*., 2014).

To find out if KCNE1 alters KCNQ1 voltage-sensing, Nakajo & Kubo (2007) analysed the movement of S4 in the absence and presence of KCNE1, and found that KCNE1 stabilises the channel in the resting state and slows the transition of S4 to the activated conformation. It has been suggested that by interacting with the S4 domain, KCNE1 disrupts the positive charges in the C-terminal end of S4 that

stabilise the activated state of the channel, consequently destabilising the activated state (Wu *et al*., 2010). Contradicting these observations, Rocheleau & Kobertz (2008) found that the S4 domain reaches equilibrium quickly upon membrane depolarisation in the presence of KCNE1, and concluded that the KCNE1 cytoplasmic domain slows the opening of the activation gate.

Others have said that KCNE1 drastically slows the movement of the voltage sensor, as in the presence of KCNE1, KCNQ1 gating currents could not be resolved (Ruscic *et al*., 2013). In the same study, the gating and ionic currents of KCNQ1 channels coincided closely with each other, suggesting a tight coupling of voltage sensor movement and pore-opening. The gating and ionic currents were slowed to the same extent in the presence of KCNE1, and it was concluded that it is the KCNE1-dependent slowing of voltage sensor movement that creates the rate-limiting step in the activation process (Ruscic *et al*., 2013).

The slow activation of $I_{Ks}$ is not the only modification KCNE1 affords KCNQ1 that is crucial to its role in ventricular repolarisation; KCNE1 grants the channel multiple closed states that are near the channel's open state. This collection of closed states allows the channel to be in a state primed for rapid opening when required, particularly at higher heart rates in conditions of increased sympathetic tone (Silva & Rudy, 2005).

Not only is KCNE1 crucial to the formation of the $I_{Ks}$ channel, enabling the contribution of the $I_{Ks}$ channel in cardiac repolarisation, it is also required in the inner ear to facilitate $K^+$ recycling in the endolymph. The association of KCNE1 with KCNQ1 causes opening of the channel at membrane potentials positive of -40 mV, and abolishes channel inactivation. These properties of the channel allow its constitutive activity at the $V_m$ of the apical membrane of inner ear cells, which is typically between 0 mV and +10 mV, creating a sustained $K^+$ current (Hibino *et al*., 2009). Due to this crucial role in the inner ear, mutations in either KCNE1 or KCNQ1 can affect a mutation carrier's hearing as well as their cardiac function, causing the condition JLNS.

*Regulation by other KCNE subunits*

Elsewhere in the body, KCNQ1 associates with other members of the KCNE family. Whilst KCNE1 allows prolonged channel opening in depolarised cardiac cells due to the lack of channel inactivation, other KCNE subunits can confer constitutive activity at resting membrane potentials by modifying the state of the voltage-sensing domain. In contrast to other $K_v$ channels, KCNQ1 contains a lower net positive charge in its S4 domain (+3 compared to +7 in *Shaker* and +5 in other KCNQ channels) (Panaghie & Abbot, 2007). Mutation of KCNQ1 to neutralise one positive residue in the N-terminal

portion of the S4 domain (Arg231Ala) rendered the channel voltage-independent. Mutation of the KCNQ4 S4 domain to resemble that of the KCNQ1(Arg231Ala) S4 domain allowed channel opening even at hyperpolarised potentials, suggesting that the propensity to switch from a voltage-activated channel to a 'leak' (i.e. constitutively active) $K^+$ channel was determined by the S4 domain and not any properties of the KCNQ1 pore. This study also highlighted that the change in gating in response to voltage is not due to the gate gaining independence from the voltage sensor and becoming locked in the open state, but due to the voltage sensor becoming locked in the active configuration and communicating this to the channel gate (Panaghie & Abbot, 2007).

Association of KCNQ1 with KCNE2 occurs in polarised epithelial cells in, for example, the thyroid and gastric epithelium. Here, the constitutive activity of the KCNQ1-KCNE2 complex is important for its function. The KCNE2 subunit stabilises the S4 VSD in the active position, rendering the channel insensitive to changes in membrane potential and consequently facilitating a $K^+$ current at hyperpolarised potentials (Tinel *et al*., 2000). KCNQ1-KCNE2 channels have reduced current amplitude compared to the homomeric KCNQ1 channel, which is thought to be a result of the interactions between KCNQ1 and the KCNE2 N-terminus (Li *et al*, 2014).

An additional way in which the KCNE2 subunit regulates the KCNQ1 channel is by altering the channel's sensitivity and reaction to extracellular pH. Homomeric KCNQ1 channels are inhibited by extracellular protons, and the $I_{Ks}$ channel is also inhibited, but is less sensitive. When KCNE2 is complexed with KCNQ1, the channel has the complete opposite response; KCNQ1-KCNE2 currents are augmented by increased extracellular protons, hence the channel's importance in the gastric epithelium (Heitzmann *et al*., 2007).

When KCNQ1 is in complex with KCNE3, it behaves as a constitutively active channel like the KCNQ1-KCNE2 complex, but the KCNQ1-KCNE3 channel is not sensitive to extracellular pH. KCNE3 is also thought to exert its effect on the KCNQ1 channel through stabilisation of the S4 domain in the active configuration, even at resting membrane potentials (Nakajo & Kubo, 2007).

These complexes are found in intestinal and airway epithelium. In the intestines, the KCNQ1-KCNE3 channel is found in the basolateral membrane of colonic crypt cells (Schroeder *et al*., 2000), and tracheal epithelial cells (Preston *et al*., 2010). Their function in these cells is thought to involve the recycling of $K^+$ to stimulate the secretion of $Cl^-$ ions by increasing the electrochemical driving force for $Cl^-$ across the apical membrane (Preston *et al*., 2010).

Expression of KCNE4 with KCNQ1 was found to cause almost complete inhibition of the KCNQ1 current at all membrane potentials tested. KCNE4 mRNA is found predominantly in embryo and

uterus, where KCNQ1 is also found (Grunnet *et al*., 2002). KCNE4 contains a tetraleucine motif in the juxtamembranous region of the C-terminus that confers CaM binding in a $Ca^{2+}$-dependent manner. Mutation of this binding region or $Ca^{2+}$ chelation reduced the ability of KCNE4 to inhibit KCNQ1 Ciampa *et al*., 2011). Further supporting a role in the regulation of KCNQ1, the KCNE4 subunit was not found to regulate the KCNQ2–5 or hERG channels (Grunnet *et al*., 2002).

KCNE5 also imposes an inhibitory effect on the KCNQ1 subunit; when KCNE5 associates with KCNQ1, the time- and voltage-dependent mechanisms are altered drastically, and there is approximately a 140 mV depolarising shift in the voltage-dependence of activation curve. In addition, the KCNQ1-KCNE5 complex activates slowly and deactivates rapidly, meaning the channel is largely inactive at physiological potentials. KCNE5 is expressed in cardiac myocytes, and it has been hypothesised that this accessory subunit, along with KCNE1, may regulate the contribution of the $I_{Ks}$ current to cardiac repolarisation (Angelo *et al*., 2002).

*Regulation by phosphoinositides*

It is well documented that the $I_{Ks}$ channel requires the presence of $PIP_2$ to function, and it is thought that it stabilises the open state of the channel (Loussouarn *et al*., 2003). Other KCNQ channels also require $PIP_2$ for voltage-dependent activation (Suh & Hille, 2002; Zhang *et al*., 2003). The M channel, consisting of the KCNQ2 and KCNQ3 subunits, requires $PIP_2$ to open, and as a result of the dependency on $PIP_2$ for function it was concluded that $PIP_2$ depletion is the mechanism used by the muscarinic acetylcholine (M1) receptor to induce M channel closure and resulting inhibition of the M current (Li, *et al*., 2005; Zhang *et al*., 2003). This is supported by Suh *et al*. (2006), who observed M current inhibition when using an inducible phosphatase to directly deplete $PIP_2$ from the PM.

The region of basic residues thought to be responsible for $PIP_2$ binding is conserved throughout the KCNQ family, but not in other channels where $PIP_2$ is not required for function. Despite $PIP_2$ binding being crucial for channel opening, the rate-limiting step of the whole activation process is voltage-sensor movement, which does not require $PIP_2$ (Zaydman *et al.*, 2013).

A $PIP_2$ binding region in the proximal C-terminus of the channel was identified by Thomas *et al*., (2011), the most important residues in this region being Lys358 and Arg360. Even though $PIP_2$ bound to the channel with the highest affinity, other phosphoinositide (PI) species could also bind. It is possible that other membrane phospholipids can assume the role of $PIP_2$ if it is in low abundance, or perhaps other phosphoinositides bind to the channel at different stages between its production and degradation.

The two CaM-binding domains in the C-terminus of the KCNQ1 channel partially overlap with a PI binding region. In a competition assay, $PIP_2$ and phosphatidylinositol-3,4,5-trisphosphate ($PIP_3$) were both able to displace CaM binding from one of the CaM-binding domains, and $PIP_3$ was able to reduce CaM binding from the other. $PIP_3$ was the most potent at disrupting CaM binding to these two regions, and may play a role in regulating the binding of CaM to the channel (Kwon *et al*., 2008).

Phosphatidylinositol-3,5-bisphosphate ($PI(3,5)P_2$) is required for the RAB11-dependent cell-surface delivery of the channel after SNS activation (Seebohm *et al*., 2007). Release of cortisol during SNS activation causes activation of serum- and glucocorticoid-inducible kinase 1 (SGK1), a serine/threonine kinase that promotes surface delivery of a number of ion channels (Debonneville *et al*., 2001). SGK1 has a dual effect with regards to KCNQ1 surface delivery: SGK1 inactivates Nedd4-2, a ubiquitin ligase that ubiquitinates the channel and prepares it for degradation, and activates PIKfyve, a phosphatidylinositol-3-phosphate (PI3P) 5-kinase that converts PI3P to $PI(3,5)P_2$.

## 1.6 Phosphoinositides

### 1.6.1 Phosphoinositides and their synthesis

PIs are a small family of acidic phospholipids that contains 8 members, each differing in the phosphorylation of their *myo*-inositol ring. These phospholipids are present on the cytosolic side of cellular membranes and are involved in almost all biological processes (Di Paolo & De Camilli, 2006). The simplest PI in structure, phosphatidylinositol (PtdIns), contains a phosphodiester linkage with diacylglycerol, and forms the backbone of all PIs (Balla, 2013). From this core PI structure, each of the 7 other members of the PI family can be produced (figure 10). The nomenclature of the *myo*-inositol ring was introduced by Bernard William Agranoff in 1978, who described the structure as similar to the shape of a turtle, where the body represents the ring, and the legs, tail and head represent the 6 OH groups (figure 9). Since the OH at position 1 is occupied by the phosphodiester linkage, 5 OH groups remain free for phosphorylation purposes, although physiologically only positions 3, 4 and 5 are phosphorylated (figure 9).

The journey of PI species begins at the ER, where PtdIns is synthesised. From cytidine-diphosphate diacylglycerol (DAG) and *myo*-inositol, PtdIns is synthesised by a PtdIns synthase enzyme, after which PtdIns is transported to other cellular compartments via PtdIns-transfer proteins (PITPs) or by vesicles. Transport of PtdIns to other cellular locations is required for the synthesis of polyphosphoinositides (PPIs) because PI kinases, which catalyse the transformation of PtdIns into each of the 7 PIs by phosphorylation, are localised to the specific cellular compartments relevant to

the PI that they produce. Each of the phosphorylated PI species, or PPIs, concentrates at a particular cellular membrane. For example, $PIP_2$ is predominantly localised to the PM, phosphatidylinositol-4-phosphate (PI4P) to the Golgi and PI3P to the early endosomes.

Once PPIs are produced in their respective locations within a cell, their functions are not static – phosphorylation and dephosphorylation by PPI kinases and PPI phosphatases, respectively, allows PPIs to transfer between different phosphorylated states, enabling their involvement in many cellular processes. This can occur during specific signalling events, for example. One demonstration of this is the phosphorylation of $PIP_2$ to $PIP_3$ during growth factor signalling – despite $PIP_2$ being an important signalling molecule in its own right, it is also the substrate for $PIP_3$ synthesis.

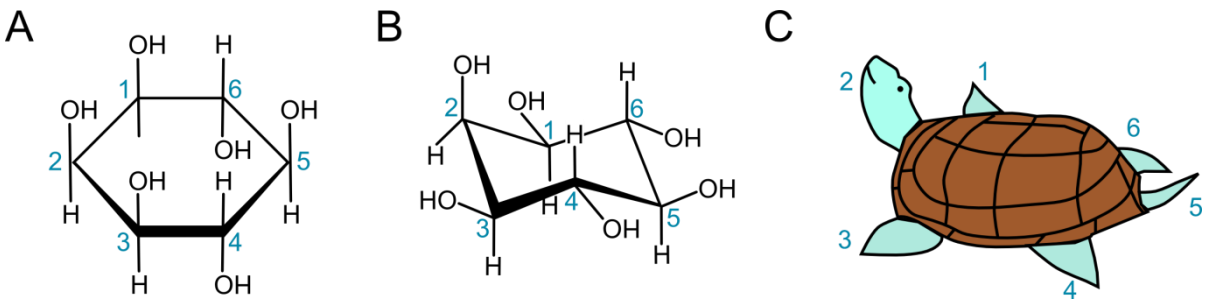


**Figure 9. Nomenclature of the phosphoinositide *myo*-inositol head group**. **A** – the *myo*-inositol head group in the Haworth projection, and **B** – in a more accurate representation of the 'chair' structure, both showing the nomenclature of the phosphorylation sites in the ring. **C** – A schematic interpretation of Agranoff's turtle. Agranoff noted that the structure of the ring (ignoring the hydrogen atoms) superficially resembles a turtle. The numbering begins on the turtle's right flipper and proceeds anticlockwise.

### 1.6.2 PI- and PIP-kinases

Kinase enzymes that add phosphate groups onto PtdIns are termed PI-kinases, and those that phosphorylate PPIs are known as PIP-kinases. This terminology is used to describe the primary function of the kinase or the position of the inositol ring that the enzyme phosphorylates, but some may also be able to phosphorylate both PtdIns and PPIs.

*4-kinases*

There are 4 mammalian PtdIns 4-kinases (PI4Ks): PI4KIIα, PI4KIIβ, PI4KIIIα and PI4KIIIβ. The PI4KIII enzymes are in part characterised by their sensitivity to wortmannin (Nakanishi *et al.*, 1995), whilst the PI4KII enzymes are insensitive. The localisation and function of these enzymes has been better

characterised using yeast PI4Ks, but this does not always align with what is currently known about eukaryotic PI4K enzymes, and not all eukaryotic enzymes have corresponding yeast homologues.

PI4KIIα and PI4KIIβ are both membrane-bound proteins, and were found to be expressed at the trans-Golgi network (TGN) and endosomes (Balla *et al*., 2002; Wang *et al*., 2003), where they are involved in the regulation of intracellular trafficking events (Jovic *et al*, 2012). Wei and colleagues found that PI4KII enzymes may have slightly overlapping functions, but PI4KIIβ is activated by recruitment from the cytosol to the PM where it then stimulates $PIP_2$ synthesis (Wei *et al*, 2002).

PI4KIIIα plays a major role in the synthesis of $PIP_2$ at the PM as it is the primary kinase that produces the precursor pool of PI4P (Balla *et al*., 2005; Bojjireddy *et al.,* 2014), despite originally thought to only reside in the Golgi membranes (Nakagawa *et al*., 1996).

PI4KIIIβ, the yeast homologue of which was the first PI-kinase to be cloned (Flanagan & Thorner, 1992), mainly resides at the Golgi in an ADP-ribosylation factor (ARF)1-dependent manner (Godi *et al*., 1999). This enzyme has also been found at the PM and nucleus, although the functional significance of this is unknown (De Graaf *et al*., 2002).

*3-Kinases*

*In vivo*, the class III PtdIns 3-kinase (PI3KCIII) is the dominant subtype that produces PtdIns 3-P (PI3P) from PtdIns. The yeast homologue of this enzyme, Vps34p, is the sole source of PI3P in yeast (Backer, 2008). Among the 3-kinases, PI3KCIII is unique in that its only substrate is PtdIns, and it cannot phosphorylate PPIs. Like the yeast Vps34p, the mammalian PI3KCIII produces PI3P at endocytic membranes, which may bind a number of PI3P-binding domains such as the FYVE domain. Recruitment of such domains and the pathways downstream of this leads to processes including endocytic sorting and autophagy (Wirth *et al*., 2013). Despite the existence of other 3-kinase enzymes that also produce PI3P, it is thought that the activity of PI3KCIII produces the main source of PI3P that is involved in endocytic regulation (Ikonomov *et al*., 2015).

Class II PI3Ks (PI3KCII) can also produce PI3P, but are involved to a lesser extent than PI3KCIII. PI3KCII also phosphorylates PI3P to $PI(3,5)P_2$ (Falasca &Maffucci, 2012). There are 3 types of PI3KCII enzymes: PI3KCIIα, PI3KCIIβ and PI3KCIIγ. PI3KCIIα is reported to be involved in endocytosis (Posor *et al*., 2013), cell growth and survival. This role is shared with PI3KCIIβ, which also regulates cell cycle progression and cell migration, whilst PI3KCIIγ is involved in the homing of leukemic cells (Falasca & Maffucci, 2012). PI3KCII and PI3KCIII enzymes both produce PI3P, but this has been shown to occur in

different cellular compartments, suggesting that redundancy is not present in this system (Falasca & Maffucci, 2012).

The class I PI3Ks (PI3KCI) consist of two subunits – a catalytic subunit that occurs in 4 isoforms: p110α, p110β, p110γ and p110δ, and a regulatory subunit. P110α, β and δ mainly associate with the regulatory subunit p85, whilst p110γ associates with the regulatory subunit p101 (Zhao & Vogt, 2008). PI3KCIs are the only PI3K that can convert $PIP_2$ to $PIP_3$, and due to the important role of this PI in cell growth and survival, dysregulated PI3KCI is often involved in oncogenesis.

These various PI and PIP 3-kinases can be characterised based on their sensitivity to wortmannin (WTM) and LY294002. In contrast to the WTM-sensitive PI4Ks, which are inhibited by micromolar concentration of WTM, PI3Ks are inhibited at nanomolar concentrations. However, Domin *et al*. (1997) found that the PI3KCIIα isoform is less sensitive to WTM inhibition than other isoforms, with a half-maximal inhibitory concentration (IC50) value of 420 nM compared to, for example, the IC50 of 5 nM for p110α and 1.6 nM for PI3KCIIβ (Arcaro *et al*., 1998).

*5-kinases*

The 5-kinase known as the type I PIP-kinase (type I PIPK, or PIPKI) phosphorylates PI4P at the D-5 position on the inositol ring to produce $PIP_2$ (Rameh *et al*., 1997). This represents the second and more-common pathway of $PIP_2$ synthesis after phosphorylation of PtdIns-5-P (PI5P) at the D-4 position by type II PIP kinases. There is debate as to the location of $PIP_2$ synthesis in the cell, but evidence exists to support synthesis at the Golgi. Jones *et al*. (2000) showed that PIPKIs directly interacts with ARF1, which is localised to the Golgi, and the subsequent activation of the kinase leads to production of $PIP_2$ at the Golgi. Supporting this is a study that used the PH domain from phospholipase C (PLC) δ (PLCδ-PH), which binds to $PIP_2$ and hence localises to the PM in a resting cell. Upon depletion of $PIP_2$ from the PM, PLCδ-PH translocated to the cytoplasm and was then observed at the Golgi where *de novo* $PIP_2$ synthesis is thought to occur. PLCδ-PH then translocated to the PM over time as the $PIP_2$ concentration at this membrane returned to basal levels (Várnai & Balla, 1998).

In addition to $PIP_2$ synthesis at the Golgi, $PIP_2$ synthesis at the PM is suggested due to the presence of PI4P. Although PI4P may have a regulatory role in its own right, it can be synthesised at the PM and Golgi by different PI 4-K enzymes, and thus there is the assumption that it resides in the PM as the precursor for $PIP_2$ synthesis at this site (Hammond *et al*., 2009; Sarkes & Rameh, 2010).

There are 3 PIPKI isoforms: PIPKIα, PIPKIβ and PIPKIγ (Ishihara *et al*., 1996; Ishihara *et al.,* 1998). There is evidence to suggest that the PIPKI isoforms are responsible for the production of distinct pools of $PIP_2$ in the cell that may be functionally specialised (Sasaki *et al*., 2006). There are numerous splice variants of each PIPKI isoform (3 α, 4 β and 6 γ), which are localised to different parts of a cell to enable the production of $PIP_2$ at various sites in response to different stimuli, including the nucleus, PM and Golgi (Choi *et al*., 2015).

Another crucial 5-kinase is PIKfyve, which phosphorylates PtdIns to PI5P, and PI3P to $PI(3,5)P_2$. This enzyme is conserved across most eukaryotes, and the yeast homologue is named Fab1 (McCartney *et al*., 2014). The activity of this kinase has been shown to be required for successful trafficking of a number of receptors (Hayashi *et al*., 2015; McCartney *et al*., 2014), and has been found localised to the early endosomes where it regulates retrograde trafficking from the endosomes to the TGN by producing $PI(3,5)P_2$ (Rutherford *et al*., 2006).

**1.6.3 Phosphoinositide-binding domains**

One of the most important properties of PIs is their ability to bind a vast range of proteins, which can be critical to their regulation. Proteins regulated by PIs contain PI binding domains, which usually facilitate binding to the PI in question in a 1:1 stoichiometry. The discovery of the pleckstrin homology (PH) domain, which binds to $PIP_2$ (and inositol trisphosphate ($IP_3$)) (Garcia *et al*., 1995), provided a breakthrough in the knowledge of how PIs regulate a wide range of cellular processes. Since then, many other binding domains have been discovered, each with differing preference for the phosphorylation state of the inositol head group (table 3).

Hammond and Balla (2015) detail a number of principles underlying the regulation of proteins by PI binding:

- High-affinity binding recruits proteins to a particular cellular membrane. However, not all binding domains hold such high affinity, and the binding to a particular PI may not be strong enough to dictate protein localisation (Yu *et al.,* 2004).

- PI binding occurs alongside a second interaction, which together control membrane localisation. This phenomenon is termed 'coincidence detection', and is demonstrated by the localisation of the four phosphate adapter protein (FAPP) 1 domain to the TGN through binding to PI4P and ARF1 (Godi *et al*., 2004; Liu *et al*., 2014).

- PI binding contributes to the membrane localisation of a protein, but this time in a less specific manner. Many proteins harbour polybasic domains that can interact with anionic lipids, namely $PIP_2$ and PI4P in the PM (Hammond *et al*., 2012), where any of the lipids can fulfil the requirement for membrane-targeting.

- PIs are not only involved in protein targeting, and binding of PIs can alternatively result in activation of the protein in question. This is demonstrated in the case of the $PIP_3$-dependent activation of the ARF GTPase activating protein (GAP), ARAP1 (Campa *et al*., 2009).

- The hydrophilic head and hydrophobic acyl tail groups of the PI species may bind to lipid-transfer proteins in order to facilitate movement of these lipids between cellular membranes (Mesmin *et al*., 2013).

All of these principles allow the regulation of PI-binding proteins in time and space.

The known PI-binding proteins differ in their specificity for particular PIs, and, as a consequence, vary in their value in experiments that have a need to exploit the compartmentalised nature of PI localisation. For example, PLCδ1-PH was first thought to bind with high specificity to $PIP_2$, but it was later found that this domain also binds with high-affinity to $IP_3$, one of 2 products of $PIP_2$ hydrolysis. This hinders the quantification of $PIP_2$ loss from the PM due to hydrolysis because as $PIP_2$ levels decrease, $IP_3$ levels increase, altering the ratio of PLCδ1-PH bound to each. Other PI-binding domains have high specificity, such as SidM, a protein found in *Legionella pneumophila.* SidM binds with high affinity to PI4P, and has been used as an effective biosensor due to its ability to detect lower levels of this lipid than other known PI4P-binding proteins (Schoebel *et al*., 2010). Table 3 contains a number of currently known PI-binding proteins that are used experimentally for PI detection and protein targeting. Not all are fully characterised, and for some it is unknown if binding to its PI binding partner is sufficient for membrane localisation.

| PI species | Protein binding domain | Cellular localisation | Is PI binding specific? | Is PI sufficient for localisation? |
|---|---|---|---|---|
| PI3P | FYVE-Hrsx2 | Early endosomes | Yes | Unknown |
| | PX-p40phox | Early endosomes | Yes | Unknown |
| PI4P | PH-OSBP | Golgi/PM | Also binds $PIP_2$ | ARF1-dependent |
| | PH-FAPP1 | Golgi | Also binds $PIP_2$ | ARF1-dependent |
| | P4M-SidM | Golgi/PM/Late endosomes | Yes | Yes |
| PI5P | PHD-Ing2x3 | Nucleus/PM | Also binds PI3P | Yes at PM, unknown in nucleus |
| PI(3,4)P2 | TAPP1-PH-CT | PM | Yes | Yes |
| PI(3,5)P2 | ML1-Nx2 | Late endosomes | Yes | Unknown |
| PI(4,5)P2 ($PIP_2$) | PH-PLCδ1 | PM | Also binds $IP_3$ | Yes |
| | Tubby | PM | Also binds PI(3,4)P2 and $PIP_3$ | Yes |
| PI(3,4,5)P3 ($PIP_3$) | PH-Akt | PM | Also binds $IP_4$ and PI(3,4)P2 | Unknown |
| | PH-Btk | PM | Also binds $IP_4$ | Unknown |

**Table 3. The specificity and localisation of PI-binding domains.** PI-Binding domains used experimentally for determining PI localisation and for protein targeting (adapted from Hammond & Balla, 2015).

### 1.6.4 Phosphoinositides and the secretory pathway

From the synthesis of a protein to the delivery of that protein to its final destination within a cell, the protein encounters a number of different membrane-bound organelles, each with a unique PI signature. Proteins involved in trafficking include soluble *N*-ethylmaleimide-sensitive factor attachment protein receptor (SNARE) proteins, which mediate fusion of membrane bilayers, coat proteins of transport vesicles and motor proteins that move cargo along the cytoskeleton. It is the disparity in PI make-up of secretory pathway membranes that allows the specific recruitment of these trafficking effector proteins via their PI-binding domains to their respective sites of action (Behnia & Munro, 2005).

*Endoplasmic reticulum*

Despite being the most abundant PI, the location and mechanism of mobility of PtdIns is not fully understood. PtdIns is synthesised in the ER, and evidence now suggests that PtdIns is transported to various membranes in highly mobile membrane compartments derived from the ER, although the precise mechanisms are yet to be determined (Kim *et al*., 2011).

Despite being synthesised in the ER, PtdIns has no role in recruiting proteins to the ER to drive membrane trafficking. Surprisingly, PI3P, which has always been thought to be concentrated at the early endosomes, was found in relatively large concentrations in the ER/Golgi using subcellular fractionation techniques (Sarkes *et al*., 2010). Supporting the presence of PI3P in the ER, Amoasii and colleagues identified a PI-phosphatase involved in regulating PI3P in the SR of skeletal muscle (Amoasii *et al*., 2013). This pool of PI3P may be involved in membrane trafficking, as it was found that UV radiation resistance-associated gene protein (UVRAG), a PI-binding protein, depends on PI3P for ER-localisation. UVRAG is recruited to the ER where it is involved in a complex that docks COPI vesicles (from Golgi–ER retrograde trafficking) (He *et al*., 2013).

*Golgi Apparatus*

PI4P is the classical PI associated with the Golgi, where it recruits many proteins involved in the formation of vesicles, and the PH-domains of proteins that are involved in delivering lipids and proteins to the Golgi (Wang *et al*., 2003).

In yeast, the PI4K enzymes Pik1 and STT4 are crucial to yeast viability, and deletion of either enzyme is lethal. Pik1 and STT4 both phosphorylate PI to PI4P, and mutation of these enzymes results in a

lower abundance of PI4P at the Golgi and consequent disturbance of Golgi functions including trafficking, actin cytoskeleton organization and secretion (Audhya *et al*., 2000).

Despite PI4P playing important roles in Golgi function, 3-phosphorylated PIs also appear to serve functions at the TGN. Jones & Howell (1997) observed that $p62^{cplx}$, the regulatory subunit of a PI3K, was required for the transport of polymeric IgA-receptor-containing vesicles from the TGN (Jones & Howell, 1997). Supporting the involvement of 3-phosphorylated PIs in protein trafficking from the Golgi, a class II PI3K, PI3KC2α, was found by Domin & colleagues to be localised to the TGN in several mammalian cell types (Domin *et al*., 2000). One role of 3-phosphorylated PIs at the Golgi could be to modulate the activity of ARFs, for example the ARF GAP known as ARAP1 is activated by binding $PIP_3$ (Campa *et al*., 2009).

*Plasma Membrane*

The most abundant PI at the PM is $PIP_2$, amounting to approximately 1–2 % of total PM lipids. In addition to the many roles $PIP_2$ plays in ion channel regulation, cell motility and polarity, $PIP_2$ also plays a part in endocytosis and fusion/exocytosis events.

Exocytosis is the process by which an intracellular vesicle fuses with the PM of a cell, and in the process incorporates its membrane with that of the PM, releasing any vesicular contents from the cell. Constitutive exocytosis of vesicles trafficking directly from the Golgi, or via endosomal intermediates, occurs in a $Ca^{2+}$-independent manner, while the regulated exocytosis of 'dense-core' vesicles in neuronal/exocrine/endocrine cells occurs upon elevation of intracellular $Ca^{2+}$ levels (Martin, 2009). The latter requires $PIP_2$ for vesicle priming, which is a prerequisite to regulated exocytosis and was discovered through the ATP requirement and PITP involvement during this process (Eberhard *et al*., 1990; Hay & Martin, 1993).

There is evidence to suggest that $PIP_2$ may form clusters in the PM, enabling functional 'hotspots' to arise. These hotspots have been shown to concentrate at sites of $Ca^{2+}$-dependent exocytosis, or release sites (Koch & Holt., 2012). Although the mechanism these $PIP_2$-rich domains use to maintain the $PIP_2$ concentration gradient is largely unknown, it has been suggested that the binding of proteins via their PI-binding domains could sequester $PIP_2$ and concentrate the lipid at the sites of function. For example, at the site of endocytosis, the large GTPase dynamin binds $PIP_2$ through its PH domain, and it was found that this led to a clustering of $PIP_2$ at clathrin-coated pits (CCPs). Also, the adaptor protein (AP)-2 complex binds to multiple PI5Ks, which phosphorylate PI4P at the 5-position to form $PIP_2$ (Posor *et al*., 2015).

It is evident that $PIP_2$ is involved in both exocytosis and endocytosis, and Koch & Holt (2012) argue that in the case of regulated exocytosis, $PIP_2$ acts as the central 'hub' to recruit and coordinate proteins involved in both processes, possibly using synaptotagmin as an effector protein.

Endocytosis is a mechanism used by the cell to internalise membrane proteins and engulf extracellular particles. The resulting intracellular vesicle is initially composed of the same constituents of the PM (where it originates from), but its identity changes as it travels through the endocytic pathway.

Clathrin-mediated endocytosis (CME) is the most-studied method of endocytosis in eukaryotic cells, and the local $PIP_2$ concentration is crucial to its different stages, from initiation to maturation and budding. Clathrin, which was first identified and isolated by Barbara Pearse (1975), forms a three-legged triskelion structure composed of 3 clathrin light chains and 3 clathrin heavy chains (the original component identified by Pearse). Clathrin triskelia form a lattice of pentagons and hexagons around the outer surface of the forming vesicle, which is thought to give the vesicle its spherical structure. $PIP_2$ is known to be involved in clathrin-coated vesicle (CCV) formation (Jost *et al*., 1998), and deletion of a PI 5-phosphatase, synaptojanin 1 (which dephosphorylates $PIP_2$), was found to increase CCV formation at synaptic terminals (Cremona *et al*, 1999). In addition, acute depletion of $PIP_2$ resulted in a loss of CCPs and a dissociation of CME-associated adapter proteins (Zoncu *et al*., 2007). Supporting this, Sun and colleagues suggested that a dynamic modulation of $PIP_2$ is required for the complete CME process. They observed that the presence of $PIP_2$ is required for CCV formation, but for the process to culminate in CCV budding, turnover (and hence loss) of $PIP_2$ is required (Sun *et al*., 2007).

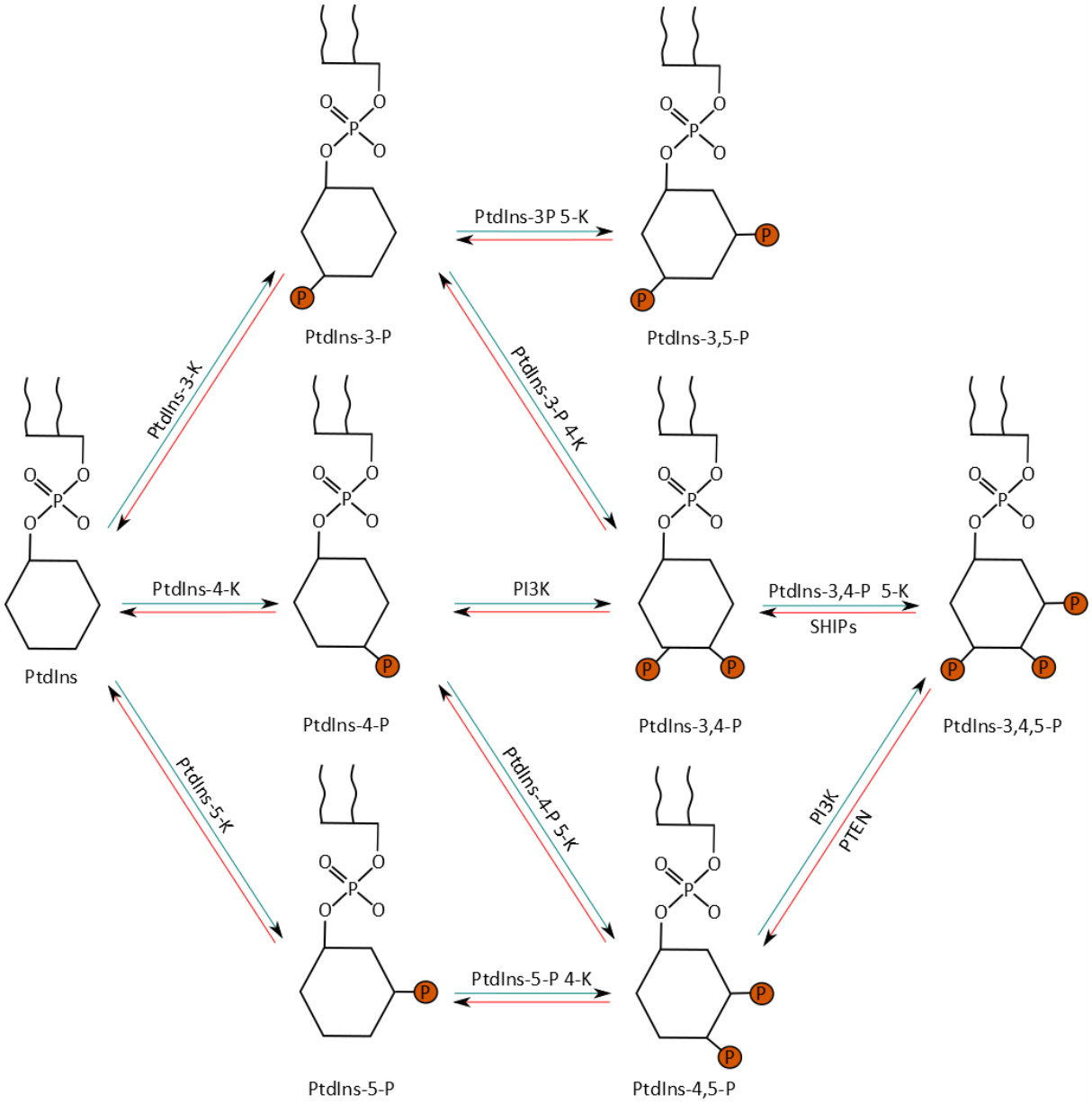


**Figure 10. The synthesis of phosphoinositides from PtdIns.** PtdIns is the phosphoinositide (PI) that each of the 7 phosphorylated PIs originate from. PtdIns can be phosphorylated on the 3, 4 or 5 position, and the products of this phosphorylation can further be phosphorylated to form PIs phosphorylated on the 3 and 5, 3 and 4 or 4 and 5 position. PtdIns-3,4-P and PtdIns-4,5-P can also be phosphorylated again on the 5 or 3 position, respectively, to form the only PI that is phosphorylated at 3 positions. PI kinases perform the phosphorylation step, whilst PI phosphatases remove the phosphate groups from the PIs.

## 1.7 Phosphotidylinositol-4,5-bisphosphate

$PIP_2$ is a minor constituent of the PM PI pool in mammalian cells, contributing just 1–2% of the total acidic lipids (Suh & Hille, 2008). $PIP_2$ can be synthesised by the sequential phosphorylation of PtdIns at the D-4 and -5 positions, which can be via PI4P or PI5P. However, as discussed in section 1.6.2, the

major pool of $PIP_2$ is produced by the action of type I PIP-kinases on PI4P. $PIP_2$ can also be produced by dephosphorylation of $PIP_3$ by the phosphatase named phosphatase and tensin homologue (PTEN) (Lemmon, 2008).

### 1.7.1 Phosphatidylinositol-3,4,5-trisphoshate synthesis

$PIP_2$ can be further phosphorylated at the D-3 position to produce $PIP_3$, which occurs as a result of PIP 3-kinase activation resulting from either GPCR or receptor tyrosine kinase (RTK) activation. One of the key targets of $PIP_3$ synthesis is the serine/threonine kinase Akt, also known as protein kinase B.

Akt and its upstream activator, phosphoinositide-dependent kinase (PDK) 1 are recruited to $PIP_3$ at the PM via their PH domains. Once in close proximity PDK1 activates Akt at Thr308, which partially activates Akt. Full activation of Akt is achieved by further phosphorylation by mTORC2 at Ser473. The activation of this pathway is regulated by PTEN, which dephosphorylates $PIP_3$, and by protein phosphatase 2a, which dephosphorylates Akt.

Akt has many downstream effectors that are involved in cell growth, proliferation and survival. Dysregulation of this pathway, for example by mutation of PTEN, upregulation of PI 3-kinase activity or gain-of-function mutations in Akt, has been implicated in diseases including cancer, cardiovascular disease and some neurological diseases.

### 1.7.2 Hydrolysis by G protein-coupled receptors

$PIP_2$ levels are not only controlled by the action of PIP-kinases and PIP-phosphatases. Activation of Gq-GPCRs and RTKs that lead to the activation of different PLC isoforms also cause loss of $PIP_2$ from the PM by hydrolysis. Hydrolysis of $PIP_2$ by PLC results in the production of $IP_3$ and DAG, as this enzyme hydrolyses $PIP_2$ at the phosphodiester bond, releasing the *myo*-inositol head with 3 phosphates attached (at the D-1, 4 and 5 positions) and the 1,2-diacylglycerol tail (figure 12). $IP_3$ is released into the cytoplasm, while DAG remains in the membrane. The cellular effects of $PIP_2$ hydrolysis diverge down the two different pathways: the $IP_3$ pathway and the DAG pathway.

In the $IP_3$ pathway, $IP_3$ binds to its name-sake receptor (which is a ligand-gated $Ca^{2+}$ channel) at the ER, resulting in the release of $Ca^{2+}$ from the intracellular stores. $Ca^{2+}$ is tightly controlled within the cytoplasm due to the activity of $Ca^{2+}$ pumps that actively transport $Ca^{2+}$ out of the cell or into the ER. When $Ca^{2+}$ is released from the intracellular stores, the $Ca^{2+}$ concentration in the cell increases

dramatically, causing activation of $Ca^{2+}$-dependent proteins and pathways. One such protein is CaM, a calcium-binding protein that is a major transducer of calcium-dependent signalling in eukaryotic cells.

The DAG pathway involves the direct activation of protein kinase C family members, which are involved in growth and differentiation, by DAG. Some of these enzymes also require $Ca^{2+}$ for activation, and thus depend on both pathways resulting from $PIP_2$ hydrolysis. DAG is also an intermediate in the synthesis of phosphatidic acid and 2-arachidonylglycerol, both of which act as second messengers.

In addition to the release of $IP_3$ and DAG, the loss of $PIP_2$ that occurs during this hydrolysis event also gives $PIP_2$ a significant role in cellular signalling. In T lymphocytes, for example, PLC activation through GPCR signalling is involved in cell migration, and it was found that $PIP_2$ depletion by PLC activation or activity of a PM-recruitable phosphatase caused the dissociation of ezrin/radixin/moesin (ERM) proteins from the PM due to dephosphorylation (Hao *et al*., 2009). ERM proteins link the cytoskeleton to the PM, so depletion or reduction of PM $PIP_2$ could be involved in controlling cytoskeletal arrangement and reorganisation.

Although this is a major role that $PIP_2$ plays in the PM, the loss of $PIP_2$ from the PM as a result of hydrolysis may also be a regulatory mechanism that the cell uses to control membrane-restricted proteins such as ion channels.

### 1.7.3 Regulation of ion channels and transporters

Evidence that $PIP_2$ could directly regulate the function of ion channels and transporters first came from Hilgemann and Ball (1996). In their study of the $Na^+/Ca^{2+}$ exchanger, they observed that ATP hydrolysis was required for activation and that this generated $PIP_2$ from PI, which could be mimicked by addition of exogenous $PIP_2$. They also found that the ATP-sensitive $K^+$ channel ($K_{ATP}$) was regulated by $PIP_2$ and, conversely, that the $Na^+$ channel and the $Na^+$ and $K^+$ pumps were insensitive. Hilgemann and Ball asserted that $PIP_2$ may be an important regulator of ion channels and transporters.

Since this discovery, $PIP_2$ has been found to be involved in the regulation of many different channels and transporters (Hilgemann *et al.*, 2001; Logothetis *et al.*, 2007; Suh & Hille, 2007). Although a full characterisation of $PIP_2$ regulation is not available for most channels, a large body of evidence has been collected for many that is highly supportive of a $PIP_2$-dependent mechanism of regulation. Within this group of $PIP_2$-regulated channels (and transporters), there exists scales of $PIP_2$ selectivity

and $PIP_2$ sensitivity. $PIP_2$ selectivity describes a scale where at the most selective end a channel will only bind $PIP_2$, and at the opposite end of the scale a channel will bind a broad range of PIs. $PIP_2$ sensitivity relates to a channel's affinity for $PIP_2$, where a low-affinity channel will be more sensitive to changing $PIP_2$ levels than a channel with a high $PIP_2$ affinity.

Two theories as to why some channels are regulated by $PIP_2$ have been put forward. The first suggests that due to the unique PI signature of different membranes, the maturation and activation of channels can be regulated throughout the secretory pathway. When a channel finally reaches the PM, the high relative concentration of $PIP_2$ allows the regulation of activation (Hilgemann *et al*., 2001). On the other hand, a second theory suggests that the depletion or reduction of $PIP_2$ from the PM that can occur in some signalling events is the mechanism of regulation. $PIP_2$ depletion by hydrolysis occurs as a result of Gq-GPCRs/RTK activation, and could be a mechanism of rapid regulation for particularly $PIP_2$-sensitive channels.

*Regulation of Kir channels by $PIP_2$*

One of the most-studied groups of channels with regards to $PIP_2$ regulation is the Kir channels. After the observation that the $K_{ATP}$ channel was sensitive to $PIP_2$ levels it was suggested that $PIP_2$ may bind to positive charges in the cytoplasmic domains of the Kir6.2 subunit and stabilise the open state of the channel as a result, as well as antagonising the inhibitory effect of ATP (Fan & Makielski, 1997; Shyng & Nichols, 1998).

More recently, it has been shown that as well as regulating the activity of $K_{ATP}$ channels through interaction with Kir6.2, $PIP_2$ sequesters Syntaxin-1A (part of the SNARE complex involved in membrane fusion and secretion) and limits its availability for binding to sulphonylurea receptor (SUR) subunits (the auxiliary subunit of the $K_{ATP}$ channel). In this way, $PIP_2$ can regulate $K_{ATP}$ channels in islet β-cells in a dual and highly-controlled manner (Liang *et al*., 2014).

Kir channels exhibit differing affinities for $PIP_2$ as well as other PIs. For example, the GIRK1/4 channel, which has a weak interaction with $PIP_2$, is also activated with similar efficacy by $PI(3,4)P_2$, $PI(3,5)P_2$ and $PIP_3$ (Rohacs *et al*., 1999). Similarly, $K_{ATP}$ channels have a low selectivity for $PIP_2$, also binding $PI(3,4)P_2$ and $PIP_3$ (Krauter *et al*., 2001). Supporting this broad binding ability of the $K_{ATP}$ channel, the negatively charged long-chain (LC) acyl-coenzyme A (CoA) could also activate the channel. LC acyl-CoA did not, however, result in activation of other Kir channels tested, but could activate mutant Kir2.1 channels that exhibited a low PI specificity (Rohacs *et al*., 2003).

The positively charged residues Arg67, Lys118, Arg189, Arg218 and Arg312 in Kir2.1 are involved in $PIP_2$ binding. It has been suggested that polyamines regulate the $PIP_2$-dependent activation of Kir2.1 channels by acting as cofactors, and Xie *et al*. (2005) concluded that long polyamines such as spermine play a dual role in channel regulation by influencing the effects of $PIP_2$ and inducing inward rectification. Others have found that mutants with a lower $PIP_2$-binding affinity decreased single-channel open probability and led to the emergence of sublevels of activation (Lopes *et al*., 2002). Xie *et al*. (2008) show that the interaction of $PIP_2$ with a single Kir2.1 subunit is sufficient to shift the channel into an 'available' mode for opening with a high open probability, and that further binding of $PIP_2$ to other subunits increases this further.

*Regulation of the $I_{Ks}$ channel by $PIP_2$*

The role that $PIP_2$ plays in $I_{Ks}$ channel function is known, but the mechanism underlying this role is yet to be fully elucidated. Thomas and colleagues (2011) identified a cluster of basic residues in the proximal C terminus that are involved in the binding of PIs, including $PIP_2$. Using charge neutralisation scanning, 9 residues were also identified by another group, which may form 2 distinct binding pockets (Eckey *et al*., 2014). The residues identified here were in the C-terminal portion of S6 (Lys354, Arg360, and Lys362), the S2-S3 intracellular linker (Arg181, Lys183, Arg190 and Arg192) and the intracellular S4-S5 linker (Arg249 and Arg259). $PIP_2$ binding was only studied in the C terminus by Thomas and colleagues, but Zaydman *et al*. (2013) also found that Arg190 and Arg192 in the S2-S3 linker and Arg259 in the S4-S5 linker were involved in $PIP_2$ binding, and mutation of these residues mimicked the effect of $PIP_2$ depletion. Mutations introduced to neutralise other positive residues in the distal C-terminus of the channel (Arg234His, Arg539Trp and Arg555Cys) were also found to reduce the $I_{Ks}$ channel's $PIP_2$ binding affinity (Park *et al.*, 2005).

The crystal structure of the GIRK2 channel (Whorton & MacKinnon, 2011), and biochemical assays performed on the $K_{ATP}$ channel (Shyng *et al*., 2000) and the Kir3 channel family (Thomas *et al*., 2006) have previously revealed $PIP_2$ binding regions outside of the C terminus, and it is therefore possible that this is also the case for the $I_{Ks}$ channel. Eckey *et al*. (2014) postulate that binding of $PIP_2$ at the two separate binding regions that were identified leads to a stabilisation of the overall channel structure in both the open and closed conformation. This group also found that when $PIP_2$ was absent from the PM there was higher structural flexibility of the pore domain and a distortion of the channel in both conformations, but they concluded that the closed conformation may be structurally more stable in the absence of $PIP_2$.

The crystal structure of KCNQ1 has not been solved, but a model of the open and closed state has

been constructed by Smith *et al.* (2007). Using the rat $K_v1.2$ structure that had recently been determined (Long *et al*., 2005), the open state of the $I_{Ks}$ channel was modelled, and using the crystal structures of bacterial $K^+$ channels and the closed state model of $K_v1.2$ (Yarov-Yarovoy *et al*., 2006), the closed state of the $I_{Ks}$ channel was modelled.

Using this model, Zaydman *et al*. (2013) were able to identify a region of 16 basic residues located at the VSD-PD interface, which is thought to be involved in $PIP_2$ binding. Each of these 16 residues was neutralised and the effect on $I_{Ks}$ current density was investigated using two-electrode clamp. There were 8 different mutations in this region that caused a reduction in current density whilst retaining channel cell-surface expression and voltage-sensor movement, indicating that $PIP_2$ that binds at this site couples voltage-sensor movement to pore opening. This group also measured the time course of current rundown after patch excision, where PIs are gradually lost from the PM. Supporting the role of the 8 basic residues in $PIP_2$ binding was the observation that these mutant channels experienced an increased rate of rundown after patch excision compared to WT and gain-of-function mutants, suggesting a reduced affinity for $PIP_2$.

The dependence on $PIP_2$ for $I_{Ks}$ channel function has been demonstrated using a number of methods. For example, voltage-sensitive phosphatases that deplete $PIP_2$ from the PM (Hossain *et al*., 2008), chemically inducible dimerisation systems involving $PIP_2$-specific phosphatases that can be recruited to the PM (Kruse *et al*., 2012), and activation of receptors that leads to depletion of $PIP_2$ through activation of PLC (Matavel & Lopes, 2009).

Due to the sensitivity to $PIP_2$ depletion that the $I_{Ks}$ channel exhibits, it has become of great interest to establish whether this mechanism of regulation is used physiologically. A cell can manipulate the concentration of phosphoinositides in a given membrane through the activation of PI phosphatases, or at the PM by activation of $G_q$-coupled GPCRs. Activation of members of this family of GPCRs and the downstream hydrolysis and concomitant depletion of $PIP_2$ can occur in the cardiac myocyte. The rapid manipulation of PIs in the PM could be a mechanism to silence the channel during periods of $G_q$-coupled GPCR agonist signalling**.**

## 1.8 G protein-coupled receptors

### 1.8.1 GPCR overview

G protein-coupled receptors (GPCRs) are the largest group of cell-surface receptors in the eukaryotic kingdom. This diverse group of receptors act to convey extracellular messages to effectors inside the cell, and can react to light, lipids, sugars, peptides and proteins. This large family of receptors share a

common structure: one large polypeptide that forms 7 TM domains (hence these receptors are occasionally called the 7-TM receptors). The extracellular loops between TM segments commonly form part of the binding pocket for the receptor's specific ligand.

Humans possess more than 800 GPCRs, most of which can be grouped into 5 main families: Glutamate, rhodopsin, adhesion, frizzled/taste2 (frizzled) and secretin (Fredriksson *et al*., 2003). To be classed as a GPCR, receptors have to satisfy two criteria. The first is that the receptor should contain 7 stretches of sequence that are predicted to show a high degree of hydrophobicity, correlating to the 7 α-helices that span the membrane. The second criterion is that the receptor should be able to interact with a heterotrimeric G protein (Fredriksson *et al*., 2003). Despite these criteria, the homology between GPCR families is limited as they share little sequence similarity and contain different N-termini. Within GPCR families, for example the rhodopsin-like family (which contains approximately 700 members), there can be many subfamilies. The members of each subfamily share a higher degree of structural similarity than each large GPCR family. The differences between subfamilies, for example in the extracellular loop regions and side chains, confer the high diversity of ligand binding pockets and give rise to the vast number of physiological processes that GPCRs are involved in. Although many GPCRs are well characterised and their ligands are known, the ligands and function of a number of GPCRs are still unknown, and these are known as orphan receptors (Tang *et al*., 2012).

*Heterotrimeric G proteins*

G proteins (also known as guanine nucleotide-binding proteins) can bind guanosine triphosphate (GTP) and guanosine diphosphate (GDP), and act as molecular switches that regulate the 'on' and 'off' state of particular proteins in a myriad of signalling pathways. They can exist in a monomeric form, called small GTPases, which are homologous to the α-subunit of heterotrimeric G proteins. Heterotrimeric G proteins are comprised of 3 parts: α, β and γ subunits (Gα, Gβ and Gγ, respectively). Gα and Gγ are tethered to the membrane by lipid anchors, and it is Gα that is responsible for binding GTP/GDP.

When a GPCR is in the inactive state (i.e. in the absence of an activating ligand), Gα is bound to GDP, which allows Gα to also bind the β- and γ-subunits (in a dimer known as Gβγ) creating an inactive heterotrimeric complex. When the GPCR is in the active state (i.e. in a ligand-bound state) the dissociation of GDP from Gα is catalysed, allowing GTP to bind. A conformational change in the GPCR causes dissociation of Gα and Gβγ from the GPCR, and a conformational change in Gα after the exchange of GDP for GTP causes a decrease in affinity for Gβγ, leading to their dissociation (Lambert,

2008). The G protein subunits are still tethered to the membrane, but are no longer bound to the receptor. In this way, the subunits are able to move laterally in the membrane and interact with effector proteins in the signalling cascade, for example adenylyl cyclase (AC) or PLC (Purves *et al*., 2001). Gα possesses intrinsic GTPase activity that converts GTP to GDP, but this process is relatively slow. GAPs are responsible for the rapid deactivation of Gα by binding to this subunit and accelerating the intrinsic GTP hydrolysis. GAPs that catalyse GTP hydrolysis of heterotrimeric G proteins include PLC-β1 (Berstein *et al*., 1992) and p115 RhoGTPase nucleotide exchange factors (RhoGEF) (Kozasa *et al*., 1998), which catalyse the hydrolysis of GTP on their respective upstream activators. Members of the regulators of G protein signalling (RGS) family are also GAPs. They increase the rate of Gα-bound GTP hydrolysis, effectively inhibiting Gα and Gβγ signalling pathways. When Gα is once again bound to GDP it reverts back to the inactive state, re-associates with Gβγ and binds to the inactive GPCR.

*G-protein subunits*

The signal that is relayed by the activity of G-protein subunits can be stimulatory or inhibitory, and GPCRs associate with specific types of G-protein subunits in order to transmit the correct signal. There are 16 mammalian genes encoding 23 α-subunits that belong to one of 4 subfamilies: $G\alpha_s$, $G\alpha_i$, $G\alpha_{q/11}$ and $G\alpha_{12/13}$. The βγ dimer is made from one of 5 Gβ-subunits and one of 12 Gγ-subunits (Hurowitz *et al*., 2000; Zhang *et al*., 2015).

$G\alpha_s$ subunits, when in complex with GTP, are able to bind to all isoforms of AC (AC1–9). By binding to and activating AC, signalling through $Ga_s$ increases the intracellular concentration of cyclic adenosine monophosphate (cAMP) as AC converts ATP to cAMP and pyrophosphate. $G_i$ subunits, on the other hand, selectively inhibit AC1, AC5 and AC9 to reduce in intracellular concentration of cAMP (Godinho *et al*., 2015). $G\alpha_{q/11}$ subunits activate PLCβ, which hydrolyses $PIP_2$ and releases $IP_3$ and DAG into the cell (O'Connell *et al*., 2014). Gα12/13 involves the activation of RhoGEFs. RhoGEFs bind to and activate RhoA, which regulates downstream effectors including cytoskeletal proteins (Siehler, 2009).

### 1.8.2 GPCRs in the heart

To fulfil the body's changing heart-rate requirements in the many different situations it encounters including periods of stress or exercise, the function of ion channels responsible for shaping the cardiac action potential can be regulated by GPCRs (among other mechanisms). Modulation of ion channel function in this way allows extracellular factors to influence heart rate. For example, the release of the catecholamines epinephrine and norepinephrine from the adrenal glands during

stress, physical activity and excitement results in increased heart rate and contractility. This occurs through the binding of these hormones to their receptors, which in turn transduce the signal into the cell, causing an alteration in ion channel function. These signals may also originate from the cardiovascular centre in the brain, which sends signals via the sympathetic and parasympathetic nervous systems to the heart, releasing norepinephrine and acetylcholine, respectively.

*Stimulatory effects on cardiac ion channel function*

Via sympathetic stimulation of the nerve fibres innervating the myocardium, norepinephrine is released onto the heart. Norepinephrine (along with epinephrine) is the chemical ligand for α- and β-adrenergic receptors (ARs), but it is the β-ARs that are the predominant subtypes expressed in the heart, with the total β-AR population in the heart comprising approximately 80% β1-AR and 20% β2-AR (Lohse *et al*., 2003; Xiao *et al*., 2006). When norepinephrine binds to the β1-AR the receptor becomes stabilised in the active conformation, allowing coupling to the G protein subunits. The $G\alpha_s$ subunit can then dissociate from GDP and bind GTP. The active $G\alpha_s$ subunit activates AC, which generates cAMP. Increased cAMP activates PKA by binding to its regulatory subunit and alleviating inhibition of the catalytic subunit, and this kinase phosphorylates a number of effector proteins including troponin I and phospholamban (Madamanchi, 2007; Wegener *et al*., 1989; Zhang *et al*., 1995), leading to an increased rate of dissociation of $Ca^{2+}$ from troponin C and an increased SR $Ca^{2+}$ influx during diastole, respectively, together enabling more rapid muscle contraction and relaxation (Kang *et al*., 2007).

In addition to these effectors that are involved in excitation-contraction coupling, PKA activation through β1-AR activation also leads to phosphorylation of a number of ion channels involved in shaping the cardiac action potential. The L-type $Ca^{2+}$ current is a crucial component of the repolarisation phase of the cardiac action potential, and an increase in $I_{Ca,L}$ is one of the major causes of an increase in inotropy. Phosphorylation of the L-type $Ca^{2+}$ channel results in an increase in $I_{Ca,L}$ due to an increase in channel open time and open probability, rather than an increase in single-channel conductance (Van der Heyden *et al*., 2005).

Despite β1-AR expression dominating in the heart, β2-AR activation has been shown to increase $I_{Ca,L}$. In contrast to β1-AR activation, however, this occurs without the accompanying modulation of troponin I and phospholamban (Xiao & Lakatta, 1993). This is suggested to occur through extremely localised elevation of cAMP levels, likely due to the fact that the β2-AR couples to $G\alpha_i$ as well as $G\alpha_s$. In addition, the β2-AR has been shown to couple to the L-type $Ca^{2+}$ channel in a signalling microdomain (Davare *et al*., 2001), together causing a rapid and spatially restricted signalling

pathway that is incapable of affecting regulatory proteins outside of its immediate vicinity. This observation is supported by studies in frog ventricular cells, where β2-AR expression predominates. Application of isoprenaline to cells had limited effect on L-type $Ca^{2+}$ channels located at the opposite end of a cell. This effect was not reproduced with addition of forskolin (an AC activator), and was reduced when a phosphodiesterase inhibitor was added in combination with isoprenaline (Jurevicius & Fischmeister, 1996).

An increase in $I_{Ca,L}$ would lead to prolongation of the cardiac action potential if left unopposed. To shorten the APD, an enhancement of $I_{Ks}$ also occurs as a result of β1-AR activation. The ability of β1-AR activation to result in $I_{Ks}$ augmentation is due to localisation of proteins involved in the signalling pathway to the channel complex, and this process is discussed in section 1.8.3.

In addition to causing an increase in the $I_{Ks}$ current, β1-AR activation has been shown to result in an increase in the $I_{Kr}$ current. In canine ventricular myocytes, ISO, forskolin or intracellular application of cAMP analogues led to an increase in the $I_{Kr}$ current by 30–50% (Harmati *et al*., 2011). Also, inhibition of PKA had no effect on the baseline $I_{Kr}$ current.

*Inhibitory effects on cardiac ion channel function*

In contrast to the observations of Harmati and colleagues, other groups have found that the $I_{Kr}$ channel is inhibited by PKA-dependent phosphorylation downstream of adrenergic stimulation.

A study in guinea pig myocytes showed that application of the selective β1-AR agonist xamoterol caused inhibition of the $I_{Kr}$ current in a concentration-dependent manner (Wang *et al*., 2014). In addition to this, previous investigations found that the elevation in cAMP concentration resulting from β-AR activation not only leads to activation of PKA and hence phosphorylation of the hERG channel, but also regulation of the channel via direct binding to cyclic nucleotide binding sites on the channel itself (Cui *et al*., 2000). Again, the phosphorylation of the hERG channel through the mechanisms downstream of β-AR activation was found to cause a rapid inhibition of the hERG current.

Similar to the $I_{Ks}$ channel, PKA is thought to be localised to the hERG channel through binding to an AKAP protein. Li *et al*. (2008) reported that the PKA-RII-specific AKAP inhibitory peptide, AKAP-IS, reduces the PKA-dependent phosphorylation of the hERG channel, suggesting that PKA is localised to the channel by an AKAP. However, this group could not demonstrate an interaction between hERG and any cardiac-specific AKAPs in heterologous co-transfection experiments.

The inhibition of hERG by β1-AR activation could explain why the majority of cardiac events in individuals with KCNH2 mutations occur during episodes of emotional stress. However, the precise mechanism of regulation by PKA has not been elucidated. This is likely due to the differing origin of cell types used in the studies mentioned here.

*Chronic activation of cardiac GPCRs*

The above mentioned changes in ion channel function as a result of GPCR activation serve to provide a rapid and acute manipulation of cardiac contractility to ensure sufficient oxygenation of vascular tissue. In some circumstances, however, GPCR activation can give rise to more prolonged, chronic changes in the heart. This is known as 'remodelling', and may come in the form of an increase in cell size, organ size or chamber dimensions (Kang *et al*., 2007).

Cardiac remodelling may occur through the activation of various different GPCRs, including catecholamines activating the α- and β-ARs, endothelin (ET)1 activating the endothelin $ET_A$ and $ET_B$ receptors or angiotensin (AT) II activating the ATI and ATII receptors.

Activation of these GPCRs is usually intended to be a short-term event, such as in the fight-or-flight response in which β1-adrenergic stimulation occurs to increase contractility and heart rate. Chronic activation of such receptors can contribute to the onset and progression of heart failure. This is supported by the fact that β-AR antagonists are the standard therapy for individuals with heart failure (Bristow, 2000), and ATI antagonists and angiotensin-converting enzyme (ACE) inhibitors have been shown to reverse cardiac remodelling and slow the progression of heart failure (Cohn *et al*., 2001; Lindholm *et al*., 2002; Pfeffer *et al*., 1992).

### 1.8.3 Regulation of the $I_{Ks}$ channel by GPCRs

The increase in adrenergic drive that occurs during periods of increased sympathetic tone leads to enhancement of $I_{Ks}$ activation. The β-AR-induced increase in the $I_{Ks}$ current supresses the β-AR-induced afterdepolarisations that may arise through the increased $Ca^{2+}$ current (Burashnikov & Antzelevitch, 2000; Marban *et al*., 1986; Shimuzu *et al*., 1991).

*$I_{Ks}$ regulation by β-adrenergic activation*

The exact mechanism by which β1-AR-dependent PKA activation results in enhanced $I_{Ks}$ activity is still largely unknown. It is known, however, that the $I_{Ks}$ signalling complex centres around AKAP9, or yotiao, which anchors PKA, phosphodiesterase (PDE) 4D3 (PDE4D3), AC9 and protein phosphatase

(PP) 1 in close proximity to the channel (Li *et al*., 2012; Marx *et* al., 2002; Terrenoire *et al*., 2009). The increase in cAMP concentration resulting from AC activation activates PKA, which phosphorylates the channel at Ser27 (Kurokawa *et al*., 2004) and Ser92 (Lopes *et al*., 2007). This is thought to cause a conformational change that leads to enhanced channel activation (figure 11).

There have not yet been studies performed to investigate how the channel changes conformation following phosphorylation of the $I_{Ks}$ channel, and how this causes activation. However, studies have suggested that $PIP_2$ may be involved. In these experiments, the $I_{Ks}$ channel was inhibited by activation of the α1-AR (a $G_q$-coupled GPCR), and this inhibition was reduced when 100 nM isoproterenol (a β1-AR agonist) was applied for 2 minutes (Lopes *et al*., 2007).

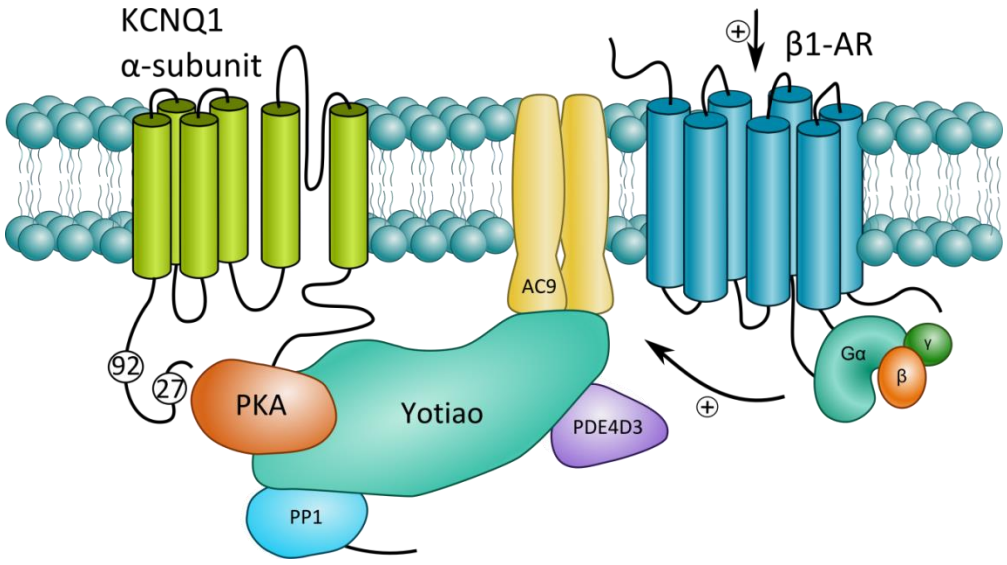


**Figure 11. Activation of the β1-AR leads to activation of the $I_{Ks}$ channel**. Activation of the β1-AR by the binding of agonists such as norepinephrine leads to the dissociation of Gα and Gβγ. Gα activates adenylate cyclase (AC), which catalyses the production of cAMP, resulting in an increase in the local concentration. Increased cAMP activates PKA, which phosphorylates the $I_{Ks}$ channel on the KCNQ1 α-subunit at Ser27 and Ser92, leading to enhanced channel activation. Yotiao, also known as AKAP9, anchors the effector proteins in a macromolecular signalling complex, allowing rapid signal transduction downstream of β1-AR activation.

*$I_{Ks}$ regulation by $G_q$-coupled GPCRs*

Cardiac $G_q$-coupled GPCRs include the ATI, ET1 and α1-AR. Activation of $G_q$-coupled GPCRs results in the depletion of $PIP_2$ through activation of PLC. Several studies have shown that $PIP_2$ depletion leads to inhibition of the $I_{Ks}$ current (Kruse *et al*., 2012; Loussouarn *et al*., 2003; Matavel & Lopes, 2009) However, one of the second messengers produced from the hydrolysis of $PIP_2$, DAG, subsequently

activates PKC, which has been shown to lead to activation of the $I_{Ks}$ channel; Matavel & Lopes (2009) showed that the depletion of $PIP_2$ and activation of PKC causes biphasic modulation of the $I_{Ks}$ channel by $G_q$-coupled GPCRs (figure 12).

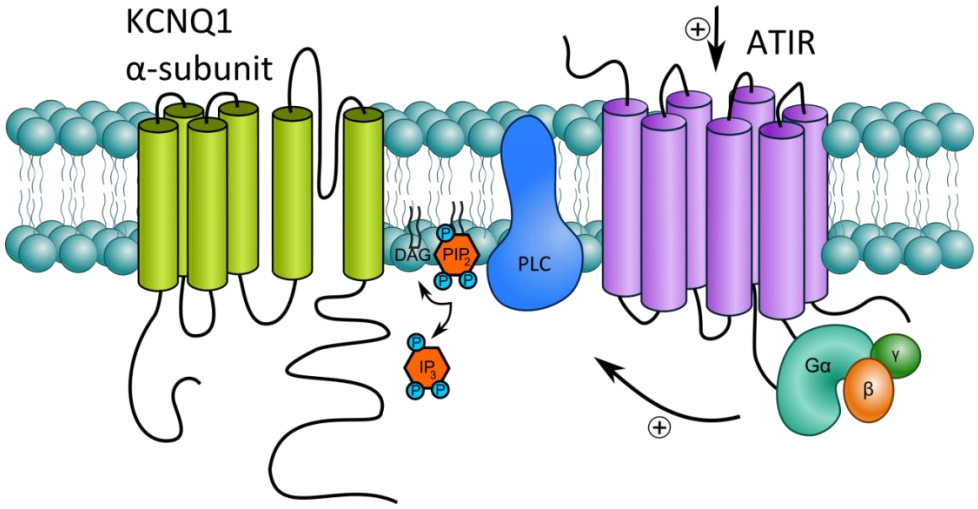


**Figure 12. Activation of Gq-coupled GPCRs leads to $PIP_2$ hydrolysis.** Activation of $G_q$-coupled GPCRs, such as the ATIR, results in dissociation of the Gα and Gβγ subunits. Gα activates PLC, which hydrolyses $PIP_2$ in the PM to $IP_3$ and DAG. DAG resides in the PM, whereas $IP_3$ is released in the cytosol. $PIP_2$ depletion arising from Gq-coupled GPCR activation is thought to cause inhibition of the $I_{Ks}$ channel.

In their study, activation of the M1 receptor and the AT1 receptor by acetylcholine and angiotensin II, respectively, resulted in an inhibition phase followed by an activation phase. This group also activated the bradykinin (BK) 2 receptor using BK, but observed only inhibition of the $I_{Ks}$ current, suggesting that an activation phase was not present or was concurrent with the inhibition phase and therefore masked. $PIP_2$ hydrolysis was responsible for the $I_{Ks}$ inhibition phase, whereas activation of PKC by DAG and the subsequent phosphorylation of the $I_{Ks}$ channel were responsible for the activation phases observed.

On the other hand, others have shown that PKC causes the downregulation of the $I_{Ks}$ channel through phosphorylation of KCNE1 at Ser102. This occurs in human and rat, but not guinea pig as KCNE1 possesses an asparagine residue at this position in place of serine in this species (Varnum *et al*., 1993). The mechanism behind the downregulation of $I_{Ks}$ by PKC-dependent phosphorylation of KCNE1 in humans is thought to be via an increase in channel internalisation (Kanda *et al*., 2011). This mechanism could be pathologically relevant, as α1-AR agonists (such as norepinephrine) activate PKC in cardiac myocytes.

In contrast to the results showing $I_{Ks}$ inhibition resulting downstream of ATIR activation, are the findings that activation of the ATIR in guinea pig myocytes leads to activation of the $I_{Ks}$ channel (Zankov *et al*., 2006; Zankov *et al*., 2009). These results may vary due to the different cell types used in the studies. These results do, however, support the presence of an activation phase in the experiments of Matavel & Lopes (2009).

Activation of the $ET1_a$ receptor was found to cause inhibition of the $I_{Ks}$ current in guinea pig ventricular myocytes (Washizuka *et al*., 1997). This is thought to be through a pertussis toxin-sensitive mechanism and the resulting inhibition of AC, and it can result in a prolongation of the APD.

*Dual regulation by different GPCR families*

Dvir *et al*., (2014) investigated the molecular mechanism of a number of LQT-associated mutations in KCNQ1 and KCNE1 that are located in KCNQ1 helix C and the KCNE1 distal C terminus – two regions that are thought to interact. This group reported that the mutations in KCNQ1 helix C highlighted that this region is important for channel modulation by $PIP_2$, and the KCNE1 distal C-terminus mutations suggested that this region is essential in $I_{Ks}$ channel regulation by yotiao-mediated PKA phosphorylation.

These experiments suggest that $PIP_2$ could be involved in transforming the signal from $I_{Ks}$ phosphorylation and conformational change of the channel into activation, but also that there could be crosstalk between the β1-AR and $G_q$-coupled GPCR regulation of the $I_{Ks}$ channel *in vivo*.

Matavel *et al*. (2010) found that as well as PKA, PKC also regulates the response of the $I_{Ks}$ channel to $PIP_2$-mediated inhibition. In this study, several LQT-associated mutations that affect the $I_{Ks}$-$PIP_2$ interaction (Arg174Cys, Arg243Cys, Arg366Gln and Arg555Cys) were shown to affect the PKA- and $G_q$-coupled GPCR-mediated regulation of the $I_{Ks}$ channel, and the effects were diverse across the mutations studied. Matavel and colleagues proposed that the effects on channel regulation could be important in the risk stratification of LQT patients, and may also influence the treatment strategies employed.

The mechanisms of $I_{Ks}$ regulation by different cardiac GPCRs have not been fully elucidated, and the interplay between these remains an area of research that could help to understand mechanisms of arrhythmia generation in particular arrhythmias, such as LQTS.

## 1.9 Conclusion and thesis content

The $I_{Ks}$ channel binds $PIP_2$, and it has been show experimentally that this channel is inhibited by a loss

of $PIP_2$ from the PM. It is also widely thought that the open conformation of this channel is stabilised by $PIP_2$. Other KCNQ channels, namely the M channel, require $PIP_2$ for opening, and physiologically this mechanism is used by the M1R to inhibit the M current. How $PIP_2$ regulates the $I_{Ks}$ channel and whether experimental data translates to physiological environments, however, is largely unknown.

Physiologically, the $I_{Ks}$ current contributes to phase-3 repolarisation during periods of increased sympathetic tone, but contributes little at resting heart rates. The mechanism behind this is via activation of the β1-AR, but how the activation of this receptor and the downstream activation of PKA transmits into enhanced $I_{Ks}$ channel activation has not been investigated.

When either of the $I_{Ks}$ channel subunits, KCNQ1 or KCNE1, harbour mutation(s), the $I_{Ks}$ current can become compromised and lead to LQTS types 1 and 5, respectively. The mechanisms underlying these mutations may be due to disrupted channel trafficking or function. In this laboratory, mutations in a $PIP_2$ binding region in the proximal C-terminus of the $I_{Ks}$ channel led to impaired channel trafficking.

As well as studying how $PIP_2$ regulates $I_{Ks}$ channel function, and whether $PIP_2$ is involved in the β1-AR-induced enhancement of the $I_{Ks}$ current, this thesis will detail experiments that determine whether $PIP_2$ is involved in the anterograde trafficking of the $I_{Ks}$ channel.

In addition to investigating mechanisms of $I_{Ks}$ channel regulation by PIP, this thesis will describe the compatibility of the rapamycin-inducible dimerisation system for studying the function of the $I_{Ks}$ channel, and the efforts made to improve this methodology.

# CHAPTER 2: Methodology

## 2.1 Cell culture

### 2.1.1 Passaging cells

To provide a continuous supply of heterologous cells for use in the experiments within this project, cells were passaged approximately once per week. This practice discards the majority of cells during each passage and takes only a small portion, or subculture, to continue growing. This process may carry on with the same cells for a few months, before replacing them with new, earlier passage cells.

Human embryonic kidney (HEK) 293 cell lines were grown in 75 $cm^2$ (T75) cell culture flasks in minimum essential media (MEM [31095-029, Thermo Fisher Scientific] supplemented with 10% heat-inactivated foetal bovine serum (FBS) (10500-064, Life technologies) and 100 units/ml penicillin and 100 µg/ml streptomycin (15140-122, Life technologies), described from here onwards as HEK293 media. Chinese Hamster Ovary (CHO)-K1 cells were grown in 75 $cm^2$ cell culture flasks in Ham-F12 media (D8900, Sigma) supplemented with 10% FBS and 100 units/ml penicillin and 100 µg/ml streptomycin. Cells were kept at 37°C and 5% $CO_2$ in a humidified incubator.

HEK293 and CHO-K1 cells were passaged when they reached approximately 80% density. Cells were first washed with 8 ml phosphate buffer saline (PBS [D8537, Sigma]) to remove any residual culturing media, then detached from the flask using 2 ml 0.25% trypsin (5 ml 2.5% trypsin [15090, Life technologies] in 45 ml PBS). Trypsin activity was terminated with the addition of 8 ml culture media. The required fraction of HEK293 or CHO-K1 cells was transferred to a new T75 flask containing 15 ml HEK293 or Ham-F12 media, respectively. Cells were commonly passaged using a 1:10 dilution: from 10 ml of trypsinised cells, 1 ml was taken and transferred to the new flask.

Cells were then incubated at 37°C and 5% $CO_2$ for a minimum of 2 days before being passaged again.

### 2.1.2 Seeding cells

In order to use cells in experiments, a portion were taken from the main culture and adhered to a medium suitable for the desired experiment in a process known as ‘seeding’. Commonly, cells were seeded onto glass coverslips. Cells adhered onto glass coverslips were required for patch clamp and confocal microscopy experiments. Alternatively, cells were adhered to the bottom of a well in multi-well plate. This was required for the in/on-cell western experiments.

To obtain the cells required, a portion were taken from the main culture after trypsinisation and added to wells in a multi-well plate. These wells either contained 4–5 x 10 mm coverslips (for patch clamp), 1 x 25 mm coverslip (for confocal microscopy) or were empty (for in/on-cell western assays).

When untransfected cells were required on coverslips, they were seeded into wells containing coverslips 48 hours before use at a density of approximately 10%. The low density allowed space for cell division to occur so that on the day of experimentation the cells were at an appropriate density.

When transfected cells were needed (i.e. for patch clamp experiments), they were seeded into wells without coverslips, 72 hours before use, at a density of approximately 50%. A higher density was used to allow cells to be effectively transfected before being passaged and re-seeded into new wells containing coverslips at a density of approximately 10%.

When a monolayer of transfected cells was required for the experiment (i.e. in the in/on-cell western assay), cells were seeded at a density of 50%, 72 hours before transfection. After transfection, the cells were not passaged again and seeded into new wells, but left to divide in the original well to reach a high density.

**2.1.3 Transfection**

Transient transfection was routinely used throughout the project, and it allowed the transient expression of foreign cDNA in the heterologous cell lines used. Transient expression (in contrast to stable expression) occurs due to the lack of incorporation of cDNA into the cell's own genome, meaning that the cDNA is lost when the cell divides (Kim & Eberwine, 2010). As the transfected cDNA can be changed from experiment to experiment, the transient transfection method provided a quick and flexible way to study the function of many different proteins in the same cell line.

On the other hand, a stable transfection was occasionally performed, which involved the incorporation of cDNA into the cell's own genome. This resulted in the expression of the transfected cDNA in the original cell, but also in new cells arising from cell division. A number of different cell lines were used throughout the project, each stably expressing one or more desired proteins. The production of stably expressing cell lines was performed in this project to prolong the expression of proteins that were to be constant through the experiments, allowing transient expression of other proteins in these cells.

Viruses, calcium phosphate, cationic lipids and direct injection of cDNA are all valid methods of transfection, each with their own advantages and disadvantages (Kim & Eberwine, 2010). Cationic

lipids are most commonly used in the type of cells and the nature of experiments used throughout this project, and was the method chosen here.

This method was effective at transfecting cDNA into the heterologous cell lines used, and the efficiency of transfection was routinely between 40–80%. The success of this method relies on the fact that the positively charged transfection lipids attract the negatively charged cDNA molecules, forming a complex that is endocytosed or phagocytosed by the cell and delivered to the nucleus.

Fugene HD (E2311, Promega) and Lipofectamine 2000 (11668019, Thermo Fisher Scientific) were both used throughout the project. Depending on the experiment the cells were destined for, one transfection agent was favoured over the other; Fugene HD was used to transfect cells for electrophysiological experiments, while Lipofectamine 2000 was used to transfect cells for imaging experiments and in/on-cell western assays.

***Transfection of cells in a 6-well plate using FuGENE HD***

- The appropriate volume of cDNA and 200 µl Opti-MEM I (11058-021, Life technologies) were added to a 1.5 ml sterile microcentrifuge tube. The cDNA and Opti-MEM I were mixed by vortexing. 5 µl FuGENE HD (E2311, Promega) was then added and the solution was mixed by gently tapping/flicking the tube. The cDNA/FuGENE HD/Opti-MEM I solution was then left for complexes to form for 20 minutes at room temperature (RT).
- The cells to be transfected were washed with 1 ml Opti-MEM I, and media was replaced with 2 ml antibiotic-free media. After 20 minutes, the total volume of cDNA/FuGENE HD/Opti-MEM I solution (200 µl) was taken and added to the cells. Cells were incubated with the cDNA/FuGENE HD complexes at 37°C and 5% $CO_2$.
- After 4 hours, media (containing complexes) was removed and cells were washed using 1 ml PBS. Cells were then incubated with 400 µl trypsin at RT for approximately 5 minutes, and an appropriate volume of cell suspension was removed for seeding in a new well containing culture media and coverslips (e.g. 40 µl of cell suspension taken for seeding at 10% density).

| *Transfection of cells in a 6-well plate using Lipofectamine 2000* |
| --- |
| • The appropriate volume of cDNA and 200 µl Opti-MEM I were added to a 1.5 ml sterile eppendorf tube. The cDNA and Opti-MEM I were mixed by vortexing. In a separate sterile eppendorf tube, 195 µl Optimem I and 5 µl Lipofectamine 2000 (Life technologies, 11668-019) were added, mixed by gently pipetting and incubated at RT for 5 minutes.<br>• The Opti-MEM I/Lipofectamine 2000 solution was added to the tube containing cDNA/Optimem I, and the solution was mixed by gently tapping/flicking the tube. The cDNA/Lipofectamine 2000/Opti-MEM I solution was incubated at RT for 15 minutes in order for cDNA-Lipofectamine 2000 complexes to form.<br>• Cells to be transfected were washed as in the FuGENE HD protocol, and the remaining steps are the same, apart from the total volume of transfection mixture added to the cells was 400µl. Cells were left for 5 hours, after which, media was removed and cells were passaged and transferred to a new well, as in the FuGENE HD protocol. |

### 2.1.4 Generation of stably expressing cell lines

A number of stably expressing HEK293 cell lines were made during this project. A stably expressing KCNH2 cell line and KCNJ2 cell line were made, and a stably expressing KCNQ1-GFP/KCNE1 cell line had been produced prior to the start of the project by Dr Stephen Harmer.

In order to generate a stably expressing cell line, the cDNA used for transfection must contain an antibiotic-resistance gene. By incorporating antibiotic resistance into the cDNA plasmid, cells that successfully incorporate the plasmid into their genome are selected for by using antibiotic-containing culture media (known here as selection media). To ensure stably transfected cells had been selected for, untransfected cells were cultured in selection media in parallel, and the death rate of these two populations of cells was monitored. When the untransfected cells had died, the remaining cells in the transfected-cell population were assumed to have successfully incorporated the antibiotic-resistance gene (and therefore also the gene of interest) into their genome. Individual colonies of cells were left to divide until their density reached approximately 60–80 % of a well in a 6-well plate.

Commonly, the protein of interest is tethered to a fluorescent tag to enable visualisation of protein expression during experiments. This was exploited during the process of cell colony selection to ensure that cells that had survived contained the gene of interest in addition to the antibiotic-resistance gene, but also to check that the colonies of cells were clonal (i.e. all cells originated from

the same cell, and hence expressed the fluorescently-tagged protein). Colonies that were not clonal were discarded.

Unfortunately, the KCNH2 and KCNJ11 proteins were not fluorescently tagged, so to identify clonal colonies the electrophysiological properties of each respective colony were assessed using whole-cell patch clamp (WCPC). In order to do this, cells were seeded onto 10 mm coverslips, as detailed in section 2.1.2. The colony in which cells produced acceptable and reproducible current densities corresponding to the respective ion channel was kept, and inferior colonies were discarded.

***Production of a stably expressing cell line***

- Cells were first seeded into 1 well of a 6-well plate at a density of approximately 50%. The following day, cells were transfected using Lipofectamine 2000, as described in section 2.1.3.
- After transfection, cells were passaged, similar to the method detailed in section 2.1.2. Here, however, cells were seeded into 100 mm cell culture dishes at various dilutions (1:20, 1:100, 1:1000 and 1:10,000). A control plate of untransfected cells was seeded in parallel. Cells were incubated at 37°C and 5% $CO_2$, in culture media containing the appropriate antibiotic (determined by the antibiotic-resistance gene contained within the plasmid).
- Cells were left in all dishes to divide until 100% cell death occurred in the control plate. Then, antibiotic-selection media was removed from the transfected cells and replaced with PBS (10 ml). PBS (100 µl) was drawn into a pipette tip whilst scraping an isolated colony, and this cell suspension was placed into a well in a 6-well plate containing antibiotic-free media (2 ml). 12–18 colonies were picked, and each placed in a separate well. Antibiotic-free media was replaced with antibiotic-selection media after 24 hours.
- Cells were left to divide until they reached a density of 60–80 %, then either passaged onto coverslips for electrophysiological investigation or viewed under a microscope to identify the most suitable clonal line for use in further experiments.

## 2.2 Molecular Biology

Molecular biology techniques were used throughout the project in order to isolate, amplify and manipulate DNA.

Manipulation of the gene of interest, for example, through the introduction of mutations or restriction sites, was performed using the polymerase chain reaction (PCR). Bacterial amplification

was performed once a complete plasmid had been made, which allowed the production of a sufficient amount of plasmid for use in procedures such as transfection.

A number of techniques were commonly used in sequence to produce the desired DNA plasmid constructs needed for progression of this project. These were the PCR, restriction digest, agarose gel electrophoresis, ligation and transformation, and a simplified cloning workflow is shown in figure 13.

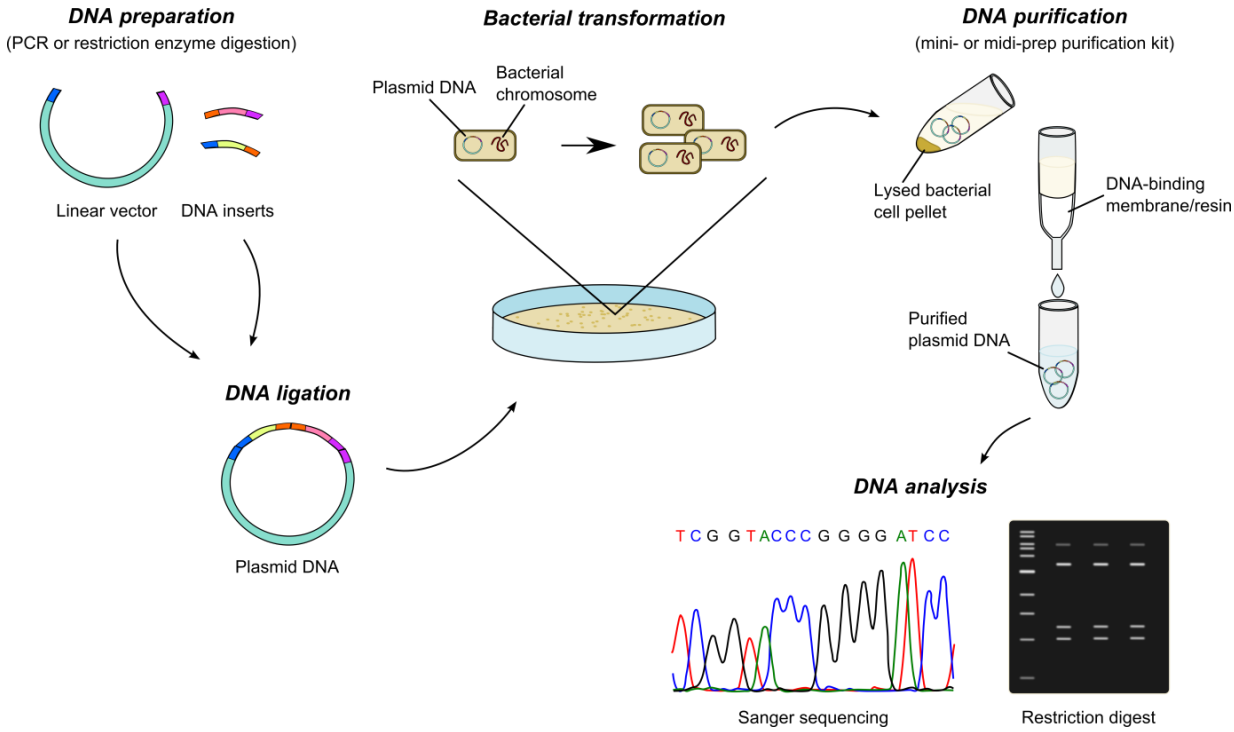


**Figure 13. Molecular biology workflow.** An overview of the step used to produce and amplify a DNA plasmid. DNA vectors and inserts can be produced using PCR or by restriction enzyme digestion. The resulting lengths of DNA (which are designed to have compatible ends) are ligated together, before being amplified using competent bacterial cells. To extract the DNA, the bacterial cells are lysed and the DNA plasmids are purified. The purified plasmid DNA can then be analysed to check the correct sequence has been produced. This is commonly done using a restriction digest or by Sanger sequencing.

### 2.2.1 Polymerase Chain Reaction

The polymerase chain reaction, or PCR, has long been used for the manipulation and amplification DNA fragments, and was invented by Mullis and his team in the 1980s (Saiki *et al.*, 1985). In this project, PCR was used for molecular cloning and site-directed mutagenesis.

For the purpose of molecular cloning, regions of DNA from DNA plasmids or libraries (known as template DNA) were amplified using primers complementary to the 5' and 3' ends of the desired DNA sequence. The region between the forward and reverse primers is known as the target DNA, and is the region that was amplified.

A thermally stable DNA polymerase was used to enable DNA denaturation at high temperatures before amplification, whilst keeping the DNA polymerase active throughout the heat cycle. Once amplified, the region of target DNA was purified and used in subsequent molecular cloning reactions.

*PCR DNA Polymerases*

The DNA polymerase from *Thermus aquaticus* (Taq) is commonly used in PCR reactions due to its thermostability (Saiki *et al*., 1988). The optimum temperature for Taq polymerase activity is 75°C, which enables high temperatures to be used during the PCR extension step of each cycle. High temperatures ensure that primers bind with a higher specificity, producing less unwanted amplification products as a result of non-specific binding (Lawyer *et al*., 1989).

Throughout this project, however, Q5 high-fidelity DNA polymerase (M0491, New England Biolabs) was used due to its higher fidelity (>100 times higher than Taq polymerase) and low error rates. The Q5 high-fidelity DNA polymerase consists of a novel polymerase fused to the DNA binding domain of Sso7d, a chromatin protein from the hyperthermophillic archaebacterium *Sulfolobus solfataricus* (Su *et al*., 2000).

*Extraction of DNA from a completed PCR reaction*

Different methods exist to enable the extraction of DNA from a completed PCR reaction. Up to 10 µg of DNA can be purified quickly and efficiently using the QIAquick PCR purification kit (28104, Qiagen), which uses a silica gel that binds DNA in a high-salt buffer and allows elution of DNA in a low-salt buffer (or water). Once eluted, the DNA can be used immediately in downstream reactions.
Alternatively, the completed PCR reaction can be loaded into an agarose gel, where DNA fragments are separated by size. The isolated PCR product can then be excised, but needs to be extracted from the gel before use in further reactions. This method is described in section 2.2.3.

***Performing PCR using Q5 DNA polymerase***

**The following were added to an RNase/DNase-free 0.2 ml microcentrifuge tube:**

DNA (50 ng)

Forward primer (0.5 µl)

Reverse primer (0.5 µl)

5x Q5 reaction buffer (10 µl)

10 mM deoxynucleotide triphosphates (dNTPs) (1 µl)

Q5 DNA polymerase (1 µl)

$H_2O$ (make up to 50 µl)

**Tubes were placed in a PCR machine, and the following protocol was started:**

1. Initialisation – Reaction was heated to 98°C for 2 minutes.
2. Denaturation – Reaction was heated to 98°C for 30 seconds in order to denature the double-stranded DNA (dsDNA), yielding single-stranded DNA (ssDNA).
3. Annealing – Reaction temperature was lowered to 60°C (variable, depending on experiment) for 30 seconds, allowing primer annealing to the template DNA.
4. Extension – Reaction temperature was increased to 72°C for 1–5 minutes (variable, depending on experiment), to allow complementary dNTP addition to the DNA template via the action of Q5 DNA polymerase.
5. Final extension – Reaction was held at 72°C for 5 minutes to ensure all extension was complete.
6. Final hold – Immediately after completion, reactions were held for an indefinite amount of time at 4°C.

- Steps 2–4 form 1 cycle. These steps were repeated for 35 cycles, between step 1 and 5

### 2.2.2 Site-directed mutagenesis

Site-directed mutagenesis (SDM) enables the introduction of specific alterations in a gene of interest using the PCR technique. Point mutations, replacement of amino acids and insertion or deletion of single amino acids can be performed using SDM. There are a number of different ways to introduce mutations into a plasmid, and many commercially available kits exist for this technique.

Early SDM techniques used two PCR reactions to create complementary DNA plasmids. The completed PCR reactions were combined to allow complementary DNA strands to anneal. The primers used in these reactions were complementary, and both contained the mutation to be introduced, but the positioning of the primer resulted in the 'break point' of the plasmid ending up in a different position. This resulted in a plasmid containing staggered single-stranded break points, which were subsequently repaired when expressed in a host cell (Jones *et al*., 1990).

Current SDM methods use the same principles as the earlier method. However, the use of two PCR reactions is no longer required. Completely overlapping primers are now used within the same PCR reaction, each complementary to opposite DNA strands. After generation of each single-stranded circular plasmid, complementary strands anneal. In this project, the QuikChange II XL Site-Directed Mutagenesis kit (200521, Agilent Technologies) was used.

The QuikChange II XL kit makes use of a genetically engineered version of *Pfu* DNA Polymerase, named *Pfu*Ultra high-fidelity DNA polymerase, which allows the highly precise replication of both plasmid strands as it exhibits an error rate many times lower than that of other commercially used polymerases (i.e. 18-fold lower than Taq polymerase). In addition to the high fidelity of this polymerase, it promotes the rapid extension and higher yield through the presence of the ArchaeMaxx polymerase-enhancing factor. This converts the inhibitory dUTP (generated from dCTP deamination) to harmless dUMP, improving PCR performance (Agilent Technologies Inc, 2015).

The primers used in this method are synthetic, and bind to their complementary sequences on the DNA plasmid (at the site where the mutation is to be introduced). These primers are extended by *Pfu*Ultra high-fidelity DNA polymerase during the PCR temperature cycling stage, creating a circular plasmid with staggered nicks, which are repaired when expressed in a cell.

Following the production of the mutated plasmids, the *Dpn* I endonuclease is added to the reaction mix. *Dpn* I (target sequence: 5′-Gm6ATC-3′) selectively digests the dam-methylated parental (template) DNA over the unmethylated mutation-containing synthesised DNA.

***To perform SDM using QuikChange II XL Site-Directed Mutagenesis kit***

**The following were added to an RNase/DNase-free 0.2 ml microcentrifuge tube:**

DNA (50 ng)

Forward primer (0.5 µl)

Reverse primer (0.5 µl)

5x Q5 reaction buffer (10 µl)

10 mM deoxynucleotide triphosphates (dNTPs) (1 µl)

Q5 DNA polymerase (1 µl)

$H_2O$ (make up to 50 µl)

**Reaction tubes were placed in a PCR machine and the following PCR cycle was commenced:**

1. 98°C for 2 minutes (initialisation)
2. 98°C for 30 seconds (denaturation)
3. 60 ± 5°C (variable, depending on experiment) for 30 seconds (annealing)
4. 68°C for 2 minutes per kb of plasmid (extension)d
5. 72°C for 5 minutes (final extension)
6. 4°C (final hold)

Steps 2–4 form 1 cycle. These steps were repeated for 18 cycles, in between step 1 and 5.

*Dpn* I (1 µl) was then added to each reaction tube and incubated at 37°C for 1 hour. 10 µl of each reaction mixture was then used to transform XL10-Gold Ultra-competent cells. The transformation procedure is detailed in section 2.1.3.

When the DNA plasmid containing the new mutation was amplified and purified, Sanger sequencing was performed to determine whether the mutation had successfully been introduced.

### 2.2.3 Restriction digest

Restriction digests allow the production of DNA fragments that can be joined (ligated) together in further reactions to create a desired construct or sequence. Restriction enzymes, also called restriction endonucleases, were first used in 1971 to produce fragments of simian virus 40 DNA (Danna & Nathans, 1971). The use of restriction enzymes in molecular biology became routine as the number of known restriction enzymes increased, giving increased flexibility to DNA manipulations.

Restriction enzymes recognise specific short stretches of DNA sequence and create double-stranded cuts in the DNA. These cuts produce either 'sticky ends' or 'blunt ends'. When sticky ends are created, there is a 3' or 5' overhang of ssDNA (depending on the enzyme that was used).

Naturally occurring restriction enzymes are classified into 4 groups (type I, II, III and IV). Type I restriction enzymes cut DNA sequences at random, at sites that are far from the recognition sequence. Type II restriction enzymes cut DNA at a specific point at, or close to, the recognition sequence (Pingoud & Jeltsch, 2001). The most common type II enzymes, known as orthodox type II restriction enzymes, assemble as a homodimer and recognise symmetric, or palindromic, sequences. In order to perform their function, these enzymes require the presence of $Mg^{2+}$, which enables the cleavage of DNA at the specific sequence to give 5'-phosphate and 3'-OH ends. Other subtypes of the type II group of restriction enzymes include those that recognise asymmetric sequences (due to being formed from a heterodimer of subunits), those that interact with two copies of their recognition sequence, those that cleave DNA at both sides of the recognition sequence and those that recognise methylated DNA (Pingoud & Jeltsch, 2001).

Artificial enzymes that recognise larger sequences of DNA can be created by fusing a DNA-binding domain to a nuclease domain. In this way, a restriction digest can be performed on any DNA sequence desired. Zinc-finger nucleases and transcription-activator-like effector nucleases are commonly used artificial enzymes, which are created by fusing the zinc-finger binding domain or the TAL effector binding domain to a nuclease domain (Townsend *et al*., 2009).

For molecular cloning purposes, type II restriction enzymes are used due the predictable DNA binding and cleavage that they possess. Restriction enzymes that create sticky ends are more desirable than those that create blunt ends because of the relative ease of ligating two complementary sticky ends. Figure 14 depicts how a commonly used restriction enzyme, BglII, digests dsDNA. The enzyme recognises a specific sequence in the DNA (AGATCT), and cuts here to produce 5' overhang sticky ends.

In single-digest reactions of circular plasmids, i.e. those that involve DNA digestion with only one restriction enzyme, complementary ends are produced that can easily re-ligate within the same reaction. In order to prevent this, the removal of the 5' phosphate from each end can be performed with the addition of either calf-intestinal alkaline phosphatase (CIP) (M0290, New England Biolabs) or Antarctic phosphatase (AnP) (M0289, New England Biolabs) to the reaction.

All restriction enzymes used in this project were purchased from New England Biolabs, and the reaction buffer (NEBuffer 1–4 [or 1.1–3.1 and Cutsmart]) in which the enzyme had the highest activity was used.

| ***Performing a restriction digest (20 µl reaction)*** |
| --- |
| **The following were added to a sterile microcentrifuge tube:**<br>DNA (2–10 µg)<br>10x NEBuffer (2 µl)<br>Restriction enzyme(s) (1 µl each)<br>CIP/AnP (if required, 1 µl)<br>$H_2O$ (make up to 20 µl)<br><br>• Reaction tubes were incubated at 37°C for 2–3 hours, after which the completed reactions were loaded into an agarose gel to enable purification of the digested DNA. |

**2.2.4 Agarose gel electrophoresis and gel extraction**

The development of agarose gel electrophoresis revolutionised the separation of nucleic acid fragments, as previously separation could only approximate fragment size. Throughout this project, this technique was used for separation of DNA.

Agarose is isolated from the seaweed *Gelidium* and *Gracilaria*, and once polymerised it forms a network of bundles containing pores that act like a DNA sieve. The extent to which DNA fragments move through the agarose gel is determined by their size, with smaller DNA fragments moving further through the agarose gel than larger DNA fragments. To induce the movement of DNA fragments (as this does not occur spontaneously) an electric field is applied across the agarose gel. The negatively charged DNA is attracted to the positively charged anode and migrates through the gel.

To determine fragment size, a 'DNA ladder' is run in parallel, which contains DNA of a known size as a reference to which the sample DNA is compared. The distance over which a fragment of DNA travels is inversely proportional to the log of its molecular weight, as DNA has a uniform mass to charge ratio. The distance travelled by DNA fragments is also dependent on the agarose concentration of the gel, conformation of the DNA (i.e. linear or supercoiled), voltage applied to the gel and the type of electrophoresis buffer used (Lee *et al*., 2012).

After completion of electrophoresis and sufficient separation of DNA fragments, extraction of DNA from the agarose gel was sometimes performed. This was required when DNA was to be used in further reactions, for example, ligation.

The QIAquick gel extraction kit (28704, QIAGEN) enables the extraction of up to 10 µg of DNA from agarose gel by using a buffer to dissolve the agarose followed by the use of a silica gel to bind the DNA in a high-salt buffer. The DNA can then be eluted in a low-salt buffer (or water). These DNA extraction methods ensure the removal of primers, nucleotides, enzymes, mineral oil, salts, and agarose.

*To perform agarose gel electrophoresis*

The appropriate amount of agarose (1–2% w/v – depending on the size of DNA fragments) was added to 150 ml TAE buffer (40 mM Tris-acetate, 1 mM EDTA [disodium ethylenediaminetetraacetate in $H_20$, pH 8.0 with NaOH]) and heated to solubilise the agarose. Once cooled but not set, Midori green DNA stain (7.5 µl; Nippon Genetics, MG04) was added and the gel solution was left to set in a prepared gel tray with gel comb(s) inserted.

Gel loading dye (1:10; B7021S, New England Biolabs) was added to each restriction digest reaction. The set agarose gel was placed into a gel tank, and the reaction mixtures were added to individual wells of the gel along with 1 kb (N3232, New England Biolabs) and 100 bp (N3231, New England Biolabs) DNA ladders.

A 90 mV potential difference was applied across the agarose gel and fragments were run for approximately 1 hour, until the bands were separated by an appropriate distance. Bands were then visualised using a UV AlphaImager system, and images were acquired using AlphaImager software on a PC. Fragments were cut out of the main agarose gel if required in downstream reactions, and extracted from the gel using the QIAquick gel extraction kit.

### 2.2.5 Ligation

Ligation reactions catalyse the formation of a phosphodiester bond between the 5'-phosphate and 3'-hydroxyl ends of DNA (figure 14). The fragments of DNA with complementary sticky ends created in restriction digest reactions, described in section 2.2.3, are used here to assemble new DNA constructs. This technique uses naturally occurring enzymes that are usually involved in DNA repair.

In this project, T4 DNA ligase (M0202, New England Biolabs), an ATP-dependent ligase, was used. As well as its use in joining sticky ends, T4 DNA ligase can also join blunt ends and repair single-stranded nicks in DNA and RNA (Rossi *et al*., 1997).

For an efficient ligation it is recommended that a 3:1 ratio of insert to vector DNA is used, although this varies depending on the size of the fragments and the concentration of the DNA in the sample.

After ligation, the new plasmid DNA can be inserted into bacterial cells for amplification. A control ligation reaction containing only vector DNA and DNA ligase should be performed in parallel to ensure the vector has cut properly and that the phosphatase (CIP/AnP) activity was successful (i.e. the digest was successful and the sticky ends created did not re-ligate with each other). There are commonly bacterial colonies that grow from transformation of this control ligation, but the number of colonies that grow from each ligation reaction should be far in excess of those grown from the control ligation.

| *Performing DNA ligation with T4 DNA ligase (20 µl reaction)* |
|---|
| **The following were added to a sterile microcentrifuge tube:**<br>Vector DNA (50 ng)<br>Insert DNA (37.5 ng)<br>T4 DNA Ligase buffer (2 µl)<br>T4 DNA Ligase (1 µl)<br>$H_20$ (make up to 20 µl)<br><br>• Reaction tubes were incubated at RT for 3 hours, and the reactions were gently mixed every hour.<br>• Reactions were then stored at 4°C until required for transformation. |

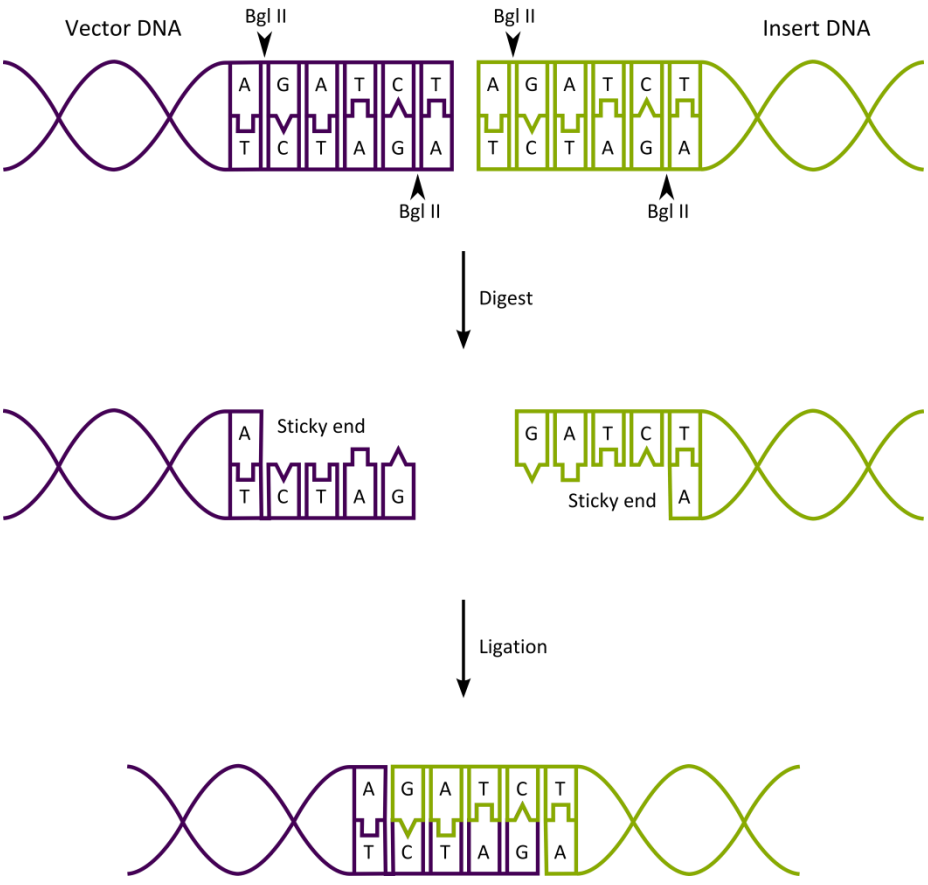


**Figure 14. An example of restriction digests and the ligation of sticky ends.** Restriction digest using BglII (AGATCT) of vector and insert DNA, forming sticky ends, and the subsequent ligation of complementary sticky ends of the vector and insert DNA.

### 2.2.6 Transformation

Transformation occurs when a bacterial cell takes up foreign DNA, and this process is replicated here in order to yield a sufficient quantity of DNA for use in mammalian cell transfection. The bacterial transformation method exploits the rapid rate of bacterial growth, which allows amplification of DNA in a short time frame. Artificial induction of bacterial transformation requires the use of cells that have been made 'competent' (Griffiths *et al*., 2000). For DNA uptake to occur, a short 'heat shock' step is performed, which is thought to increase membrane fluidity and allow entry of DNA through membrane pores (Panja *et al*., 2008).

The level of competency of bacterial cells differs between strains. Routine amplification of plasmids was performed using Top10 competent *E*. *coli* cells, but when smaller concentrations of plasmid (e.g. in ligation products) were used, XL10-Gold Ultra-competent cells were used because the proportion of total DNA successfully transformed is greater.

Despite the fact that the DNA plasmids used in this project were destined for use in mammalian cells, they also contained a bacterial-resistance gene. For selection of bacterial colonies successfully transformed with the amplified plasmid, cells were incubated overnight on LB agar plates that contained the antibiotic corresponding to the antibiotic-resistance gene within the plasmid. Bacterial cells that were not successfully transformed do not survive the action of the antibiotic, and only plasmid-containing bacteria remain.

A number of colonies are then picked and grown overnight at 37°C in either 5 or 50 ml LB media (depending on whether a mini or midi prep was performed, respectively).

| ***Performing a bacterial transformation using Top10 competent E. coli cells*** |
| --- |
| • Top10 competent *E. coli* (TT) cells were thawed on ice for 15 minutes. Plasmid DNA (1–5 µl) was then added to TT cells (30–50 µl) in a sterile microcentrifuge tube, and the TT cell/DNA mix was incubated on ice for 30 minutes.<br>• The TT cell/DNA mix was subject to heat shock by incubating at 42°C for 1 minute, and the mixture was immediately incubated on ice for 2 minutes.<br>• LB media (800 µl) was added to each tube and incubated at 37°C for 45 minutes. The cell suspension was mixed by inverting the tube, and was performed every 15 minutes.<br>• The cell suspension was centrifuged at 13,000 rpm for 1 minute. The supernatant was removed and the pellet was re-suspended in LB media (100 µl). The cell re-suspension (100 µl) was spread onto LB agar plates containing the appropriate antibiotic and incubated at 37°C for 16 hours. |

### 2.2.7 DNA purification

After amplification of DNA in bacterial cells, for example the TT or XL10-Gold Ultra-competent cells, the DNA requires extraction and purification before it can be used. For the purification of small volumes of DNA (i.e. yielded from amplification in bacterial cells that are then grown in 5 ml LB media overnight), the Plasmid Miniprep Kit (27405, Qiagen) was used, and for purification of larger volumes (i.e. when the same bacteria was grown in 50 ml overnight) the Qiagen Plasmid Purification Midiprep Kit (12145, Qiagen) was used. The Miniprep Kit allows isolation of up to 20 µg DNA, which is released from the bacterial cells after their lysis under alkaline conditions. The lysate produced is neutralised and adjusted to high-salt binding conditions. The DNA is then purified from the lysate by using a silica membrane, which binds the DNA in high-salt conditions, and DNA is subsequently eluted in low-salt conditions. The salt concentration of the buffer ensures that RNA, proteins and metabolites are not bound to the membrane, to ensure elution of these before the DNA.

| ***Purification of DNA using the Qiagen Plasmid Miniprep Kit*** |
| --- |
| • Bacterial cultures (1.5 ml) were transferred into a round-bottomed microcentrifuge tube and centrifuged at 13,000 rpm to pellet the bacterial cells. Supernatant was removed and this process was repeated.<br>• The bacterial pellets were resuspended and the bacterial cells lysed by adding the appropriate buffers. The resulting reaction mixture was then added to a spin column containing the silica membrane, and tubes were centrifuged for 60 seconds at 13,000 rpm.<br>• Supernatant was discarded and columns were washed twice with a high-salt buffer. DNA was then eluted into new microcentrifuge tube using 20 µl $H_2O$. |

The Midiprep Kit uses similar alkaline conditions to the Miniprep Kit in order to perform bacterial cell lysis, after which the technique uses low-salt and low-pH conditions to bind DNA to QIAGEN resin. RNA, proteins, dyes and low-molecular-weight impurities do not bind to the resin and are hence removed. DNA can then be eluted in high-salt conditions, then concentrated and de-salted using isopropanol precipitation.

| *Purification of DNA using the Qiagen Plasmid Purification Midiprep Kit* |
| --- |
| • Bacterial cultures (50 ml) were transferred to a 50 ml falcon tube and centrifuged for 30 minutes at 4000 rpm and 4°C to pellet the bacterial cells. The supernatant was then removed.<br>• The bacterial pellets were resuspended and the bacterial cells lysed by adding the appropriate buffers. The lysate was then removed from the DNA-containing solution by gravity-flow filtration.<br>• The resulting solution was then added to gravity-flow Qiagen resin columns, and DNA was bound, washed and then eluted into 15 ml falcon tubes by sequentially adding the appropriate buffer.<br>• Isopropanol (3.5 ml) was added to each tube and reaction tubes were centrifuged for 90 minutes at 4000 rpm. Supernatant was removed and the DNA pellet was resuspended in 70% ethanol (1.5 ml), whilst transferring to a new microcentrifuge tube.<br>• Reaction tubes were centrifuged for 10 minutes at 13,000 rpm to pellet the DNA, and this was repeated once more.<br>• Supernatant was removed and the DNA pellet was left at RT for the remaining ethanol to evaporate. The DNA pellet was then resuspended and solubilised in 200 µl $H_2O$. |

## 2.3 Confocal Microscopy

Marvin Minsky developed the technique of confocal microscopy (CM) (Minsky, 1988) and contributed substantially to the advancement of biological imaging over the decades. Compared to conventional fluorescence microscopy using a digital camera, CM allows the acquisition of higher-resolution images. However, the relative simplicity of optical microscopy still allows a high magnification of a sample, and is consequently the preferred method in some applications when in depth observations are not required. An additional factor taken into account when deciding the method of microscopy is cost; wide-field fluorescence microscopy is much cheaper than CM.

On the other hand, when a higher degree of image resolution is required, CM may be used. The need for CM usually results from the expression of fluorescently tagged proteins or fluorescent organelle markers in cells. These fluorescent tags can be imaged using optical microscopy optimised for the use of fluorescence detection (i.e. using different filters for each fluorescent protein [FP]). However, the spatial resolution is poor in these conventional methods and their use is consequently limited to fluorescence detection rather than fluorescence localisation. The most common type of CM is laser scanning confocal microscopy (LSCM), which was used throughout this project.

### 2.3.1 Principles of confocal microscopy

The way in which CM achieves high-resolution images is by means of point-by-point illumination and the elimination of out of focus emission light (Charman, 1998). In detail, light of the excitation wavelength travels through a pinhole before being focused on the specimen by the objective lens, allowing only a specific point in the specimen to be illuminated (the focal plane). Point-by-point illumination refers to the fact that each point in the focal plane is sequentially illuminated by a single beam of laser light. This excitation light is absorbed by the FPs in the focal plane, and light is emitted from them. The emission light is detected in the point-by-point order in which they were excited.

In a perfect system, only the focal plane would be illuminated and only a single pinhole would be required. In reality, however, a small amount of light is absorbed by FPs that neighbour the focal plane, so a second pinhole is used. This pinhole is placed in a conjugate focal plane to the focal point of the objective lens. Light emitted from the specimen passes through this second pinhole before reaching the detector in order to eliminate out of focus light (i.e. light not originating from the focal plane). The detector used in CM is a photomultiplier tube.

The aperture of the second pinhole can be altered to change the amount of light able to reach the detector. Decreasing the pinhole size allows more accurate detection of the light emitted from the focal plane, but this also limits the signal intensity. Accordingly, increasing the size of the pinhole yields stronger signal intensity, but has the risk of allowing light emitted from outside of the focal plane to be detected.

In order for different light wavelengths to be passed through the same light path (i.e. excitation and emission wavelengths), a dichroic mirror is used. This mirror allows the excitation wavelength to be passed through to the cells whilst only letting the wavelength of the emission light back through to the detector.

### 2.3.2 Considerations for image acquisition

Using LSCM, image acquisition is performed by illuminating the specimen and collecting the emission light. In multicolour experiments, this first round of light detection is then followed by the illumination of the same focal plane using a different wavelength of light in order to excite a second FP within the specimen. The collection of emission light from this second FP then follows. Due to the sequential (rather than simultaneous) nature of point-by-point illumination and excitation of multiple FPs, the temporal resolution is LSCM is limited.

In order to ensure the detected signal is at a high enough level, the pinhole aperture needs to be of sufficient diameter. However, this can cause a reduction in resolution along the Z axis. Reducing the pinhole aperture produces images of higher constrast and better image quality, indicating that a compromise in pinhole aperture is required. In this project, the pinhole aperture was set to 1 Airy unit at all times. This describes the pinhole aperture that matches the diameter of the Airy disc, which is the circular diffraction pattern created by a light source passing through an aperture.

If the signal intensity from a particular cell is weak, the gain of the photomultiplier tube can be increased, but this comes at the cost of also amplifying the signal of background noise.

In addition to acquiring single images as described above, LSCM can be used for different multi-image purposes. For example, time-series and Z-stacks can be created from multiple images taken of the same specimen.

A time-series is constructed by acquiring subsequent images of the same focal place at predetermined, regular intervals. Post image-acquisition, these images can be compiled to reveal any changes in the localisation of fluorescently tagged proteins that occur over time.

By acquiring multiple images along the Z-axis of a specimen, a Z-stack can be created. These 2-dimensional images, only varying in depth along one axis, can be assembled to create one 3-dimensional image. This can reveal relative spatial information about fluorescently tagged proteins within a cell.

| ***Acquiring an image using confocal microscopy*** |
| --- |
| • Cells (adhered to a coverslip) were placed on the microscope stage and the focus was altered to position the cells in an approximate focal plane. A more accurate focus of the desired focal plane was achieved using controls within the PC software (ZEN, ZEISS Microscopy).<br>• Once the focal place was set, the excitation/emission protocol was started. The protocol sequentially excited the FPs and detected light emitted from them. Within multicolour experiments, the excitation and emission cycle was sequentially performed for each FP.<br>• The image produced was subject to a number of offline corrections, including background filtering and contrast adjustment. |

| Fluorescent protein | Excitation wavelength (nm) | Emission wavelength (nm) |
|---|---|---|
| Wild type GFP | 396, 475 | 508 |
| eGFP | 488 | 507 |
| eCFP | 434 | 477 |
| eYFP | 514 | 527 |
| mRFP1 | 584 | 607 |
| mCherry | 587 | 610 |

**Table 4. The excitation and emission of commonly used fluorescent proteins**. WT GFP was isolated from *A. Victoria* and has subsequently been enhanced to produced eGFP, eCFP and eYFP. mRFP1 and mCherry are monomeric RFPs originating from DsRed, an RFP isolated from D. Striata.

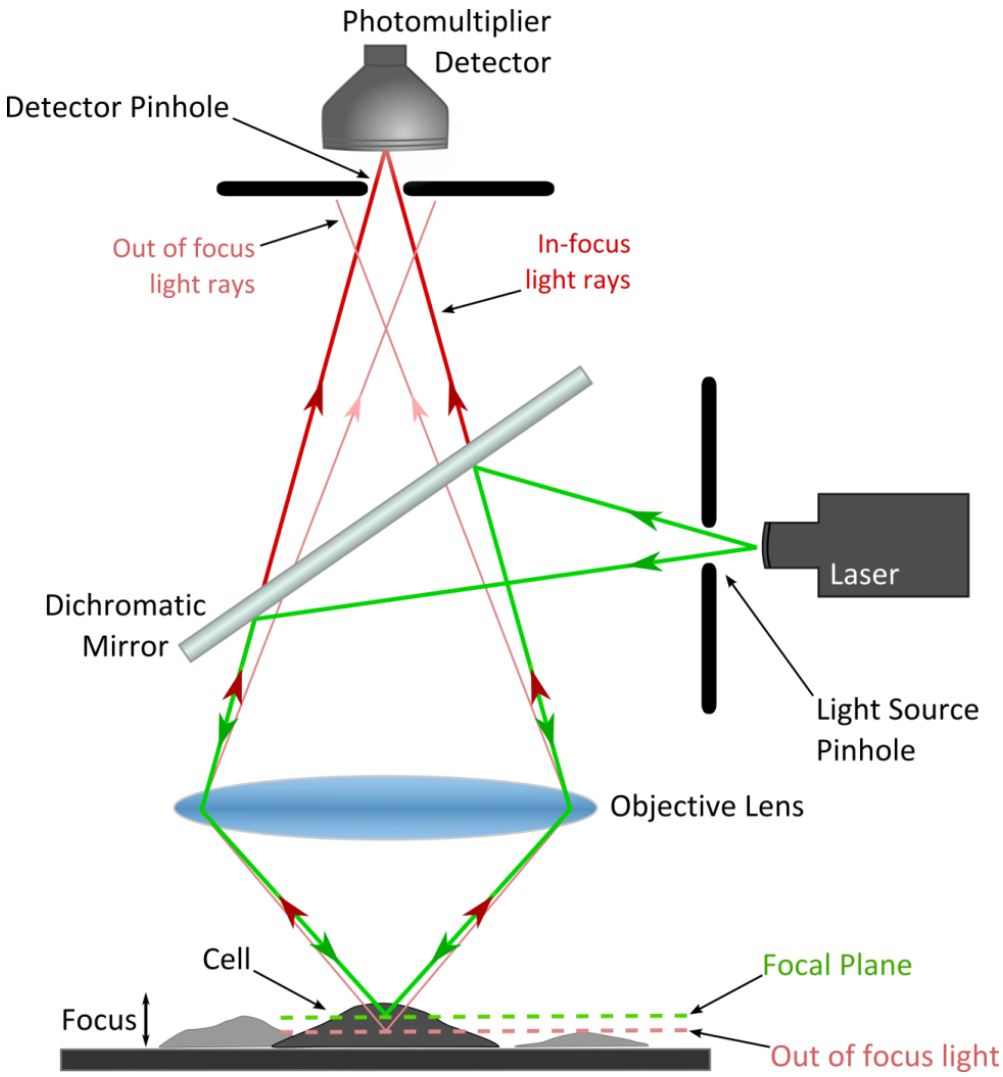


**Figure 15. Princples of confocal microscopy.** Light from a laser passes through the illumination pinhole and is reflected onto the specimen to be imaged, where it is absorbed by molecules from the fluorescent protein tags. Light emitted from the focal point then passes through the confocal pinhole, in a conjugate focal plane to the point of illumination, and is detected. Light emitted from round the focal point will be out of focus when reaching the confocal pinhole, so will not reach and detector and is eliminated. 'Confocal Microscopy' adapted from the John Innes Centre (2012).

## 2.4 Fluorescent dyes and proteins

To illuminate regions of a cell for the purpose of identifying the location of proteins and cellular organelles, fluorescent dyes and proteins are used. Fluorescent molecules enable their visualisation by absorbing light of a certain wavelength and emitting light of a different wavelength. Synthetic fluorescent dyes, or fluorophores, were commonly used in the past for this, and are sometimes still used today. The most common of these are the xanthene derivatives, such as fluorescein and rhodamine. Even though the synthetic dyes were often successfully used, they still had many downfalls. For example, fluorescein has a high photobleaching rate and broad emission spectra, the latter of which limits its use in multi-colour experiments.

Many features of fluorescent tags have to be considered when choosing the most suitable for use in microscopy experiments. Low cell toxicity is important as these fluorescent molecules are expressed in cells for a number of days before experiments are performed. Photostability also has to be considered; excessive photobleaching can occur from high-intensity excitation light during an experiment, and the reduced emission signal can cause artefacts to emerge in results. A third important factor is the Stoke's shift: the difference between the optimal emission and excitation wavelength. A large Stoke's shift is desirable as this prevents the crossover of emission and excitation wavelengths. During multicolour experiments, the Stoke's shift of all fluorescent tags must be considered as the emission from one fluorescent molecule may excite another (Day & Davidson, 2012), which is not usually the aim in standard confocal experiments.

Today, FPS are more commonly used instead of synthetic fluorescent dyes as they possess more desirable characteristics. In the 1960s, Osamu Shimomura isolated the chemiluminescent protein, aequorin, from the green-glowing jellyfish, *Aequorea Victoria (A. Victoria)*. Aequorin, however, emits blue light. Along with his colleagues, Shimomura identified that *A. Victoria* also contains a green fluorescent protein (GFP), and the energy in the form of the blue light from aequorin was absorbed by GFP and emitted at a different wavelength, resulting in the visible green luminescence of *A. Victoria* (Morise *et al*., 1974).

Furthering this discovery, it was found that GFP consists of a single peptide chain over 200 amino acids in length, 3 of which (Ser-Tyr-Gly) form the chromophore (Cody *et al*., 1993). This, along with the fact that GFP can be excited in the absence of *A. Victoria*-specific proteins, means that GFP can be cloned and expressed in other systems. This meant that by simply linking GFP to a protein of interest, protein localisation can be visualised in a myriad of cells types. Within this project, a number of different FPs were used due to the interest in localisation of the $K_v7.1$ channel and other

constructs.

WT GFP has been modified to produce an enhanced version, named eGFP, via the addition of a point mutation (Ser65Thr). eGFP possesses increased emission light intensity and increased photostability compared to WT GFP, and also has only one excitation maxima. eGFP was used as a template to produce an array of different coloured FPs. Table 4 includes some of these (cyan fluorescent protein [eCFP] and yellow fluorescent protein [eYFP]) along with other FPs used in this project. The monomeric red fluorescent protein (mRFP1) was created through the optimisation of DsRed, a red fluorescent protein (RFP) isolated from the coral *Discosoma Striata* (*D.* Striata), which naturally forms a tetramer (Campbell *et al*, 2002). Another monomeric red fluorescent protein from *D. Striata* used in this project is named mCherry.

Many of the protein constructs used in this project contain FPs. When investigating the trafficking of $K_v7.1$ using imaging techniques these FPs are indispensable, as without them the visualisation of construct localisation would not be possible. Illumination of different cellular organelles and the PM also plays an important role in microscopy experiments, as this gives reference to the localisation of the construct/protein of interest.

Although the attachment of a FP to the $K_v7.1$ protein is required in imaging experiments, this fluorescent tagging also proves helpful in electrophysiological experiments, where identification of cells expressing the protein of interest is required.

## 2.5 Electrophysiology

Electrophysiological approaches are used to measure the transmembrane potential and the electrical changes that occur as a result of an applied stimulus. Changes in $V_m$ can occur from externally applied electrical stimuli, direct pharmacological activation/inhibition of ion channels or indirect activation/inhibition of ion channels, e.g. via GPCR activation. The ability to measure the changes in $V_m$, and therefore ion flow across the membrane, allows the function of PM ion channels to be investigated.

Some of the early iterations of electrophysiological recordings were performed by Hodgkin and Huxley in the 1940s and early 1950s. The pair first inserted a fine capillary electrode into a squid giant axon to record the potential difference across the nerve membrane. This revealed an action potential characterised by a large depolarising overshoot beyond 0 mV followed by a small hyperpolarisation beyond the baseline potential (Hodgkin & Huxley, 1939). Following this, Hodgkin and Huxley introduced the concept of voltage-clamp, where the membrane is maintained at a

constant potential, allowing the current flowing across the squid axonal membrane to be recorded. With the help of Katz, the voltage sensitivity and kinetics of the ion channels within the membrane were also investigated (Hodgkin *et al*., 1952). This collection of work provided the crucial first understandings of nerve excitability and the action potential.

Since then, the principles of this method have been adapted and developed, and now the function of endogenous channels in native cells can be investigated as well as the function of transiently expressed channels in heterologous cell lines. In addition to this, the development of different electrophysiological methods has enabled the measurement of single-channel activity or macroscopic whole-cell currents.

### 2.5.1 Patch clamp

The patch clamp technique was developed by Neher and Sakmann, who published this method in 1976. This new technique was first used to record the single-channel currents from nicotinic acetylcholine receptors in denervated frog muscle fibres (Neher & Sakmann, 1976). This method was more sensitive than previously used electrophysiological methods and enabled a high enough resolution of currents for single channel fluctuations to be detected.

In the most commonly used patch-clamp configuration, the voltage-clamp principle is employed to enable the membrane potential to be held constant. In a physiological environment, the depolarisation in a cell's membrane potential as a result of ion flux may lead to the activation of $K_v$ channels and the consequent return of the membrane potential to $R_m$. This is not the case in patch clamp – the membrane potential is 'clamped' to prevent its alteration by ion channel activity. In this way, the ionic current that passes through the membrane via any active ion channels can be measured. An alternative configuration is occasionally used, known as *current-clamp*, which allows the change in membrane potential to be recorded when the cell is subject to fixed amplitudes of current. Throughout this project, the voltage-clamp method of patch clamp was used, and the term 'patch clamp' will be used from here on synonymously with the term 'voltage clamp'.

### 2.5.2 Patch clamp equipment

*Microscope:*

An inverted light microscope is required in the patch clamp setup for visualisation of the cell and pipette. Without this, the fine control and manipulation of the pipette onto the cell to form a seal would not be possible. Microscopes for patch-clamp use are engineered to reduce the vibration caused when controlling the magnification and focus.

*Micromanipulator:*

A micromanipulator allows movement of the patch pipette in 3 axes, usually with the option of a coarse (fast) and fine (slow) control. The fine control is used to carefully guide the pipette onto the cell membrane. Once a seal is formed, the pipette must stay in place and not drift, to ensure a GΩ seal can be maintained throughout the experiment.

*Pipettes:*

Pipettes for patch-clamp come in various different sizes and glass types. Commonly used for electrophysiological experiments are borosilicate glass pipettes, due to their desirable properties: low softening temperature, high electrical resistivity and chemical resistance. Pipettes commonly contain a filament running the length of the inside to aid pipette filling. Pipettes come in either thin- or thick-walled varieties, the thick-walled being ideal for single-channel experiments because the noise and pipette capacitance are low. Thin-walled pipettes are ideal for WCPC experiments, however, as they provide a lower access resistance (Rycroft *et al*., 2006).

The glass for patch-clamp pipettes is pulled to yield two similar pipettes. This can be performed in manual vertical pullers, or newer, automated horizontal pullers. The pipettes are pulled in 2 stages: the first determines the taper of the pipette tip, and the second determines the final diameter of the pipette tip.

Once pulled, the pipettes can be fire-polished. This makes the tip smoother, and higher-resistance seals can usually be achieved by fire-polishing.

*Silver-chloride electrode:*

In order for electric current to be converted to ionic current, and vice versa, a silver-chloride (Ag-Cl) electrode is used. A silver electrode is coated with Ag-Cl either by dipping it in bleach containing hypochlorite or through electrophoresis in a chloride solution (Zhao *et al*., 2008). This electrode is wired to the amplifier, and is present in the glass pipette in contact with the high KCl-containing intracellular solution during recordings. Ag-Cl electrodes are widely used due to the reversible reaction responsible for current transduction: when electrons pass down the electrode, $Cl^-$ dissociates from the Ag-Cl electrode into the intracellular KCl solution, hence converting electrical current to an ionic one. As this reaction is reversible, chloride ions in the intracellular solution can reform the Ag-Cl coating, providing a free electron that converts the ionic current to the electrical current. This redox reaction can be seen in equation 2.1.

$$AgCl + e^- = Ag + Cl^-$$ Equation 2.1

*Amplifier:*

The amplifier allows the manipulation of the membrane potential or current. A representative voltage-clamp protocol is shown in figure 17. The Axopatch 200B (Axon), used in this project, provides low-noise patch-clamp recordings, and can actively cool the amplifier headstage for low thermal noise. The amplifier in a patch-clamp setup allows pipette and membrane capacitance cancellation, and series resistance compensation and prediction to be performed.

*Digitiser:*

A digitiser converts one or more channels of analog signal into a series of digital values, which is does using an A/D converter. For example, when recording the current through one or a number of ion channels, a digitiser may calculate the output of the patch clamp amplifier at regular time intervals and provide the digital value to the computer.

*Storage and analysis equipment:*

To record and store the data from patch-clamp experiments, PC software is used. The pClamp software (Axon) is used in this project, and includes Clampex 10 for data acquisition and Clampfit 10 for offline analysis.

*Solutions:*

Depending on the patch-clamp configuration and the ion channels being investigated, the extracellular and intracellular (pipette) solutions differ in composition. Standard extracellular solutions contain a low $K^+$, high $Na^+$ concentration, while the intracellular solution contains a high $K^+$ and low $Na^+$ concentration. Solutions also contain a $Ca^{2+}$ chelator, for example, EGTA, to buffer the intracellular free $Ca^{2+}$ levels to a minimum. ATP is also commonly added to intracellular solutions in WCPC experiments to maintain ATP-dependent processes.

**2.5.3 Patch clamp principles**

*Patch clamp electronics:*

The way in which a patch-clamp amplifier clamps the $V_m$ at a particular voltage is via a feedback system (figure 16). To clamp the membrane potential, current flows from the amplifier's output if the two inputs are not equal. The two amplifier inputs are the command potential ($V_{cmd}$) (positive input)

and the pipette potential ($V_p$) (negative input). If the membrane potential (or $V_p$, as it is the tip of the pipette that is clamped) is the same as $V_{cmd}$, there will be no current flow. When membrane current flows, $V_p$ will change and move away from $V_{cmd.}$ To restore $V_p$ to $V_{cmd}$, current of an equal amount, but opposite sign, will be applied through the output via a feedback resistor ($R_f$).

According to Ohm's law, the voltage drop ($V_{out} - V_p$) that occurs across the resistor determines the current that flows though the pipette ($I_p$). As $V_p$ is clamped at $V_{cmd}$, the amplifier continuously measures the difference between $V_{out}$ and $V_{cmd}$, and adjusts $I_p$ accordingly to clamp the membrane potential at the desired voltage (Rycroft *et al*., 2006).

$$I_p = \frac{(V_{out} - V_{cmd})}{R_f} \qquad \text{Equation 2.2}$$

For large macroscopic recordings, low resistance feedback resistors are used. Larger resistance values give higher sensitivity to recordings and ensure that $V_p$ comes closer to $V_{cmd}$. However, the resistance of $R_f$ is limited when recording larger currents due to the power supply of the amplifier. Typically, with a 12 V amplifier and 500 MΩ $R_f$, the amplifier will saturate at an $I_p$ value of 24 nA.

*Cellular electrical characteristics:*

The electrical workings of the patch-clamp technique can be demonstrated using simple equivalent circuits, where $V_m$ is the membrane potential, $C_m$ is the membrane capacitance and $R_m$ is the membrane resistance. A capacitor is defined as an insulator that separates two areas of conducting regions (e.g. the PM lipid bilayer, which separates two high conducting regions, the intracellular and extracellular solutions).

In a cell, the membrane potential creates a driving force for ion movement across the PM. Ohm's law (V = IR, that can be rearranged to I = V/R) denotes that that at a particular voltage (V), the current (I) is proportional to the resistance (R) across the membrane. In a physiological setting, the membrane potential is not fixed. As the membrane resistance changes (with the opening and closing of ion channels in the PM) and the current flow through the capacitance is charged and discharged, the membrane potential changes.

*Recording artefacts:*

While the PM capacitance is charging during a patch-clamp experiment, the current recorded is not the total current, but the current passing through the capacitor. This also occurs when the capacitor discharges. These capacitive currents can be seen in WCPC experiments after breaking into the cell whilst subjecting the cell to a test pulse.

The glass walls of the pipette also act as a capacitor, between the intracellular and extracellular solutions (Ogden & Stanfield, 1994). This capacitance can be reduced by coating the pipette with SigmaCote, a silicone coating that thickens the pipette wall. To further reduce pipette capacitance, the depth of solution in the bath can be lowered so only the very tip of the pipette remains in the solution.

The electrode resistance ($R_e$) also introduces unwanted error to recordings. As the voltage is clamped to the end of the electrode, and not the PM, a voltage drop across $R_e$ will cause the voltage reaching the PM to differ.

The $R_e$ can interact with the capacitance properties of the PM and cause problems when performing patch-clamp recordings. As the capacitor needs to be charged and discharged it slows any change in membrane voltage, and therefore slows the effect of membrane potential change on current characteristics. This time course (T) of voltage change follows an exponential relationship, and is the combination of the electrode resistance and membrane capacitance (equation 2.3).

$$T = R_e C_m \qquad \text{Equation 2.3}$$

Similarly, any current that flows across the membrane will be subject to the same time course error, meaning any fast current signals will be filtered by $C_m$ and $R_e$.

*Capacitance cancellation:*

Cancellation of the pipette and cell capacitance is important for a number of reasons. Firstly, it prevents saturation of the amplifier at large voltage steps (Ogden & Stanfield, 1994). When the power supply of the amplifier is exceeded, the correct current is not driven round the circuit, and the current or voltage cannot be clamped correctly. Secondly, cancellation allows the capacitance to be

charged by an extra 'capacity current' that bypasses the recording amplifier (and therefore does not alter the cell response). The pipette capacitance is cancelled upon sealing to the PM, and the cell capacitance is cancelled when sufficient access to the cell is gained (i.e. in WCPC, when the patch is ruptured).

*Series resistance compensation:*

Series resistance ($R_{series}$) is the term given to the summed resistances of the pipette and cell, which cause unwanted filtering effects and voltage errors in the recording circuit, causing $V_m$ to differ significantly from the $V_{cmd}$. Any current injected into the cell from the amplifier will be subject to a voltage drop across electrode resistance, and Ohm's law (V=IR) denotes that an increase in either current or resistance increases the voltage drop (Barbour, 2014). It is important to account for this during set-up and recordings. Resistance can be lowered to an extent by choosing low-resistance pipettes. This can be achieved by widening the pipette tip, but widening the tip too far can cause problems in producing high-resistance seals with the PM.

The effects of $R_{series}$ can be predicted (i.e. the voltage error that will result), and because of this, a current can be injected to compensate for these effects. Driving extra current through the electrode mimics the situation that would occur by having a lower-resistance pipette, and the PM is therefore clamped at a voltage closer to $V_{cmd}$ (Barbour, 2011). In theory, $R_{series}$ can be compensated for by around 90%, but in practice $R_{series}$ is compensated for by approximately 70%.

For effective $R_{series}$ compensation it is required that pipette and cell capacitance cancellation be performed. Any current transients arising from charging the capacitance can interfere with the current recorded, and therefore the extra current injected for $R_{series}$ compensation.

*Transient prediction:*

By performing cell capacitance cancellation prior to $R_{series}$ compensation, the voltage drop caused by charging the membrane capacitance is not estimated as accurately as possible, and the compensation that is applied may not be sufficient. By measuring the cancellation current used to cancel the cell capacitive currents, an extra correction can be made to the current injected through the electrode. This effectively 'overshoots' the pipette potential at the beginning of a command, and as a result, the cell's capacitance is charged more quickly than if the cancelled capacitance current had not been considered (Sigworth, 2014). This transient prediction is also called supercharging.

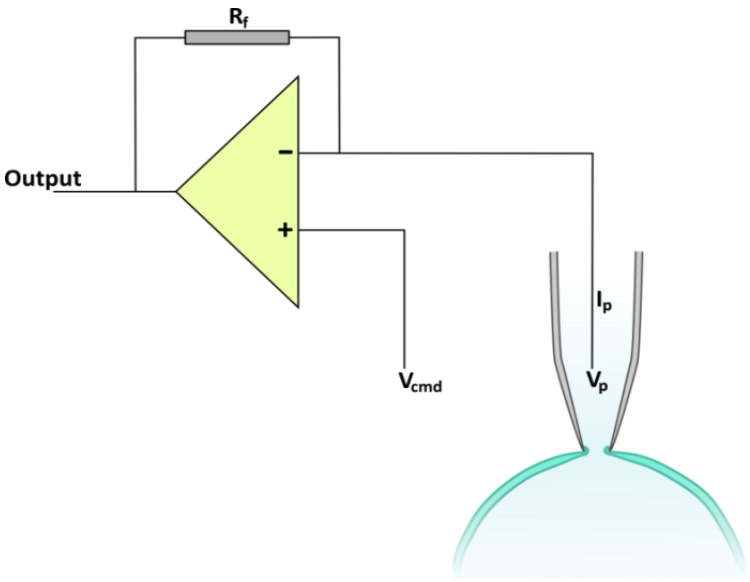


**Figure 16. The patch-clamp feedback system equivalent circuit.** The amplifier output is determined by the difference between the positive ($V_{cmd}$) and negative ($V_p$) inputs. Deviation of $V_p$ from $V_{cmd}$ causes current to be driven across the feedback resistor ($R_f$), and a current ($I_p$) is supplied to bring $V_p$ back to $V_{cmd}$. Adapted from Rycroft et al. (2006).

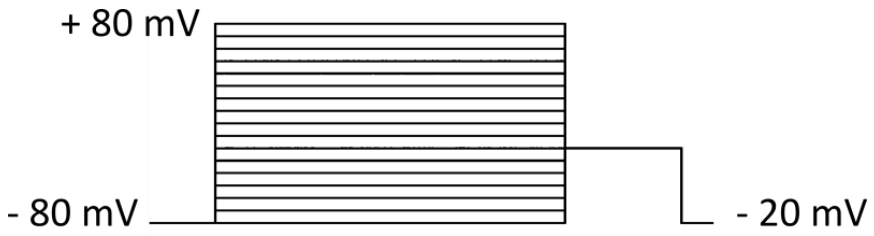


**Figure 17. Patch-clamp I-V voltage protocol.** Representative voltage protocol used in patch clamp experiments to record the relationship between current and voltage (when recording the $I_{Ks}$ current) Voltage is held at -80 mV for 1 second before a depolarising step for 6 seconds between -80mV and +80mV, which then steps to -20 mV for 2 seconds, before returning to -80 mV for 1 second.

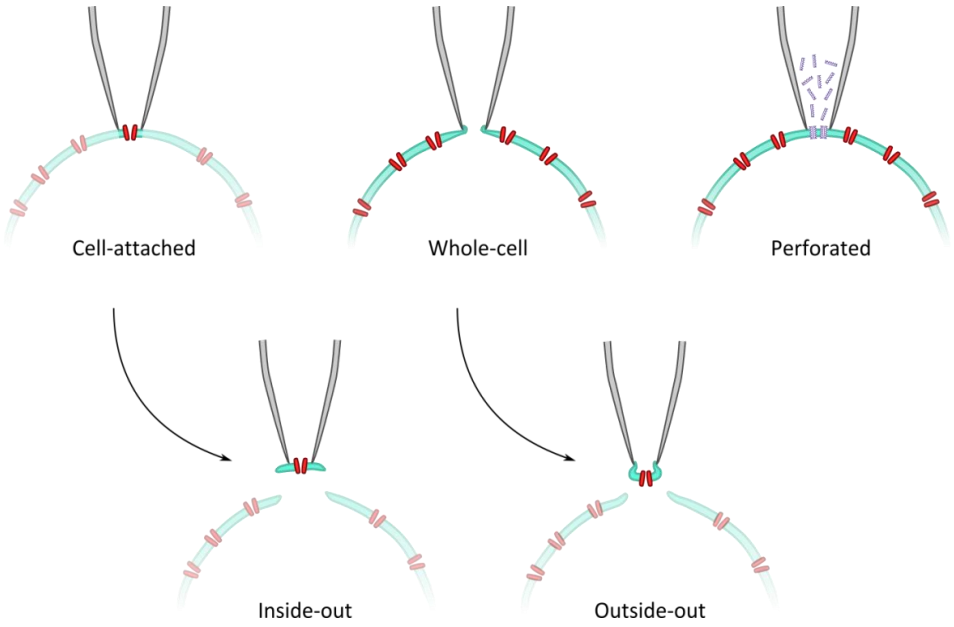


**Figure 18. Configurations of the patch clamp technique.** From cell-attached, inside-out can be achieved by pulling the pipette away from the cell. By stretching the membrane slowly from the whole-cell configuration until it breaks, outside-out can be performed. Perforated patch is achieved by forming small pores in the membrane with, for example, amphotericin B. The whole-cell and perforated patch configurations measure the total ionic current in the cell, whereas cell-attached, inside-out and outside-out record the ionic current present only in the membrane patch.

### 2.5.4 Patch-clamp configurations

A standard patch-clamp procedure involves forming a high-resistance giga-ohm (GΩ) seal (>1 GΩ) between a glass pipette and the PM of a cell. The patch of membrane in the tip of the pipette is then ruptured, pulled away from the cell, left intact or perforated, depending on the patch clamp configuration (figure 18). The different patch-clamp configurations are briefly described below:

*Cell-attached:*

This configuration of the patch-clamp technique is arguably the simplest, as it requires only a tight seal between the patch pipette and cell membrane. It is commonly used for investigation of single-channel activity and recordings of spontaneous action potential firing (Perkins, 2006). This configuration is also the most physiological, because none of the intracellular environment is disrupted by dialysis with the pipette solution.

*Inside-out:*

After forming a GΩ seal, pulling the membrane patch away from the cell will result in a small area of membrane in the tip of the pipette for recording, with the intracellular side of the cell exposed to the bath solution. In this method, all cytoplasmic constituents are lost, therefore providing a method for investigating the influence of exogenously applied intracellular constituents on the membrane (Rycroft *et al*., 2006).

*Whole-cell:*

In the whole-cell configuration, the patch of membrane in the tip of the pipette is ruptured by applying gentle suction. While running a test pulse protocol, it is clear when access to the cell is gained due to the sharp cell capacitance spikes that appear, indicating that electrical access to the whole cell has been successfully obtained. Because the membrane patch is ruptured there is a continuous environment between the pipette and cell intracellular solutions, meaning the cell's cytoplasmic constituents will become diluted over time.

*Outside-out:*

After rupturing the membrane patch, i.e. going to whole-cell configuration, the pipette can be slowly withdrawn from the cell until the membrane stretches and breaks. The broken edges of membrane should seal with each other, resulting in the extracellular membrane being in contact with the bath solution, and the intracellular membrane being in contact with the pipette solution. Similar to the cell-attached configuration, this allows investigation of single-channel activity, but using outside-out

patch-clamp means the effect of extracellular agents on the single channels can also be studied (Rycroft *et al*, 2006).

*Perforated patch:*

A slight variation of the WCPC, perforated patch does not rupture the whole patch inside the pipette, but instead perforates it using pore-forming substances in the pipette solution. Nystatin and amphotericin B are two antibiotics that are used for membrane perforation. Perforating the PM in the tip of the pipette rather than rupturing it, gives limited access to the cell. However, $K^+$, $Na^+$ and $Cl^-$ ions are permeable, giving electrical access. $Ca^{2+}$ cannot cross the membrane through the pores that are made, along with higher molecular weight cellular constituents such as ATP (Lippiat, 2008). Perforated patch, therefore, maintains an intracellular environment that is physiological while recording.

## 2.6 Methods of phosphoinositide manipulation

The role of $PIP_2$ and other PIs in the regulation of ion channels can be assessed by mutation of the proposed $PIP_2$-binding regions within these proteins, but is also commonly investigated by altering the levels of membrane PIs themselves. The benefit of this latter method is that the channel in question remains in its WT state, containing no mutations that may or may not interfere with properties other than PI binding.

### 2.6.1 Non-specific methods of altering phosphoinositide concentration

Activation of $G_q$-coupled GPCRs is a common method used to induce PLC activation and the resulting reduction of $PIP_2$ at the PM by hydrolysis (Lee & Rhee, 1995). This method was used by Daleau & Turgeon (1994), who observed that angiotensin II reduced the $I_{Ks}$ current in guinea pig ventricular myocytes, and Matavel & Lopes (2009) in their study into the effects AT1, M1 and BK2 receptor activation on $I_{Ks}$ channel function, who found that activation of $G_q$-coupled receptors regulates $I_{Ks}$ channels in a biphasic manner.

In these kinds of experiments $PIP_2$ depletion occurs, but a multitude of other cellular signalling pathways are also set in motion upon GPCR stimulation. Solely from the hydrolysis of $PIP_2$ to form $IP_3$ and DAG, there are many downstream effects: $IP_3$ binds to the Ins3PR, resulting in $Ca^{2+}$ release from the SR (Lee *et al*., 2003), and DAG activates PKC (Tewson *et al*., 2012) (figure 19). Using receptor activation in an attempt to determine the precise role of $PIP_2$ in a physiological process greatly complicates the interpretation of results.

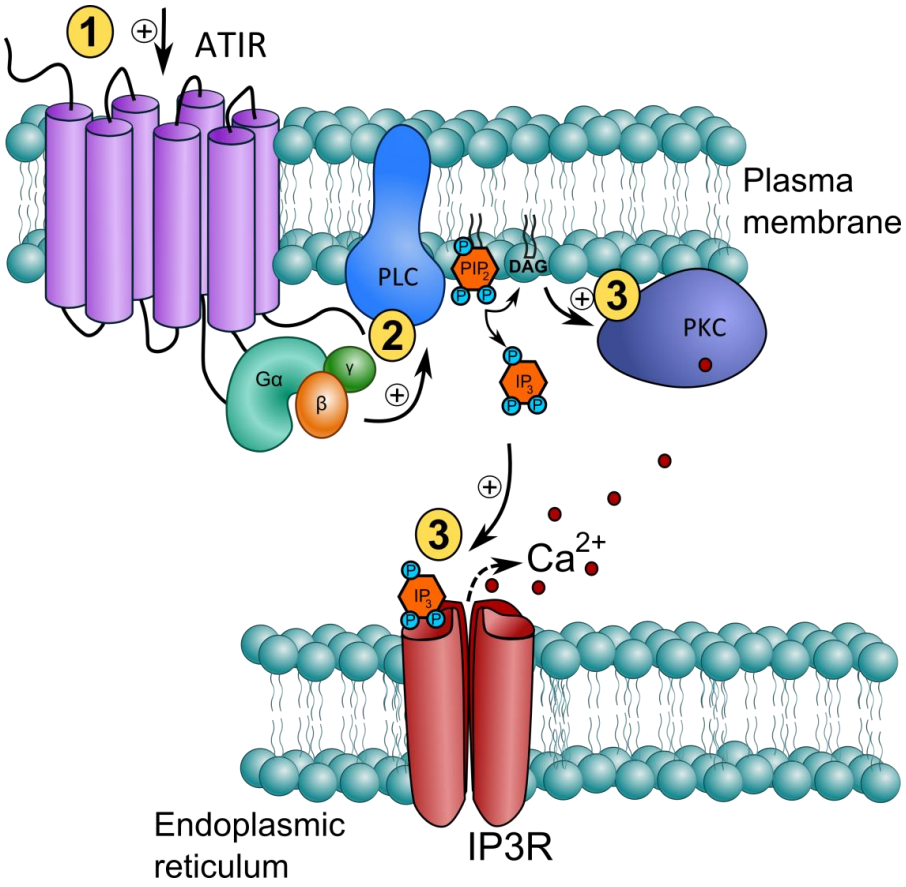


**Figure 19. Signalling downstream of Gq-coupled GPCR activation**. (1) Activation of a $G_q$-coupled GPCR, for example the ATIR by angiotensin II, causes activation of PLC. (2) PLC hydrolyses $PIP_2$ to DAG and $IP_3$. $IP_3$ is released into the cytoplasm while DAG remains anchored in the PM. (3) $IP_3$ binds to the inositol-3-phosphate receptor (Ins3PR) in the ER membrane, which when activated releases $Ca^{2+}$ from the ER (or SR) into the cytoplasm, and DAG activates PKC.

Other methods that can be used, but are unfortunately also non-specific, include the inhibition of PI-kinase activity by wortmannin, the steroid metabolite of the fungi *Penicillium funiculosum*. This technique is widely used to study the effects of $PIP_2$ depletion, because at micromolar concentrations wortmannin inhibits PI4K activity leading to loss of PI4P, the precursor PI to $PIP_2$ (Nakanishi *et al*., 1995; Meyers & Cantley, 1997). This method does not take into account effects on PI4P or the fact that at lower (nanomolar) concentrations, wortmannin inhibits PI3K activity. PI3K inhibition will halt the synthesis of $PIP_3$, a PI shown to bind to KCNQ1 along with many other anionic phospholipids (Thomas *et al*, 2011). Nonetheless, wortmannin has been used by various groups in

studies investigating the effects of $PIP_2$ depletion on $K_v$ channels (Brown *et al*, 2007; Suh & Hille, 2002; Rodriguez-Menchaca *et al*, 2012).

Despite the use of wortmannin providing a means for $PIP_2$ depletion, that lack of its specificity for one PIK means it can only provide crude answers regarding the effects of $PIP_2$ depletion. Distinguishing between the effects of $PIP_2$ and $PIP_3$ depletion on the channel in this situation is not possible. However, using wortmannin as a quick tool to uncover any striking effects of $PIP_2$ depletion can be beneficial and precede more specific studies, and Matavel & Lopes (2009) reported that 100 nM WTM treatment (a concentration that completely inhibits PI3K activity) caused no inhibition of $I_{Ks}$ current in their studies.

### 2.6.2 Phosphoinositide phosphatases

PI phosphatases dephosphorylate a certain PI to another PI without releasing second messengers into the cell, and provide an answer to the problem of non-specific PI-depletion methods. For example, PI 4-phosphatases and PI 5-phosphatases are able to dephosphorylate $PIP_2$ on the 4 and 5 positions, respectively. This results in a decrease of the $PIP_2$ concentration without activation of downstream pathways.

*Voltage-sensitive phosphatases*

In the recent past it was recognised that the voltage-sensor domains contained within some ion channels, such as $K_v$ channels, are not unique in their ability to convert the input of a change in membrane potential to an output of an alteration in protein function (Hossain *et al*., 2008; Murate *et al*., 2005; Sasaki *et al*., 2006).

Voltage-sensitive phosphatases (VSPs) act in a similar way to ion channels, in the respect that a VSP can convert a change in membrane potential into alteration in protein function – in VSPs this is the activation of a phosphatase domain. VSPs are endogenously expressed in some organisms, but can be expressed in experimental systems to enable manipulation of $PIP_2$ levels in the PM. Like voltage-gated ion channels, these phosphatases contain an integral membrane VSD, but instead of a PD the VSP contains a cytoplasmic phosphatase domain. VSPs from ascidian, *Ciona intestinalis,* (Ci-VSP) and zebrafish, *Danio rerio,* (Dr-VSP) both contain a VSD that is homologous to S1–4 (i.e. the VSD) of $K_v$ channels, and a phosphatase domain similar to that of PTEN (Hossain *et al*., 2008).

When the membrane potential changes these VSPs exhibit a gating charge, which suggests a conformational change in the VSD in response to the change in membrane voltage. This conformational change in the VSD is translated into activation of the phosphatase domain, leading to

depletion of surrounding lipid molecules (Murata *et al*., 2005). Murata & Okamura (2007) found that VSPs are activated in response to depolarisation of the membrane, and unlike PTEN, whose substrate is $PIP_3$, these VSPs dephosphorylate $PIP_2$.

The activation of Dr-VSP and Ci-VSP occurs at physiologically relevant membrane potentials, i.e. those that are experienced by myocytes during the cardiac action potential (figure 20). Because of this, these VSPs are useful in deciphering how cellular processes respond to $PIP_2$ depletion. In this project, both Ci-VSP and Dr-VSP were used to deplete $PIP_2$ at the PM whilst recording the response of the $I_{Ks}$ current.

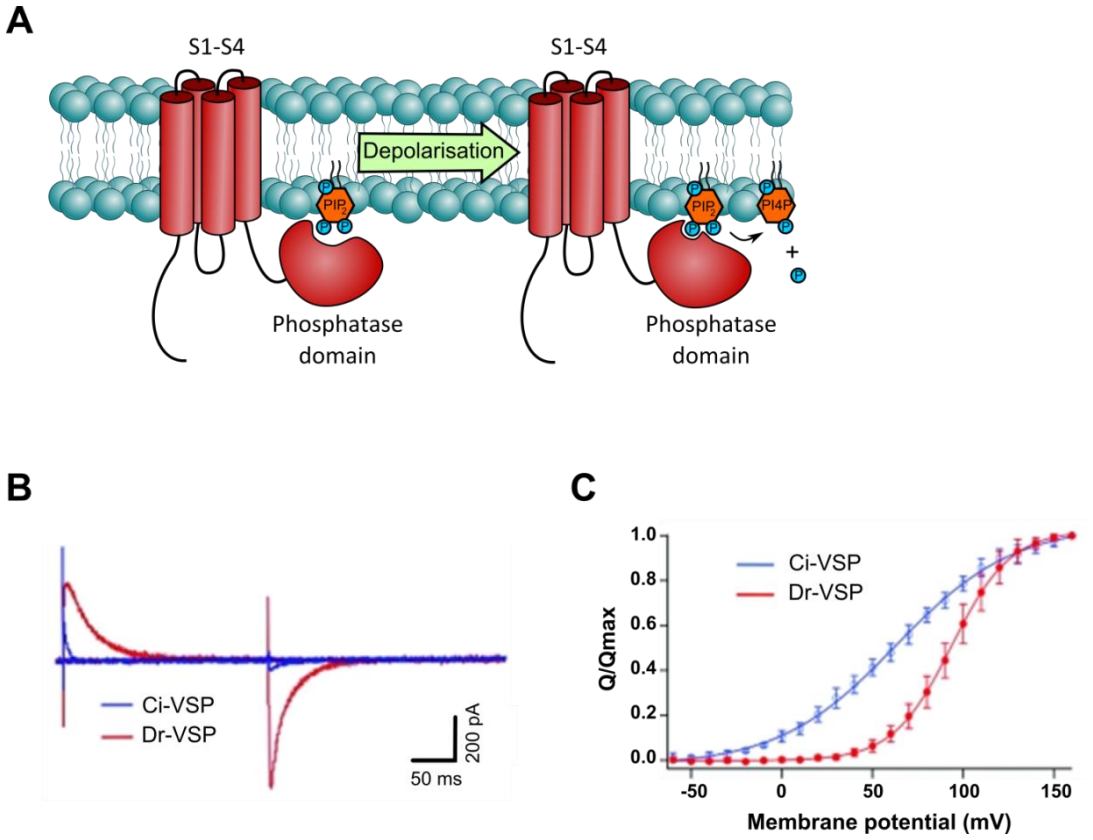


**Figure 20. Structure and activation of voltage-sensitive phosphatases**. **A** – Schematic representation of voltage-sensitive phosphatases. The transmembrane S1–S4 domains are linked to an intracellular phosphatase domain. Depolarisation of the PM activates the voltage-sensitive phosphatase, causing a conformational change in the phosphatase domain to enable dephosphorylation of $PIP_2$ to PI4P. **B** – 'Gating' or sensing currents evoked at 160 mV under whole-cell patch clamp from tsA201 cells transfected with Ci-VSP (blue) and Dr-VSP (red). **C** – charge–voltage (Q–V) relations of Ci-VSP (blue) and Dr-VSP (red). Normalised values of Off-charges are shown as mean and standard deviations, collected from 6 and 5 cells for Ci-VSP and Dr-VSP, respectively. Maximum Off-charges were 2.89 ± 0.3 pC $pF^{-1}$ and 0.11 ± 0.1 pC $pF^{-1}$ for Ci-VSP and Dr-VSP, respectively. **B** and **C** adapted from Okamura et al. (2009).

### 2.6.3 Chemically induced dimerisation systems

The chemically induced dimerisation (CID) systems that have been developed also make use of PI phosphatase activity, but induce lipid depletion in a different way. These systems also avoid the problems faced by other non-specific methods by being selective for particular PI species and preventing the release of second messengers into the cell. CID systems exploit the ability of certain chemicals to bind two different proteins simultaneously, which results in the dimerisation of the two proteins. One such chemical, rapamycin, is an immunosuppressant drug that is used in cancer treatment as it possesses anti-tumour and immunosuppressant properties (Law, 2005).

Rapamycin binds to FK506 binding protein (FKBP) 12, a member of the immunophillin family. This structurally diverse group of proteins possess peptidylprolyl cis-trans isomerase activity (Ballou & Lin, 2008), which is inhibited upon binding of the drug. Tacrolimus (FK506) also binds to FKBP and, like the structurally unrelated cyclophillins, displays immunosuppressant activity when in the protein-drug complex by docking with the protein phosphatase 2B (PP2B) and inhibiting its phosphatase activity. This leads to the phosphorylation of PP2B substrates, including nuclear factor of activated T cells, and as a result of this, a number of genes important in the T cell immune response are not expressed and the immune response is supressed (Barik *et al*., 2006).

The FKBP-rapamycin complex exerts its function in a different way – by binding to the mammalian target of rapamycin (mTOR). mTOR is a serine/threonine kinase that is part of the PI3K-related kinase family, as its catalytic site closely resembles that of PI3K. mTOR has many functions physiologically, including promoting cell growth, proliferation and survival. The binding of mTOR to the FKBP-rapamycin complex via one of its catalytic pockets, known as the FKBP-rapamycin binding (FRB) domain (figure 21), results in the inhibition of some of its functions. As mTOR is upregulated in many cancers, inhibition of mTOR activity can be useful in cancer therapy (Porta *et al*., 2014).

Given that rapamycin binds to both FRB and FKBP, and that these protein domains can be linked to a variety of effector proteins, this system can be used for a wide variety of PI manipulations within a cell. Throughout this project, various constructs containing the FRB and FKBP domains were used. These constructs were either tethered to the location of phosphoinositide (i.e. the PM or Golgi) or contained phosphatase domains (to dephosphorylate PIs).

### 2.6.4 Lipid-depleting constructs used in CID

Constructs that were tethered to cell membranes containing the PIs of interest were linked to the FRB domain. Untagged LYN11-FRB (LYN11-targeted-FRB) (20147, Addgene; deposited by Tobias

Meyer), LYN11-FRB-CFP (38003, Addgene) and LYN11-FRB-mCherry (38004, Addgene; both deposited by Robin Irvine), and Tgn38-FRB from Tamas Balla were used in this project. Only the fragment of mTOR that binds the FKBP-rapamycin complex was contained in the FRB-containing constructs. LYN11-FRB constructs are tethered to the PM by a LYN11 sequence (GCIKSKGKDSA) (Inoue, 2005) which is then attached to the FRB domain, and Tgn38-FRB is tethered to the TGN by using the integral TGN membrane protein, Tgn38, in which a Tyr motif in the cytoplasmic domain is responsible for its localisation (Bos *et al*., 1993). A fluorescent tag was also attached to a number of these constructs to allow their visualisation, and was attached to the C-terminal end of the constructs used here. The names and characteristics of these constructs are shown in table 5.

FKBP-containing constructs were ones that included phosphatase domains or kinase domains: PJ (37999), PJ-SAC (38000), PJ-INPP5E (38001) and PJ-DEAD (38002) (all from Addgene; all deposited by Robin Irvine). All these constructs contain an RFP tag at the N-terminal end. Each of these constructs consists of an RFP domain, SAC1 domain, INPP5E domain and an FKBP domain. The SAC1 domain of these constructs codes for the SAC1 PI-phosphatase, which dephosphorylates PIs on the 4-position. However, interestingly this phosphatase has no activity against $PIP_2$. The INPP5E domain codes for an $IP_3$ 5-phosphatase, which dephosphorylates $PIP_2$ on the 5 position.

In PJ, named so because of its similarity to synaptojanin, both phosphatase domains are active. PJ-SAC contains an inactivating mutation (Asp1263Ala) in the INPP5E domain, and PJ-INPP5E contains an inactivating mutation (Cys779Ser) in the SAC1 domain. Therefore, PJ-SAC dephosphorylates only PI4P at the 4-position, and PJ-INPP5E dephosphorylates only $PIP_2$ at the 5-position. PJ-DEAD contains both inactivating mutations (Asp1263Ala and Cys779Ser). Hence, PJ-DEAD is a control construct (figure 22).

Due to the membrane-tethered nature of FRB-containing constructs, rapamycin addition causes the translocation of the FKBP-containing constructs to that same membrane. Figure 23 uses PJ and LYN11-FRB as an example, showing that after rapamycin is applied to the cells containing these constructs and the consequent dimerisation has occurred, the FKBP-containing construct can exert its phosphatase activity on the PI substrates in the membrane.

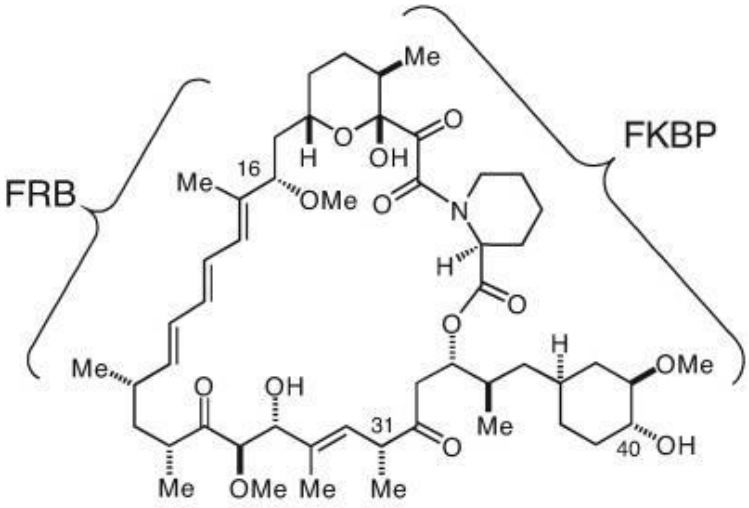


**Figure 21. FRB-Rapamycin-FKBP binding.** The chemical tructure of rapamycin showing the FKBP and FRB binding domains (Edwards *et al*, 2007). FRB and FKBP bind to separate sites on the rapamycin molecule, and as such can bind simultaneously.

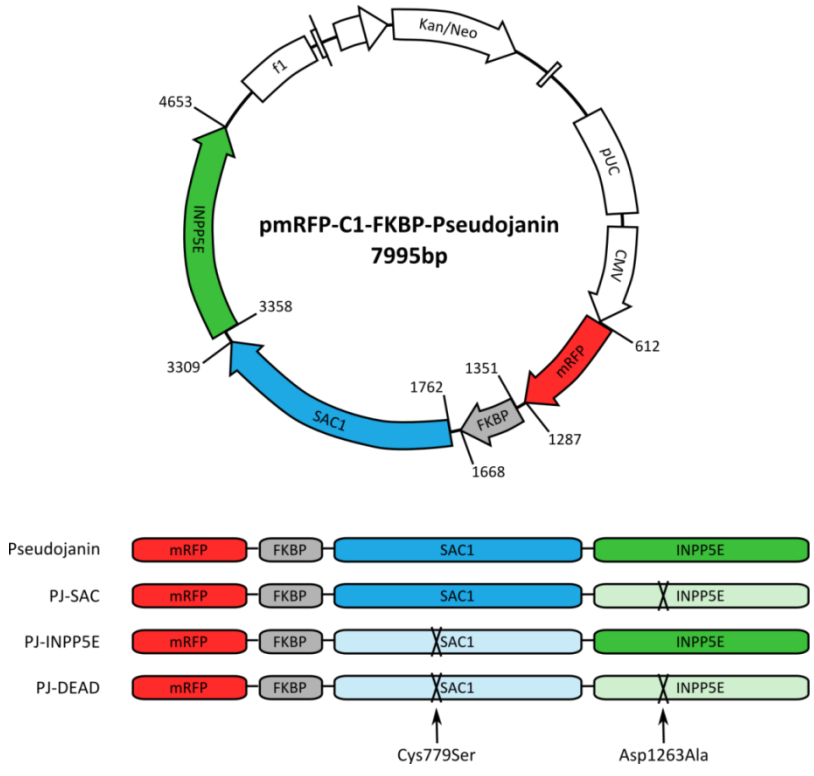


**Figure 22. Lipid-depleting construct plasmid map and mutation location.** Top: plasmid map of the Pseudojanin construct, and bottom: each of the lipid-depleting constructs showing the location of the inactivating mutation (X) and remaining active domains (solid colour).

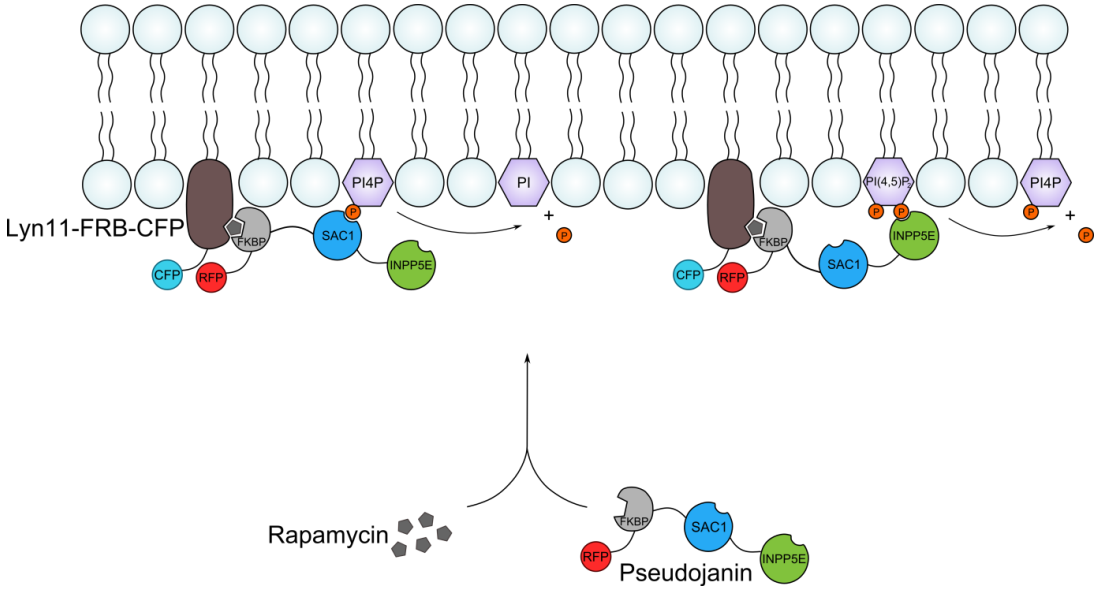


**Figure 23. Rapamycin-induced recruitment of lipid-depleting constructs to the plasma membrane.** Pseudojanin (PJ), a fusion of RFP, SAC1 phosphatase, INPP5E phosphatase and an FKBP domain, and its rapamycin-induced recruitment to the plasma membrane-bound LYN11-FRB-CFP through the simultaneous binding of the FKBP and FRB domains to the rapamycin molecule. The SAC1 phosphatase converts PI4P to PI, and the INPP5E phosphatase converts PI(4,5)$P_2$ ($PIP_2$) to PI4P.

| CID construct | Function |
|---|---|
| Pseudojanin | $PIP_2$ and PI4P depletion |
| PJ-INPP5E | $PIP_2$ depletion |
| PJ-SAC | PI4P depletion |
| PJ-DEAD | No PI depletion (Control) |
| CF-PIPKi | $PIP_2$ synthesis |
| LYN11-FRB-CFP | PM-tethered FRB, tagged with CFP |
| LYN11-FRB-mCherry | PM-tethered FRB, tagged with mCherry |
| LYN11-targeted-FRB | PM-tethered FRB (untagged) |
| Tgn38-FRB | TGN-tethered FRB, tagged with YFP |

**Table 5. CID constructs and their functions.** Each construct used in the rapamycin-induced dimerisation and a summary of its function. PJ, PJ-SAC, PJ-INPP5E, PJ-DEAD and CF-PIPKi are FKBP-containing constructs, and the LYN11- and Tgn38-containing constructs are linked to FRB.

## 2.7 Statistics

All statistical tests were performed in Graphpad Prism. Paired and unpaired Student's T tests and one-way analysis of variance (AVONA) with Dunnett's or Bonferroni's post hoc test were performed

in this project. A Boltzmann function was applied to steady state of activation graphs to fit a sigmoidal curve to the data. These will all be described below.

*Student's t-test*

A Student's t-test is used to determine if the mean of two samples from a normally distributed small population with assumed equal variance are significantly different from one another, taking into account the variability of the data. A t-test calculates the difference between group means divided by the variability within each group (standard error of the difference). To calculate the standard error of the difference, the variance for each group is divided by the number of samples in each respective group, and these two values are then added and the square root of these taken. The formula for a t-test is shown in equation 2.4

$$t = \frac{\overline{X}_T - \overline{X}_C}{\sqrt{\frac{var_T}{n_T} + \frac{var_C}{n_C}}} \qquad \text{Equation 2.4}$$

The t value is then looked up in a table of significance to determine whether the t value is large enough to say that the difference is not likely to have occurred by chance. The confidence level is commonly set at 95%, which means that 5% of the time statistical significance would be found between the two small groups of samples even if there was none. To determine statistical significance using the table of significance, the degrees of freedom must also be known. This is calculated as the sum of the number of samples in both groups minus 2. The p value that is produced must be <0.05 (using a 95% confidence level) to reject the null hypothesis.

A paired t-test is performed when the two sample groups are linked, for example through a 'before and after' observation or when two treatments are applied to the same subject. In this project a paired t-test was used to determine statistical significance before and after drug application. An unpaired t-test is used to determine significance between two groups that are not related in this way.

*One-way ANOVA*

A one-way ANOVA is used to determine statistical significance between the means of 2 or more independent (unrelated) groups in which the samples are normally distributed and have assumed equal variance (although in this project this test was used only when 3 or more groups were compared).

The sum of squares (SS) values for between-group SS ($SS_A$) and within-group SS ($SS_{s/A}$) need to be

calculated to perform a one-way ANOVA. $SS_A$ represents the variation due to treatment, and $SS_{s/A}$ represents variation due to individual differences in the score. $SS_A$ examines the difference between the group means by calculating the variance of each mean around the grand mean, and $SS_{s/A}$ examines error variation around each group mean. The df is calculated for each SS value as shown in equations 2.5 and 2.6, where a is the number of groups, n is the number of samples within each group and N is the total number of samples across all groups.

$$df_A = a - 1 \qquad \text{equation 2.5}$$

$$df_{s/A} = a(n-1) = N - a \qquad \text{equation 2.6}$$

The mean sum of squares (MS) is then calculated for both between- and within-group SS by diving by the df. These values are then used to calculate the F ratio, shown in equation 2.7

$$F = \frac{MS_A}{MS_{s/A}} \qquad \text{equation 2.7}$$

If the estimates of the variance between groups is almost the same (i.e. the null hypothesis is true), then the F ratio will be close to 1. Using an F table, the p value can be estimated using the F ratio and df values.

On its own, a one-way ANOVA determines significance between any groups compared, but does not specify between which groups this is. To do this, a post hoc test is performed.

The Dunnett's multiple comparison test calculates significance between the mean of one group and the means of every other group, and this test determines the confidence levels for each individual comparison. Using this test, each group can be compared to a single control group. The Bonferroni test can be used to compare all pairings of groups to specifically determine statistical significance between groups. This test suggests that the p value should be equal to the alpha value divided by the number of groups, which increases the confidence level. This is introduced because the Bonferroni test takes into account familywise error, which represents the probability that any one of a set of comparisons is a Type I error (due to chance). The more tests that are performed means that the likelihood that significance is proven due to chance increases. To keep the pairwise alpha value at 0.05, the Bonferroni test recalculates the familywise alpha value. For this reason, however, this test can lack power and can lead to a non-significant p value even when a one-way ANOVA has proven significance between one (unknown) pair of groups.

*Boltzmann function*

The Boltzmann function is a form of nonlinear regression analysis that allows a nonlinear curve to be fit to the data to describe it in the form of *y=f(x)*, where *y* is the dependent variable that is measured in the experiment and *x* is the independent variable and its value on the *x* axis is fixed. *f* is the function used to describe the relationship between *y* and *x*. The Boltzmann equation is shown in equation 2.8.

$$y = \frac{1}{\left[1+exp\frac{(V-x)}{Slope}\right]} \qquad \text{equation 2.8}$$

## CHAPTER 3: Characterisation of the rapamycin-induced dimerisation system for investigating the role of $PIP_2$ in $I_{Ks}$ function

### 3.1 Introduction

Among the many mechanisms that regulate the function of the $I_{Ks}$ channel, including β-subunit association (Barhanin *et al*., 1996; Sanguinetti *et al*., 1996; Tinel *et al*., 2000) and β-adrenergic signalling through PKA (Walsh & Kass, 1988), is the interaction between the channel and $PIP_2$. This minor PM PI and major signalling molecule is thought to regulate the $I_{Ks}$ channel by binding near the VSD-PD interface, where it stabilises the open conformation of the channel (Loussouarn *et al*., 2003; Zaydmann *et al*., 2013). Physiologically, $G_{q/11}$-coupled receptor activation leads to $PIP_2$ depletion through activation of PLC (Lee & Rhee, 1995; Rhee & Choi, 1992). The hydrolysis of $PIP_2$ by PLC results in the production of DAG and $IP_3$. It is now known that the loss of $PIP_2$ from the PM in this signalling event is the cause of reduced $I_{Ks}$ current in experimental systems, and that the presence of $PIP_2$ is required for $I_{Ks}$ function (Matavel & Lopes, 2009). The experiments leading to these conclusions included excised-patch recordings, where it was observed that upon excision of the membrane patch the $I_{Ks}$ current would run down. Additionally, subsequent addition of $PIP_2$ to the exposed patch could restore the $I_{Ks}$ current (Loussouarn *et al*., 2003).

Several groups have been involved in locating the region of the KCNQ1 subunit where $PIP_2$ binds or interacts, and a number of regions have been identified. Park and colleagues mutated residues thought to be involved in $PIP_2$ binding and found that $I_{Ks}$ channels containing the KCNQ1 mutations Arg243His, Arg539Trp or Arg555Cys had a reduced affinity for a soluble analogue of $PIP_2$. The mutant channels had a reduced current density, which could be counteracted by direct application of $PIP_2$ to the intracellular side of the PM in excised patches (Park *et al*., *2005*).

Previous work in this laboratory (Thomas *et al*., 2011) identified a $PIP_2$ binding region in the proximal C-terminus of the KCNQ1 subunit. Additionally, in unpublished work it was found that mutations in this $PIP_2$ binding region resulted in an increased level of channel retention in the ER. The ER-retention was observed using confocal microscopy, where co-localisation of the GFP-tagged KCNQ1 subunit with DsRed2-ER, a fluorescent ER-marker, was used as a surrogate marker for retention of the channel in the ER. I have subsequently repeated these experiments and found a similar trend (figure 24). The mechanisms that lead to increased ER-retention of the channel are unknown, but could be due to a role that $PIP_2$-binding plays in anterograde trafficking of the channel from the ER through the secretory pathway to the PM. Alternatively, the introduced mutation(s) could cause protein misfolding and consequently reduce the ability of the channel to exit the ER.

The study of $PIP_2$-binding-region mutations in KCNQ1 has shed some light on how the $I_{Ks}$ channel is regulated by $PIP_2$. However, studies that manipulate $PIP_2$ levels whilst recording the effect on the WT channel are mostly limited to those using non-selective $PIP_2$-depletion mechanisms that may also result in complex downstream effects. Examples include the activation of $G_{q/11}$-coupled receptors, which leads to $PIP_2$ depletion via PLC activation and the release of the second messengers DAG and $IP_3$ into the cell, or addition of wortmannin, which inhibits PI4K activity (and hence the production of PI4P, the precursor to $PIP_2$) at higher concentrations than those that cause PI3K inhibition (Matavel & Lopes, 2009), meaning that effects of both PI3K and PI4K inhibition will be observed. Other limitations of previous studies aiming to investigate the effect of $PIP_2$ manipulation on channel function include the use of the inside-out configuration of patch clamp (Li *et al*., 2005). In the inside-out – or excised-patch – method, the glass micropipette is pulled away from the cell membrane after the formation of a giga-seal, revealing the intracellular side of the PM. This method leads to the gradual loss of $PIP_2$ from the PM and concomitant rundown of the $I_{Ks}$ current (Loussouarn *et al*., 2003). This method is employed as it creates the lower baseline reading of $I_{Ks}$ current density to which the current density after $PIP_2$ addition can be compared, but all other intracellular contents are lost with unknown consequences. Another drawback of this method is that the use of soluble $PIP_2$ analogues is non-physiological (Park *et al*., 2005), and a channel's interaction and reaction with different isoforms of membrane phospholipids may be far more diverse than we imagine. The rapamycin-induced dimerisation system provides an answer to these pitfalls of previously used methods, in that it does not require the use of non-physiological methods of recording (i.e. WCPC and P-WCPC can be used), neither does it result in the release of second messengers (as in the case of GPCR activation).

The rapamycin-induced dimerisation system has been used quite extensively to investigate the effect of manipulating local pools of PIs. For example, Fili and colleagues recruited myotubularin, a PI 3-phosphate, to Rab5-positive endosomes to elucidate whether targeted depletion of PI3P led to disruption of normal endocytic trafficking through these endosomes (Fili *et al*., 2006), and Dickson and colleagues depleted PI4P at the PM, Golgi or both to determine the location of $PIP_2$ precursor pools of PI4P, using the $PIP_2$-sensitive KCNQ2/3 current as an indicator of $PIP_2$ depletion (Dickson *et al*., 2014). This system has also been used to selectively deplete $PIP_2$ at the PM to determine the role of $PIP_2$ in transient receptor potential (TRP)M8 channel activity, and transferrin and epidermal growth factor receptor internalisation (Varnai *et al*., 2006). Others have also used this system to investigate how manipulation of $PIP_2$ at the PM affects a range of different ion channels (Kruse *et al*., 2012; Lukacs *et al.*, 2007; Suh & Hille, 2006)

Despite its extensive and varied use in PI manipulation over the past decade, the rapamycin-induced dimerisation system has not been used solely for the purpose of investigating the role of $PIP_2$ in the regulation of trafficking and function of the $I_{Ks}$ channel. As a consequence, a number of experiments were initially performed to characterise whether this dimerisation system can be used to model the effect of $PIP_2$ depletion on the $I_{Ks}$ channel.

This chapter describes the characterisation of this system, which involves direct dephosphorylation of PI4P and/or $PIP_2$ at the PM (Suh & Hille, 2006; Varnai *et al*., 2006). Rapamycin is used as a dimerising agent, which is added to cells expressing two constructs that bind to distinct sites on the rapamycin molecule. When rapamycin is added to the cells, a construct containing PI-phosphatase domains is recruited to a PM-anchored construct. The dimerisation of the two constructs brings the phosphatase domains into close proximity to the PM, where $PIP_2$ and PI4P may reside. By dephosphorylating instead of hydrolysing $PIP_2$ during intact cellular recordings, this system avoids the problems associated with other PI manipulation systems.

**Aims:** To characterise and establish the effectiveness of the rapamycin-inducible dimerisation system in investigating the role of $PIP_2$ in the regulation of function and trafficking of the $I_{Ks}$ channel.

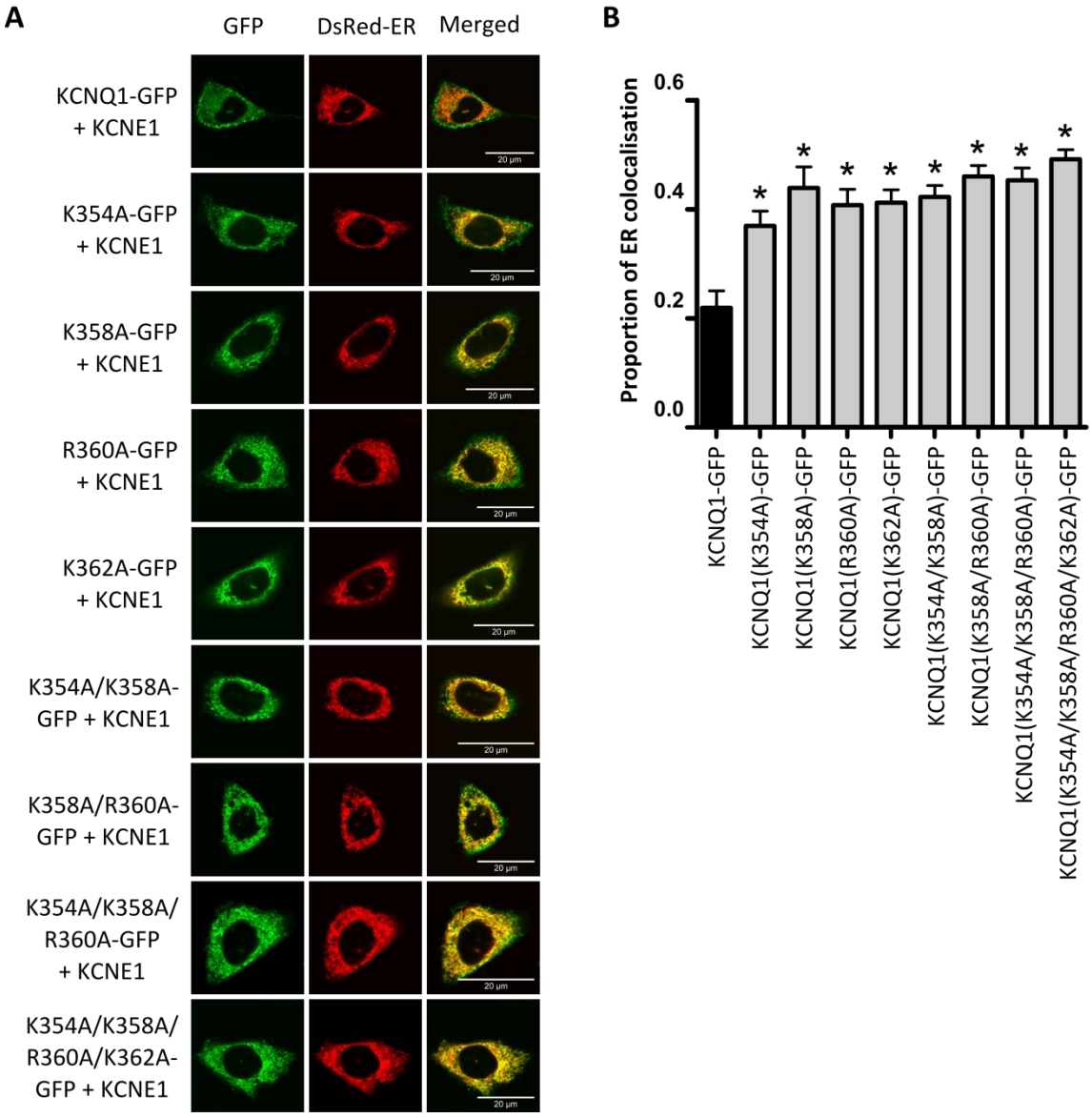


**Figure 24. The effect of introducing mutations into a $PIP_2$-binding region in the C-terminus of KCNQ1 on the localisation of the KCNQ1 subunit in CHO-K1 cells. A** – The localisation of WT and mutant KCNQ1-GFP in CHO-K1 cells. The left column shows the GFP-tagged KCNQ1 subunit, the middle column shows DsRed-ER, an ER marker, and the right column shows the merged images. The top row shows the localisation of the WT KCNQ1-GFP with KCNE1, while all rows below show the localisation of the mutant KCNQ1 subunits investigated (all n=25, except KCNQ1(R360A-GFP), where n=24). **B** – A bar graph showing the proportion of ER colocalisation of the WT and mutant KCNQ1-GFP subunits. Data are presented as mean ± SE.

## 3.2 Methods

### 3.2.1 Constructs

The following plasmids were obtained from Addgene and were deposited there by the Irvine laboratory, with exception of LYN11-targeted-FRB, which was deposited by the Tobias Meyer laboratory.

PJ (#37999), PJ-SAC (#38000), PJ-INPP5E (#38001) and PJ-DEAD (#38002) consist of the same domains. PJ-SAC contains the Asp1263Ala mutation to inactivate the INPP5E domain, and PJ-INPP5E contains the Cys779Ser mutation to inactivate the SAC1 domain. PJ-DEAD contains the inactivated version of both enzymes. These four constructs are contained within the pmRFP-C1 mammalian expression vector (figure 22). For full cloning details please refer to Hammond *et al*. (2012).

LYN11-FRB-CFP (#38003) and LYN11-targeted-FRB (#20147) contain both the PM-targeted LYN11 sequence and the FRB domain, while LYN11-FRB-CFP also contains a C-terminal CFP domain. LYN11-targeted-FRB is contained in the pC4-RHE mammalian expression vector, and LYN11-FRB-CFP is contained in the pmCherry-N1 mammalian expression vector. Both of these PM-targeted FRB-containing constructs were used interchangeably throughout the project, and the term LYN11-FRB will be used in their place.

### 3.2.2 Electrophysiology

Currents were recorded from a KCNQ1-eGFP/KCNE1 stably expressing HEK293 cell line (referred to as HEK-$I_{Ks}$ cells from here onwards) either untransfected or transiently transfected. Untransfected HEK-$I_{Ks}$ cells were used 48–72 hours after seeding, and transfected HEK-$I_{Ks}$ cells were used 48–72 hours after transfection. For lipid-depleting experiments, 500 ng PJ, PJ-SAC, PJ-INPP5E or PJ-DEAD were transfected with 500 ng of LYN11-FRB. Additionally, where stated, 100 ng empty eYFP-C1 vector was transfected for identification of successfully transfected cells by epifluorescence. All transfections were performed using FuGENE HD as described in section 2.1.3.

WCPC was used to record the $I_{Ks}$ current in HEK-$I_{Ks}$ cells, and $I_{K1}$ or $I_{Kr}$ currents from HEK-$I_{K1}$ and HEK-$I_{Kr}$ cells, respectively. WCPC experiments were carried out at room temperature using an Axopatch 200B amplifier (Axon Instruments) and transfected cells were identified using epifluorescence. Extracellular bath solution for all experiments with HEK-$I_{Ks}$ and HEK-$I_{K1}$ cells contained (mM) 150 NaCl, 5 KCl, 10 HEPES, 2 $MgCl_2$ and 1 $CaCl_2$ (pH 7.4 with NaOH). Extracellular bath solution for all experiments with HEK-$I_{Kr}$ cells contained (mM) 150 NaCl, 4 KCl, 10 HEPES, 1 $MgCl_2$, 1.8 $CaCl_2$ and 5

glucose (pH 7.4 with NaOH). In all experiments, $R_{series}$ was compensated for by 70% using the amplifier circuitry.

The intracellular pipette solution contained (mM) 150 KCl, 10 HEPES, 5 EGTA, 2 $MgCl_2$, 1 $CaCl_2$ and 5 $(Na)_2ATP$ (pH 7.2 with KOH). Pipette resistance, when pipettes were filled with intracellular solution, was 2–3 MΩ. Pipette tips were coated with SigmaCote (SL2, Sigma) after being filled with intracellular solution, to reduce pipette capacitance. After seal formation and successful membrane-patch rupture, cells were left to dialyse for 2 minutes before recording. I-V protocols were recorded by holding the cells at -80mV before a 6-second activation pulse, from -80 mV to +50 mV or +80 mV, in 10 mV increments. After the 6-second pulse, a 2-second repolarising step to -20 mV was used to record tail currents, before stepping back to -80 mV.

In experiments involving the perfusion of rapamycin (sc-3504, Santa Cruz) over the cells, extracellular solution containing rapamycin (5 µM) was perfused for 2 minutes, and perfusion was then returned to rapamycin-free extracellular solution.

Inclusion criteria for recordings to be analysed included: a leak current of less than 10% macroscopic current amplitude, maximum current amplitude of 19 nA and maximum $R_s$ of 10 MΩ. Data from all experiments was analysed using Clampfit (Molecular Devices, CA, U.S.A) and GraphPad Prism (San Diego, CA, U.S.A). Current density (CD) was calculated by normalising the peak current value at the end of each activating pulse to the cell capacitance (nA/pF). Peak tail current density (PTCD) was calculated by normalising the peak tail current value at the start of the repolarising pulse to cell capacitance (pA/pF). Steady state activation (SSA) curves allow the voltage at which half-maximal activation occurs ($V_{0.5}$) to be calculated. These were constructed by plotting normalised PTCD density values ($y/y_{max}$) against membrane potential ($V_m$). Curves were fitted and $V_{0.5}$ values were determined using a Boltzmann function.

### 3.2.3 Statistical analysis

Data are expressed as mean ± SE, and Boltzmann functions were generated using GraphPad Prism. A Student T Test was used to determine statistical significance for single comparisons ($p < 0.05$), and a one-way ANOVA ($p < 0.05$) was used to determine significance when multiple groups were compared. For one-way ANOVA analyses, a Bonferroni's multiple comparison test was used to compare each pair of conditions. Where possible, an asterisk (*) was added to graphs to indicate that the comparison to control reached statistical significance.

### 3.2.4 Confocal microscopy

Live cells were imaged using a Zeiss LSM510 (Mark 4) (Carl Zeiss, Oberkochen, Germany) confocal microscope and a Plan-Apochromat 63x oil lens objective. CFP and YFP were excited with a multiline argon laser (CFP: wavelength 458 nm; YFP: wavelength 488 nm) and RFP was excited using a helium/neon laser (wavelength 543 nm). When imaging CFP, a 465-510 bandpass (BP) filter was used, and when imaging GFP a 505–530 BP filter was used, which prevented bleedthrough of the GFP fluorescence into the spectrum of the RFP signal. YFP was also imaged using the 505–530 BP filter to avoid overlap between the YFP and RFP spectra. Images were taken at 1024 x 1024 frame size, a bit depth of 16bit, and a pinhole aperture of 1 Airy unit.. The two FPs expressed were excited sequentially to prevent crosstalk. Post image acquisition, images were median-filtered, converted to RGB format and saved in a JPEG/TIFF format.

## 3.3 Results

### 3.3.1 Cellular localisation of lipid-depleting constructs, and their rapamycin-induced dimerisation

Before using the lipid-depleting constructs for patch clamp experiments, their cellular localisation and ability to translocate after the addition of rapamycin was determined using confocal microscopy. When lipid-depleting constructs were transiently expressed in HEK293 cells they showed a cytoplasmic and nuclear localisation, which was observed using confocal microscopy. In the same cells, the LYN11-FRB-containing constructs were localised to the PM (figure 25A).

To assess the effectiveness of rapamycin at inducing the dimerisation of the FRB- and FKBP-containing constructs, rapamycin (5μM) was added to cells so the movement of the constructs could be visualised. When rapamycin was added to cells expressing PJ and LYN11-FRB, PJ visibly translocated to the PM in approximately 30 seconds (figure 26). Quantification of PJ and LYN11-FRB signal intensity confirm that PJ moved from the cytoplasm to the PM on addition of rapamycin (figure 26B), and this is supported by the observation that the RFP signal intensity in the cytoplasm reduced by approximately 60% and 70% after 1 and 2 minutes of rapamycin (5 μM) perfusion, respectively (figure 26C).

### 3.3.2 Effect of transiently expressing lipid-depleting constructs in HEK-$I_{Ks}$ and CHO-K1 cells on the $I_{Ks}$ current

After the cellular localisation of the constructs and ability to induce translocation of PJ to the PM upon the addition of rapamycin was confirmed, these constructs were transiently expressed in HEK-$I_{Ks}$ cells, and the $I_{Ks}$ current was recorded using WCPC (figure 26). The enzymatically dead mutant of the lipid-depleting constructs, PJ-DEAD, was expressed with LYN11-FRB in these cells to ensure no change in the $I_{Ks}$ current occurred that could not be attributed to the phosphatase domains. Expression of PJ-DEAD and LYN11-FRB had no effect on the $I_{Ks}$ current density or peak tail current density (figure 26B).

Next, PJ-SAC, PJ-INPP5E or PJ were transiently expressed with LYN11-FRB in HEK- $I_{Ks}$ cells, and the $I_{Ks}$ current was recorded in each condition. Expression of PJ-SAC with LYN11-FRB had no effect on the $I_{Ks}$ current density or peak tail current density (p=NS), while expression of PJ-INPP5E with LYN11-FRB resulted in a reduction of the $I_{Ks}$ current density and peak tail current density by approximately 50% ($p<0.005$ across all voltages analysed for both CD and PTCD). The current in the presence of PJ-INPP5E and LYN11-FRB was also significantly reduced compared to PJ-DEAD and LYN11-FRB ($p<0.001$ across all voltages analysed for both CD and PTCD). Expression of PJ with LYN11-FRB in HEK-$I_{Ks}$ cells caused a complete loss of the $I_{Ks}$ current ($p<0.001$ across all voltages analysed for CD and PTCD when compared to control or PJ-DEAD). It was therefore not possible to normalise tail current values for currents recorded when the cells were expressing PJ and LYN11-FRB, and the voltage-dependence of activation curve could not be plotted. Analysis of the voltage-dependence of activation during expression of PJ-DEAD, PJ-SAC or PJ-INPP5E with LYN11-FRB showed there was an effect on the $V_{0.5}$ values (figure 26C), which was significant ($p<0.05$) between control and PJ-DEAD and PJ-INPP5E, respectively. There was also a significant difference ($p<0.05$) between the $V_{0.5}$ values for PJ-SAC and PJ-INPP5E.

Due to the complete loss of $I_{Ks}$ current that was observed in the HEK-$I_{Ks}$ cells when expressing PJ with LYN11-FRB, a similar experiment was performed in CHO-K1 cells to rule out cell-type-specific effects. The $I_{Ks}$ channel subunits, KCNQ1 and KCNE1, were expressed in CHO-K1 cells with LYN11-FRB and PJ-DEAD, and the resulting current was recorded in WCPC. While expressing PJ-DEAD, an $I_{Ks}$-like current was recorded. However, the expression of PJ in place of PJ-DEAD caused almost a complete loss of the current (figure 30) as previously seen in HEK-$I_{Ks}$ cells, which was significant ($p<0.0001$) across all voltages analysed for both CD and PTCD.

### 3.3.3 The effect of rapamycin-induced recruitment of lipid-depleting constructs on the cellular localisation of Tubby in HEK293 cells

To determine if the loss of $I_{Ks}$ current observed in both HEK-$I_{Ks}$ cells and CHO-K1 cells transiently expressing the $I_{Ks}$ channel subunits was due to loss of $PIP_2$, Tubby-YFP was used as an indicator of $PIP_2$ depletion. Tubby-YFP binds to $PIP_2$ through its $PIP_2$-binding domain, and upon depletion of $PIP_2$, Tubby-YFP will move from the PM (Quinn *et al*., 2008).

PJ-DEAD or PJ were transiently expressed with LYN11-FRB and Tubby-YFP in HEK293 cells, and a time series experiment was performed using confocal microscopy. When rapamycin (5 µM) was added to cells expressing PJ-DEAD or PJ with LYN11-FRB and Tubby-YFP, both PJ-DEAD and PJ translocated from the cytosol/nucleus to the PM in 30–45 seconds (figures 28A & 29A). In cells expressing PJ-DEAD, there was no movement of Tubby-YFP after translocation of PJ-DEAD to the PM (figure 28). However, in cells expressing PJ, Tubby-YFP underwent a rapid redistribution after the translocation of PJ to the PM. At 45 seconds after rapamycin addition, Tubby-YFP had partially moved from the PM to the cytosol, and at 60 seconds had showed a complete redistribution (figure 29). Quantification of PJ/PJ-DEAD and Tubby-YFP signal intensity before and after rapamycin (5 µM) addition confirms that as PJ-DEAD moved from the cytoplasm to the PM on addition of rapamycin (figure 28B), the fluorescence intensity did not alter for Tubby-YFP; however, when PJ translocated from the cytoplasm to the PM, Tubby-YFP moved from the PM to the cytoplasm. These observations are supported by the analysis of fluorescence signal intensity in a region of cytoplasm, which showed the decrease in RFP signal intensity from both PJ and PJ-DEAD after rapamycin (5µM) addition, and the concomitant increase in Tubby-YFP in cells expressing PJ, but not in those expressing PJ-DEAD (figure 28C & 29C).

### 3.3.4 Effect of transiently expressing PJ in the absence of LYN11-FRB in HEK-$I_{Ks}$ cells

Due to the inhibition of the $I_{Ks}$ current that occurred when PJ or PJ-INPP5E were transiently expressed with the PM-located LYN11-FRB in both HEK-$I_{Ks}$ and CHO-K1 cells, PJ was expressed in HEK-$I_{Ks}$ cells without its dimerisation partner, LYN11-FRB.

Expression of PJ alone in HEK-$I_{Ks}$ cells did not cause complete inhibition of the $I_{Ks}$ current, as previously seen when PJ was expressed with LYN11-FRB. Instead, only a partial reduction (approximately 50%) of the $I_{Ks}$ current and tail current densities was observed, but this was also a significant reduction compared to control cells (current density: 30 mV & 40 mV = $p<0.05$; 50 mV = $p<0.01$; peak tail current density: 30 mV = $p<0.05$; 40 mV & 50 mV = $p<0.01$) (figure 31).

### 3.3.5 Effect of incubating HEK-$I_{Ks}$ cells in OptiMEM I whilst transiently expressing lipid-depleting constructs

In all previous experiments, HEK293 cells and cell lines were incubated in MEM media (detailed in section 2.1.1). This media is supplemented with FBS and antibiotics to support the growth of the cultured cells. Whilst this does not commonly interfere with experiments, FBS does contain many non-defined growth-promoting and survival-enhancing factors, which could potentially interfere with the dimerisation system components. To ensure that contents of the culture media were not interfering with the dimerisation system and causing the $I_{Ks}$ inhibition observed, OptiMEM I was used in place of MEM media to culture the cells in the 24 hours prior to patch clamp experiments.

Incubation of HEK-$I_{Ks}$ cells expressing PJ and LYN11-FRB in OptiMEM I for 24 hours prior to WCPC recording still resulted in complete inhibition of the $I_{Ks}$ current, showing no difference between the incubation of cells in OptiMEM I and the normal culture media. There remained a significant ($p<0.0001$) inhibition of the $I_{Ks}$ current in the OptiMEM I-incubated cells compared to control (figure 32).

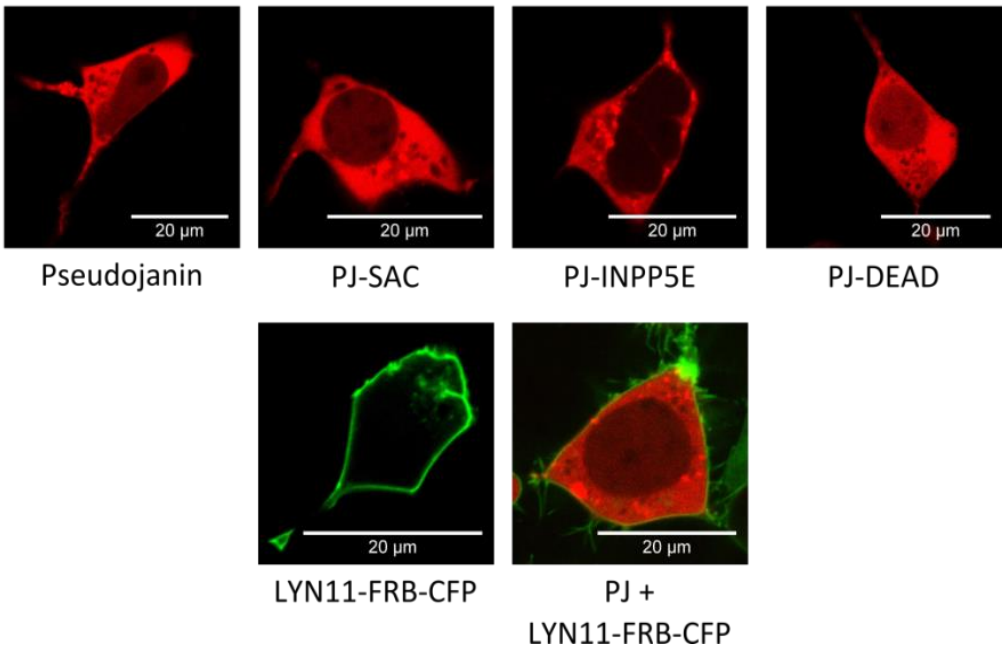


**Figure 25. The localisation of lipid-depleting constructs in HEK293 cells.** Cellular localisation of lipid-depleting constructs and LYN11-FRB-CFP construct. LYN11-FRB-CFP has a plasma membrane localisation, and the lipid-depleting constructs are expressed throughout the cytoplasm and nucleus. Pseudojanin and LYN11-FRB-CFP show the same expression pattern when expressed together. Images were taken using confocal microscopy. Images taken using confocal microscopy.

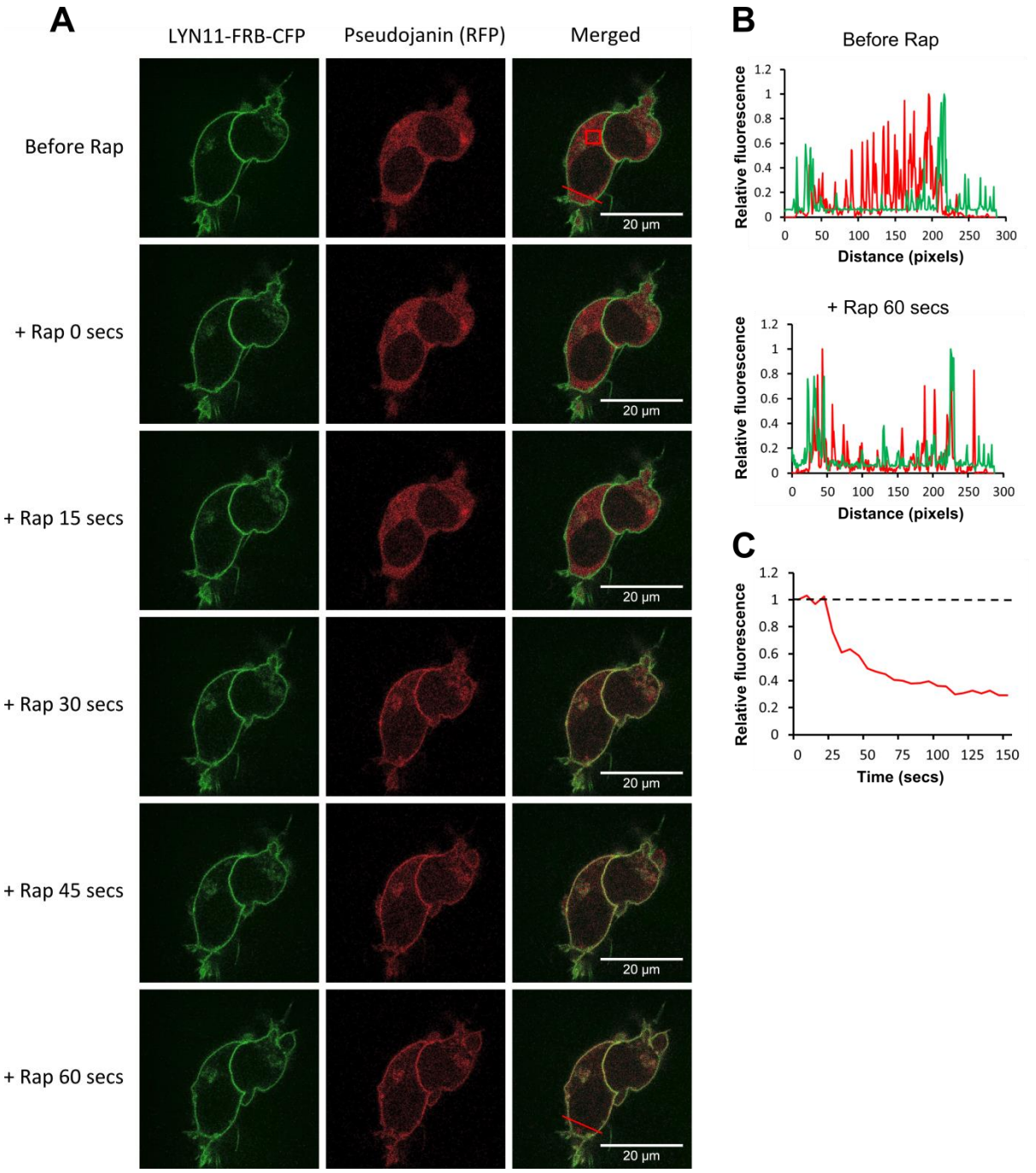


**Figure 26. The localisation of pseudojanin (PJ) in HEK293 cells before and after the rapamycin-induced recruitment of PJ to the PM in HEK293 cells. A –** Rapamycin(Rap)-induced dimerisation of PJ and LYN11-FRB-CFP. Pseudojanin contains the FKBP domain, which translocates to the PM, the location of LYN11-FRB, upon addition of Rap. Top panel: Before rapamycin addition. Lower panels: Increasing time after addition of rapamycin showing the increased PM signal of the PJ construct. Images taken using confocal microscopy. **B** – Normalised ($y/y_{max}$) intensity of fluorescence of CFP and RFP along the red line illustrated in the top right-hand image (before Rap) and bottom right-hand image (+ Rap 60 secs) in **A**. Green represents LYN11-FRB-CFP and red represents PJ in both **B** and **C**. **C** – Change in fluorescence intensity over time measured from region of interest shown by red box in top right-hand image in **A** (relative to value from image 1 of time series). Representative cell response (n=3).

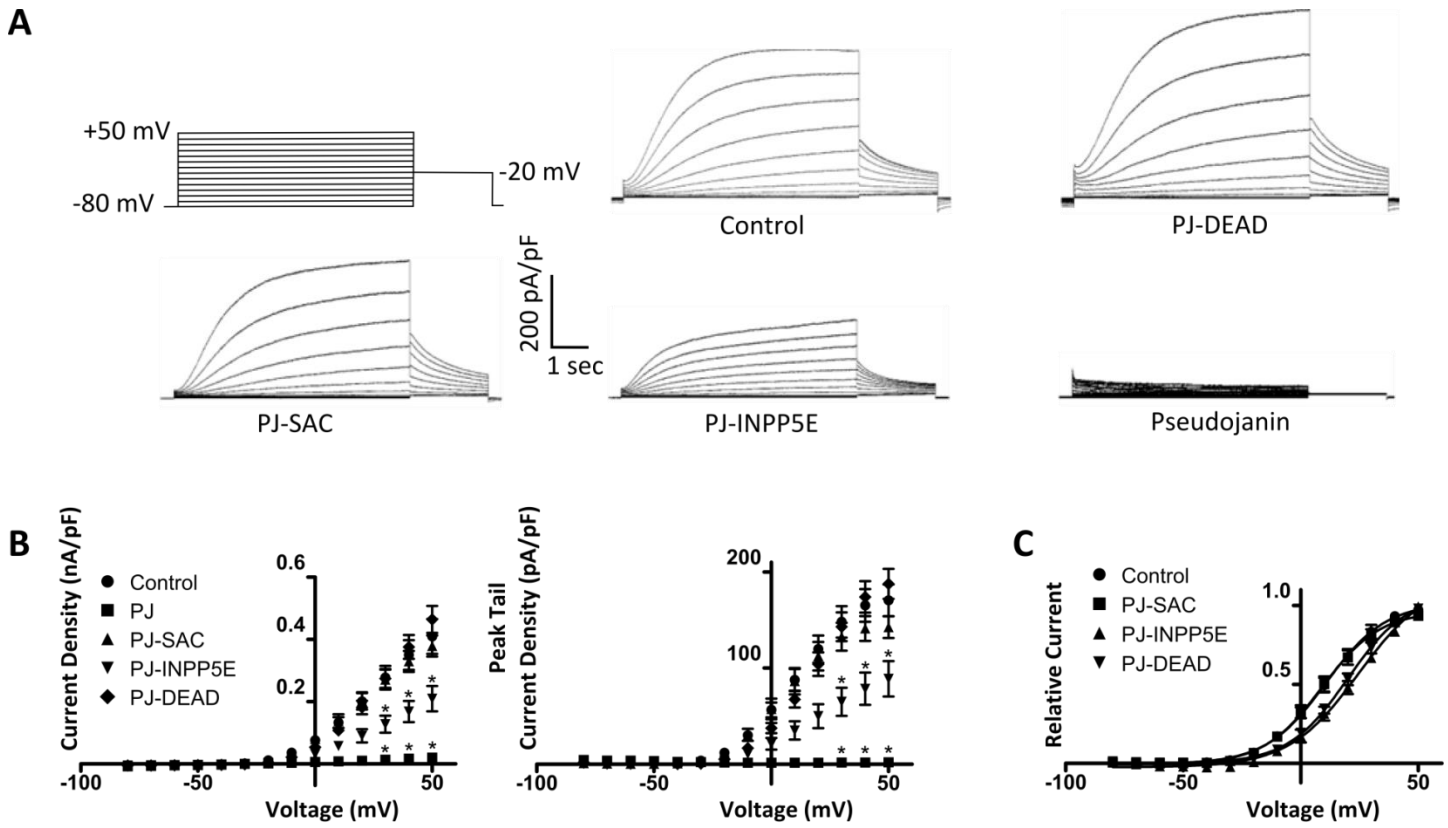


**Figure 27. The effect of expressing lipid-depleting constructs on the $I_{Ks}$ current in HEK-$I_{Ks}$ cells.**

**A –** Voltage protocol and representative traces of currents recorded in WCPC from HEK-$I_{Ks}$ cells (control), and HEK-$I_{Ks}$ transiently expressing PJ-DEAD, PJ-SAC, PJ-INPP5E or Pseudojanin (PJ) with LYN11-FRB. **B –** Mean current density (left) and peak tail current density (right) of currents recorded in WCPC from HEK-$I_{Ks}$ cells while transiently expressing PJ (n=11), PJ-SAC (n=23), PJ-INPP5E (n=24) or PJ-DEAD (n=16) with LYN11-FRB. **C –** Steady state of activation curve, constructed by plotting normalised peak tail current densities ($y/y_{max}$) against test potential with a Boltzmann function (solid lines) Data are presented as mean ± SE. A one-way ANOVA with Bonferroni's post hoc test was used to determine statistical significance between all group pairs in **B**, between +30 mV and +50 mV, and between $V_{0.5}$ values obtained from **C**. A Boltzmann function was applied to data in **C** to fit a sigmoidal curve.

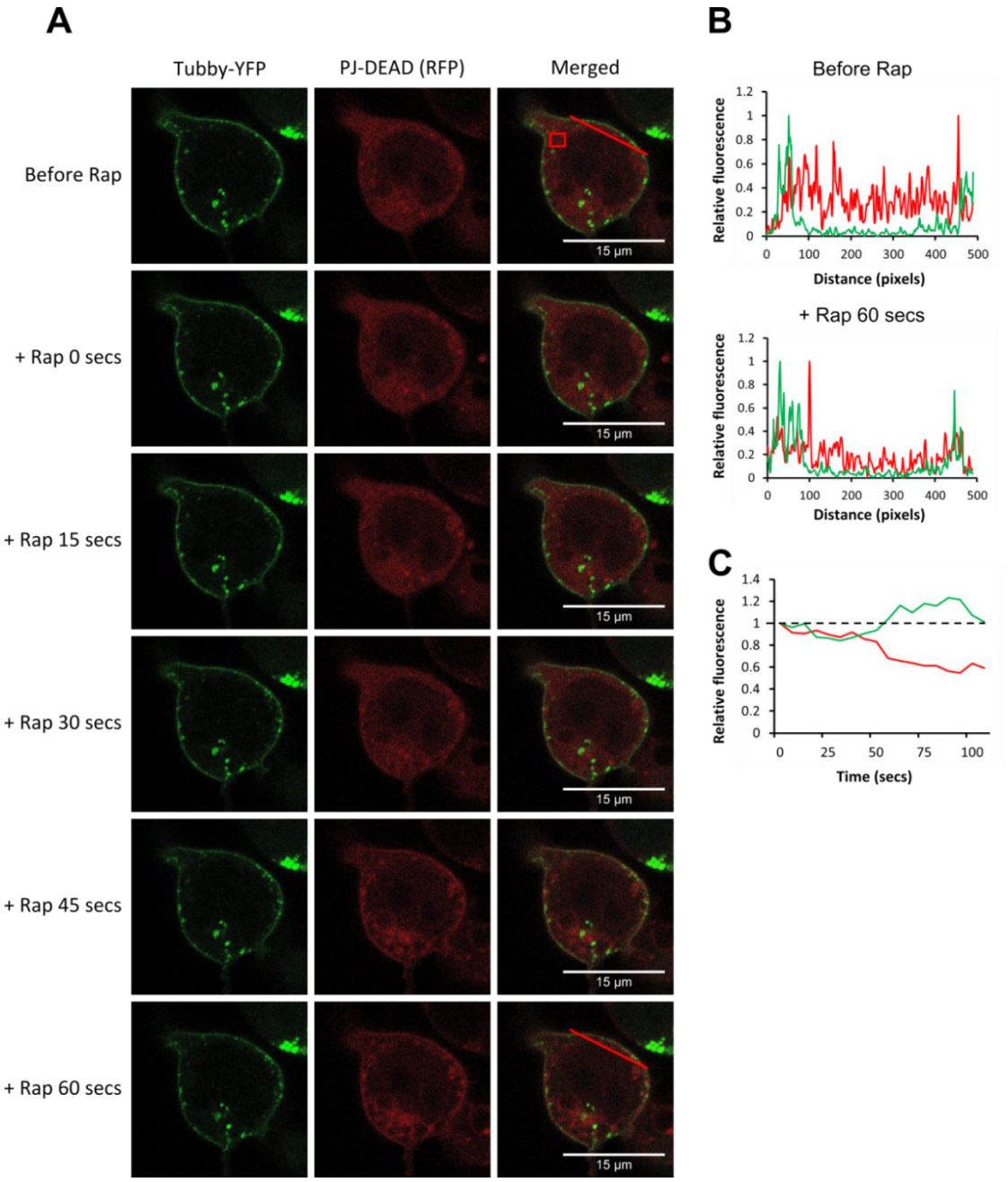


**Figure 28. The localisation of Tubby-YFP in HEK293 cells before and after the rapamycin-induced recruitment of PJ-DEAD to the PM in HEK293 cells**. **A –** Rapamycin (Rap)-induced dimerisation of PJ-DEAD and LYN11-targeted-FRB (the untagged version of LYN11-FRB) and the localisation of Tubby-YFP. Pseudojanin contains the FKBP domain, which translocates to the PM, the location of LYN11-targeted-FRB, upon addition of rapamycin (Rap). Tubby localises to the PM in the presence of a sufficient concentration of $PIP_2$. Top panel: Before rapamycin addition. Lower panels: Increasing time after addition of rapamycin showing the increased PM signal of PJ-DEAD, whilst Tubby-YFP remains at the PM. Images taken using confocal microscopy. **B** – Normalised ($y/y_{max}$) intensity of fluorescence of YFP and RFP along the red line illustrated in the top right-hand image (before Rap) and bottom right-hand image (+ Rap 60 secs) in **A**. Green represents Tubby-YFP and red represents PJ-DEAD in both **B** and **C**. **C** – Change in fluorescence intensity over time measured from region of interest shown by red box in top right-hand image in **A** (relative to value from image 1 of time series). Response from one cell (n=1).

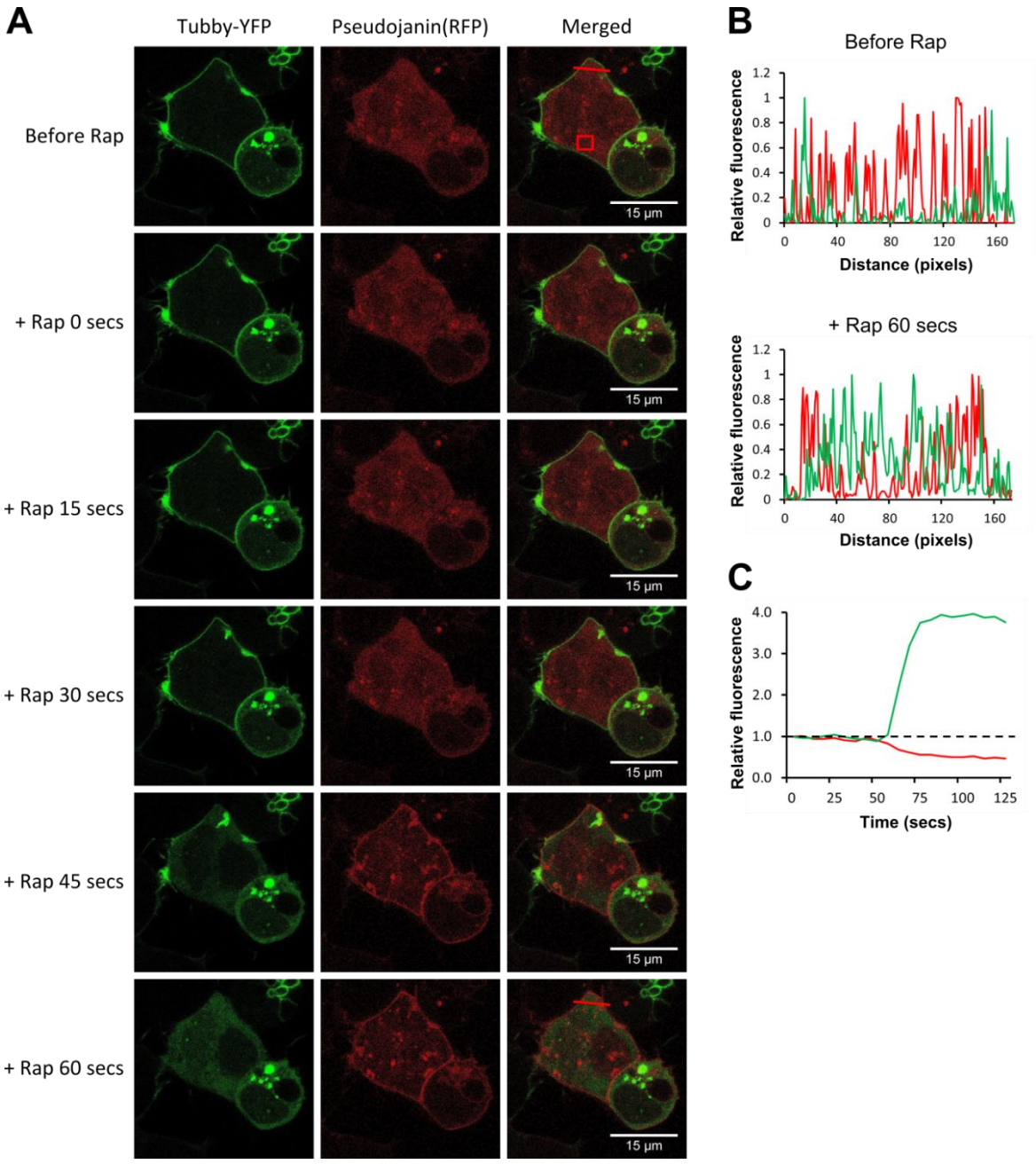


**Figure 29. The localisation of Tubby-YFP in HEK293 cells before and after the rapamycin-induced recruitment of PJ to the PM in HEK293 cells. A** – Rapamycin (Rap)-induced dimerisation of Pseudojanin (PJ) and LYN11-targeted-FRB (the untagged version of LYN11-FRB) and the localisation of Tubby-YFP. Pseudojanin contains the FKBP domain, which translocates to the PM, the location of LYN11-targeted-FRB, upon addition of rapamycin (Rap). Tubby localises to the PM in the presence of a sufficient concentration of $PIP_2$. Top panel: Before rapamycin addition. Lower panels: Increasing time after addition of rapamycin showing the increased PM signal of PJ and the redistribution of Tubby-YFP from the PM to the cytosol. Images taken using confocal microscopy. **B** – Normalised ($y/y_{max}$) intensity of fluorescence of YFP and RFP along the red line illustrated in the top right-hand image (before Rap) and bottom right-hand image (+ Rap 60 secs) in **A**. Green represents Tubby-YFP and red represents PJ in both **B** and **C**. **C** – Change in fluorescence intensity over time measured from region of interest shown by red box in top right-hand image in **A** (relative to value from image 1 of time series). Representative cell response (n=4).

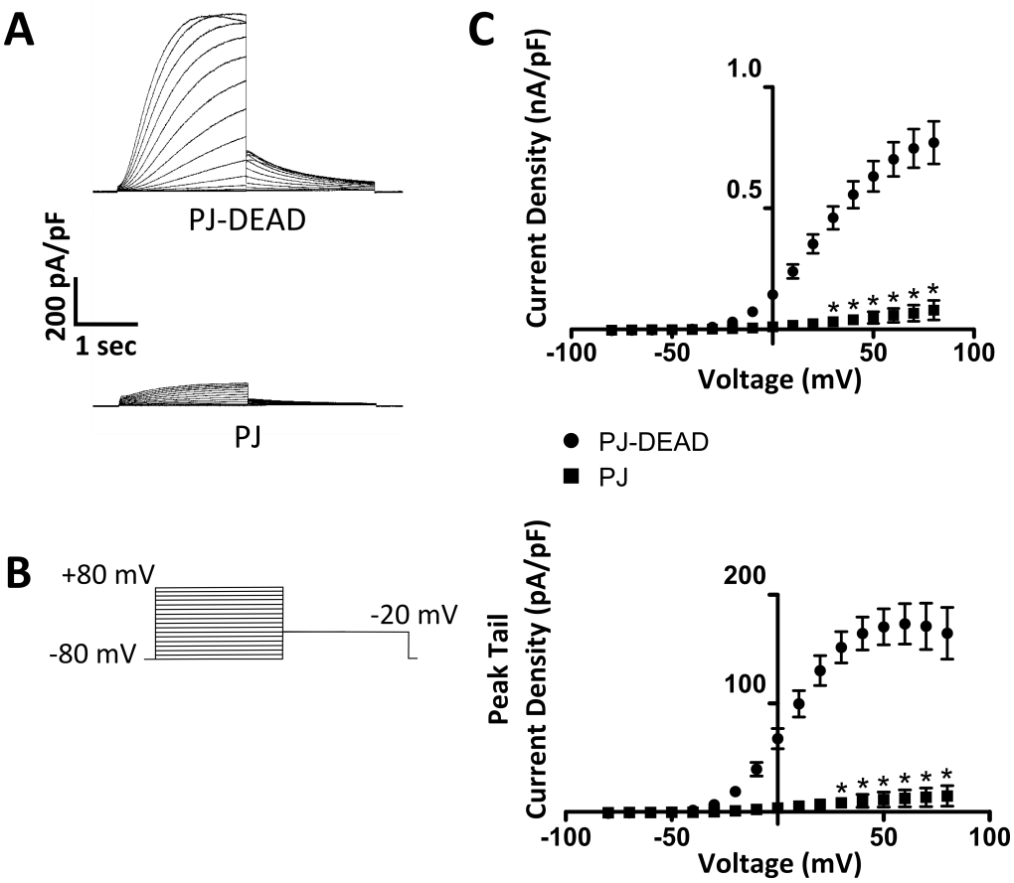


**Figure 30. The effect of expressing CID constructs in CHO-K1 cells expressing the $I_{Ks}$ channel**. **A –** Representative traces of currents recorded in WCPC from CHO-K1 cells transiently expressing the KCNQ1 and KCNE1 subunits with LYN11-FRB and either PJ-DEAD or PJ. **B –** Voltage protocol used to elicit current recorded. **C –** Mean current density (top) and peak tail current density (bottom) of currents recorded in WCPC from CHO-K1 cells transiently expressing the KCNQ1 and KCNE1 subunits with LYN11-FRB and either PJ-DEAD (n=12) or Pseudojanin (PJ) (n=11). Data are presented as mean ± SE. An unpaired t-test was performed to determine statistical significance between groups in **C**, at voltages between +30 mV and +80 mV.

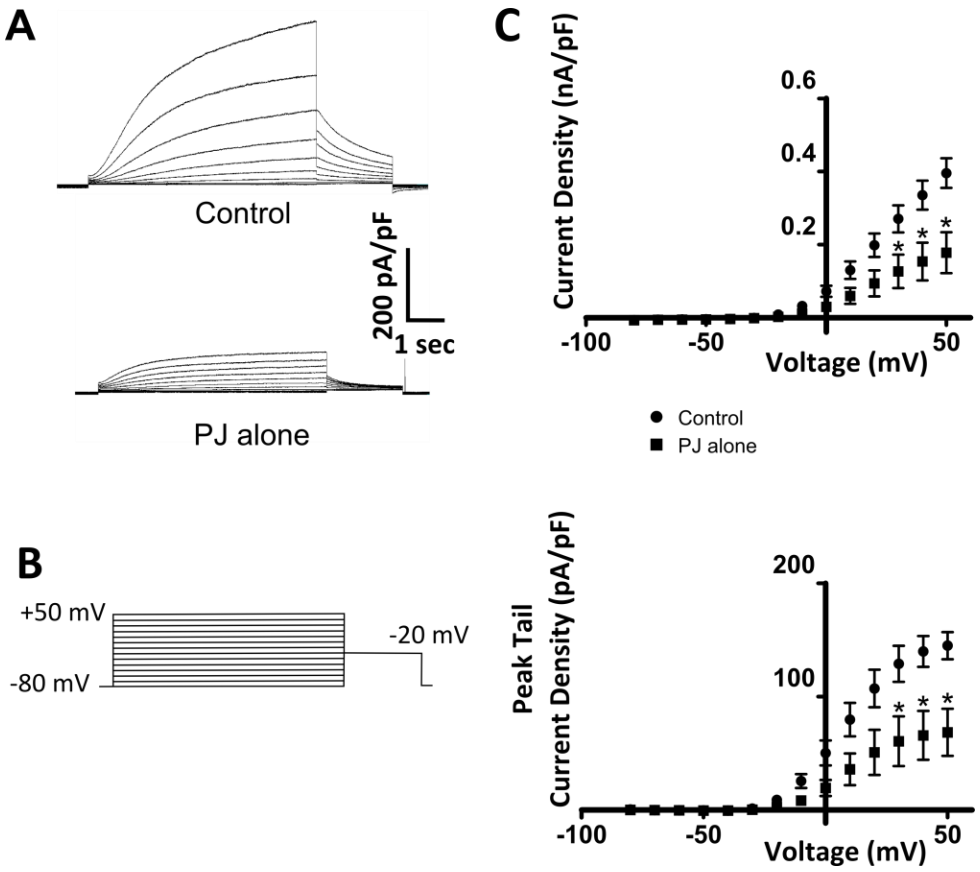


**Figure 31. The effect of expressing pseudojanin alone on the $I_{Ks}$ current in HEK-$I_{Ks}$ cells. A –** Representative traces of currents recorded in WCPC from untransfected HEK-$I_{Ks}$ cells (control), and HEK-$I_{Ks}$ cells transiently expressing PJ. **B** – Voltage protocol used to elicit current recorded. **C –** Mean current density (top) and peak tail current density (bottom) of currents recorded in WCPC from untransfected HEK-$I_{Ks}$ cells (control; n=12) and HEK-$I_{Ks}$ cells transiently expressing PJ (n=12). Data are presented as mean ± SE. An unpaired t-test was performed to determine statistical significance between groups in **C**, at voltages between +30 mV and +50 mV.

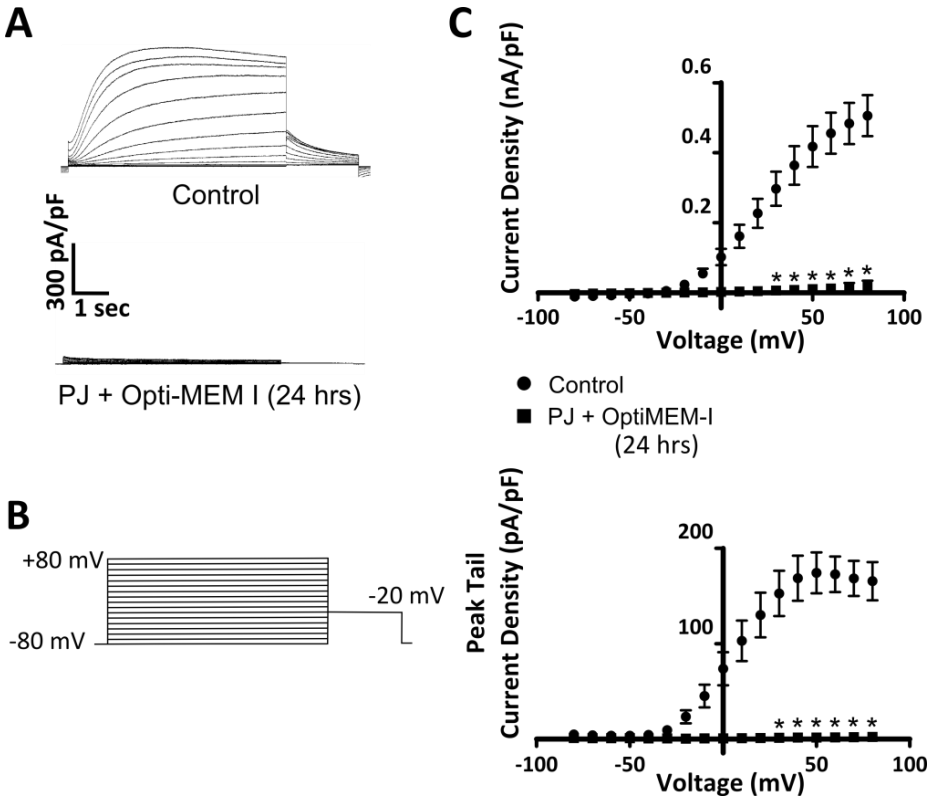


**Figure 32. The effect of expressing lipid-depleting constructs on the $I_{Ks}$ current in HEK-$I_{Ks}$ cells incubated in Opti-MEM I. A** – Representative traces of currents recorded in WCPC from untransfected HEK-$I_{Ks}$ cells (control; n=9), and HEK-$I_{Ks}$ cells transiently expressing PJ and LYN11-FRB that were incubated in Opti-MEM I for 24 hours prior to recording (n=10). **B** – Voltage protocol used to elicit current recorded. **C** – Mean current density (left) and peak tail current density (right) of currents recorded in WCPC from untransfected HEK-$I_{Ks}$ cells (control) and HEK-$I_{Ks}$ cells transiently expressing PJ and LYN11-FRB that were incubated in Opti-MEM I for 24 hours prior to recording. Data are presented as mean ± SE. An unpaired t-test was performed to determine statistical significance between groups in **C**, at voltages between +30 mV and +80 mV.

### 3.3.6 Effect of transiently overexpressing lipid-depleting constructs in CHO-K1 cells transiently expressing KCNQ1 without KCNE1

To investigate whether the KCNE1 subunit plays a role in the $I_{Ks}$ inhibition that occurred in HEK-$I_{Ks}$ cells and CHO-K1 cells expressing the $I_{Ks}$ channel subunits, the KCNQ1 subunit was transiently expressed in CHO-K1 cells with LYN11-FRB and either PJ or PJ-DEAD. CHO-K1 cells were used here instead of HEK-$I_{Ks}$ cells because the outward steady state current from the homomeric KCNQ1 channel is not large enough to be effectively distinguished from the macroscopic endogenous outward HEK293-cell current.

Expression of KCNQ1 with PJ-DEAD and LYN11-FRB in CHO-K1 cells elicited a current resembling that of the homomeric KCNQ1 channel in WCPC. However, when PJ and LYN11-FRB were expressed together, there was a drastic and significant loss of the KCNQ1 steady state ($p<0.0001$ across all voltages analysed) and tail currents ($p<0.0005$ across all voltages analysed) (figure 33). As there was virtually no resulting tail current when expressing PJ with LYN11-FRB, the voltage-dependence of activation curve could not be plotted.

### 3.3.7 Effect of transiently overexpressing lipid-depleting constructs in HEK-$I_{K1}$ cells, and the effect of recruiting the lipid-depleting constructs to the plasma membrane using rapamycin

As other $K^+$ currents contribute to phase-3 repolarisation, the sensitivity of these to expression of the lipid-depleting constructs was investigated. For comparison with the $I_{Ks}$ channel expressed in the HEK-$I_{Ks}$ cell line, the $I_{K1}$ (Kir2.1) channel was stably expressed in HEK293 cells, and the resulting cell line named HEK-$I_{K1}$. The use of this cell line enabled further investigation into whether the effect of lipid-depleting construct expression is specific to KCNQ1-containing channels.

LYN11-FRB and either PJ-DEAD, PJ-INPP5E or PJ were transiently expressed in HEK-$I_{K1}$ cells, and inward currents were recorded in WCPC using the voltage protocol shown in figure 34B.

Transient expression of PJ-DEAD, PJ-INPP5E or PJ with LYN11-FRB in HEK-$I_{K1}$ cells caused no change to the $I_{K1}$ current when compared to untransfected HEK-$I_{K1}$ cells (p=NS) (figure 34A & C). As the $I_{K1}$ current was not affected by expression of the lipid-depleting constructs with LYN11-FRB, it was possible to record the effect of FRB-FKBP dimerisation by perfusing rapamycin over the cells.

First, untransfected HEK-$I_{K1}$ cells were subjected to repeated I-V protocols every 1 minute to record the stability of the $I_{K1}$ current over a prolonged period of time. When repeated I-V relationships were recorded in untransfected HEK-$I_{K1}$ cells, there was no change in peak inward current density (p=NS) and no change in the I-V relationship over time (figure 35A, E & F).

Once it had been established that the $I_{K1}$ current remained stable over a prolonged recording period in WCPC, the rapamycin-induced dimerisation experiments were performed. Rapamycin (5μM) was perfused over HEK-$I_{K1}$ cells expressing PJ-DEAD and LYN11-FRB for 2 minutes after the completion of the first I-V recording. The $I_{K1}$ current was recorded every minute for 8 minutes. Over a period of 8 minutes, there was no change in peak inward current density (p=NS) or I-V relationship over time (figure 35B & G). The same experiment was repeated in HEK-$I_{K1}$ cells expressing PJ-INPP5E and LYN11-FRB, and after 8 minutes there was no change in the peak inward current density (p=NS). Finally, rapamycin was added to cells expressing PJ and LYN11-FRB. After rapamycin (5 μM) perfusion for 2 minutes there was a gradual but complete inhibition of the peak inward $I_{K1}$ current density over approximately 6 minutes ($p<0.05$ at +1 min rap, and $p<0.005$ at +2 minutes rap onwards), with only endogenous HEK293 current remaining from 6 minutes (figure 35C & G). This current at all time points after the addition of rapamycin was significantly reduced compared to control ($p<0.001$ across all time points analysed) and PJ-DEAD ($p<0.001$ across all time points analysed).

### 3.3.8 Effect of transiently overexpressing lipid-depleting constructs in HEK-$I_{Kr}$ cells, and the effect of recruiting the lipid-depleting constructs to the plasma membrane using rapamycin

In addition to the $I_{Ks}$ and $I_{K1}$ currents, the $I_{Kr}$ current plays a major role in phase-3 repolarisation, and is a major component of the repolarisation reserve. In light of the different response to lipid-depleting construct expression of the $I_{Ks}$ and $I_{K1}$ currents, the effect of this expression on the $I_{Kr}$ current was also investigated. Similar to the HEK-$I_{Ks}$ and HEK-$I_{K1}$ cell lines, a HEK-$I_{Kr}$ cell line was made (HEK293 cells stably expressing the $I_{Kr}$ [hERG] channel) to allow effective comparison between the different channels.

PJ or PJ-DEAD were expressed with LYN11-FRB in HEK-$I_{Kr}$ cells, and the resulting current was recorded using WCPC using the voltage protocol shown in figure 36B.

Transient expression of LYN11-FRB with either PJ-DEAD or PJ in HEK-$I_{Kr}$ cells had no effect on the $I_{Kr}$ current when compared to the current elicited from untransfected HEK-$I_{Kr}$ cells (figure 36A & C). As the $I_{Kr}$ current was not affected by co-expression of PJ or PJ-DEAD with LYN11-FRB, it was possible to record the effect of FRB-FKBP dimerisation by perfusing rapamycin over the cells.

First, untransfected HEK-$I_{Kr}$ cells were subjected to repeated I-V protocols every 2 minutes to record the $I_{Kr}$ current and its stability over 10 minutes. When repeated I-V relationships were recorded in untransfected HEK-$I_{Kr}$ cells there was only a minor reduction in the peak tail current density (p=NS) (figure 37 A & E) and no change in the I-V relationship over the period of the experiment (p=NS) (figure 37D).

Once the relative stability of the $I_{Kr}$ current in untransfected HEK-$I_{Kr}$ cells was established, rapamycin (5 µM) was perfused onto HEK-$I_{Kr}$ cells expressing PJ-DEAD and LYN11-FRB for 2 minutes after completion of the first I-V recording. Over a period of 10 minutes, there was a small reduction in peak tail current density, which was not significant (p=NS) and was similar to untransfected cells, and there was no change in the I-V relationship over time (figure 37B & F). When rapamycin was perfused over HEK-$I_{Kr}$ cells expressing PJ and LYN11-FRB for 2 minutes, there was a small inhibition of the peak tail current (figure 37B & F) beyond that seen in untransfected HEK-$I_{Kr}$ cells and cells expressing PJ-DEAD and LYN11-FRB, but this was not significant (p=NS). At t=0 mins, there was no significant difference between PJ or PJ-DEAD compared to control, and PJ compared to PJ-DEAD (assessed using a one-way ANOVA with Bonferroni's multiple comparison test). From t=2 mins onwards there remained no significant difference between PJ and control, whilst there was a significant difference between PJ-DEAD and control ($p<0.05$).

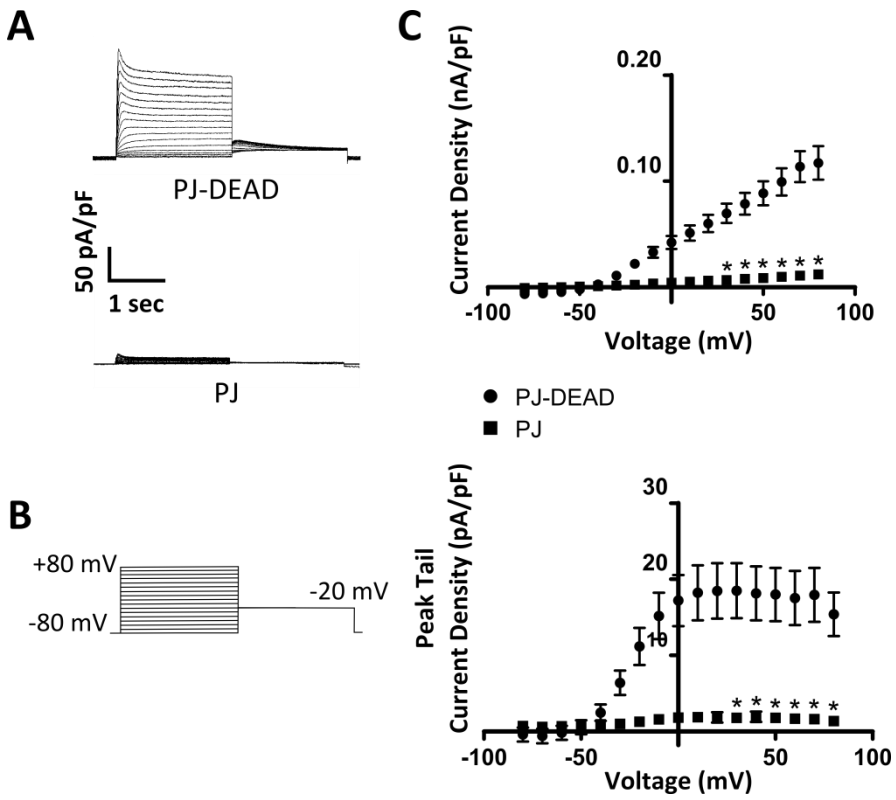


**Figure 33. The effect of expressing lipid-depleting constructs in CHO-K1 cells expressing the homomeric KCNQ1 channel. A –** Representative traces of currents recorded in WCPC from CHO-K1 cells transiently expressing the KCNQ1 subunit with LYN11-FRB and either PJ-DEAD or PJ. **B –** Voltage protocol used to elicit current recorded. **C –** Mean current density (left) and peak tail current density (right) of currents recorded in WCPC from CHO-K1 cells transiently expressing the KCNQ1 subunit with LYN11-FRB and either PJ-DEAD (n=11) or Pseudojanin (n=10). Data are presented as mean ± SE. An unpaired t-test was performed to determine statistical significance between groups in **C**, at voltages between +30 mV and +80 mV.

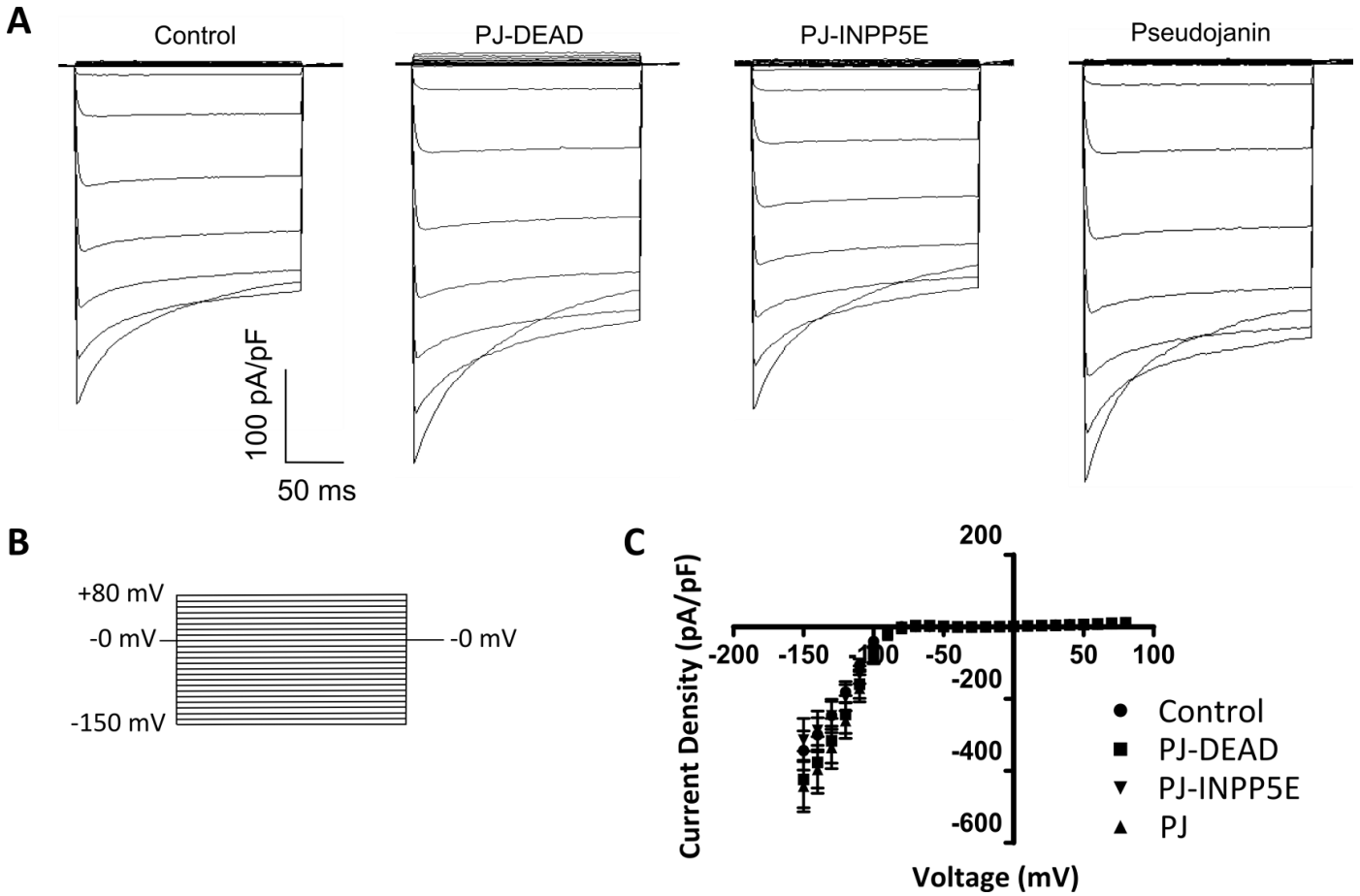


**Figure 34. The effect of expressing lipid-depleting constructs on the $I_{K1}$ current in HEK-$I_{K1}$ cells.**

**A –** Representative traces of currents recorded in WCPC from HEK-$I_{K1}$ cells (control), and HEK-$I_{K1}$ transiently expressing PJ-DEAD, PJ-INPP5E or PJ with LYN11-FRB. **B** – Voltage protocol used to elicit the currents recorded. **C –** Mean current density of currents recorded in WCPC from untransfected HEK-$I_{K1}$ cells (control; n=11) and HEK-$I_{K1}$ cells transiently expressing PJ (n=9), PJ-INPP5E (n=11) or PJ-DEAD (n=9) with LYN11-FRB. Data are presented as mean ± SE.

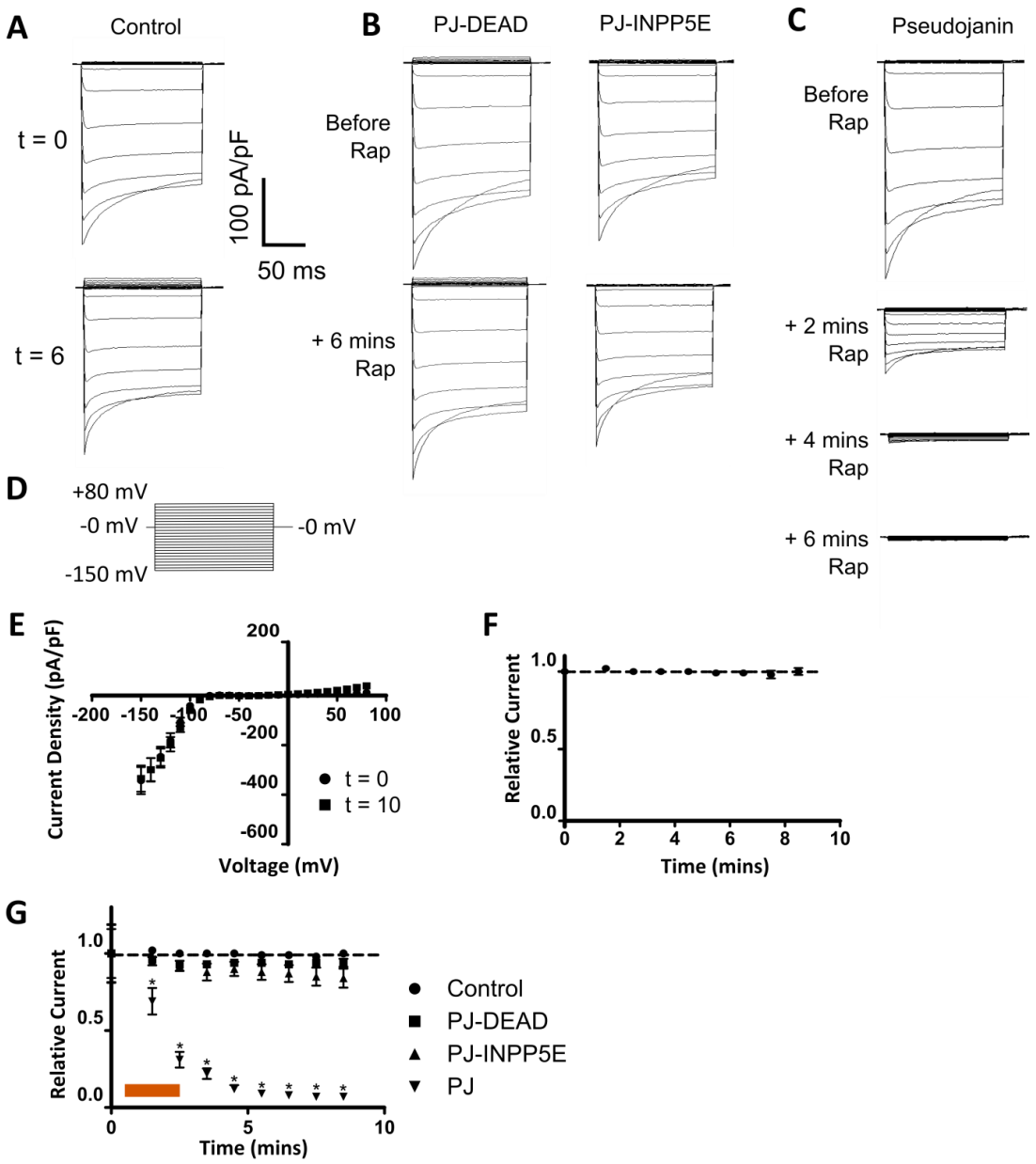


**Figure 35. Stability of the $I_{K1}$ current and the effect of rapamycin-induced recruitment of lipid-depleting constructs on the $I_{K1}$ current in HEK-$I_{K1}$ cells in whole-cell patch clamp. A** – Representative current traces from HEK-$I_{K1}$ cells recorded at t = 0 and 6 minutes in WCPC. **B** – Representative current traces recorded in WCPC from HEK-$I_{K1}$ cells expressing PJ-DEAD or PJ-INPP5E with LYN11-FRB, before and 6 minutes after the start of rapamycin (5µM) addition. **C** – Representative current traces recorded in WCPC of HEK-$I_{K1}$ cells expressing PJ with LYN11-FRB, before and 2, 4 and 6 minutes after the start of rapamycin (5µM) addition. **D** – Voltage protocol used to elicit the currents recorded in WCPC. **E** – Mean current density from untransfected HEK-$I_{K1}$ cells recorded at t = 0 and t = 10 minutes in WCPC. **F** – Current density at -150 mV over approximately 8 minutes, relative to that at t = 0, from untransfected HEK-$I_{K1}$ cells recorded in WCPC. **G** – Current density at -150 mV recorded in WCPC over a period of 8 minutes after the start of rapamycin (5µM) addition (orange bar), relative to the value before rapamycin addition, in HEK-$I_{K1}$ cells (control; n=11) or HEK-$I_{Ks}$ cells expressing PJ-DEAD (n=9), PJ-INPP5E (n=11) or PJ (n=9) with LYN11-FRB. Data are presented as mean ± SEM.

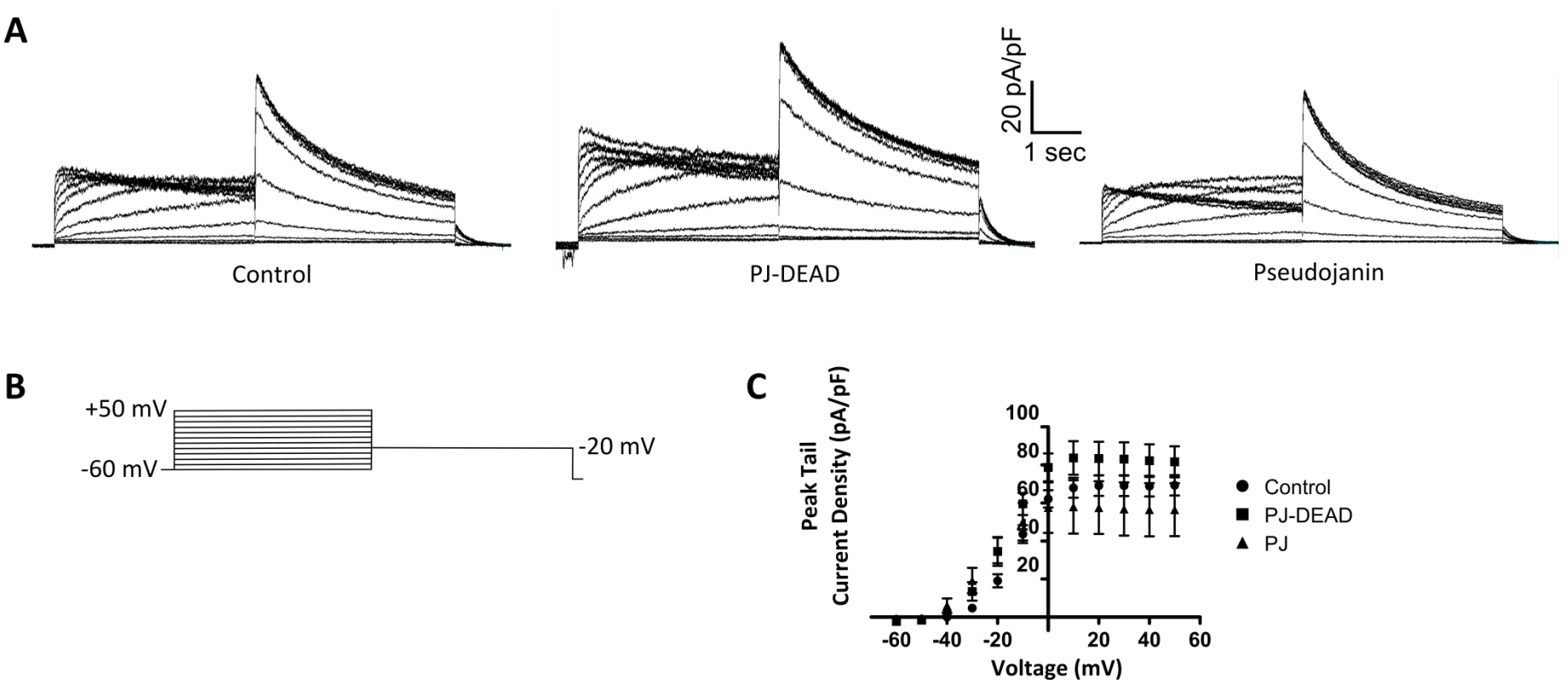


**Figure 36. The effect of expressing lipid-depleting constructs on the $I_{Kr}$ current in HEK-$I_{Kr}$ cells**. **A –** Representative traces of currents recorded in WCPC from HEK-$I_{Kr}$ cells (control), and HEK-$I_{Kr}$ cells transiently expressing PJ-DEAD or PJ with LYN11-FRB. **B** – Voltage protocol used to elicit the currents recorded. **C –** Mean current density of currents recorded in WCPC from HEK-$I_{Kr}$ cells (control; n=9) and HEK-$I_{Kr}$ cells transiently expressing PJ (n=10) or PJ-DEAD (n=10) with LYN11-FRB. Data are presented as mean ± SE.

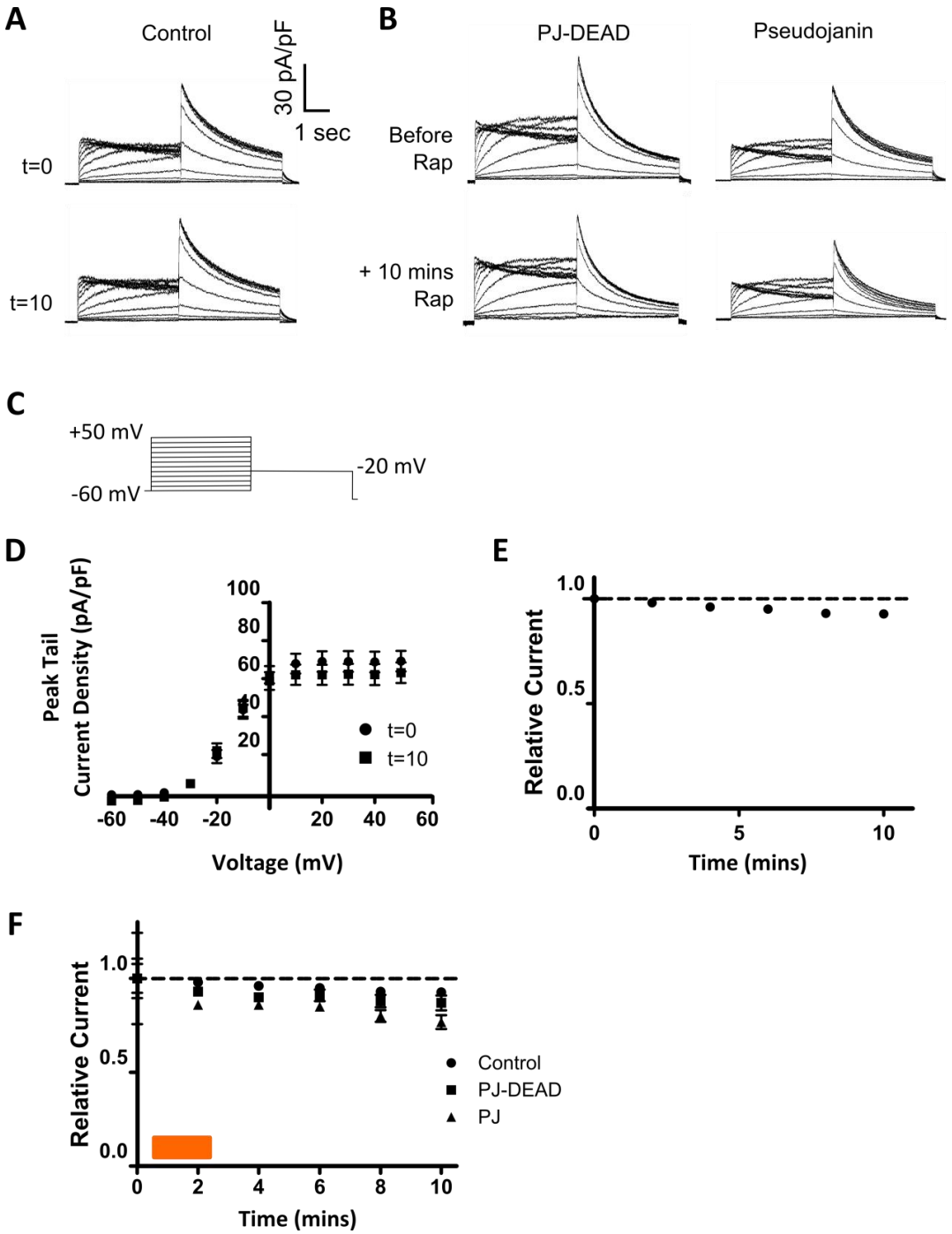


**Figure 37. Stability of the $I_{Kr}$ current and the effect of rapamycin-induced recruitment of lipid-depleting constructs on the $I_{Kr}$ current in HEK-$I_{Kr}$ cells in whole-cell patch clamp. A** – Representative current traces from HEK-$I_{Kr}$ cells (control) recorded at t = 0 and 10 minutes in WCPC. **B** – Representative current traces recorded in WCPC from HEK-$I_{Kr}$ cells expressing PJ-DEAD or PJ with LYN11-FRB, before and 10 minutes after the start of rapamycin (5µM) addition. **C** – Voltage protocol used to elicit the currents recorded in WCPC. **D** – Mean current density recorded in WCPC from untransfected HEK-$I_{Kr}$ cells (control; n=9) recorded at t = 0 and t = 10 minutes. **E** – Current density at 0 mV over approximately 10 minutes, relative to that at t = 0, from untransfected HEK-$I_{Kr}$ cells (control; n=9). **F** – Current density recorded in WCPC at 0 mV over a period of 10 minutes after the start of rapamycin (5µM) addition (orange bar), relative to the value before rapamycin addition, in HEK-$I_{Kr}$ cells expressing PJ-DEAD (n=10) or PJ (n=10) with LYN11-FRB. Relative current density from untransfected HEK-$I_{Kr}$ cells (n=9) included for comparison. Data are presented as mean ± SEM.

### 3.3.9 Effect of titrating active lipid-depleting construct expression with pcDNA3.1 or PJ-DEAD on the $I_{Ks}$ current

To try to reduce the inhibition that occurs when expressing PJ or PJ-INPP5E with LYN11-FRB in cells expressing the $I_{Ks}$ current, a titration of the lipid-depleting constructs was attempted. There was hope that a reduction in the amount of lipid-depleting construct expressed in the cell would lead to a concomitant reduction of the inhibition caused by expression of said construct. Previously, expression of PJ-INPP5E or PJ with LYN11-FRB caused partial and total loss of the $I_{Ks}$ current, respectively. This occurred when using 500 ng of each plasmid DNA for transfection. Titration of PJ using the pcDNA3.1 empty vector as a transfection bulking agent (to total 500 ng) was attempted to try to recover the $I_{Ks}$ current. Using 200 ng PJ per transfection enabled partial recovery of the $I_{Ks}$ current, and titration of PJ to 50 ng per transfection led to a further recovery of the $I_{Ks}$ current. Full recovery of the $I_{Ks}$ current was deemed to be when the current density reached a similar level to that recorded when PJ-DEAD and LYN11-FRB were expressed together in HEK-$I_{Ks}$ cells (figure 38 A & C)

The lipid-depleting constructs contain a fluorescent tag (RFP), and due to this, successfully transfected cells can be identified by exciting the fluorescent protein and detecting the emitted fluorescence by eye. As the amount of PJ was titrated to just 50 ng per transfection, however, there were difficulties in visualising transfected cells. To overcome this, YFP can be co-transfected with LYN11-FRB, PJ (50 ng) and pcDNA3.1 (450 ng), but the $I_{Ks}$ current density recorded in the presence of these constructs varied to such an extent that there became uncertainty regarding the actual level of PJ in each cell.

To solve this problem, PJ-INPP5E was titrated, but this time PJ-DEAD was used in place of pcDNA3.1 The use of PJ-INPP5E allows a larger ratio of PJ-INPP5E to PJ-DEAD, because PJ-INPP5E expression previously caused a less severe reduction in $I_{Ks}$ current density. The use of PJ-DEAD not only allows titration of PJ-INPP5E plasmid uptake during transfection, but also titration of the expression of PJ-INPP5E in the cell (which pcDNA3.1 cannot provide).

Titration of PJ-INPP5E from 500 ng per transfection to 200 ng per transfection, using PJ-DEAD to total 500 ng, resulted in recovery of the $I_{Ks}$ current to a comparable level compared to control cells (figure 39 A & C). Despite not being able to successfully recover the $I_{Ks}$ current using PJ using feasible means, PJ-INPP5E can still be used to investigate the role of $PIP_2$ in the regulation of the $I_{Ks}$ channel. Due to the fact that that all 4 lipid-depleting constructs contain RFP tags, however, means that using PJ-DEAD to titrate PJ-INPP5E expression introduced uncertainty regarding the ratio of PJ-INPP5E to PJ-DEAD in each cell (i.e. two cells of equal RFP intensity may contain vastly different amounts of PJ-DEAD and PJ-INPP5E).

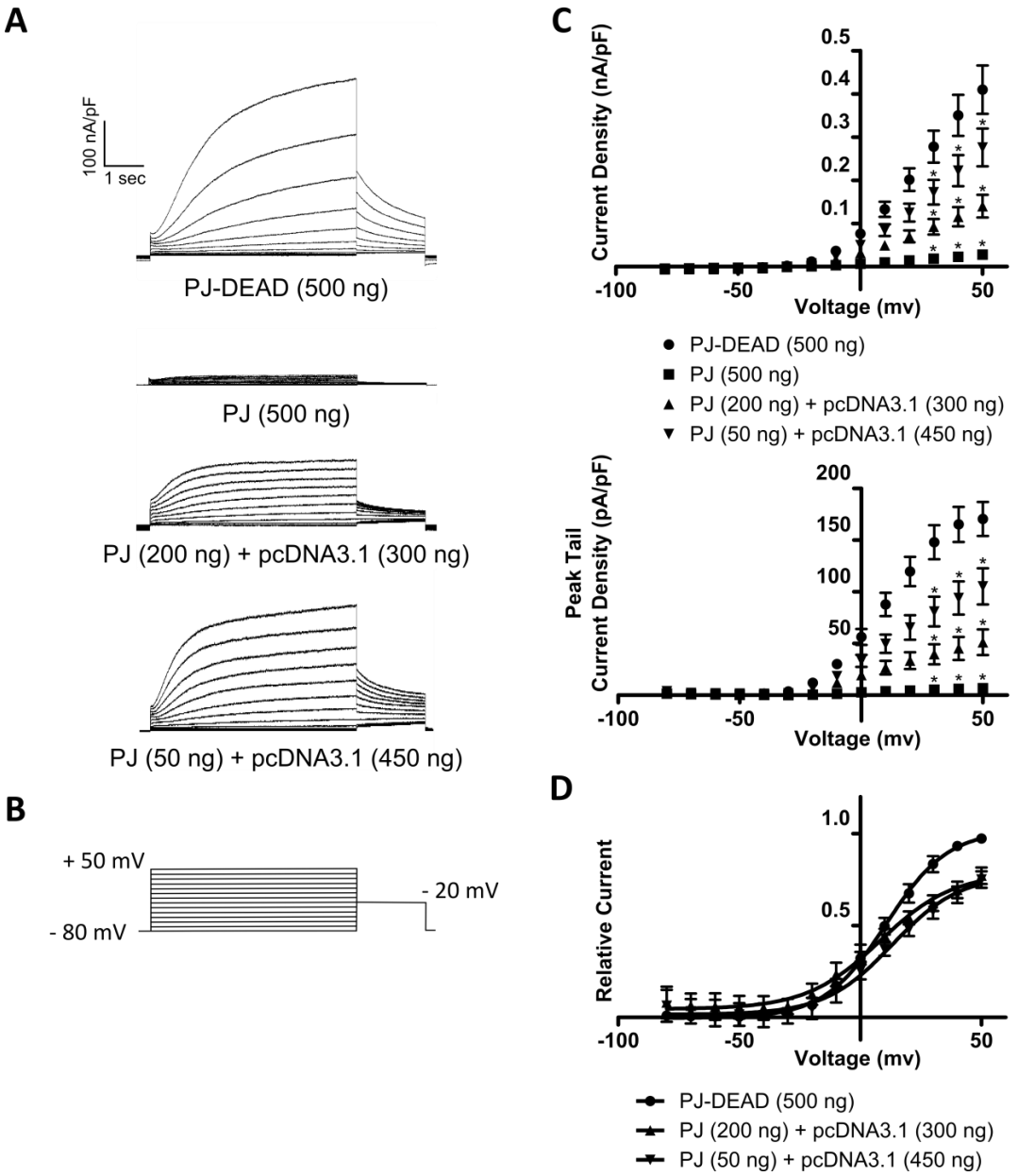


**Figure 38. The effect of titrating PJ with pcDNA3.1 on $I_{Ks}$ current inhibition in HEK-$I_{Ks}$ cells. A -** Representative traces of currents recorded in WCPC from HEK-$I_{Ks}$ cells transiently expressing PJ-DEAD (500 ng) with LYN11-FRB) (n=16), and HEK-$I_{Ks}$ cells transiently expressing PJ at 500 (n=11), 200 (n=23) or 50 ng (n=33), which were also transfected with 0, 300 and 450 ng pcDNA3.1, respectively. **B** – Voltage protocol used to elicit current recorded. **C –** Mean current density (top) and peak tail current density (bottom) of currents recorded in WCPC from HEK-$I_{Ks}$ cells expressing PJ-DEAD with LYN11-FRB or PJ at 500, 200 or 50 ng with LYN11-FRB. **D** – Steady state of activation curves, constructed by plotting normalised peak tail current densities ($y/y_{max}$) against test potential with a Boltzmann function (solid lines). Data are presented as mean ± SE. A one-way ANOVA with Dunnett's post hoc test was used to determine statistical significance between PJ-DEAD and other groups in **B**, between +30 mV and +50 mV, and between $V_{0.5}$ values obtained from **C**. A Boltzmann function was applied to data in **C** to fit a sigmoidal curve.

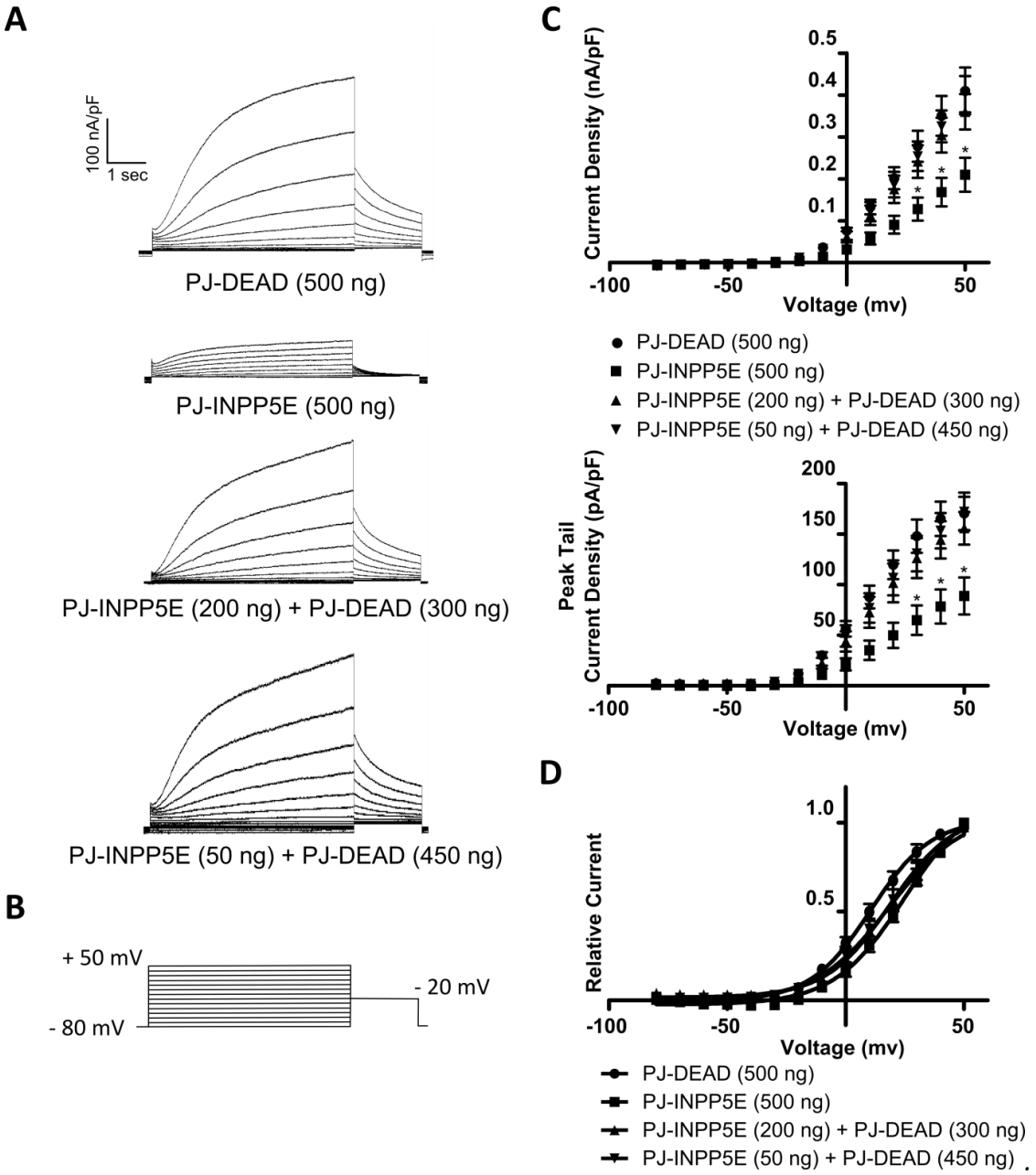


**Figure 39. The effect of titrating PJ-INPP5E with PJ-DEAD on $I_{Ks}$ current inhibition in HEK-$I_{Ks}$ cells**. **A –** Representative traces of currents recorded in WCPC from HEK-$I_{Ks}$ cells transiently expressing PJ-DEAD (500 ng) with LYN11-FRB) (n=16), and HEK-$I_{Ks}$ cells transiently expressing PJ-INPP5E at 500 (n=24), 200 (n=18) or 50 ng (n=18), which also expressed 0, 300 and 450 ng PJ-DEAD, respectively. **B** – Voltage protocol used to elicit current recorded. **C –** Mean current density (top) and peak tail current density (bottom) of currents recorded in WCPC from HEK-$I_{Ks}$ cells expressing PJ-DEAD with LYN11-FRB or PJ-INPP5E at 500, 200 or 50 ng with LYN11-FRB and 0, 300 and 450 ng PJ-DEAD, respectively. **D** – Steady state of activation curves, constructed by plotting normalised peak tail current densities ($y/y_{max}$) against test potential with a Boltzmann function (solid lines). Data are presented as mean ± SE. A one-way ANOVA with Dunnett's post hoc test was used to determine statistical significance between PJ-DEAD and other groups in **B**, between +30 mV and +50 mV, and between $V_{0.5}$ values obtained from **C**. A Boltzmann function was applied to data in **C** to fit a sigmoidal curve.

## 3.4 Discussion

Manipulation of cellular $PIP_2$ levels using methods such as excised-patch recordings (Loussouarn *et al*., 2003), $G_{q/11}$-coupled receptor activation (Matavel & Lopes, 2009) and exogenous application of $PIP_2$ analogues (Park *et al*., 2005) gave insights into the dependence of the $I_{Ks}$ channel on $PIP_2$ for function. However, what these experimental methods did not allow was a combination of direct and physiological manipulation of $PIP_2$ levels within the cell.

The rapamycin-induced dimerisation system allows the selective and inducible depletion of endogenous $PIP_2$ and/or PI4P, the effect of which can be observed in real-time. The rapamycin-induced dimerisation system has been previously used to investigate the depletion of many different ion channels, including the $I_{Ks}$ channel and other members of the KCNQ family.

In this chapter, I have shown that whilst the lipid-depleting constructs are expressed and recruit in the same way as previously shown (Hammond *et al*., 2012), expression of these constructs in HEK-$I_{Ks}$ cells alters the function of the $I_{Ks}$ channel in WCPC, hindering the investigation into the role of $PIP_2$ in regulation of the $I_{Ks}$ current in this project.

*Lipid-depleting constructs cause inhibition of the $I_{Ks}$ current in heterologous cells*

Using confocal microscopy, the cellular localisation of each lipid-depleting construct and LYN11-FRB were found to be consistent with the localisation of the same constructs used by Hammond *et al*. (2012), and the recruitment of these constructs using rapamycin behaved in the same way as similar constructs (containing the same rapamycin-binding domains) used by Suh *et al*. (2006). The time-course of recruitment of these constructs also paralleled that seen by Suh *et al*. (2006). These observations suggest that when expressed in cells for patch-clamp experiments, the lipid-depleting constructs possess the correct localisation and recruitment properties.

To confirm that as a result of lipid-depleting construct recruitment, lipid depletion occurs at the PM, the Tubby-YFP construct was co-transfected with PJ/PJ-DEAD and LYN11-FRB. Tubby is a transcription factor that localises to the PM due to the presence of a PI-binding domain that selectively binds $PIP_2$. By recruiting PJ-DEAD to LYN11-FRB at the PM with rapamycin (5 μM) and observing the localisation of Tubby-YFP over time, it was clear that $PIP_2$ levels at the PM were not affected as Tubby-YFP remained localised at the PM. This is in contrast to the rapid redistribution of Tubby-YFP from the PM to the cytosol after recruitment of PJ to the PM, showing that $PIP_2$ depletion occurs after rapamycin-induced recruitment of PJ.

Kruse *et al*. (2012) used the rapamycin-induced dimerisation system to investigate the effect of direct $PIP_2$ depletion on a number of $K_v$ channels, as this had only previously been performed with the KCNQ2/3 channel. Interestingly, this group used PJ to deplete $PIP_2$ and PI4P with all channels apart from the $I_{Ks}$ channel, where they used Inp54p in place of PJ. Inp54p is similar to PJ-INPP5E, in that it only depletes $PIP_2$.

In my experiments, when PJ or PJ-INPP5E (which deplete $PIP_2$ and PI4P, or only $PIP_2$, respectively) were expressed with LYN11-FRB in HEK-$I_{Ks}$ cells, inhibition of the $I_{Ks}$ current occurred. In the case of PJ, a complete loss of the $I_{Ks}$ current was observed. This effect could only be due to the active phosphatase domains that dephosphorylate $PIP_2$ and PI4P, because when PJ-SAC (which depletes solely PI4P) or the inactive construct, PJ-DEAD, were expressed with LYN11-FRB there was no change in the $I_{Ks}$ current characteristics. I would argue that in the experiments of Kruse *et al*. (2012) they experienced the same or similar difficulties as I did with PJ and LYN11-FRB, and used Inp54P in the place of PJ to enable a greater $I_{Ks}$ current density to be recorded. In the same study, the current density in the presence of PJ-DEAD and LYN11-FRB (or even $I_{Ks}$ in the absence of any construct) was not shown, and so any inhibition caused by the expression of Inp54p with LYN11-FRB could not be assessed.

Kruse *et al*. (2012) performed their studies in tsA-201 cells, which could cause some difference in results as HEK293 cells were used here. To rule out cell-type-specific effects, LYN11-FRB and either PJ or PJ-DEAD were expressed in CHO-K1 cells that were also transiently expressing the $I_{Ks}$ channel subunits, KCNQ1 and KCNE1. Confirming that this observation was not cell-type-specific, the same loss of current was noted upon expression of LYN11-FRB with PJ, but not PJ-DEAD.

*Could a low level of lipid depletion occur by expressing active lipid-depleting constructs, even in the absence of rapamycin?*

The phosphatase domains of the lipid-depleting constructs are constitutively active (with the exception of those in PJ-DEAD and the mutated domains in PJ-SAC and PJ-INPP5E), which could, in theory, confer a lower steady-state baseline level of cellular $PIP_2$ (and/or PI4P in the case of PJ and PJ-SAC, respectively). Using confocal imaging it is clear that the lipid-depleting constructs are expressed throughout the cell. Whilst rapamycin-induced dimerisation concentrates the lipid-depleting constructs at the PM, the constitutive phosphatase activity combined with the cytosolic expression of the constructs could allow a low level of lipid depletion by constructs that are coincidentally close to the PM in the absence of rapamycin, as suggested by DeRose *et al*. (2013).

Even without LYN11-FRB, expression of PJ in HEK-$I_{Ks}$ cells caused a 50% reduction in $I_{Ks}$ current density, supporting the notion that expression of the phosphatase-containing constructs may lead to lipid depletion due to constitutive activity of these domains. In addition to this, the fact that LYN11-FRB expression confers increased inhibition of the $I_{Ks}$ current indicates that there may be a low level interaction between these two constructs, possibly between the FRB and FKBP domains in the absence of rapamycin.

*Could there be an interaction between the FRB and FKBP domains?*

Based on the studies that were performed in different cell types and with different incubation media, it appears that no exogenous component was responsible for the $I_{Ks}$ inhibition caused, which led to the conclusion that there could be an interaction between the lipid-depleting constructs. An interaction between the two constructs could concentrate the phosphatase-containing construct at the PM.

Choi *et al*. (1996) reported protein domains involved in an FKBP–FRB interaction in the absence of rapamycin. These were Tyr2105 (in the 40s loop) of FRB with the oxygen atom of Lys47 (in the α4 domain) of FKBP, and Arg2042 (in the 80s loop) of FRB with Thr85 and Gly86 (in the α1 and α2 domains respectively) of FKBP. In 1999, a 2.2 Angstrom resolution structure of the FRB-rapamycin-FKBP complex was solved, which showed many more residues involved in the protein-protein interaction between FRB and FKBP (Liang *et al*., 1999).

Despite a conflicting report that these two domains do not interact (Banaszynski *et al.*, 2005), the previous structural studies do provide an explanation as to why LYN11-FRB may confer an increased inhibitory effect of PJ on the $I_{Ks}$ current. Rapamycin strengthens the dimerisation of FRB and FKBP, but even a transient and weak interaction could provide a slight concentration of the lipid-depleting construct at the PM, resulting in the incompatibility of this CID system with investigation of the $I_{Ks}$ channel.

*Can titration of the lipid-depleting constructs recover the $I_{Ks}$ current sufficiently?*

Whether there is an interaction between the FRB and FKBP domains or not, reducing the concentration of lipid-depleting constructs in the cell should lead to a reduction in lipid depletion and a consequent recovery of the $I_{Ks}$ current (in the case of PJ-INPP5E and PJ). First, a proportion of PJ plasmid DNA was replaced by pcDNA3.1 plasmid DNA during transfection to reduce the uptake of PJ DNA into the cells. By using 200 ng PJ a partial recovery occurred, and a larger recovery occurred by using 50 ng PJ (bulked to 500 ng using pcDNA3.1). However, it was obvious that the expression of PJ

varied in the cells that were co-transfected with YFP, and the detection by eye (epifluorescence) of such a low level of RFP-tagged construct was difficult and subjective.

The use of PJ-INPP5E instead of PJ would not completely hamper the investigation into the role of $PIP_2$ in $I_{Ks}$ regulation. Even though it has been shown that PI4P and $PIP_2$ can both activate the TRPV1 channel (Hammond *et al*., 2012) because the channel has a broad polyanionic lipid requirement, PI4P is mainly thought to reside in the PM as a precursor for $PIP_2$ synthesis. However, Thomas *et al.,* (2011) showed that the KCNQ1 C-terminus could bind a range of PIs, including $PIP_2$ and PI4P, but the functional role of this binding has not been investigated.

The increased $I_{Ks}$ inhibition that PJ causes over PJ-INPP5E may be due to the removal of the $PIP_2$ precursor pool, or it may be that PI4P can maintain a level of $I_{Ks}$ function in the absence of $PIP_2$, but this is also being removed. PJ-INPP5E and PJ-SAC still allow the role of these lipids to be investigated individually.

Because of the reduced level of $I_{Ks}$ inhibition caused by PJ-INPP5E expression compared to PJ expression, PJ-INPP5E was titrated in HEK-$I_{Ks}$ cells. Instead of using pcDNA3.1 as a transfection bulking agent, PJ-DEAD was co-transfected to provide a means of titrating the cellular expression of PJ-INPP5E. The presence of the inactive construct with PJ-INPP5E would reduce the number PJ-INPP5E constructs able to interact with FRB through their FKBP domain, but this solution does not address the inherent problem with using the rapamycin-inducible dimerisation system to investigate the $I_{Ks}$ channel – specifically the low level of $PIP_2$ depletion that appears to be causing inhibition of the $I_{Ks}$ current. Nonetheless, titration of PJ-INPP5E with PJ-DEAD could enable investigation into how $PIP_2$ depletion affects the $I_{Ks}$ channel.

*Other cardiac $K^+$ channels show varying sensitivities to $PIP_2$ and/or PI4P depletion*

In my experiments, the $I_{Ks}$ channel was highly sensitive to changes in $PIP_2$ levels in WCPC. It is thought that the $I_{Ks}$ channel β-subunit, KCNE1, confers an increased channel sensitivity to $PIP_2$ (Li *et al*., 2011), effectively causing amplification of the current. In order to investigate how the homomeric KCNQ1 channel (i.e. without KCNE1) was affected by co-expression of PJ and LYN11-FRB, the KCNQ1 subunit was transiently transfected into CHO-K1 cells with LYN11-FRB and either PJ or PJ-DEAD. CHO-K1 cells were used in place of HEK293 cells because of the presence of negligible endogenous outward currents, allowing accurate recording of the relatively small current elicited by homomeric KCNQ1 channels. As expected, PJ-DEAD and LYN11-FRB expression resulted in a current resembling that of the homomeric KCNQ1 channel ($K_v7.1$). The loss of this current when expressing PJ and LYN11-FRB suggests that the $K_v7.1$ channel is sensitive to PM $PIP_2$ levels, even in the absence of

KCNE1, and the low level of lipid depletion that may occur with expression of these constructs is sufficient to affect $K_v$7.1 function. As the sensitivity to $PIP_2$ levels is lower in KCNQ1 channels compared to the $I_{Ks}$ channel, this would suggest that the level to which $PIP_2$ is reduced by expression of PJ and LYN11-FRB (in addition to the effect of intracellular solution dialysis in WCPC) is far below the minimum level required for $I_{Ks}$ function.

Surprisingly, no one has attempted to overcome these problems despite a number of publications highlighting the inherent drawbacks of this CID system (Cabantous, *et al*., 2013; DeRose *et al*., 2013; Phua *et al*., 2012; Varnai *et al*., 2006). Many others have, however, successfully used the rapamycin-inducible dimerisation system to probe how these phospholipids affect different ion channels. Of the other ion channels investigated, the $K_{ir}$2.1 and $K_v$11.1 channels are also present in ventricular myocytes and are both involved in ventricular repolarisation. These channels have been reported to show differing $PIP_2$ binding affinities and as a result, differing sensitivities to $PIP_2$ depletion (Kruse *et al.*, 2012).

To investigate if the expression of the lipid-depleting constructs with LYN11-FRB affected the $I_{K1}$ and $I_{Kr}$ currents in a similar fashion to the $I_{Ks}$ current, a HEK-$I_{K1}$ and HEK-$I_{Kr}$ cell lines that stably express the $K_{ir}$2.1 and $K_v$11.1 channels, respectively, were used. Expression of PJ or PJ-DEAD with LYN11-FRB in either of these cell lines had no effect on the $I_{K1}$ or $I_{Kr}$ currents. When rapamycin was added to these cells, recruitment of PJ to the PM in HEK-$I_{K1}$ cells caused a gradual and complete depletion of the $I_{K1}$ current, and in HEK-$I_{Kr}$ cells caused a 25% reduction in the $I_{Kr}$ current over the course of the experiment. These results indicate that the rapamycin-induced dimerisation system can be an effective tool to investigate how direct $PIP_2$ depletion affects the function of an ion channel.

Ironically, due to the constitutive phosphatase activity, possible interaction with LYN11-FRB and concomitant depletion of $PIP_2$ and/or PI4P, there may be difficulties in using the system to investigate the role of $PIP_2$ in the regulation of channels highly sensitive to $PIP_2$ depletion. As previously mentioned Kruse *et al*. (2012) did not use PJ in their studies and instead used Inp54p. One can speculate that this choice was made due to the difficulties in using PJ to investigate the role of $PIP_2$ in the regulation of $I_{Ks}$ function.

### 3.5 Conclusions and future directions

Through characterisation of the rapamycin-inducible dimerisation system, it is clear that in its current state it is not optimal for use in the investigation of highly $PIP_2$-sensitive channels.

The KCNQ family of ion channels is known to be $PIP_2$ sensitive, and work on the KCNQ2/3 current has shown a role for $PIP_2$ in the regulation of this channel (Hernandez *et al*., 2009; Liu *et al*., 2008; Suh *et al*., 2006). By comparing the effect of expressing the lipid-depleting constructs on the $I_{Ks}$ channel to the $I_{K1}$, $I_{Kr}$ and $K_v7.1$ channels, each thought to have different $PIP_2$ sensitivities, it became apparent that the rapamycin-inducible dimerisation system can only be used effectively with channels that are not overly sensitive to $PIP_2$ depletion. For this reason, the investigation of the $I_{Ks}$ channel was hampered.

Unfortunately, other methods of $PIP_2$ depletion are either indirect or result in downstream effects that have unknown or complex consequences, including the release of second messengers by $G_{q/11}$-coupled GPCR activation and inhibition of multiple kinases by wortmannin. Due to this, it is important to directly dephosphorylate $PIP_2$ using a system such as rapamycin-inducible dimerisation, so the effects can be directly attributed to the loss of $PIP_2$ from the PM.

Of greatest importance in these kinds of studies are the channels with the highest $PIP_2$ sensitivity, because these channels could be regulated physiologically by manipulation of endogenous $PIP_2$ levels. Based on my findings, the rapamycin-inducible dimerisation system is not suitable for use with channels with the highest $PIP_2$ sensitivity in the most widely-used patch clamp configuration, WCPC, and researchers wishing to investigate such channels in this way would have to optimise this system or find alternative methods of selective and direct $PIP_2$ depletion. The rapamycin-induced dimerisation system will be used in Chapter 5 to investigate the role of $PIP_2$ in the regulation of $I_{Ks}$ function in P-WCPC, which is widely accepted to be the most physiological of all patch clamp configurations.

In the experiments described in this chapter, PJ-DEAD is the control construct, and is composed of the same domains as the active constructs, the only difference being the Asp1263Ala and Cys779Ser mutations in SAC1 and INPP5E, respectively. This provides the best negative control possible, as any effect of PJ (or the other active constructs) can only be attributed to the enzyme activity. It is for this reason that the $I_{Ks}$ inhibition that occurred when PJ/PJ-INPP5E and LYN11-FRB were expressed together was attributed to constitutive lipid depletion. In order to strengthen this reasoning, measurements of $PIP_2$ and PI4P concentration could be performed in the absence and presence of these constructs.

## CHAPTER 4: Optimisation of rapamycin-induced phosphoinositide depletion system

### 4.1 Introduction

The rapamycin-induced dimerisation system has previously been used to investigate the role of $PIP_2$ in KCNQ function (Suh *et al.*, 2006), clathrin-coated pit formation (Zoncu *et al.*, 2006) and receptor-mediated endocytosis (Abe *et al.*, 2008); small GTPases in neutrophil migration (Inoue & Meyer, 2008); and Akt kinase in apoptosis (Li *et al.*, 2002). Despite this method appearing to be a promising tool to investigate the role of $PIP_2$ in the regulation of $I_{Ks}$ channels, in practice there were significant set-backs, described in Chapter 3. In my experience with the rapamycin-inducible dimerisation system, the expression of PJ with LYN11-FRB in HEK-$I_{Ks}$ cells acted to inhibit the $I_{Ks}$ current before the addition of rapamycin, suggesting that lipid depletion occurs upon over-expression of these constructs.

The work in Chapter 3 highlights that the lipid-depleting constructs are not suitable in their current form to investigate the effect of $PIP_2$ depletion (with or without simultaneous PI4P depletion) on the $I_{Ks}$ channel. Based on the actions on the $I_{Ks}$ current, it appears that the phosphatase domains contained in the constructs are able to come into contact with their substrates at the PM prior to rapamycin-induced recruitment.

To overcome this, a number of different methods were attempted, which will be described below:

*Altering the rapamycin-induced dimerisation system*

DeRose *et al*. (2013) suggest that by tethering the effector protein (i.e. PJ) away from the PM, the constitutive phosphatase activity can be restricted away from the phospholipid substrates in the PM until rapamycin addition. This method was employed in the manipulation of small GTPases, where the FKBP-GTPase construct was tethered to the PI4P-binding FAPP1 domain. This domain binds to PI4P, enriched at the trans-Golgi network, through its PH domain (Phua *et al*., 2012).

Part of this chapter describes how the lipid-depleting constructs were altered in a way to restrict them away from the PM and, in an alternative attempt, LYN11-FRB mutants were made in order to disrupt the potential interaction between the FRB and FKBP domains. PJ and PJ-INPP5E were targeted to three different locations within the cell, and the extent to which this helped recover the $I_{Ks}$ current was measured. PJ was first targeted to the early endosomes using two N-terminal FYVE domains from the early endosomal antigen 1 (EEA1) protein (Gillooly *et al*., 2000). PJ was also targeted to the nucleus using either an N-terminal monopartite or bipartite nuclear localisation signal (NLS). Both of these NLS's utilise the classical nuclear import pathway, which involves the

active transport of NLS-containing proteins from the cytoplasm to the nucleus through nucleoporins, facilitated by the action of specialised carrier proteins called importins (Lange *et al*., 2007). Finally, PJ-INPP5E was targeted to the Golgi by inserting an N-terminal FAPP1 domain.

With exception of the nuclear-targeted constructs, this construct optimisation exploits the organelle-specific nature of many PI species. In order to perform specific signalling functions by targeting effector proteins to subcellular membrane compartments, PIs such as PI3P and PI4P concentrate in the early endosomes and Golgi, respectively. Many proteins contain PI-binding domains, the most well characterised being the PH domain. The FYVE zinc finger domains used here bind to PI3P, which is highly concentrated within the cell at the early endosomes. The FAPP1 PI-binding domain localises to the Golgi through a phenomenon known as coincidence detection; the FAPP1 domains requires the binding of both PI4P and ARF1 for membrane targeting, and as these are found together at the TGN, the FAPP1 domain localises here (He *et al*., 2011).

*Producing an alternative chemically induced dimerisation system*

Miyamoto *et al*. (2012) developed a CID system using components of the gibberellin signalling system as a way of creating an orthogonal CID system to the rapamycin-induced dimerisation system that also works on a timescale of seconds.

Gibberellins are a group of plant hormones that regulate growth and influence various developmental processes, including stem elongation, germination, dormancy and flowering. All identified gibberellins are diterpenoid acids, containing either 19 or 20 carbons – the former group also comprising a 5-member lactone ring. In general, the 19-carbon gibberellins are the more biologically active, and are hydroxylated on carbons 3 and 13.

One such giberrellin, known as gibberellic acid or gibberellin A3 (GA3), was the first to be structurally characterised. It is a pentacyclic diterpene acid, and promotes cellular growth and elongation. GA3 is sometimes used in the agricultural industry to exploit its growth-promoting properties.

Gibberellic acids bind to the gibberellic acid (GA) receptor, which is a soluble receptor named GA insensitive dwarf 1 (GID1). The GA-GID1 complex then binds to DELLA proteins, which belong to the GRAS family of plant-specific nuclear proteins. DELLA proteins inhibit GA-promoted processes, and binding of GA-GID1 to DELLA leads to their degradation via the ubiquitin-proteasome pathway (Eckardt, 2007). However, DELLA proteins also induce expression of upstream GA biosynthetic and GA receptor genes, implicating a role of DELLA proteins in GA homeostasis via a feedback mechanism (Sun, 2010).

The way in which GAs bind to GID1 and DELLA proteins is similar to the way that rapamycin binds to FKBP proteins and the FRB domain of mTOR, making this plant hormone of particular interest to those using CID systems. The rapamycin-induced dimerisation system utilises the fact that both FRB and FKBP bind to separate epitopes of the rapamycin molecule to induce dimerisation of these two protein domains. These two binding events are independent of each other, and there is no control over the order in which rapamycin binds to either of the domains. On the other hand, GAs cannot bind to both GID1 and a DELLA protein in any order: GAs must first bind to GID1 and undergo a conformational change that enables binding of the DELLA protein, and hence the formation of the DELLA-GA-GID1 complex.

In this CID system, GA3 was modified to increase its cell permeability by adding an acetoxymethyl (AM) group, which masks the negative charge of GA3 until endogenous esterases cleave the AM group and release the active GA3 molecule within the cell. Miyamoto and colleagues used the DELLA protein known as gibberellin-insensitive (GAI), and determined that the minimal domain required for dimerisation is residues 1–92, which incorporates the DELLA domain and a TVHYNP motif (Miyamoto *et al.,* 2012).

This group showed that the rapamycin- and gibberellin-induced dimerisation systems are completely orthogonal by inducing, in the same cell, the translocation of CFP-FKBP and YFP-GID1 to LYN11-FRB-mCherry and mCherry-GAI(1-92), respectively. By creating a system that does not originate from mammalian systems, any interactions between cellular components and the exogenously-expressed proteins should be reduced to a minimum.

*Abolishing the FKBP-FRB interaction in the rapamycin-induced dimerisation system*

In an attempt to reduce or abolish FKBP-FRB interactions that occur in the absence of rapamycin, identified by Choi *et al.* (1996), residues involved in this interaction in the FRB domain (as discussed in chapter 3) were mutated. The mutation of these residues may lead to a reduction in the affinity of the FRB and FKBP domains for each other, and I hypothesise that this will reduce the inhibition of the $I_{Ks}$ current that occurs when the lipid-depleting constructs and LYN11-FRB are expressed together. To test this hypothesis, site-directed mutagenesis will be used to mutate residues in FRB that are involved in the FRB-FKBP interaction to alanine. The mutant LYN11-FRB constructs will be expressed with PJ in HEK-$I_{Ks}$ cells, and the resulting $I_{Ks}$ current will be recorded to determine whether the mutation was successful.

**Aims:** 1) To determine whether the restriction of PJ and PJ-INPP5E away from the PM can rescue the $I_{Ks}$ current.

2) To assess whether the mutation of interacting residues in the FRB domain will reduce the potential interaction in the absence of rapamycin.

3) To incorporate the lipid-depleting constructs into an alternative CID system

The overall aim of this chapter is to generate a CID system that is compatible with studying the $I_{Ks}$ current.

## 4.2 Methods

### 4.2.1 Design of constructs

All PCR primers were from Integrated DNA Technologies, and all restriction enzymes were from New England Biolabs.

*Nuclear-targeted constructs*

Mono-NLS-PJ was made by incorporating the monopartite NLS (mono-NLS) sequence into the PCR primers (shown below), using the PJ plasmid as the template DNA. Specifically, the mono-NLS forward primer (FPr) contained an NheI restriction site (GTAAGC), a Kozak sequence, the mono-NLS sequence and the first 12 residues of mRFP in the 5' to 3' direction. The mono-NLS sequence was taken from Kalderon *et al.* (1984), and is the SV40 Large T Antigen (TAg)-based sequence, $^{126}$PKKKRKV$^{132}$.

Bi-NLS-PJ was made using the same method as mono-NLS-PJ, but the bipartite NLS (bi-NLS) sequence replaced the mono-NLS sequence in the FPr. The bi-NLS sequence was taken from Robbins *et al.* (1991) and is the Nucleoplasmin NLS-based sequence, $^{153}$AVKRPAATKKAGQAKKKKLD$^{172}$. Primers used to create bi-NLS-PJ are shown below.

Reverse primers (RPr) for both Mono-NLS-PJ and Bi-NLS-PJ contained the last 8 residues of mRFP and the BspEI restriction site (TCCGGA) in the 3' to 5' direction.

By incorporating NheI and BspEI restriction sites at the 5' and 3' ends, respectively, the mono/bi-NLS-mRFP PCR products were easily inserted into a PJ vector (with mRFP removed using NheI and BspEI) using a ligation reaction. The inserted NLS sequences can be seen in figure 40.

*Mono-NLS Forward Primer:*

5’-AGAAGAGCTAGCCGCCACCATGCCAAAAAAGAAGAGAAAGGTAGCAGCCTCCTCCGAGGA

CGTCATCAAGGAGTTCATGCGC-3’

*NLS Reverse Primer:*

5’-TCTGAGTCCGGAGGCGCCGGTGGAGTGGCGGCCCTCG-3’

*Bi-NLS Forward Primer:*

5’-AGAAGAGCTAGCCGCCACCATGGCTGTAAAGAGGCCTGCGGCTACCAAAAAAGCAGGCCA

GGCAAAGAAGAAGAAACTTGACGCAGCCTCCTCCGAGGACGTCATCAAGGAGTTCATGCGC-3’

**Mono-NLS-PJ**

G CTA GCC GCC ACC ATG CCA AAA AAG AAG AGA AAG GTA GCA GCC TCC

**Bi-NLS-PJ**

G CTA GCC GCC ACC ATG GCT GTA AAG AAG CCT GCG GCT AAC AAA AAA

GCA GGC CAG GCA AAG AAG AAG AAA CCT GAC GCA GCC TCC

**Figure 40. DNA sequence for NLS-containing modified lipid-depleting constructs.** Both mono- and bi-NLS-containing constructs start with an NheI restriction site (orange), followed by a kozak sequence (black) and start codon (ATG; purple). The mono- or bi-NLS sequence then follows, which is immediately followed by mRFP (start of mRFP sequence shown in red). Both sequences run from 5’ to 3’ (left to right).

*Early-endosome-targeted constructs*

2xFYVE-PJ was made using PCR, with double-stranded cDNA from mouse liver (a gift from Dr Claudio Mauro, WHRI, QMUL) as the template DNA. Two Hrs (FYVE) domains, separated by a flexible linker, were amplified and fused to the N-terminus of the PJ construct, separated by a second flexible linker.

The Fpr for amplification of FYVE domain 1, FYVE(D1), incorporated an NheI restriction site (GTAAGC), a Kozak sequence and the first 10 residues of the FYVE sequence. The Rpr for FYVE(D1) contained a BamHI restriction site (GGATCC), the flexible linker (amino acid sequence: QGQGS) and the final 9 residues of the FYVE sequence.

For amplification of the second FYVE domain, FYVE(D2), the Fpr incorporated a BamHI restriction site (GGATCC) and the first 10 residues of the FYVE sequence. The Rpr for FYVE(D2) contained an NheI restriction site (GCTAGC) and the final 9 residues of the FYVE sequence.

To insert a flexible linker region between FYVE(D2) and the start of the PJ construct (mRFP), an mRFP domain preceded by the flexible linker (FL-mRFP) was created using PCR. The Fpr contained an NheI restriction site (GCTAGC) followed by the 19 residues required for the linker. This was followed by the first 13 residues of mRFP, removing the start codon, ATG, and inserting GCA (Ala). The Rpr used was the same as for mono-NLS-PJ and bi-NLS-PJ, and contained the last 8 residues of mRFP and the BspEI restriction site (TCCGGA).

In a single ligation reaction, FYVE(D1) (NheI, BamHI), FYVE(D2) (BamHI, NheI) and FL-mRFP (NheI, BspEI) were inserted into the PJ vector with RFP removed (NheI, BspEI), to create the 2xFYVE-PJ construct shown in figure 41.

*FYVE Hrs (D1) Forward Primer:*

5’-CCTCTAGCTAGCCGCCACCATGGAAAGTGATGCCATGTTCGCTGCTGAAAGAG-3’

*FYVE Hrs (D1) Reverse Primer:*

5’-GGAGATGGATCCCTGGCCCTGTGCCTTCTTGTTCAGCTGCTCATAGCAG-3’

*FYVE Hrs (D2) Forward Primer:*

5’-CCTCTAGGATCCGAAAGTGATGCCATGTTCGCTGCTGAAAGAG-3’

*FYVE Hrs (D2) Reverse Primer:*

5’-GGAGATGCTAGCTGCCTTCTTGTTCAGCTGCTCATAGCAG-3’

*Golgi-apparatus-targeted constructs*

FAPP1-PJ-INPP5E was made by PCR, using YFP-FAPP1-PH (from Dr Maria Deak, University of Dundee) as the template DNA, incorporating an NheI restriction site (GCTAGC) and the first 10 residues of the FAPP1 sequence in the FPr, and an AgeI restriction site (ACCGGT) 3' of the final 12 residues of the FAPP1 sequence in the RPr.

As the AgeI restriction site in PJ-INPP5E is not unique, PJ-INPP5E was digested using NheI and BglII, and then the resulting insert fragment (mRFP) was digested with AgeI. The digested mRFP insert (AgeI, BglII) and FAPP1 insert (NheI, AgeI) were inserted into the PJ-INPP5E vector (NheI, BglII) using a ligation reaction, resulting in the FAPP1-PJ-INPP5E construct shown in figure 41.

*FAPP1 Forward Primer:*

5'-CCAAAAGCTAGCACCATGGAGGGGGTGTTGTACAAGTGGACCAAC-3'

*FAPP1 Reverse Primer:*

5'-CCAAAAACCGGTGCTTTAGTCCTTGTATCAGTCAAACATGCTTTGGAGCTC-3'

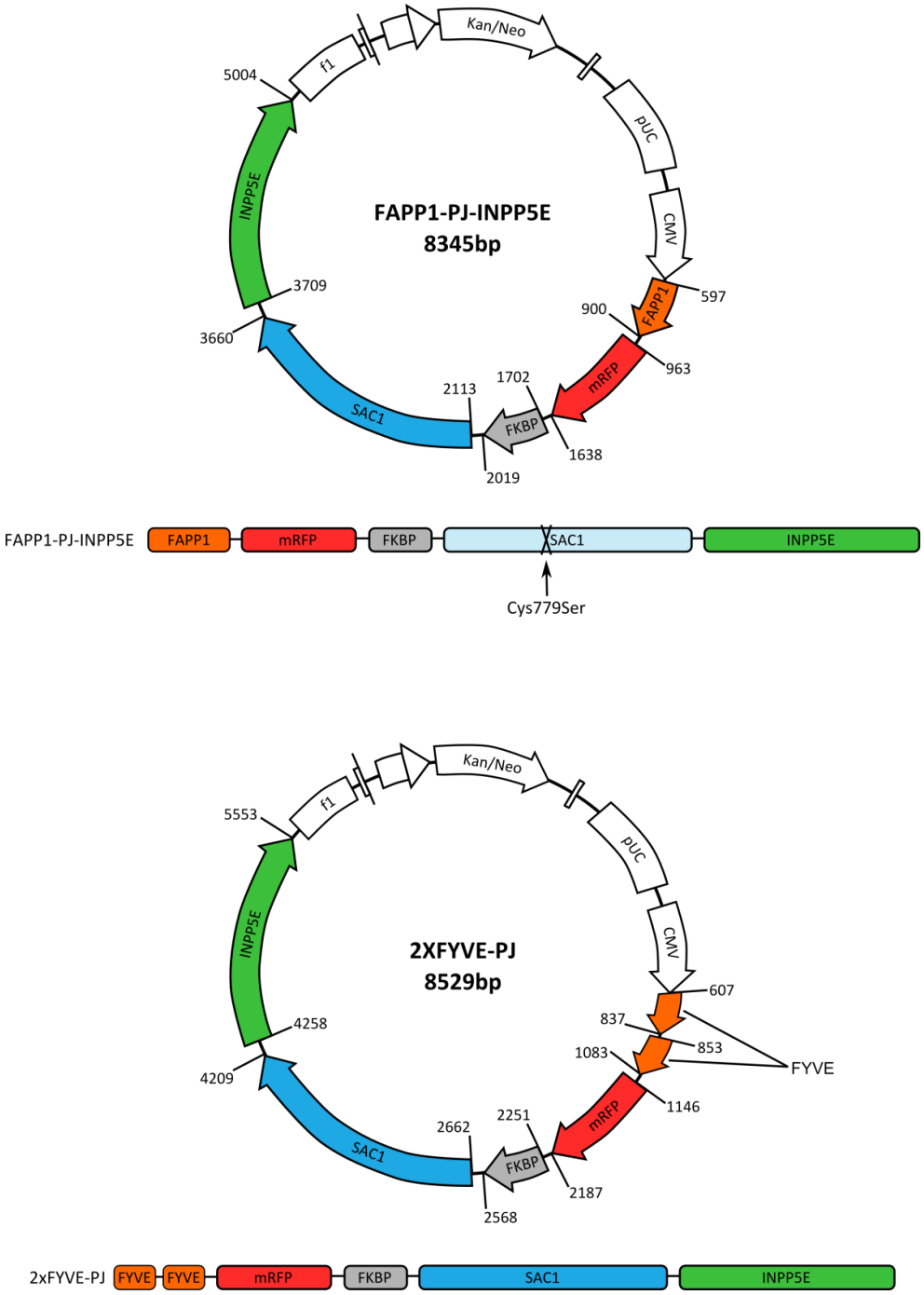


**Figure 41. Modified lipid-depleting construct plasmid maps.** Plasmid maps and representative construct image for FAPP1-PJ-INPP5E and 2xFYVE-PJ.

*PJ-GID1 constructs*

The YFP-GID1 (#37305) and LYN-CFP-GAI(1–92) (#37311) were purchased from Addgene (deposited by Takanari Inoue). To incorporate the phosphatase domains required to achieve lipid depletion upon dimerisation of GID1 and GAI, the YFP-GID1 construct was altered using molecular cloning techniques as follows:

The GID1 domain was amplified from YFP-GID1 by PCR, using customised primers (shown below) to incorporate an NheI restriction site followed by a flexible linker region, 3' of the start of the GID1 sequence, and a stop codon followed by a BamHI restriction site, 5' of the GID1 sequence. The phosphatase enzymes, INPP5E and SAC1, were amplified from PJ as one fragment, incorporating the NotI and NheI restriction sites 3' and 5' of the amplified region, respectively. These two amplified regions (GID1 and phosphatase domains) were added into a ligation reaction with a vector backbone containing RFP, created by digesting the PJ plasmid with NotI and BamHI. The resulting plasmid can be seen in figure 42.

*GID1 Forward Primer:*

5'-
GCACGCTAGCTCAGGACTCAGGCTTCGAAGCGCAGCCGCGGGAGCAGGAGGAGCAGCTCGAGCG
GCGGCAGCTGCGAGCGATGAAGTTAATCTTATT-3'

*GID1 Reverse Primer:*

5'-CGTGGGATCCTTAACATTCCGCGTTTACAAACGCCGAAAT-3'

*Enzymes Forward Primer:*

5'-GCACGCGGCCGCGAGTGCTGGTGGTAGTGCTGGTGGTAGTGCT-3'

*Enzymes Reverse Primer:*

5'-CGTGGCTAGCTGCAGAAACGGAGGCGATGGTGCTGGAGTTCTG-3'

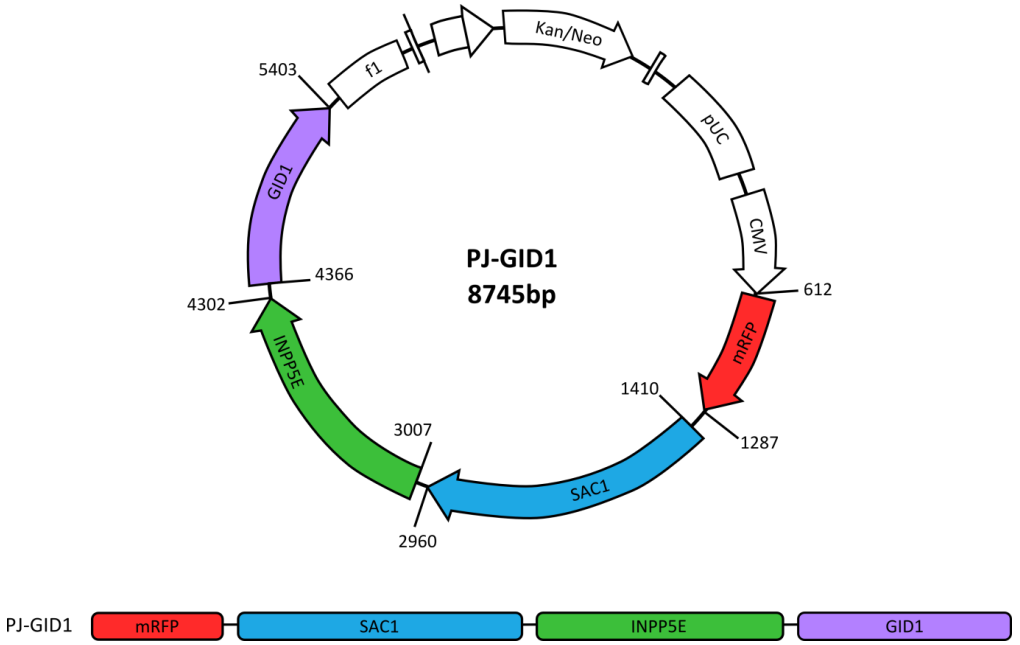


**Figure 42. GID1-containing lipid-depleting construct plasmid map.** Plasmid map and representative construct image for PJ-GID1, the lipid-depleting construct in the gibberellin-induced dimerisation system.

### 4.2.2 Confocal microscopy

Live cells were imaged using a Zeiss LSM510 (Mark 4) (Carl Zeiss, Oberkochen, Germany) confocal microscope and a Plan-Apochromat 63x oil lens objective. Images were acquired as described in section 3.2.4.

### 4.2.3 Electrophysiology

Currents were recorded from HEK-$I_{Ks}$ cells either untransfected or transiently transfected. Untransfected HEK-$I_{Ks}$ cells were used 48–72 hours after seeding, and transfected HEK-$I_{Ks}$ cells were used 48–72 hours after transfection. For lipid-depleting experiments, 500 ng of modified lipid-depleting construct was transfected with 500 ng of LYN11-FRB. All transfections were performed using FuGENE HD as described in section 2.1.3.

WCPC or P-WCPC (where stated) were used to record the $I_{Ks}$ current in HEK-$I_{Ks}$ cells. Both P-WCPC and WCPC experiments were carried out at room temperature using an Axopatch 200B amplifier (Axon Instruments) and transfected cells were identified using epifluorescence. Extracellular bath solution for all experiments contained (mM) 150 NaCl, 5 KCl, 10 HEPES, 2 $MgCl_2$ and 1 $CaCl_2$ (pH 7.4 with NaOH). In all experiments, $R_{series}$ was compensated for by 70% using the amplifier circuitry.

In WCPC, the solutions and recording procedures are as described in chapter 3. In P-WCPC, the intracellular pipette solution contained (mM) 70 $K_2SO_4$, 10 NaCl, 10 HEPES, 2 $MgCl_2$ and 1 $CaCl_2$ (pH

7.2 with KOH). The P-WCPC pipette solution was supplemented with 0.24 mg/ml amphotericin B to permeabilise the cell membrane. A stock (60 mg/ml) of amphotericin B was made, and a fresh dilution to 0.24 mg/ml was made every 1–2 hours. Before filling pipettes with amphotericin B, pipette tips were dipped into amphotericin-B-free intracellular solution, to prevent permeabilisation of the cell membrane before GΩ seal formation. Pipette resistance, after being filled with intracellular solution, was 1–2 MΩ. After seal formation, cells were left until $R_{access}$ was stable and below 20 MΩ (although most recordings achieved 15 MΩ or below), before recording. I-V protocols were recorded by holding the cells at -80 mV before a 6-second activation pulse, from -80 mV to +80 mV, in 10 mV increments. After the 6-second pulse, a 2-second repolarising step to -20 mV was used to record tail currents, before stepping back to -80 mV.

In P-WCPC experiments involving the perfusion of rapamycin over the cells, extracellular solution containing rapamycin (5 μM) was perfused for 2 minutes, and perfusion was then returned to rapamycin-free extracellular solution.

Data from all experiments was analysed as described in chapter 3.

### 4.2.3 Statistical analysis

Data are expressed as mean ± SE, and Boltzmann functions were generated using GraphPad Prism. A one-way ANOVA ($p<0.05$) was used to determine significance when multiple groups were compared, and a one-way ANOVA with Bonferroni's multiple test comparison was used to compare all pairs of groups.

## 4.3 Results

### 4.3.1 Using two FYVE domains to target PJ to early endosomes, and the ability to induce translocation of this construct to the plasma membrane with rapamycin

A first attempt at restricting PJ away from the PM led to the insertion of the 2xFYVE domain at the N-terminal end of the PJ construct, which was named 2xFYVE-PJ. Before using any of the altered constructs in patch-clamp experiments, their cellular localisation was assessed using confocal microscopy to ensure the desired localisation was achieved and, if so, whether rapamycin could induce dimerisation of these with the PM-anchored LYN11-FRB.

When the 2xFYVE-PJ construct was expressed in HEK293 cells, it was immediately apparent that the construct did not solely localise to early endosomes. The cellular localisation appeared to include early endosomes, but there was a large amount of signal also localised to the Golgi (figure 43). Despite the unsuccessful localisation of the 2xFYVE-PJ construct to the early endosomes, this construct was primarily restricted away from the PM, and only a very low level of unrestricted construct was detected in the cytosol.

As the aim was to restrict the phosphatase domains away from the PM, and this had been achieved, rapamycin was added to HEK293 cells expressing 2xFYVE-PJ and LYN11-FRB. To determine the ability of rapamycin to induce translocation of this modified lipid-depleting construct to the PM from the early endosomes/Golgi compartments, rapamycin was added and the translocation of the construct monitored. Unfortunately, addition of rapamycin (5μM) to HEK293 cells expressing 2xFYVE-PJ and LYN11-FRB did not result in translocation of the 2xFYVE-PJ construct from either the Golgi or early endosomes to the PM. The 2xFYVE-PJ construct remained localised to the early endosomes/Golgi throughout the time course of the experiment (figure 43).

### 4.3.2 Using a nuclear localisation signal to target PJ to the nucleus, and the ability to induce translocation of this construct to the plasma membrane with rapamycin

As a second attempt at restricting PJ away from the PM, the PJ construct was altered to include an NLS. Two different types of NLS were used (monopartite and bipartite), both at the N-terminal end of PJ, creating two different PJ-NLS constructs: mono-NLS-PJ and bi-NLS-PJ.

Again, to determine the localisation of these constructs, confocal microscopy was used. From this it was evident that both the mono-NLS-PJ and bi-NLS-PJ constructs successfully localise to the nucleus when transiently expressed with LYN11-FRB in HEK293 cells (figures 44 & 45). In the case of mono-NLS-PJ, there was also a small amount of unrestricted construct detected in the cytosol.

As both of these NLS-containing constructs had successfully been restricted (or mostly restricted, in the case of mono-NLS-PJ) away from the PM (and to the desired location), the ability of rapamycin to induce translocation of each construct to the PM could be tested.

Upon addition of rapamycin (5μM) to HEK293 cells expressing mono-NLS-PJ and LYN11-FRB, there was a rapid recruitment of the cytosolic (i.e. unrestricted) portion of mono-NLS-PJ to the PM (figure 44), and a ring of mono-NLS-PJ at the PM could be seen approximately 30 seconds after the addition of rapamycin. However, no detectable translocation of the nuclear-restricted mono-NLS-PJ occurred in the timeframe of the experiment. Quantification of mono-NLS-PJ and LYN11-FRB signal intensity (figure 44B) showed that mono-NLS-PJ moved from the cytoplasm to the PM on addition of rapamycin, but it was unclear upon analysing the signal intensity at a region of the PM whether the fluorescence signal intensity of mono-NLS-PJ increased over time (figure 44C). In HEK293 cells expressing bi-NLS-PJ and LYN11-FRB, there was no translocation of the nuclear-restricted construct to the PM after rapamycin (5 μM) addition over the course of the experiment.

### 4.3.3 The effect of transiently expressing mono-NLS-PJ in HEK-$I_{Ks}$ cells on the $I_{Ks}$ current, and the effect of rapamycin addition

Even though rapamycin was unable to induce translocation of the nuclear-restricted mono-NLS-PJ construct, there may have been a translocation of the unrestricted construct to the PM. Because the majority of the mono-NLS-PJ construct was restricted away from the PM and the cytoplasmic mono-NLS-PJ may translocate to the PM upon rapamycin addition, the effect of mono-NLS-PJ expression in HEK-$I_{Ks}$ cells was assessed in WCPC.

Mono-NLS-PJ and LYN11-FRB were expressed in HEK-$I_{Ks}$ cells to find out if the extent of nuclear-targeting was sufficient to recover the $I_{Ks}$ current (i.e. by preventing lipid depletion at the PM). In WCPC, there was no significant change (p=NS) in the $I_{Ks}$ current density or peak tail current density, and a small change in the steady state of activation compared to untransfected HEK-$I_{Ks}$ cells, which was significant at +10 mV ($p<0.05$) (figure 47A, B, & D). The $V_{0.5}$ changed from 9.4 mV ± 0.53 mV to 25.5 mV ± 1.6 mV, which was assessed using a Boltzmann function, but this was not significant (p=NS) (figure 47C).

As the $I_{Ks}$ current could be recorded and was at a comparable level to control in the presence of mono-NLS-PJ and LYN11-FRB, P-WCPC was used to find out whether the rapamycin-induced recruitment of cytoplasmic mono-NLS-PJ to the PM, which was visualised using confocal microscopy, had any effect on the $I_{Ks}$ current. The stability of the $I_{Ks}$ current over time in P-WCPC is shown in figure 61 in chapter 5.

First, an I-V was recorded, which was followed by perfusion of rapamycin (5 μM) for 2 minutes during a second I-V protocol. I-V relationships were recorded every 3 minutes after the start of rapamycin perfusion for a total of 12 minutes. There was no change in the steady state current density or peak tail current density of the $I_{Ks}$ current and no change in the steady state of activation 11 minutes after rapamycin exposure (p=NS) (figure 47F & G).

### 4.3.4 Using the FAPP1 domain to target PJ-INPP5E to the Golgi apparatus, and the ability to induce translocation to the plasma membrane with rapamycin

In a final attempt at optimising the CID system by restricting the lipid-depleting constructs away from the PM, the FAPP1 domain was inserted into the N-terminal end of PJ-INPP5E. The FAPP1 domain was used to target this construct to the Golgi. The FAPP1-PJ-INPP5E construct successfully localised to the Golgi when expressed in HEK293 cells with LYN11-FRB (figure 46). There was also a low level of expression detectable in the cytoplasm of most cells, but to a lesser extent than the mono-NLS-PJ or 2xFYVE-PJ constructs.

Due to the success at restricting this construct away from the PM, the ability of rapamycin to induce translocation of FAPP1-PJ-INPP5E to the PM was assessed. Addition of rapamycin (5μM) to HEK293 cells expressing FAPP1-PJ-INPP5E and LYN11-FRB caused the Golgi-localised signal to translocate in part to the PM. The movement of FAPP1-PJ-INPP5E to the PM occurred on a timescale of minutes; at 2 mins post rapamycin addition there was an accumulation of FAPP1-PJ-INPP5E at the PM, which was further increased and accompanied by a more noticeable movement of the construct from the Golgi by the 4 minute time point (figure 46). These observations are supported by quantification of the FAPP1-PJ-INPP5E and LYN11-FRB signal intensity (figure 46B), which showed that FAPP1-PJ-INPP5E increased at the PM after addition of rapamycin (5 μM). This was further supported by analysis of FAPP1-PJ-INPP5E signal intensity over time at a region of the PM, which showed that the fluorescence signal intensity of FAPP1-PJ-INPP5E increased at the PM by approximately 60% after addition of rapamycin (figure 46C).

### 4.3.5 The effect of transiently expressing FAPP1-PJ-INPP5E in HEK-$I_{Ks}$ cells on the $I_{Ks}$ current, and the effect of rapamycin addition

Because the FAPP1-PJ-INPP5E construct was successfully localised to the Golgi and there appeared to be translocation of the construct from this location to the PM after rapamycin addition, FAPP1-PJ-INPP5E and LYN11-FRB were expressed in HEK-$I_{Ks}$ cells to find out if the extent of Golgi-localisation was sufficient to recover the $I_{Ks}$ current. In WCPC, no significant change in the $I_{Ks}$ current density or peak tail current density was observed (figure 48A, B & D), and there was only a small change in the

steady state of activation compared to untransfected HEK-$I_{Ks}$ cells, which was significant at +10 mV ($p<0.05$) (figure 48C). The $V_{0.5}$ changed from 9.4 mV ±0.53 mV to 24.1 mV ±1.1 mV, but this difference did not reach statistical significance (p=NS)

As the $I_{Ks}$ current could be recorded, and was a comparable level to control in the presence of FAPP1-PJ-INPP5E and LYN11-FRB, P-WCPC was used to assess whether the rapamycin-induced recruitment of FAPP1-PJ-INPP5E to the PM that was visualised using confocal microscopy had any effect on the $I_{Ks}$ current.

In HEK-$I_{Ks}$ cells expressing FAPP1-PJ-INPP5E and LYN1-FRB an I-V was recorded, which was followed by perfusion of rapamycin (5 μM) for 2 minutes during a second I-V protocol. I-V relationships were recorded every 3 minutes after the start of rapamycin perfusion, for a total of 12 minutes. There was no change in the steady state current density or peak tail current density of the $I_{Ks}$ current and no change in the steady state of activation, 11 minutes after rapamycin exposure (p=NS) (figure 48F & G).

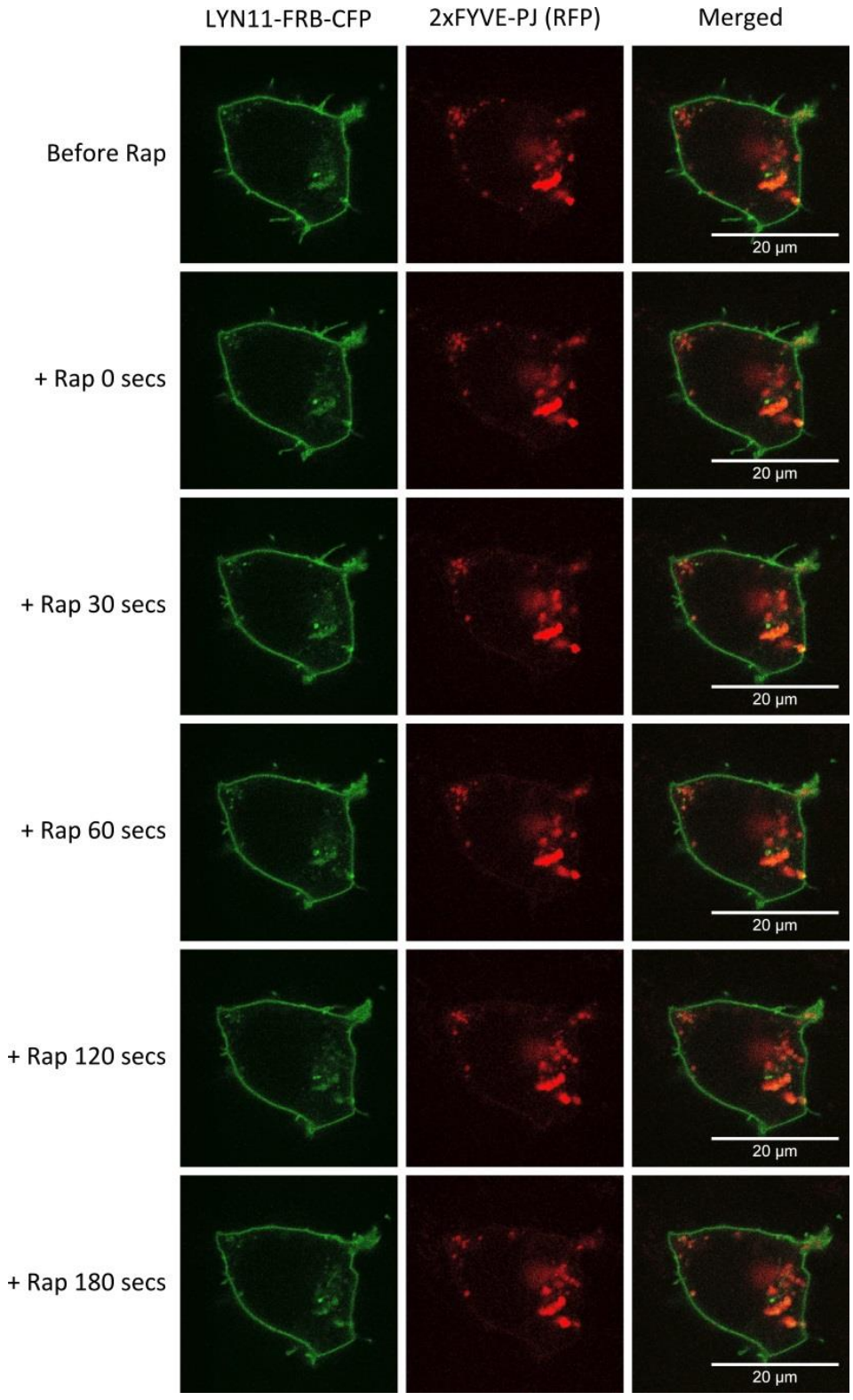


**Figure 43. The localisation of 2xFYVE-PJ in HEK293 cells before and after rapamycin addition.** The top row shows HEK293 cells transiently expressing 2xFYVE-PJ and LYN11-FRB-CFP. The 5 centre and bottom rows show the localisation of these constructs in the same cell at different time points after the addition of rapamycin (5 µM). Images were obtained using confocal microscopy. Representative cell response (n=3).

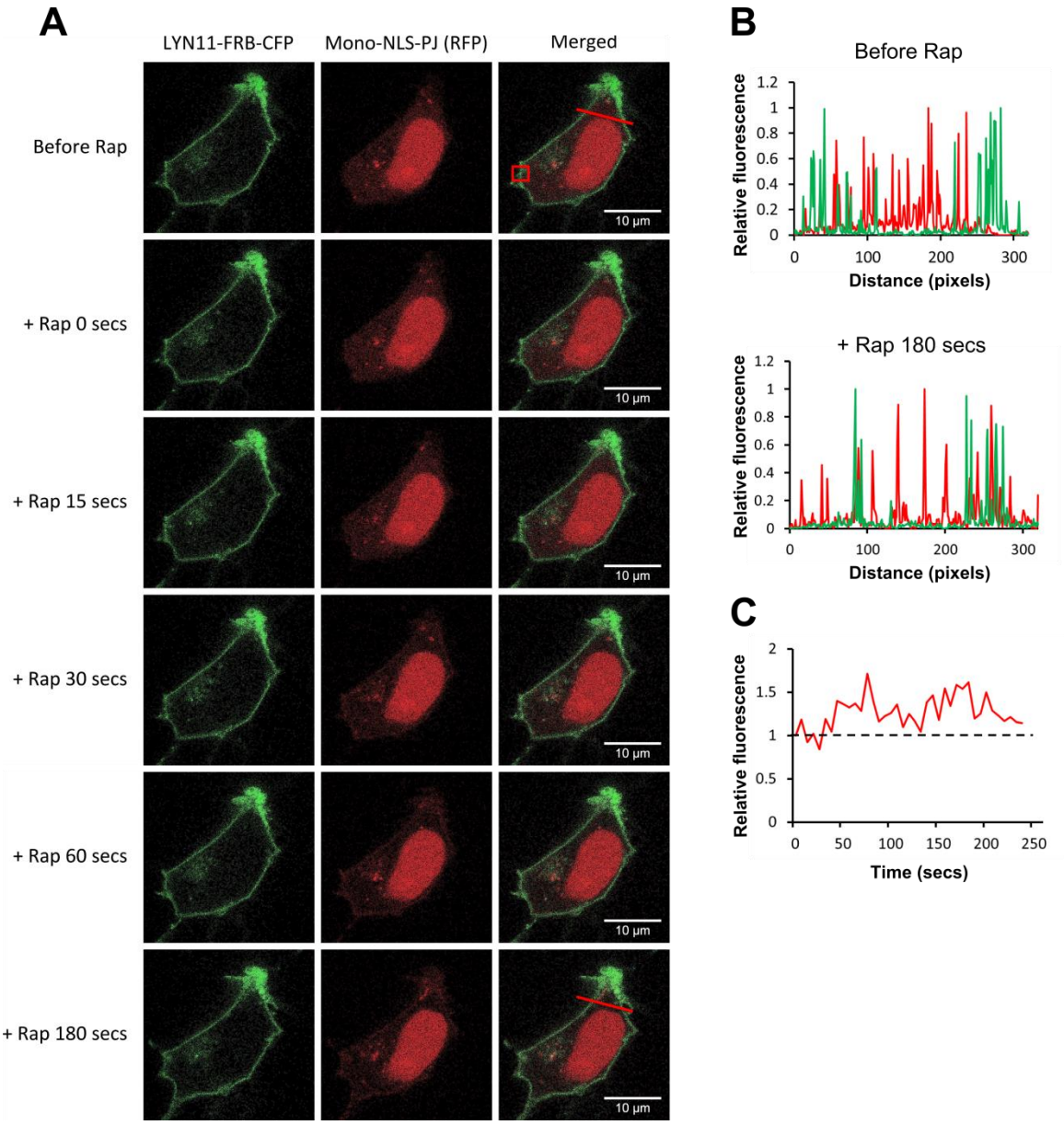


**Figure 44. The localisation of mono-NLS-PJ in HEK293 cells before and after rapamycin addition.** **A** – The top row shows HEK293 cells transiently expressing mono-NLS-PJ and LYN11-FRB-CFP. The 5 centre and bottom rows show the localisation of these constructs in the same cell at different time points after the addition of rapamycin (5 µM) to the cell. Images were obtained using confocal microscopy. **B** – Normalised ($y/y_{max}$) intensity of fluorescence of CFP and RFP along the red line illustrated in the top right-hand image (before Rap) and bottom right-hand image (+ Rap 180 secs) in **A**. Green represents LYN11-FRB-CFP and red represents mono-NLS-PJ in both **B** and **C**. **C** – Change in fluorescence intensity over time measured from region of interest shown by red box in top right-hand image in **A** (relative to value from image 1 of time series). Representative cell response (n=4).

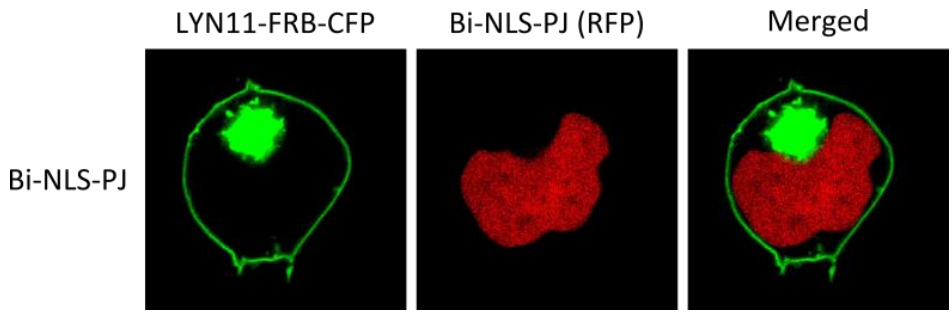


**Figure 45. The localisation of bi-NLS-PJ in HEK293 cells.** HEK293 cells transiently expressing Bi-NLS-PJ and LYN11-FRB-CFP. LYN11-FRB-CFP is localised at the PM, while bi-NLS-PJ is localised to the nucleus. Images were obtained using confocal microscopy.

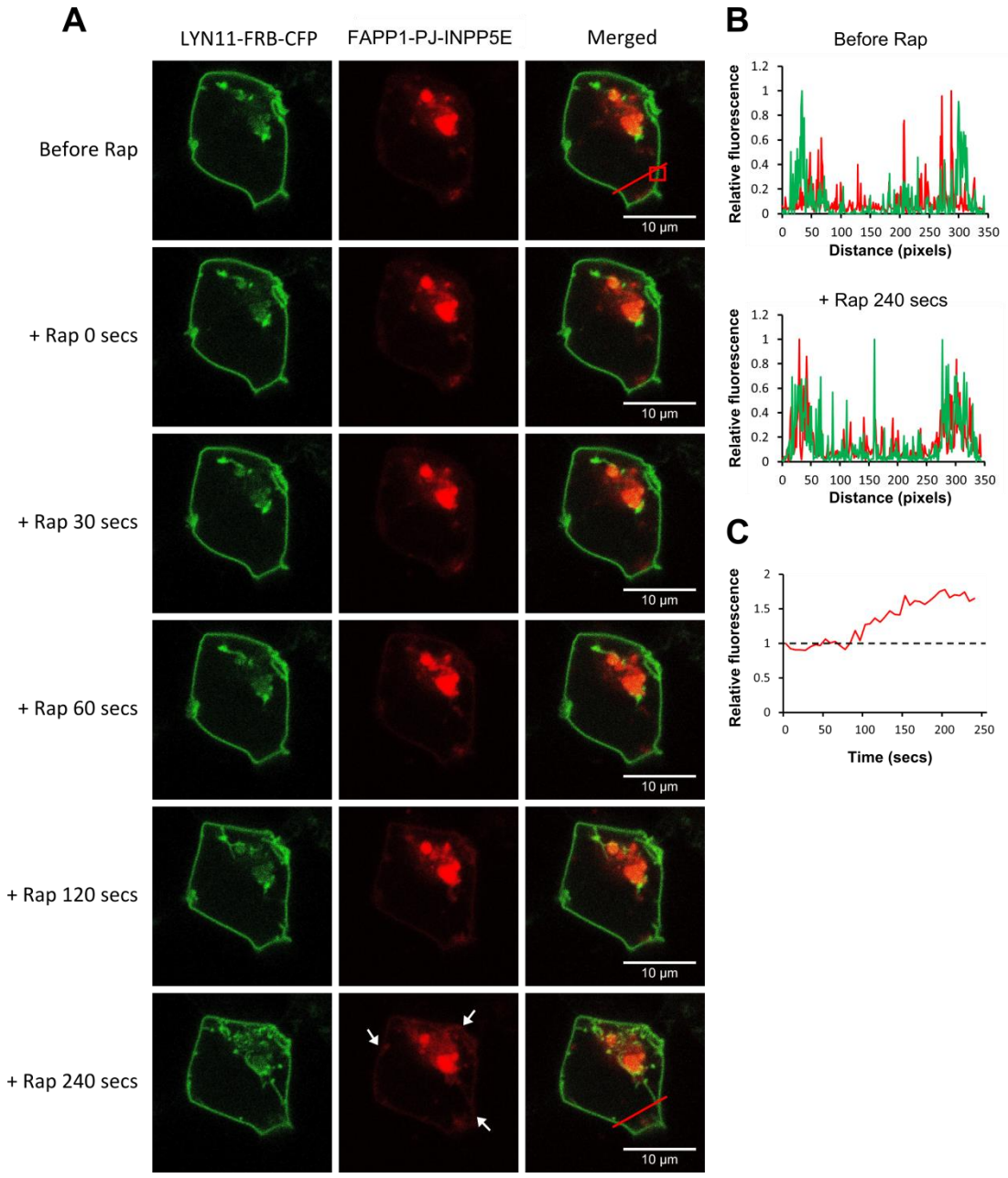


**Figure 46. The localisation of FAPP1-PJ-INPP5E in HEK293 cells, before and after rapamycin addition. A –** The top row shows HEK293 cells transiently expressing FAPP1-PJ-INPP5E and LYN11-FRB-CFP. The 5 centre and bottom rows show the localisation of these constructs in the same cell at different time points after the addition of rapamycin (5 µM). Images were obtained using confocal microscopy. Arrows highlight areas of FAPP1-PJ-INPP5E membrane localisation. **B** – Normalised ($y/y_{max}$) intensity of fluorescence of CFP and RFP along the red line illustrated in the top right-hand image (before Rap) and bottom right-hand image (+ Rap 240 secs) in **A**. Green represents LYN11-FRB-CFP and red represents FAPP1-PJ-INPP5E in both **B** and **C**. **C** – Change in fluorescence intensity over time measured from region of interest shown by red box in top right-hand image in **A** (relative to value from image 1 of time series). Representative cell response (n=3).

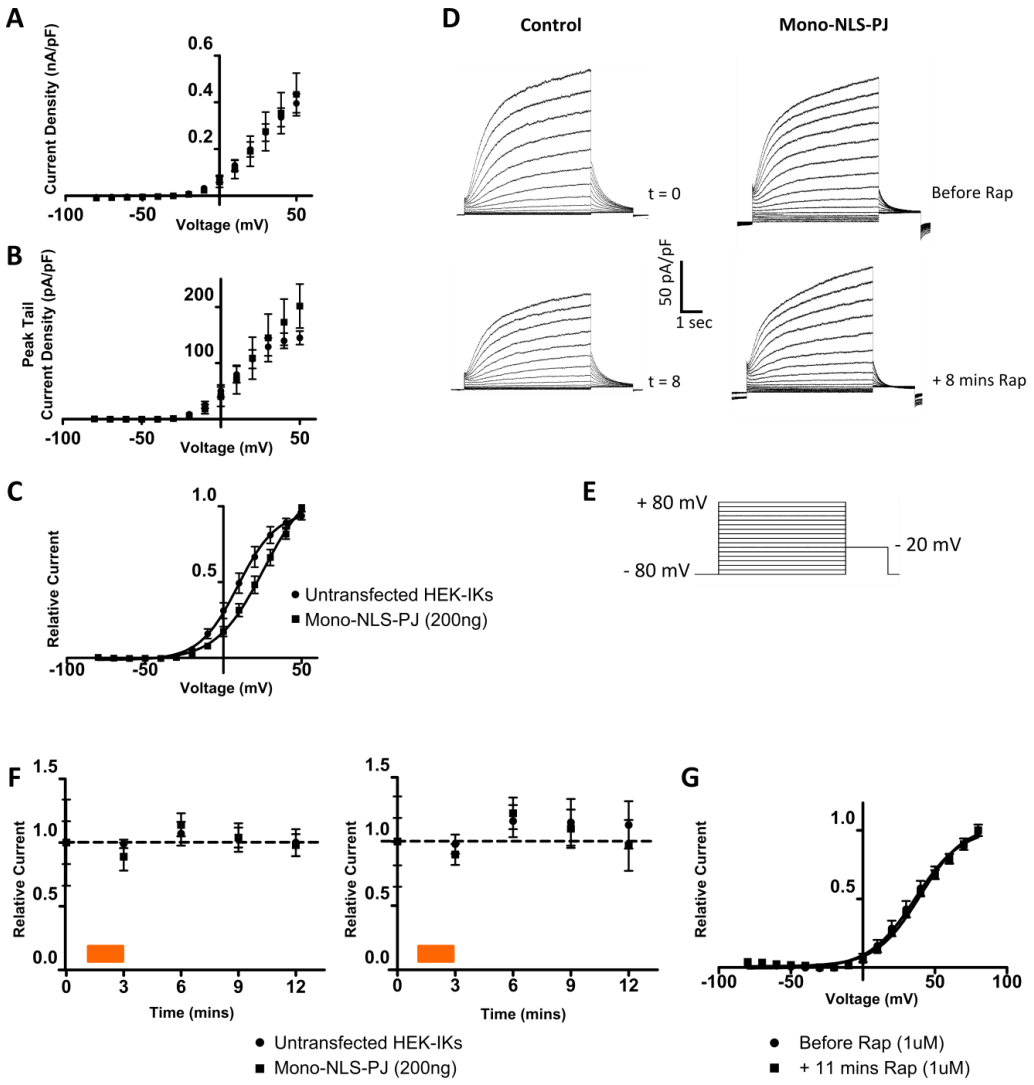


**Figure 47. The effect of recruiting a nuclear-targeted PJ construct to the plasma membrane using rapamycin, on the $I_{Ks}$ current in HEK-$I_{Ks}$ cells.** **A** – Mean current density and **B** – peak tail current density recorded in WCPC from untransfected HEK-$I_{Ks}$ cells (control; n=12) or HEK-$I_{Ks}$ cells transiently expressing mono-NLS-PJ with LYN11-FRB (n=9). **C** – Steady state of activation curve, constructed by plotting normalised peak tail current densities (y/ymax) against test potential (WCPC). **D** – Representative current traces recorded in P-WCPC from untransfected HEK-$I_{Ks}$ cells (control) at t = 0 mins and t = 8 mins, and HEK-$I_{Ks}$ cells expressing mono-NLS-PJ with LYN11-FRB, before and 8 mins after the start of rapamycin (5µM) perfusion. **E** – Voltage protocol used to elicit the currents recorded in P-WCPC. **F** – Relative current over time from untransfected HEK-$I_{Ks}$ cells (control; n=9), and HEK-$I_{Ks}$ cells transiently expressing LYN11-FRB and mono-NLS-PJ (n=10), measured at +30mV, recorded in P-WCPC. Rapamycin (5µM) was perfused over HEK-$I_{Ks}$ cells expressing mono-NLS-PJ with LYN11-FRB for 2 minutes after the 1$^{st}$ I-V recording (orange bar). **G** – Steady state of activation curve, constructed by plotting normalised peak tail current densities (y/ymax) against test potential for HEK-$I_{Ks}$ cells transiently expressing mono-NLS-PJ with LYN11-FRB before and after 11 mins of rapamycin addition (P-WCPC). Data are presented as mean ± SE. A one-way ANOVA with Dunnett's post hoc test was used to determine significance between the current at t=0 (baseline) and all other time points in **F**, unpaired t-tests were used to compare untransfected vs construct-expressing cells at each time point in **F**, the Boltzmann equation was applied to data in **C** and **G** to fit sigmoidal curves. Paired and paired t-tests were used to compare $V_{0.5}$ values obtained from Boltzmann functions in **C** and **G**, respectively.

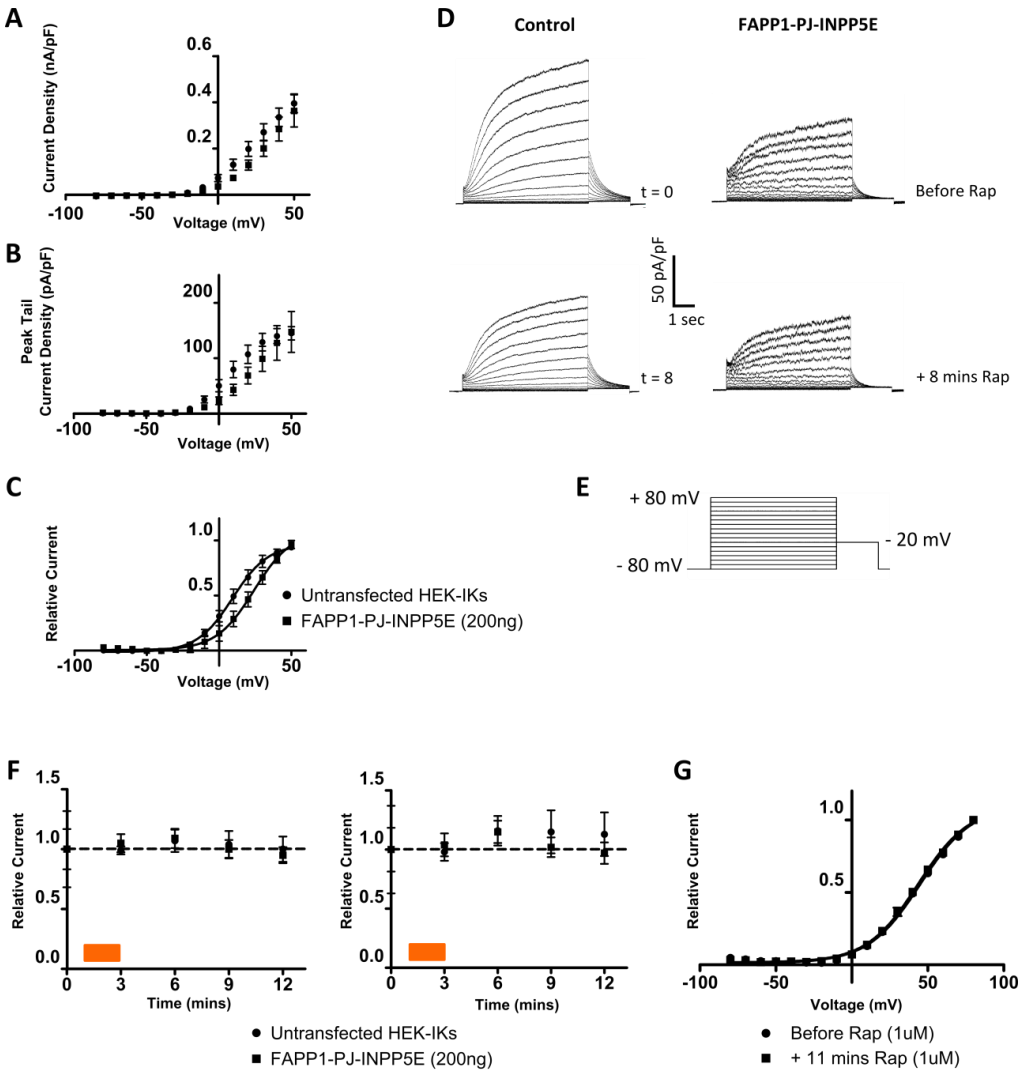


**Figure 48. The effect of recruiting a Golgi-targeted PJ-INPP5E construct to the plasma membrane using rapamycin, on the $I_{Ks}$ current in HEK-$I_{Ks}$ cells. A** – Mean current density and **B** – peak tail current density recorded in WCPC, from untransfected HEK-$I_{Ks}$ cells (control; n=12) or HEK-$I_{Ks}$ cells transiently expressing LYN11-FRB and FAPP1-PJ-INPP5E (n=9). **C** – Steady state of activation curve, constructed by plotting normalised peak tail current densities (y/ymax) against test potential (WCPC). **D** – Representative current traces recorded in P-WCPC from untransfected HEK-$I_{Ks}$ cells (control) at t = 0 mins and t = 8 mins, and HEK-$I_{Ks}$ cells expressing FAPP1-PJ-INPP5E with LYN11-FRB, before and 8 mins after the start of rapamycin (5µM) perfusion. **E** – Voltage protocol used to elicit the currents recorded in P-WCPC. **F** – Relative current over time from untransfected HEK-$I_{Ks}$ cells (control; n=9) and HEK-$I_{Ks}$ cells transiently expressing FAPP1-PJ-INPP5E with LYN11-FRB (n=9) measured at +30mV, recorded in P-WCPC. Rapamycin (5µM) was perfused over HEK-$I_{Ks}$ cells expressing mono-NLS-PJ and LYN11-FRB for 2 minutes (orange bar) after the 1$^{st}$ I-V recording (orange bar) in P-WCPC **G** – Steady state of activation curve, constructed by plotting normalised peak tail current densities (y/ymax) against test potential, for HEK-$I_{Ks}$ cells transiently expressing FAPP1-PJ-INPP5E with LYN11-FRB before and after 11 mins of rapamycin addition (P-WCPC). Data are presented as mean ± SE. A one-way ANOVA with Dunnett's post hoc test was used to determine significance between the current at t=0 (baseline) and all other time points in **F**, unpaired t-tests were used to compare untransfected vs construct-expressing cells at each time point in **F**, and the Boltzmann equation was applied to data in **C** and **G** to fit sigmoidal curves. Paired and paired t-tests were used to compare $V_{0.5}$ values obtained from Boltzmann functions in **C** and **G**, respectively.

### 4.3.6 The effect of mutating residues involved in the FRB-FKBP interaction on the $I_{Ks}$ current in HEK-$I_{Ks}$ cells

Despite confocal imaging showing that the FAPP1-PJ-INPP5E construct was effectively restricted from the PM, and WCPC recordings confirming that the inhibition seen with un-restricted PJ-INPP5E had been abrogated, the recruitment of this construct in P-WCPC did not affect the $I_{Ks}$ current. Whether this was due to insufficient recruitment of FAPP1-PJ-INPP5E to the PM or another mechanism is unknown, but results in chapter 5 would suggest that PJ may not be able to reduce the $PIP_2$ concentration to below the threshold require for $I_{Ks}$ activation in P-WCPC.

To try to reduce the $I_{Ks}$ inhibition in the presence of PJ or PJ-INPP5E with LYN11-FRB, the interaction between the FRB and FKBP domains that was postulated in chapter 3 was targeted. In order to abolish the interaction between the FRB and FKBP domains, mutations were introduced to the FRB domain by site-directed mutagenesis. Four LYN11-FRB mutants were made: Phe2039Ala (F2039A), Arg2042Ala (R2042A), Val2094Ala (V2094A) and Tyr2105Ala (Y2105A) (amino acid number refers to the original location in the full length mTOR protein). When the LYN11-FRB(R2042A), LYN11-FRB(V2094A) or LYN11-FRB(Y2105A) mutants were expressed with PJ in HEK-$I_{Ks}$ cells, a complete loss of the $I_{Ks}$ current was observed, and when the LYN11-FRB(F2039A) mutant was expressed with PJ in HEK-$I_{Ks}$ cells a small current remained, but was significantly different from control cells (CD and PTCD: $p<0.005$ across all voltages analysed) (figure 49).

A double mutant, LYN11-FRB(R2042A/Y2105A), and two triple mutants, LYN11-FRB(F2039A/V2094A/Y2105A) and LYN11-FRB(F2042A/V2094A/Y2105A) were also made, to try to further decrease any interaction between the two domains. The mutants LYN11-FRB(R2042A/Y2105A) and LYN11-FRB(R2042A/V2094A/Y2105A) caused a complete loss of the $I_{Ks}$ current in HEK-$I_{Ks}$ cells when expressed with PJ (CD and PTCD: $p<0.005$ across all voltages analysed), whereas LYN11-FRB(F2039A/V2094A/Y2105A) only resulted in a partial loss of the $I_{Ks}$ current, but this was still significant (CD: $p<0.05$ across all voltages analysed, except 70 mV, where p=NS; PTCD: $p<0.05$ across all voltages analysed) (figure 49).

As the LYN11-FRB(F2039A/V2094A/Y2105A) mutant did not cause a complete loss of $I_{Ks}$ current when expressed with PJ, the ability of rapamycin to recruit one of the lipid-depleting constructs to the mutant LYN11-FRB construct was assessed using confocal microscopy. Time series imaging showed that addition of rapamycin (5 μM) to HEK293 cells expressing PJ-DEAD and LYN11-FRB(F2039A/V2094A/Y2105A) did not result in translocation of PJ-DEAD to the PM (figure 50).

### 4.3.7 Incorporating the lipid-depleting constructs into the gibberellin-induced dimerisation system

The newly created 'PJ-GID1' construct was Sanger sequenced to confirm the correct sequence had been achieved and each PCR fragment had been inserted into the vector correctly. PJ-GID1 (500 ng) was then expressed in HEK293 cells and visualised using fluorescence microscopy to confirm that the construct could be expressed in the heterologous cell system that would be used for future experiments. Using confocal microscopy, the correct localisation of PJ-GID1 and LYN-CFP-GAI(1–92) was observed (figure 52).

In order to confirm that the construction of PJ-GID1 was successful, the ability to induce translocation to LYN-GAI in the PM had to be proven. First, the ability of GA3-AM to induce dimerisation of YFP-GID1 and LYN-CFP-GAI(1–92) was investigated by acquiring images in a time series using confocal microscopy.

Figure 51 shows that YFP-GID1 translocated to the PM in under 30 seconds after the addition of GA3-AM to HEK293 cells expressing YFP-GID1 and LYN-GAI(1–92). Quantification of YFP-GID1 and LYN-CFP-GAI(1–92) signal intensity (figure 51B) showed that YFP-GID1 moved from the cytoplasm to the PM on addition of GA3-AM. This is supported by analysis of the signal intensity of YFP-GID1 at a region of the PM, which showed that after addition of GA3-AM, YFP-GID1 signal intensity increased here over time (figure 51C). These findings confirm that the esterases required to cleave the AM group from GA3-AM (producing the active GA3) are present in HEK293 cells.

Next, the ability of GA3-AM to induce translocation of PJ-GID1 to the PM was tested. Figure 52 shows that after addition of GA3-AM to HEK293 cells expressing PJ-GID1 and LYN-GAI(1-92), there was no translocation of PJ-GID1, which remained homogenously localised throughout the cytosol and nucleus. These observations were confirmed by performing quantification of the PJ-GID1 and LYN-CFP-GAI(1–92) signal intensity (figure 52B), which showed that PJ-GID1 did not translocate from the cytoplasm to the PM on addition of GA3-AM (figure 52C), and this was supported by analysis of the signal intensity of PJ-GID1 at a region of the PM, which showed that there was no change in the PJ-GID1 signal intensity after the addition of GA3-AM (figure 52C).

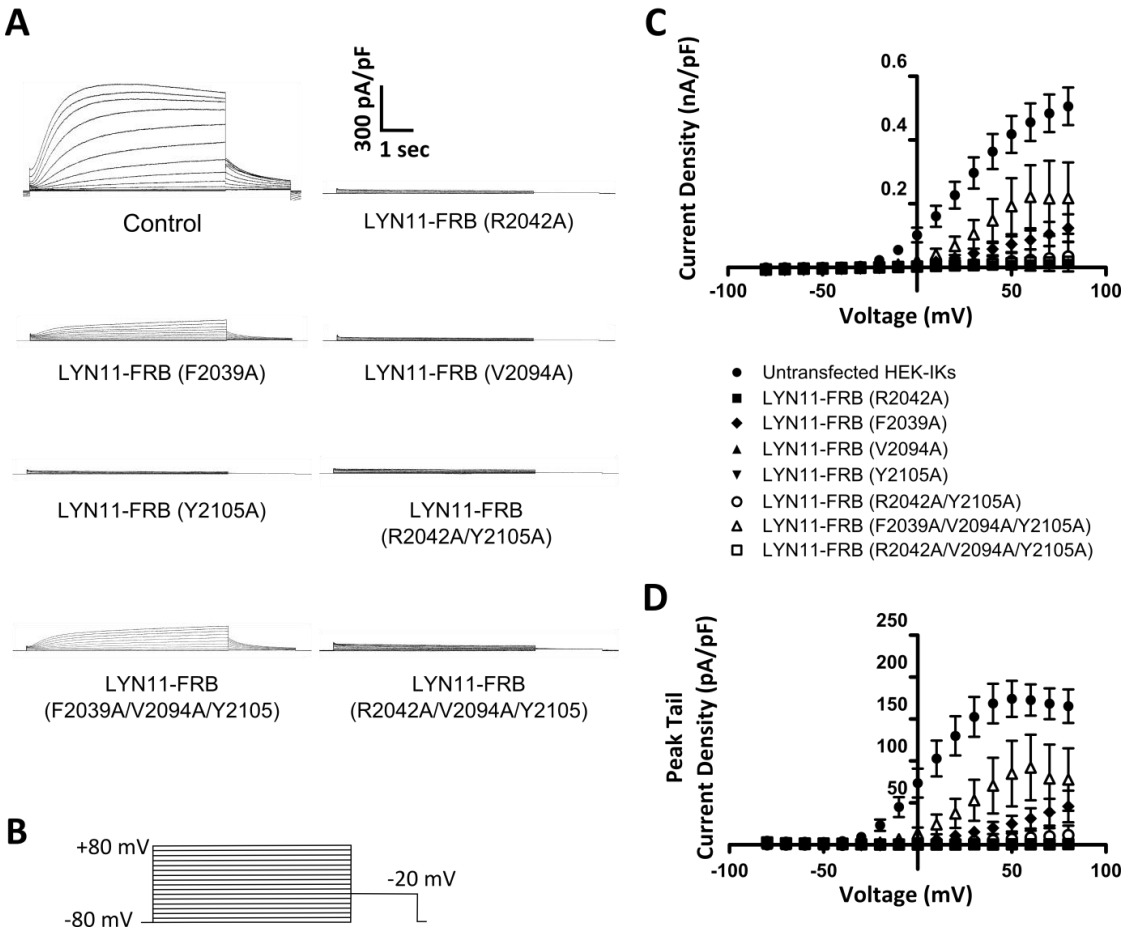


**Figure 49. The effect of expressing PJ with mutant LYN11-FRB constructs on the $I_{Ks}$ current in HEK-$I_{Ks}$ cells. A** – Representative traces recorded in WCPC of currents from untransfected HEK-$I_{Ks}$ cells (control), and HEK-$I_{Ks}$ cells transiently expressing PJ with LYN11-FRB mutants. **B** – Voltage protocol used in WCPC to elicit the currents recorded. **C –** Mean current density and **D** – peak tail current density of currents recorded in WCPC from untransfected HEK-$I_{Ks}$ cells (control; n=9) or HEK-$I_{Ks}$ cells transiently expressing LYN11-FRB containing the mutation(s) F2039A (n=4) R2042A (n=5), V2094A (n=5), Y2105A (n=5), R2042A/Y2105A (n=5), R2042A/V2094A/Y2105A (n=5) or F2039A/V2094A/Y2105A (n=6). Data are presented as mean ± SE. A one-way ANOVA with Dunnett's post hoc test was used to determine significance between the current from control cells and cells expressing a LYN11-FRB mutant in **C** and **D**.

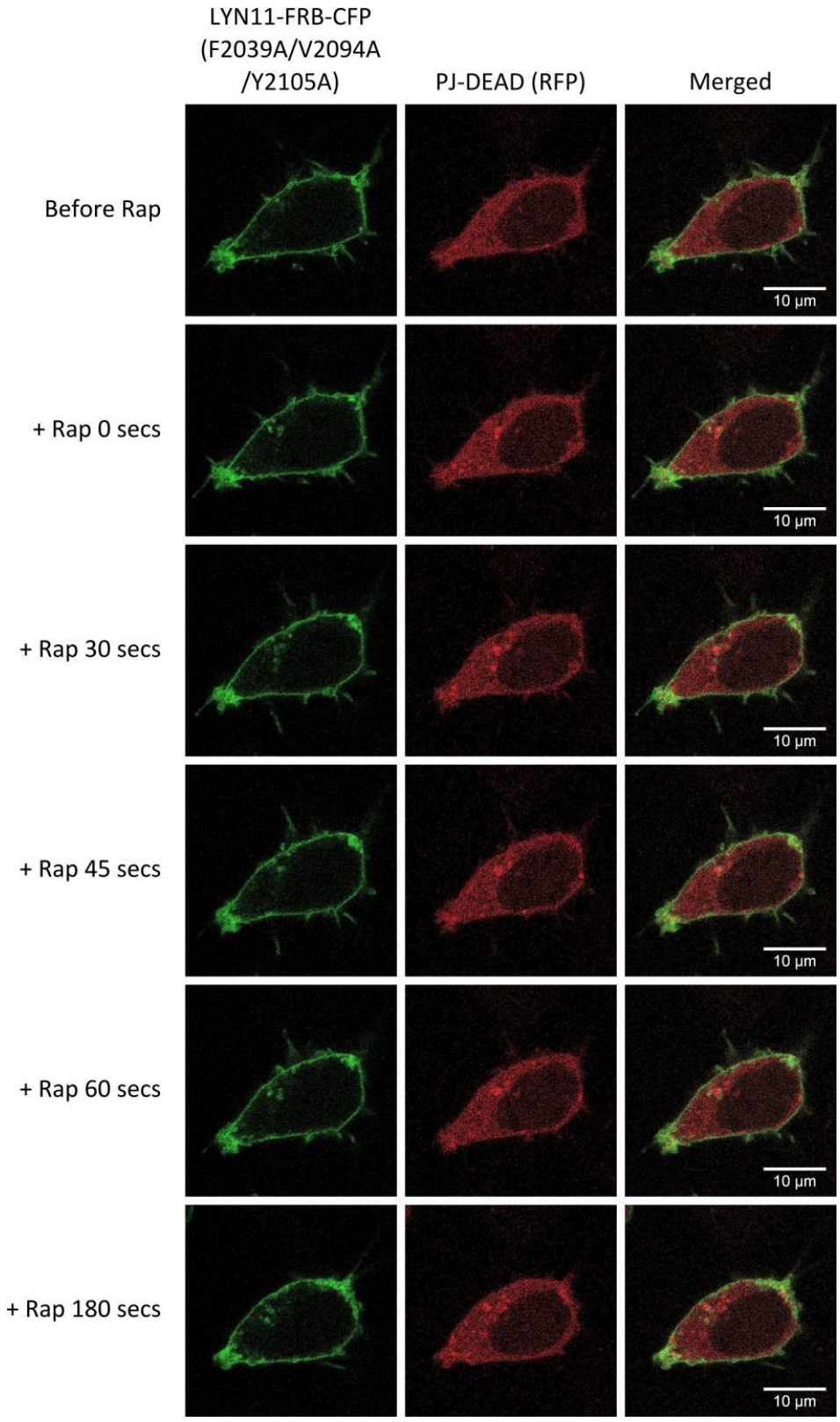


**Figure 50. The localisation of PJ-DEAD and LYN11-FRB(F2039A/V2094A/Y2105A) in HEK293 cells before and after rapamycin addition.** The top row shows HEK293 cells transiently expressing PJ-DEAD and LYN11-FRB(F2039A/V2094A/Y2105A). The 5 centre and bottom rows show the localisation of these constructs in the same cell at different time points after the addition of rapamycin (5 µM). Images were obtained using confocal microscopy. Representative cell resonse (n=4).

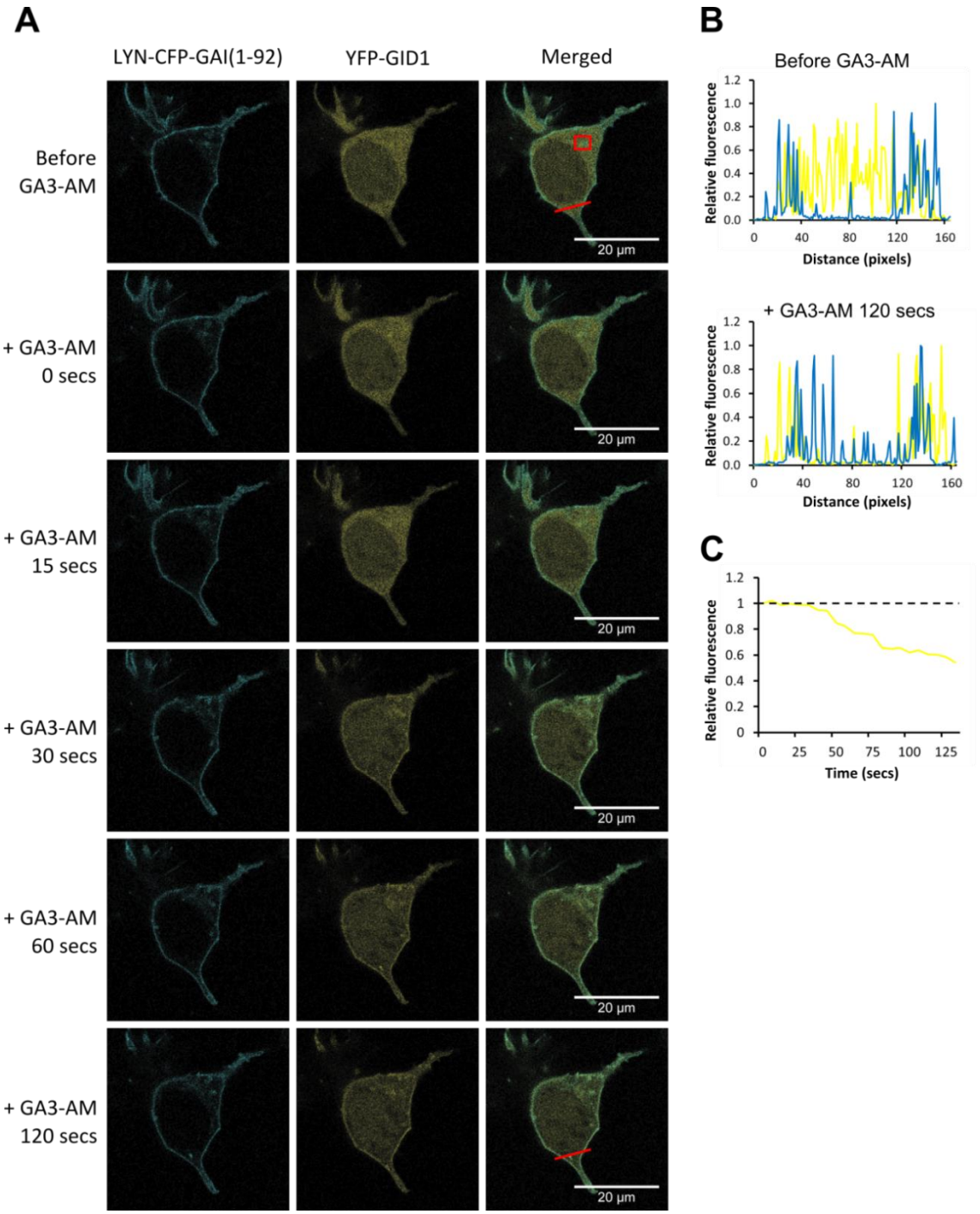


**Figure 51. The localisation of YFP-GID1 and LYN-CFP-GAI(1–92) in HEK293 cells, and the GA3-AM-induced recruitment of YFP-GID1 to LYN-CFP-GAI(1–92).** **A –** The top row shows HEK293 cells transiently expressing YFP-GID1 and LYN-CFP-GAI(1–92) before the addition of GA3-AM (100 µM). The two centre and bottom rows are of the same cell at different time points after the addition of GA3-AM (100 µM). Images were obtained using confocal microscopy. **B** – Normalised ($y/y_{max}$) intensity of fluorescence of CFP and YFP along the red line illustrated in the top right-hand image (before GA3-AM) and bottom right-hand image (+ GA3-AM 120 secs) in **A**. Blue represents LYN-CFP-GAI(1–92) and yellow represents YFP-GID1 in both **B** and **C**. **C** – Change in fluorescence intensity over time measured from region of interest shown by red box in top right-hand image in **A** (relative to value from image 1 of time series). Response from one cell (n=1).

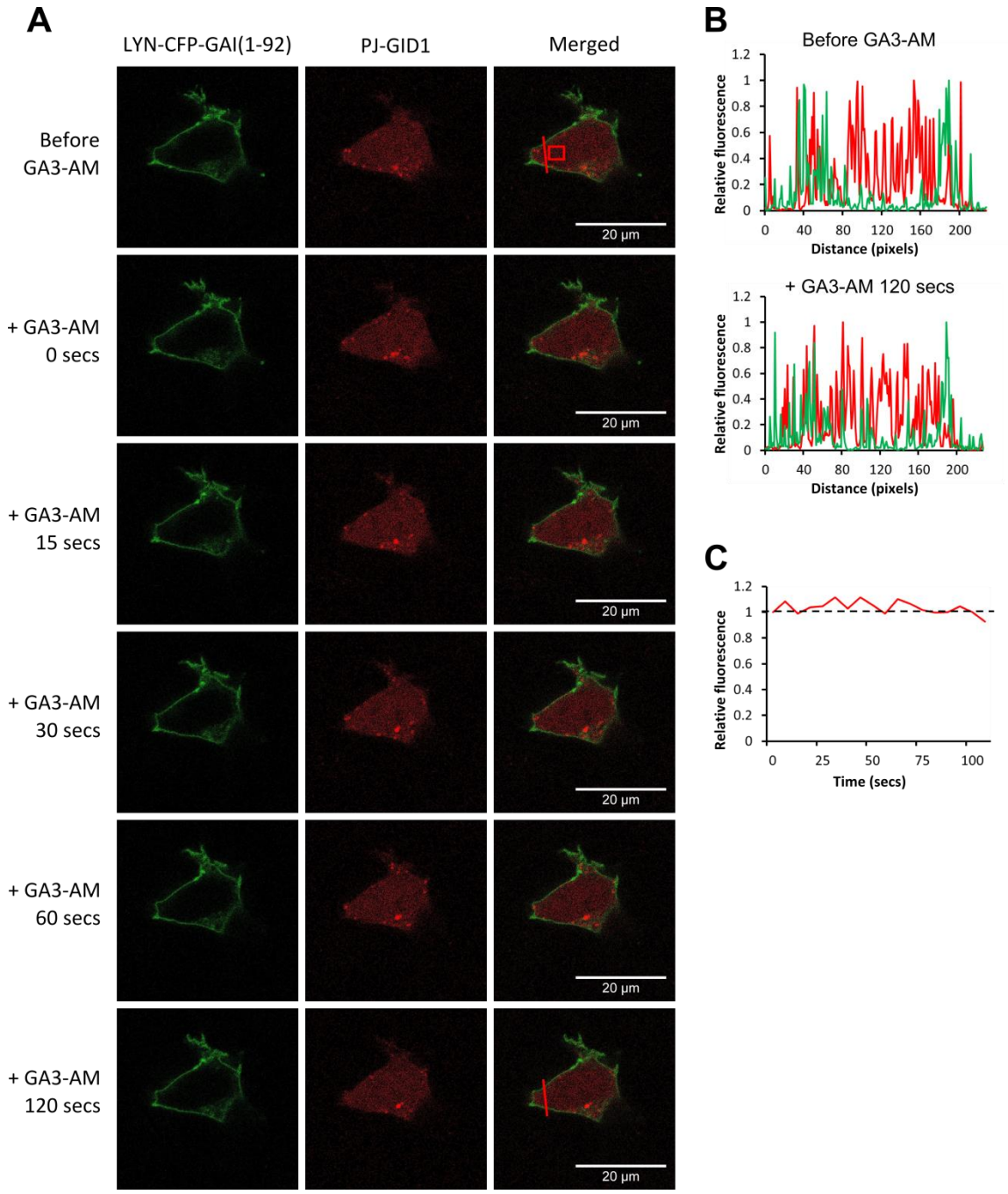


**Figure 52. The localisation of PJ-GID1 and LYN-CFP-GAI(1–92) in HEK293 cells, and the GA3-AM-induced recruitment of PJ-GID1 to LYN-CFP-GAI(1–92). A –** *T*he top row shows HEK293 cells transiently expressing PJ-GID1 and LYN-CFP-GAI(1–92) before the addition of GA3-AM. The two centre and bottom rows are of the same cell at different time points after the addition of GA3-AM (100 µM). Images were obtained using confocal microscopy. **B** – Normalised ($y/y_{max}$) intensity of fluorescence of CFP and RFP along the red line illustrated in the top right-hand image (before Rap) and bottom right-hand image (+ Rap 120 secs) in **A**. Green represents LYN-CFP-GAI(1–92) and red represents PJ-GID1 in both **B** and **C**. **C** – Change in fluorescence intensity over time measured from region of interest shown by red box in top right-hand image in **A** (relative to value from image 1 of time series). Response from one cell (n=1).

## 4.3 Discussion

In Chapter 3, I found that the rapamycin-induced dimerisation system was not optimal for investigating how $PIP_2$ depletion affects the $I_{Ks}$ channel. In contrast to other groups' work with this system investigating the function of other ion channels (Hammond *et al*., 2012; Kruse *et al*., 2012; Suh *et al*., 2006), and my own experiments with the $K_{ir}2.1$ and hERG channels (chapter 3), I found that expression of the active lipid-depleting constructs with the PM-anchored LYN11-FRB construct led to inhibition of the $I_{Ks}$ current. The constitutive activity of the lipid-depleting constructs coupled with their ubiquitous cellular-expression led to the conclusion that the constructs were in contact with, and consequently causing dephosphorylation of, the PI substrates in the PM. There also appeared to be an interaction between the lipid-depleting constructs and LYN11-FRB, which acted to increase the effect of lipid-depletion on the $I_{Ks}$ channel, even in the absence of rapamycin.

In an ideal world, an inactive construct would exist that could be switched to the active conformation when bound to rapamycin, but the creation of such a construct is unfortunately very complex and beyond the scope of my project. An alternative approach to limit the exposure of the phospholipid substrates to the active enzyme domains of the lipid-depleting constructs (in the absence of rapamycin) is to alter the localisation of the constructs within the cell. Originally expressed almost ubiquitously throughout the cell, the lipid-depleting constructs were modified in a way to restrict their expression to the Golgi, nucleus or early endosomes.

*The subcellular targeting of lipid-depleting constructs affected their ability to undergo rapamycin-induced translocation the PM*

The modified lipid-depleting constructs (mono-NLS-PJ, bi-NLS-PJ, 2xFYVE-PJ and FAPP1-PJ-INPP5E) varied in success regarding their localisation to the destination subcellular organelles.

Bi-NLS-PJ was the only construct to be entirely targeted to the desired intracellular location. Ironically, the bipartite NLS used to localise the construct to the nucleus was so successful that this construct could not translocate out of the nucleus to the PM in the presence of rapamycin in a suitable timeframe. This is not to say, however, that the bi-NLS-PJ construct would not translocate from the nucleus to the PM over a period of hours. Unfortunately, this timescale is not compatible with the patch clamp experiments required to assess the effects of construct recruitment on $I_{Ks}$ channel function.

The mono-NLS-PJ construct displayed less complete targeting to the nucleus. Again, however, the translocation of the nuclear-localised construct was unsuccessful on the timescale required, and only the low level of cytoplasmic mono-NLS-PJ could be recruited to the PM.

The importin-α receptor contains a number of different binding regions for NLS motifs, which bind monopartite and bipartite sequences in different ways. The monopartite NLS is known to interact with a few of these binding regions, whereas the bipartite NLS interacts with many more (Conti & Kuriyan, 2000). This could explain why the bi-NLS-PJ construct showed a higher extent of nuclear localisation compared to the mono-NLS-PJ construct.

The least successful modified construct was 2xFYVE-PJ, which failed to localise solely to the early endosomes as intended. A double FYVE domain (2xFYVE) was used here because the single domain has been shown to exhibit a low affinity for PI3P, whereas the inclusion of a second FYVE sequence was found to increase the affinity for PI3P (Gilooly *et al*., 2000). Instead of being localised to the early endosomes, the 2xFYVE-PJ construct was seen at the early endosomes and Golgi. This could be due to the fact that the early endosomes can shuttle cargo back to the Golgi (Grant & Donaldson, 2009), which could transfer the construct between the two compartments and lead to an accumulation of this construct at the Golgi. Nevertheless, this construct was restricted from the PM, but rapamycin addition could not induce the translocation of this construct from either location to the PM. This could be due to an extremely high affinity of 2xFYVE for PI3P, or the unexpected localisation observed may indicate logistical problems regarding movement of the construct within the cell.

The most promising of the modified constructs was FAPP1-PJ-INPP5E, which successfully localised to the Golgi and, unlike the other three modified constructs, also appeared to translocate to the PM after addition of rapamycin. The FAPP1 domain was used by Phua *et al.* (2012) to target small GTPases to the Golgi, and in line with my results, this group found that the FAPP1-conatining construct translocated to the PM after rapamycin addition. Phua *et al*. (2012) also discuss that FAPP1 binds to PI4P with a dissociation constant ($K_d$) of 230 nM, and state that the $K_d$ of FKBP for rapamycin is 0.2 nM and the $K_d$ of FRB for rapamycin is 12 nM (Banaszynski *et al*., 2005), meaning that the FKBP- FAPP1-containing GTPase construct used in their study would likely remain at the PM after rapamycin addition, once dissociated from the Golgi. This means that FAPP1-PJ-INPP5E (which contains both the FAPP1 and FKBP domains) would also dissociate from the Golgi and freely diffuse through the cytosol, where rapamycin could then concentrate it at the PM.

PJ-INPP5E was used in the place of PJ as the template for the FAPP1-modified construct here due to the presence of the active SAC1 domain in PJ, which dephosphorylates PI4P. This may have presented problems with targeting because the FAPP1 domain achieves its Golgi localisation by binding to ARF1 and PI4P in the TGN. The targeting of a PI4P-depleting construct using a PI4P-binding domain did not appear to be the most sensible option!

Phua and colleagues (2012) decided not to use a nuclear-targeted construct in their studies as they deemed the onset of dimerisation too slow due to the added step of nuclear export. However, the mono-NLS-PJ construct was selected here (because of the recruitment of cytoplasmic construct to the PM) for investigation into the effect of $PIP_2$ depletion on the $I_{Ks}$ current, in addition to FAPP1-PJ-INPP5E. These constructs were expressed in HEK-$I_{Ks}$ cells with LYN11-FRB and the effect was compared to untransfected HEK-$I_{Ks}$ cells.

WCPC experiments showed that there was no inhibition of the $I_{Ks}$ current when expressing either mono-NLS-PJ or FAPP1-PJ-INPP5E with LYN11-FRB. When rapamycin was added to the cells to induce dimerisation of these constructs with LYN11-FRB in P-WCPC, no change in the $I_{Ks}$ current was observed. This could indicate that the depletion of $PIP_2$ and/or PI4P had no effect on the $I_{Ks}$ current, or that the recruitment of the lipid-depleting constructs was unsuccessful. However, a more plausible explanation (which is also discussed in chapter 5) is that re-synthesis of $PIP_2$ is made possible in P-WCPC, and this prevents the depletion of $PIP_2$ by PJ or PJ-INPP5E (and hence the mono-NLS-PJ and FAPP1-PJ-INPP5E constructs).

*Mutating FKBP-interacting residues in FRB could not overcome $I_{Ks}$ inhibition when expressed with PJ*

Fortunately, the LYN11-FRB construct gave another route to try to optimise the rapamycin-inducible dimerisation system. In chapter 3, I suggested that there could be an interaction between the FRB domain of LYN11-FRB and the FKBP domain of the lipid-depleting constructs in the absence of rapamycin. This theory was based on the observed increase in $I_{Ks}$ inhibition when both LYN11-FRB and PJ were expressed in HEK-$I_{Ks}$ cells compared to the expression of PJ alone, and the protein-protein interaction sites identified by structural analysis of the FRB-rapamycin-FKBP complex (Liang *et al*., 1999).

There are 21 interactions between 6 residues in the FRB domain and 8 residues in the FKBP domain, of which 3 FRB residues are also involved in the binding of rapamycin (Liang *et al*., 1999). The FRB residues involved in the protein-protein interaction with FKBP are Phe2039, Arg2042, Val2094, Thr2098, Tyr2105 and Arg2109; the residues that contribute to rapamycin binding are Phe2039, Arg2042 and Tyr2105. Mutation of Phe2039, Arg2042, Val2094 and Tyr2105 to Ala altered 5, 7, 5 and 2 interactions, respectively, and the double (R2042A/Y2105A) and triple (F2039A/V2094A/Y2105A and R2042A/V2094A/Y2105A) mutants altered 9, 12 and 14 interactions, respectively. Despite altering (and possibly abolishing) up to two thirds of the interaction sites between FRB and FKBP, there was still a complete loss of the $I_{Ks}$ current when expressing the LYN11-FRB mutants with PJ, with the exception of the triple mutant LYN11-FRB(F2039A/V2094A/Y2105A). It was later discovered

that this mutant was unable to bind rapamycin (evidenced by the lack of visible PJ-DEAD translocation after rapamycin addition).

*Incorporating the lipid-depleting constructs into the gibberellin-induced dimerisation system was not successful*

The inability to recruit PJ-GID1 to the PM could be due to the arrangement of domains within the construct. I also attempted to create 2 other GID1-containing PJ constructs, but was unable to successfully clone the required domains into the vector in the other conformations.

With more time, perhaps other PJ-GID1 constructs could be created that would enable the successful investigation of the effect of $PIP_2$ depletion on the $I_{Ks}$ current.

### 4.4 Conclusions and Future Directions

The inherent problems with the rapamycin-inducible dimerisation system constructs are 1) that the lipid-depleting constructs are constitutively expressed without restriction from the PM, and 2) that the lipid-depleting constructs and LYN11-FRB appear to interact with each other even before the initiation of dimerisation.

It appears that the subcellular-organelle targeting that remedied these drawbacks could not itself be overcome by rapamycin in the case of the NLS-containing and 2xFYVE-containing constructs. The FAPP1-PJ-INPP5E construct could be recruited to the PM from the Golgi, but it had no effect on the $I_{Ks}$ current. This could be due to, for example, a higher affinity of FAPP1 for PI4P and ARF1 than of FKBP for rapamycin, which would favour the binding of FAPP1-PJ-INPP5E to the Golgi and impede the ability to recruit the construct to the PM. However, translocation of FAPP1-PJ-INPP5E was seen using confocal microscopy, so it is more likely that the level of $PIP_2$ depletion achieved was not sufficient to alter $I_{Ks}$ channel function.

Regarding the LYN11-FRB mutants that were made, it is clear that not all combinations were explored, and with more time others could have been made. However, reviewing the combinations already attempted, it seems unlikely that others would abolish the FRB-FKBP interaction and recover the $I_{Ks}$ current whilst preserving the rapamycin-binding ability of the FRB domain.

Obviously an avenue not explored was the alteration of protein structure to inactivate the enzyme domains prior to rapamycin-binding. This would negate the need to abolish the FRB-FKBP interaction, because the proximity of the enzymes to the PM would not be a problem if they were

inactive. Whether this method is possible remains to be explored, and was regrettably beyond the scope of this project.

Instead of pursuing different ways to improve the rapamycin-inducible dimerisation system, it could seem sensible to accept that this system is not optimal for use with particularly $PIP_2$-sensitive ion channels, as demonstrated by the results I have presented from my work on the $I_{Ks}$ channel so far. Instead, efforts could be focused on finding another method to allow the direct and physiological manipulation of $PIP_2$ and/or PI4P, or exploiting an alternative CID method such as the gibberellin-induced dimerisation system. I attempted to incorporate the lipid-depleting phosphatase domains from the rapamycin system into the gibberellin-induced dimerisation system, but the construct produced was not able to be recruited to the PM after addition of GA3-AM. In a personal communication with Takanari Inoue, I was told that recruitment of Inp45p-YFP-GID1 (which depletes $PIP_2$) to the PM was not very efficient and did not show a strong decrease in $PIP_2$. In addition to this, the expression of the GID1- and GAI-containing constructs appears to be compromised due to a competition for transcription and translation. The Inoue laboratory concluded that the gibberellin-based dimerisation system is not as robust as the rapamycin-based dimerisation system. In light of this communication and my own experiences, it may be in the best interest of other researchers to focus efforts on identifying other lipid-depletion techniques.

# CHAPTER 5: Investigating the role of $PIP_2$ and PI4P in the function and trafficking of the $I_{Ks}$ channel

## 5.1 Introduction

Substantial effort has been made to establish the specific mechanisms by which different KCNQ1 mutations compromise the $I_{Ks}$ current. It was previously believed that this only occurred through the assembly of dysfunctional channels that could not function correctly at the PM (Bianchi *et al.*, 2000). Since these findings, however, it has been shown that a large number of mutations in the KCNQ1 subunit cause defective anterograde trafficking of the channel to the PM (table 6).

Experimentally, many mutant channels show increased colocalisation (compared to WT channel) with a fluorescent ER marker, indicating retention in the ER. A number of KCNQ1 mutations can also cause a DN reduction of the amount of WT channel that reaches the PM (Aizawa *et al.*, 2004; Li *et al*., 2009; Thomas *et al*., 2005), where the mutant subunit acts antagonistically on the WT subunit.

*Channel trafficking and disease*

Dysfunctional membrane trafficking of cellular proteins is associated with a plethora of diseases. A well-known example is cystic fibrosis (CF), where approximately 70% of people with CF harbour a homozygous deletion of phenylalanine at position 508 of the cystic fibrosis transmembrane conductance regulator (CFTR*)* gene (ΔF508-CFTR). The ΔF508-CFTR mutation causes protein misfolding that impairs the trafficking of the CFTR channel (Cheng *et al*., 1990), leading to defective electrolyte transport and viscous secretions in the airway epithelia and other organ systems (Cutting, 2015).

Regarding cardiac disease, defective ion channel trafficking has been found to be responsible for a number of cardiac arrhythmias. For example, mutations in the $I_{Kr}$ channel (hERG) can cause LQT2, and most of the mutations identified in this channel cause a reduction of its expression at the PM (Anderson *et al*., 2006; Anderson *et al*., 2014). This is due to the production of poorly folded channels that cannot be successfully trafficked to the PM, and so are subsequently degraded in the ER or proteasome (Zhou *et al*., 1998). Baroudi and colleagues reported that a double mutation (Arg1232Trp/Thr1620Met) in the cardiac $Na^+$ channel, $Na_v1.5$, caused a reduced expression of this channel at the PM. This mutation is found in a number of people with Brugada syndrome, a ventricular arrhythmia characterised by ST-segment elevation that can lead to sudden cardiac death (Baroudi *et al*., 2002).

Mutations in the $I_{Ks}$ channel α-subunit that cause channel trafficking defects can result in different severities of LQTS. When one KCNQ1 allele is mutated causing loss of protein production or degradation of the protein, the remaining single copy may not be able to produce normal levels of KCNQ1 protein, which results in haploinsufficiency. This may not lead to severe symptoms if the level of channel production is sufficient. This can also result from the ER-retention of mutant channels whilst WT channels are successfully trafficked to the PM (Sato *et al.*, 2009; Wilson *et al.*, 2005). Other mutations may cause channels to be retained in the ER, for example, but exert a dominant negative effect over the WT channel subunit, causing a greater reduction of KCNQ1 channels able to reach the PM. DN trafficking mutations that are homozygously inherited commonly cause JLNS, because the number of functional channels that reach the PM is not sufficient to sustain the $K^+$ conductance required in the inner ear ad heart.

*Phosphoinositides and membrane trafficking*

When proteins undergo trafficking through the cell to reach their final destination, they pass through, or are embedded in the membranes of, many different cellular organelles (figure 53). These organelles have distinct membrane identities in order to recruit organelle-specific effector proteins that are required for the successful trafficking of cargo proteins. One way in which these organelles selectively recruit their required effector proteins is through PI binding.

In this chapter, specific PIs will be depleted from the Golgi and the PM, and the effect of this on $I_{Ks}$ trafficking and function will be investigated. At the PM, $PIP_2$ and PI4P are the dominant phosphorylated PI species. PI4P is thought to be present for the production of $PIP_2$ (Dickson *et al*., 2014), whilst $PIP_2$ is involved in a myriad of cellular processes (Czech, 2000; Remedios & Nosworthy, 2008; Suh & Hille, 2008). One role of $PIP_2$ is in the regulation and stabilisation of CCPs, which form CCVs that recycle membrane proteins from the PM back into the cell. It was found that selective depletion of $PIP_2$ caused the loss of endocytic CCPs, confirming that this lipid is essential for their formation (Zoncu *et al*., 2007).

| Mutation | Location | Clinical manifestation | Effect in heterologous cell systems | Reference |
|---|---|---|---|---|
| Gly58Asp | C-terminus (A domain, helix C) | RWS | Homotetrameric Gly289Asp channels show prominent trafficking defect, but measurable currents when co-assembled with WT KCNQ1 | Aromolaran *et al*., 2014 |
| Arg555His | C-terminus (A domain, helix D) | RWS | Homotetrameric Arg555His channels show significant trafficking defect that is completely rescued by WT KCNQ1 | Aromolaran *et al*., 2014 |
| ΔSer276 | S5 TMD | RWS (asymptomatic) | ΔSer276 retained in ER whilst WT KCNQ1 localised to PM – results in haploinsufficiency | Gouas *et al*., 2004 |
| Glu261Asp | S4-S5 linker | JLNS | At 1:1 ratio, Glu261Asp caused DN retention of WT KCNQ1 in ER and reduction in current density | Wilson *et al*., 2005 |
| 1008delCys | S6 TMD | JLNS | Retained in the ER and led to retention of WT KCNQ1 in ER at 1:3 ratio | Wilson *et al.,* 2005 |
| Arg518X | C-terminus (helix B) | JLNS | Retained in ER and unable to interact with WT KCNQ1 at 1:1 ratio | Wilson *et al*., 2005 |
| Tyr111Cys | Juxtamembranous N-terminus | RWS (severe symptoms) | Retained in ER as homotetrameric channel and when co-expressed with WT KCNQ1 | Dahimène *et al*., 2006 |
| Leu114Pro | Juxtamembranous N-terminus | RWS (Moderate symptoms) | Retained in ER as homotetrameric channel and when co-expressed with WT KCNQ1 | Dahimène *et al*., 2006 |
| ΔVal595 | C-terminus (A domain, helix D) | RWS (compound heterozygote with P631fs/19) | Trafficking defect and little current due to impaired subunit binding, but no DN effect over WT KCNQ1 | Sato *et al*., 2009 |
| Pro631fs/19 | Distal C-terminus | RWS (compound heterozygote with ΔV595) | Retained in the ER due to a newly-generated retention signal, but no DN effect over WT KCNQ1 | Sato *et al*., 2009 |
| Ala590Thr | C-terminus (A domain, helix D) | RWS | Reduced current and cell-surface expression, which is rescued by WT KCNQ1 | Kinoshita *et al*., 2014 |
| Arg190Gln | Cytoplasmic loop between S2 and S3 | RWS | Trafficking defect and vulnerability to catecholaminergic stress | Moretti, *et al*. 2010 |

**Table 6. KCNQ1 mutations that cause $I_{Ks}$ channel trafficking defects.** A non-exhaustive list of mutations in the KCNQ1 α-subunit of the $I_{Ks}$ channel, identified in RWS or JLNS patients, that have been found to cause abnormal trafficking of the $I_{Ks}$ channel when expressed in heterologous cell systems.

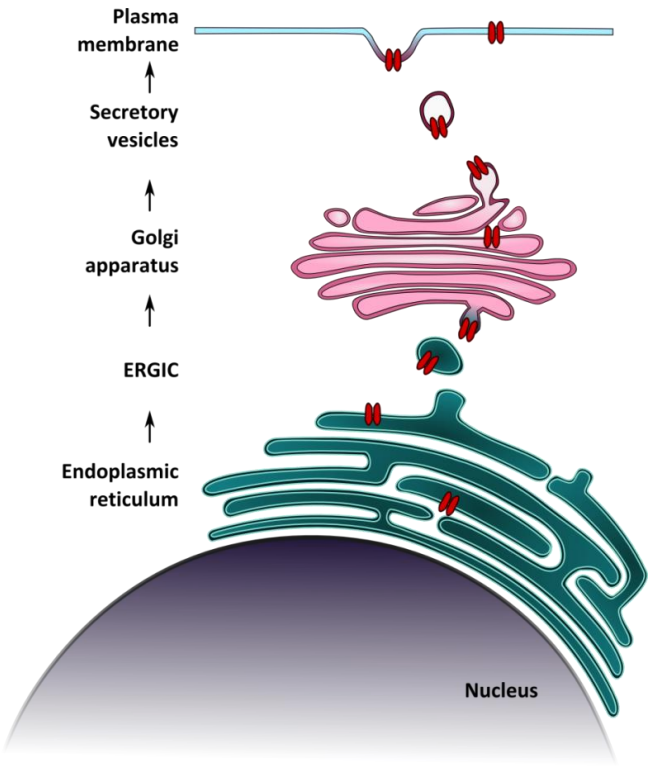


**Figure 53. Anterograde trafficking of ion channels.** After translation, ion channels are transported from the ER to the PM embedded in the membrane of organelles and vesicles. An ion channel is trafficked from the ER through the ERGIC (endoplasmic reticulum-Golgi intermediate compartment) and to the Golgi. From there it is transported to the PM in secretory vesicles that fuse with the PM.

Although the main pool of cellular $PIP_2$ is at the PM (which may contribute to the regulation of function and trafficking of the $I_{Ks}$ channel), there are also detectable levels of $PIP_2$ in the Golgi (Watt *et al*., 2002). The presence of $PIP_2$ in the Golgi is supported by the finding that PI4P 5-kinases that phosphorylate PI4P to $PIP_2$ are recruited and activated by ARF1 at the Golgi (Godi *et al.*, 1999; Jones *et al*., 2000). In addition, a $PIP_2$-binding domain was found in the Golgi-localised scaffold protein spectrin (Martin, 2001).

PI4P is the PI usually associated with the Golgi as it is highly concentrated here (Godi *et al*., 1999; Roy & Levine, 2004). PI4P aids in recruiting proteins such as FAPP1 and FAPP2. These proteins localise to the TGN via coincidence detection of PI4P and ARF1, and are involved in the budding and fission of protein-carrying vesicles destined for the PM (Godi *et al*., 2004).

*KCNQ1 trafficking*

The interactions that the KCNQ1 channel is involved in as it passes through the secretory pathway are largely unknown, but the channel is known to bind a wide variety of PIs (Thomas *et al*., 2011). $K^+$ channels, including the KCNQ1 channel, contain regions responsible for ER retention and export (Ma

*et al.*, 2001; Stockklausner *et al.*, 2001). This in part regulates and allows the timely export of the channel from the ER, which is required to control the renewed supply of channels as old ones are recycled from the PM.

Although mutations introducing ER retention motifs can result in impaired channel trafficking (Sato *et al*., 2009), mutations that cause channel trafficking defects do not necessarily have to be located in the regions responsible for ER exit or retention; mutations that cause aberrant channel trafficking have been identified throughout the length of the channel sequence, including those in the C-terminal calmodulin-binding region (Schmitt *et al*., 2007), the N-terminal domain (Dahimene *et al*., 2006) and the TM domains (Eldstrom *et al*., 2010).

Such mutations also include those investigated in this laboratory (Thomas *et al*., 2011), which are located in a $PIP_2$ binding region of the KCNQ1 subunit. In unpublished work, these mutations caused increased colocalisation with a fluorescent ER-marker compared to the WT channel. I have repeated this work to confirm the ER-retention observed for these channel mutants (figure 24). These mutations (Lys354Ala, Lys358Ala, Arg360Ala and Lys362Ala) were introduced into the KCNQ1 subunit singly and in combination with each other to create single, double, triple and quadruple $PIP_2$-binding-region mutants. In addition to showing that mutations in this region caused increased ER-retention, Thomas and colleagues (2011) found that mutation or charge neutralisation in this region caused a reduction of $PIP_2$ binding.

It is possible that the ER-retention observed when mutating the $PIP_2$ binding region could be a result of protein misfolding. Alternatively, it could be linked to the reduction in $PIP_2$ binding. It was also observed that the KCNQ1 subunit displays a broad binding affinity for other PI species (Thomas *et al*., 2011). Different PIs are involved in different stages of the secretory pathway, and whether these PIs are involved in the successful forward trafficking of the $I_{Ks}$ channel has not been investigated.

This chapter describes the use of on-cell and in-cell western assays for quantitative analysis of the cell-surface expression and total cellular expression of the VSV-KCNE1-KCNQ1 construct. This assay was developed by others in this laboratory, and is based upon previously published methods (Dahimène *et al*., 2006; Delisle *et al*., 2009). The manipulation of PI levels at the PM and Golgi was achieved using the rapamycin-induced dimerisation system, described independently in 2006 by two groups (Varnai *et al,* 2006; Suh *et al*., 2006), using either the PM-anchored LYN11-FRB or the TGN-targeted Tgn38-FRB for recruitment of the phosphatase-containing constructs to the PM and Golgi, respectively. The use of this assay made it possible to investigate the effect of direct $PIP_2$ and PI4P depletion at the PM, and PI4P depletion at the TGN, on the trafficking of the $I_{Ks}$ channel in

heterologous cells. In addition to this, patch-clamp will be used to investigate the role of $PIP_2$ in the regulation of $I_{Ks}$ function, as previously described in chapters 3 and 4.

**Aims:** To investigate the role of $PIP_2$ and PI4P in the regulation of $I_{Ks}$ channel function by depleting $PIP_2$ and/or PI4P at the PM, and $I_{Ks}$ channel trafficking to the PM by selectively depleting $PIP_2$ and/or PI4P in distinct cellular membranes, both using the rapamycin-induced dimerisation system.

## 5.2 Methods

### 5.2.1 Constructs and chemicals

The VSV-E1-Q1 construct consists of the VSV epitope (11 amino acid sequence from the vesicular stomatitis virus G protein (YTDIEMNRLGK) (Maout *et al*., 1997) fused to the extracellular side of KCNE1. The C-terminal end of KCNE1 is then fused to the N-terminal end of KCNQ1 as described in Wang *et al.* (1998). The VSV epitope is used for detecting the cell-surface expression of the KCNQ1-KCNE1 channel complex (Dahimene *et al*., 2006).

SAR1 (secretion-associated RAS-related protein 1) is a small GTPase that is involved in ER to Golgi trafficking by regulating the coat assembly and fission of new COPII vesicles at the ER (Kuge *et al.*, 1994; Long *et al.*, 2010). The SAR1 His79Gly mutant (SAR1-H79G; a gift from Philip Wedegaertner, Thomas Jefferson University, Philidelphia, USA), is a constitutively active SAR1 that cannot hydrolyse GTP and consequently prevents COPII vesicle trafficking between the ER and Golgi. The KCNQ1 Glu261Asp mutant, (KCNQ1-E261D), was created in our laboratory by Dr Andrew Wilson (Wilson *et al*., 2005). The KCNQ1-E261D subunit causes DN retention of WT KCNQ1 in the ER. The constitutively active ARF1 Gln71Leu mutant (pARF1-Q71L) was purchased from Addgene (#11385). This mutant lacks the ability to hydrolyse GTP and as a result, prevents the formation and release of COPI vesicles from the Golgi (Dascher & Balch, 1996).

PJ, PJ-SAC, PJ-DEAD, LYN11-FRB and Tgn38-FRB were used in the rapamycin-induced dimerisation system to enable depletion of phosphoinositides from the PM and Golgi. PJ-FAPP1 was made by inserting the FAPP1 domain into the N-terminal region of the PJ construct, as described in Chapter 4, and is a Golgi-localised version of PJ.

Wortmannin (#1232, Tocris Bioscience) is a steroid fungal metabolite that is used experimentally to inhibit PI 3-kinase activity at nanomolar concentrations and PI 4-kinase activity at micromolar concentrations (Hansen *et al*., 1995; Wyman *et al*., 1996). Brefeldin A (B7651, Sigma Aldrich) is a lactone antibiotic produced by fungal organisms, which inhibits anterograde protein transport from

the ER (Sciaky *et al*., 1997). Rapamycin (sc-3504, Santa Cruz) is a chemical product of an Easter Island bacterium that possesses antifungal properties (Bastidas *et al*., 2012), and is used as an anti-cancer drug (Law *et al*., 2005) and the dimerising agent for FRB- and FKBP-containing constructs in a research setting.

### 5.2.2 Electrophysiology

HEK-$I_{Ks}$ cells for WCPC and P-WCPC were incubated as described in section 3.2.2. WCPC and P-WCPC solutions and recordings were as described in section 3.2.2 and 4.2.3, respectively.

In P-WCPC experiments investigating the effect of wortmannin on the $I_{Ks}$ current, extracellular solution containing wortmannin (10 μM) was perfused after the first I-V protocol until the end of the final I-V protocol.

In experiments involving the perfusion of rapamycin over the cells, extracellular solution containing rapamycin (5 μM) was perfused for 2 minutes, and perfusion was then returned to rapamycin-free extracellular solution.

Data were analysed as described in section 3.2.2.

### 5.2.3 In/on-cell western assay

Sterile CELLSTAR 24-well plates (Greiner Bio-One Ltd., Stonehouse, UK) were coated with poly-L-lysine (P4707, Sigma Aldrich) before HEK293 cells were seeded at 30% confluence in 1 ml media. After 2 days incubation at 37°C and 5% $CO_2$, cells were transfected using Lipofectamine 2000, following the protocol in section 2.1.3. Cells were then left for 48 hours before performing the assay. How this assay is used to detect the cell-surface and total channel expression of the VSV-E1-Q1 construct can be seen in figure 54.

Cells were transfected with a total of 2 μg cDNA per well. In each well, 1 μg VSV-E1-Q1 cDNA was used, and the remaining 1 μg used was either SAR1-H79G, KCNQ1-E261D, ARF1-Q71L or a combination of 500 ng PJ/PJ-SAC/PJ-DEAD and 500 ng LYN11-FRB/Tgn38-FRB. For control wells, and those destined for the addition of wortmannin or brefeldin A, 1 μg pcDNA3.1 was transfected with VSV-E1-Q1.

For the in-cell western assay, cells were washed with $PBS^+$ (PBS supplemented with 1 mM $MgCl_2$ & 0.1 mM $CaCl_2$) then fixed with a 3.7% formaldehyde solution ($PBS^+$ + formaldehyde) for 20 minutes. After fixing, cells were washed with $PBS^+$, and then permeabilised with 0.1% triton-X100 solution ($PBS^+$ + triton-X100). Cells were washed with $PBS^+$ and incubated in HEK293 media for 30 minutes.

Primary antibody (Ab) was added (α-KCNQ1 [SC-20816, Santa Cruz]) in 500 µl HEK293 media at 1:1000 dilution, and cells were incubated on a rocking platform at room temperature for 1 hour. Cells were washed with $PBS^+$ before adding secondary Ab (α-Rabbit Dylight 800 [5151S, New England Biolabs]) in 500 µl HEK293 media at 1:1000 dilution. During secondary Ab incubation, cells were protected from light and incubated on a rocking platform at room temperature for 1 hour. Cells were then washed 3 times with $PBS^+$, and 500 µl $PBS^+$ was added to each well for visualisation. The plate was visualised using the LI-COR Odyssey Plate Reader system.

For the on-cell western assay, one of two protocols was used (noted in figure legends with either [37°C live on-cell assay] or [4°C fixed on-cell assay], respectively). The 4°C fixed on-cell assay was used when cellular processes needed to be halted at an exact timepoint.

37°C live on-cell assay: Cells were incubated at 37°C throughout. To start, primary Ab (α-VSV [V5507, Sigma]) was added in 200 µl HEK293 media at 1:500 dilution for 1 hour. Cells were then washed three times for 10 mins in HEK293 media. Secondary Ab was then added (α-mouse DyLight800 [5257S, New England Biolabs]) in 500 µl HEK293 media at 1:1000 dilution for 1 hour. Cells were washed twice with $PBS^+$, and 500 µl $PBS^+$ was added to each well for visualisation. The plate was visualised using the LI-COR Odyssey Plate Reader system.

4°C fixed on-cell assay: Primary Ab (α-VSV) was added in 200 µl ice-cold HEK293 media at 1:500 dilution for 1 hour at 4°C. Cells were then washed once in ice-cold HEK293 media and twice in ice-cold $PBS^+$. Cells were then fixed using 3.7% formaldehyde for 20 minutes. After fixing, cells were washed with $PBS^+$, then secondary Ab was added (α-mouse DyLight800) in 500 µl HEK293 media at 1:1000 dilution for 1 hour at RT. Cells were washed twice with $PBS^+$, and 500 µl $PBS^+$ was added to each well for visualisation. The plate was visualised using the LI-COR Odyssey Plate Reader system.

Rapamycin (5 µM) was added to relevant wells in 1 ml HEK293 media, either 1 hour or 24 hours before the start of the assay. Wortmannin (10 µM) was added in 1 ml HEK293 media 1 hour prior to the start of the assay, and brefeldin A (5 or 0.5 µM) was added 24 hours before the assay began.

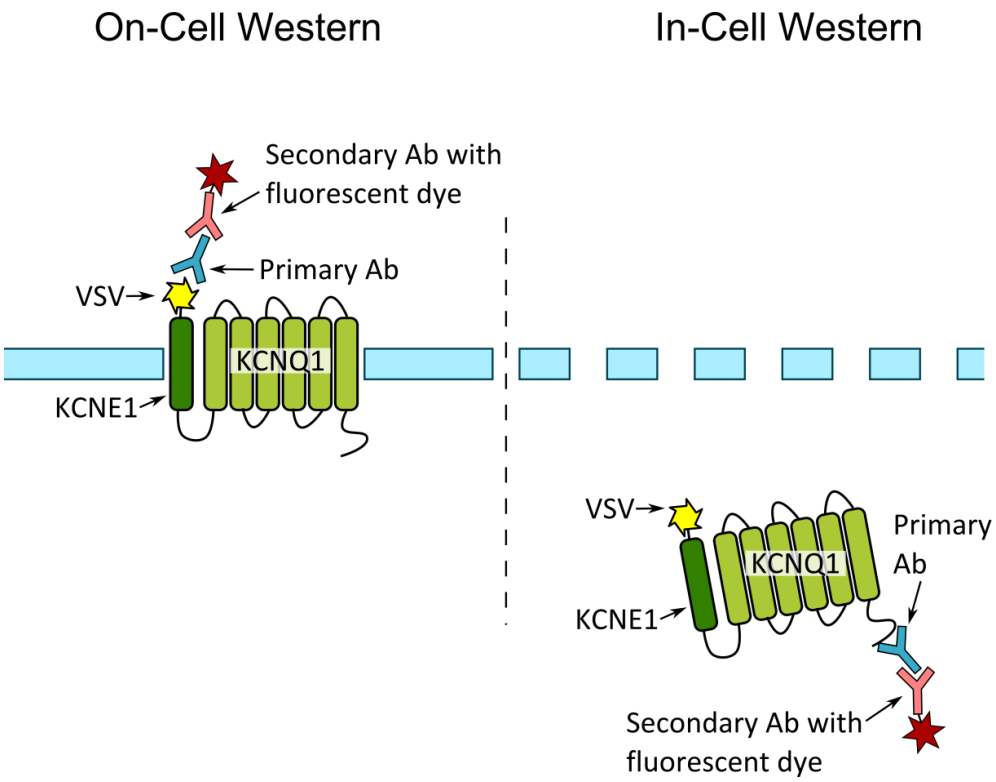


**Figure 54. Principles of the on- and in-cell western assays.** In the on-cell western assay, the VSV epitope of the VSV-E1-Q1 channel is detected by the α-VSV primary Ab. In the in-cell western assay the cells are permeabilised, and an α-KCNQ1 Ab is used to detect an epitope in the C-terminus of the KCNQ1 subunit. A secondary Ab linked to a fluorescent dye is used to detect the primary Ab in both assays to enable visualisation and quantification of VSV-E1-Q1 expression.

*Imaging setup, acquisition and analysis of the in/on-cell western assay*

To ensure the signal detected in the in/on-cell western assays was reproducible across plates, the cell density was calculated for each plate and the same cell density was used throughout. The timing of transfection was also considered due to the cell loss that can occur at low cell densities.

In each plate replicate, non-transfected cells were included as a control to ensure no differences were seen in background levels of fluorescence between plates.

Image acquisition was performed using the following settings:

Channel: 800 nm
Plate: Microplate 2 (setting for a 24-well plate)
Focus offset: 3 mm
Scan Quality: Medium (169 μm resolution)

An initial scan was performed for each plate at a scanning intensity of 5, after which a decision was made whether to rescan at a higher or lower intensity depending on the strength of the signal.

To normalise the results from different experiments relative intensity was calculated by first normalising each triplicate well against the average. The background intensity value (untransfected control) was then subtracted. All data was then normalised to averaged and background subtracted values for the control wells (VSV-E1-Q1 + pcDNA3.1). This approach has previously been used in our laboratory and is as described by (Aziz *et al*., 2012).

**5.2.4 Statistical analysis**

Data are expressed as mean ± SE, and Boltzmann functions were generated using GraphPad Prism. Each condition in the in/on-cell western assays was performed in triplicate within each plate, and each plate was repeated 3 times. A Student's T Test was used to determine statistical significance for single comparisons ($p < 0.05$), and a one-way ANOVA ($p<0.05$) was used to determine significance when multiple groups were compared. For one-way ANOVA analyses, a Bonferroni or Dunnett's multiple comparison test was used to compare groups.

## 5.3 Results

### 5.3.1 Development of in/on-cell western assay: Effect of SAR1-H79G and KCNQ1-E261D on VSV-KCNE1-KCNQ1 cell surface and total cellular expression

Before the effect of $PIP_2$ depletion using the rapamycin-inducible dimerisation system on VSV-E1-Q1 trafficking was investigated, the response to different cellular manipulations was studied to confirm that changes in VSV-E1-Q1 intracellular and/or PM expression could be detected.

To ensure that the level of VSV-E1-Q1 construct at the PM could be altered by manipulating proteins involved in KCNQ1 trafficking, the SAR1-H79G mutant or the KCNQ1-E261D mutant were expressed with the VSV-E1-Q1 construct for 48 hours.

Expression of SAR1-H79G significantly reduced the surface expression of VSV-E1-Q1 ($p<0.001$), whilst having no effect on the total level of VSV-E1-Q1 expression (p=NS). The expression of the KCNQ1-E261D mutant subunit caused a significant reduction in cell-surface expression of VSV-E1-Q1 ($p<0.005$) that was similarly not accompanied by an alteration in the total cellular expression of VSV-E1-Q1 (p=NS) (figure 55).

### 5.3.2 Development of in/on-cell western assay: Effect of wortmannin and brefeldin A on VSV-KCNE1-KCNQ1 cell surface and total cellular expression

Pharmacological manipulation of VSV-E1-Q1 expression was also performed to enable inhibition of certain cellular processes. When HEK293 cells transiently expressing VSV-E1-Q1 were incubated for 1 hour with wortmannin (10 µM), which inhibits both PI3K and PI4K activity at the concentration used (Hansen *et al*., 1995; Nakanishi *et al*., 1995; Wymann *et al*., 1996; Yano *et al*., 1993), there was no change in the total VSV-E1-Q1 channel expression. Wortmannin incubation did, however, cause a significant reduction in cell-surface expression of the VSV-E1-Q1 construct ($p< 0.01$) (figure 55).

Incubation of VSV-E1-Q1-expressing HEK293 cells with brefeldin A (5 µM) for 24 hours resulted in a small amount of cell death. The total cellular expression of VSV-E1-Q1 was significantly reduced ($p<0.001$) after 24 hours brefeldin A incubation, but it is unclear whether this was solely due to the loss of total cell number or whether there was an actual reduction in VSV-E1-Q1 protein expression. Brefeldin A incubation also significantly reduced the cell-surface expression of the VSV-E1-Q1 construct ($p<0.001$) (figure 55).

### 5.3.3 Effect of $PIP_2$ and PI4P depletion at the plasma membrane on VSV-KCNE1-KCNQ1 cell-surface and total cellular expression

To investigate whether transient expression of the lipid-depleting constructs affected VSV-E1-Q1 trafficking, VSV-E1-Q1 was expressed with LYN11-FRB and either PJ or PJ-DEAD. Expression of PJ-DEAD and LYN11-FRB for 48 hours did not result in changes in the cell-surface or total cellular expression of VSV-E1-Q1 when compared to the VSV-E1-Q1 control (VSV-E1-Q1 + pcDNA3.1). Similarly, expression of PJ and LYN11-FRB had no effect on either the total or cell-surface expression of the VSV-E1-Q1 construct (figure 56).

After it was established that the expression of the lipid-depleting constructs did not affect VSV-E1-Q1 trafficking, the effect of acute and prolonged $PIP_2$ and PI4P depletion was investigated. To induce recruitment of PJ/PJ-DEAD to the PM, cells were incubated with rapamycin (5μM) for 1 or 24 hours.

Incubation of HEK293 cells transiently expressing VSV-E1-Q1, PJ-DEAD and LYN11-FRB with rapamycin for 1 hour prior to the start of the assay had no effect on either the total or cell-surface expression of VSV-E1-Q1. Incubation of HEK293 cells expressing VSV-E1-Q1, PJ and LYN11-FRB with rapamycin for 1 hour also had no effect on the cell-surface or total expression of the VSV-E1-Q1 construct (figure 56) (p=NS). In addition, rapamycin (5 μM) incubation for 24 hours in HEK293 cells expressing VSV-E1-Q1 with PJ/PJ-DEAD and LYN11-FRB had no effect on the VSV-E1-Q1 total or cell-surface expression (figure 56) (p=NS).

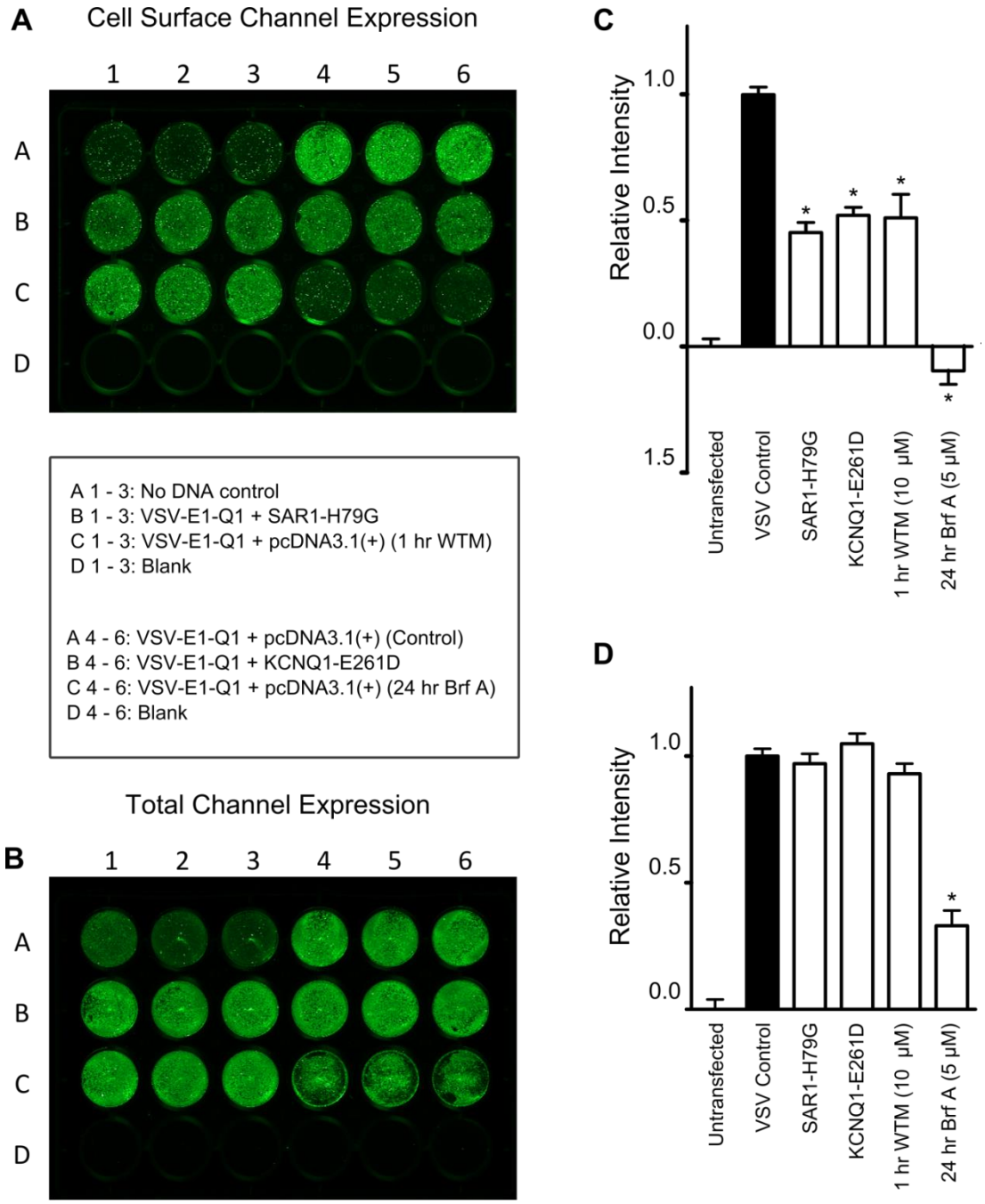


**Figure 55. Manipulating the cell-surface and total expression level of VSV-KCNE1-KCNQ1. A** and **B** show representative assay plates from the on- and in-cell western assay, enabling quantification of the cell surface and total cellular expression respectively. The VSV-E1-Q1 construct was co-expressed with either pcDNA3.1, SAR1-H79G or KCNQ1-E261D. Cells expressing VSV-E1-Q1 with pcDNA3.1 were incubated with either 10 µM wortmannin (WTM) for 1 hour or 5 µM brefeldin A (Brf A) for 24 hours. Each condition was performed in triplicate within each plate, and a total of 3 independent experiments were performed. Mean data from three independent experiments represented in **A** and **B** are shown in **C** and **D** respectively. Data represented as mean ± SEM. [37°C live on-cell western].

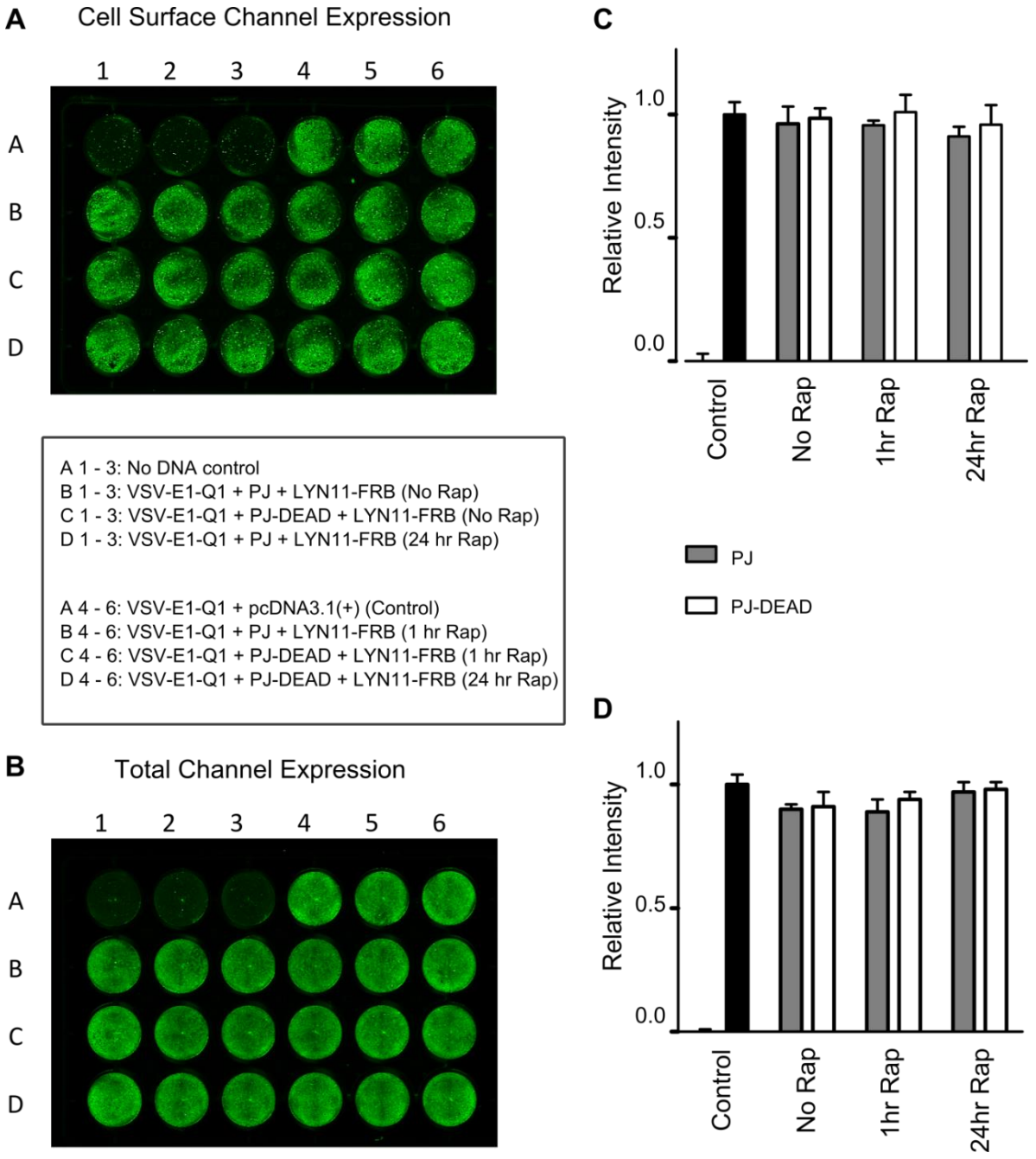


**Figure 56. Depletion of $PIP_2$ at the PM does not affect the cell-surface or total expression level of VSV-KCNE1-KCNQ1.** **A** and **B** show representative assay plates from the on- and in-cell western assay, enabling quantification of the cell surface and total cellular expression respectively. The VSV-E1-Q1 construct was co-expressed with pcDNA3.1, or with LYN11-FRB and Pseudojanin (PJ) or PJ-DEAD. Cells expressing LYN11-FRB with either PJ or PJ-DEAD were incubated in the absence of 5 µM rapamycin (Rap), or in the presence of Rap for 1 hour or 24 hours. Each condition was performed in triplicate within each plate, and a total of 3 independent experiments were performed. Mean data from three independent experiments represented in **A** and **B** are shown in **C** and **D** respectively. Data represented as mean ± SEM. [37°C live on-cell western].

### 5.3.4 Effect of PJ-FAPP1, ARF1-Q71L and brefeldin A on VSV-KCNE1-KCNQ1 cell surface and total expression levels

As the Golgi is involved in anterograde trafficking and is home to a large portion of cellular PI4P, and the KCNQ1 channel binds PI4P, the effect of depleting PI4P at the TGN was studied. First, however, alternative methods of altering cellular PI4P were attempted before using the rapamycin-induced dimerisation system to deplete solely PI4P at the Golgi.

Similar to the expression of SAR1-H79G and KCNQ1-E261D being used to alter the trafficking of the VSV-E1-Q1 construct from the ER, different ways to alter the Golgi-mediated trafficking of the VSV-E1-Q1 construct were attempted.

PJ-DEAD-FAPP1 localises to the TGN through the binding of its FAPP1 domain to ARF1 and PI4P. This could sequester PI4P, causing a reduced pool of PI4P able to interact with effector proteins and cargo at the Golgi, so the effect of this construct was investigated. Expression of VSV-E1-Q1 and PJ-DEAD-FAPP1 in HEK293 cells had no effect on the total expression of the VSV-E1-Q1 construct (p=NS) and no effect on the cell-surface expression (p=NS).

Accordingly, expression of VSV-E1-Q1 with PJ-FAPP1 in HEK293 cells had no effect on the total cellular expression of the VSV-E1-Q1 construct, but there was a small reduction (p=NS) in the cell-surface expression (figure 58).

The ARF1 mutant, ARF1-Q71L, was also used to alter Golgi function. ARF1-Q71L disrupts traffic to the Golgi and between Golgi compartments. Expression of ARF1-Q71L with VSV-E1-Q1 in HEK293 cells led to a significant reduction in cell-surface expression ($p<0.001$), but there was not an accompanying change in the total cellular expression of the construct (p=NS).

Brefeldin A was previously used as a positive control for the disruption of VSV-E1-Q1 trafficking in section 5.3.2, but the concentration and incubation time (which were based on published work) had a severe effect on cell survival. Here, HEK293 cells expressing VSV-E1-Q1 were incubated with brefeldin A (0.5 μM) for 24 hours prior to the start of the assay. In this instance, brefeldin A incubation caused a small, but significant ($p<0.001$) reduction in total VSV-E1-Q1 expression, but reduced the cell-surface expression of VSV-E1-Q1 to approximately 20% of the VSV-E1-Q1 control value (figure 58) ($p<0.05$). With this concentration of brefeldin A there did not appear to be a reduction in cell number, but the cells adhered to the bottom of the well became smaller and more circular, which affected the coverage of the wells.

### 5.3.5 Effect of $PIP_2$ and/or PI4P depletion at the Golgi on VSV-KCNE1-KCNQ1 cell surface and total level of expression

Before studying how depletion of $PIP_2$ and/or PI4P may affect trafficking of the VSV-E1-Q1 construct, the ability to recruit the lipid-depleting constructs to Tgn38-FRB was assessed using confocal microscopy (figure 57). After rapamycin (5 μM) was added to HEK293 cells expressing PJ and Tgn38-FRB, colocalisation between PJ and Tgn38-FRB occurred after 15–30 seconds.

After the ability to induce translocation of PJ to Tgn38-FRB was confirmed, the effect of this recruitment on the trafficking of VSV-E1-Q1 was studied. To investigate whether expression of the lipid-depleting constructs affected VSV-E1-Q1 trafficking in the presence of the Golgi-located Tgn38-FRB, VSV-E1-Q1 was expressed in HEK293 cells with Tgn38-FRB and either PJ, PJ-SAC or PJ-DEAD.

Expression of PJ-DEAD and Tgn38-FRB for 48 hours did not cause a change in the cell-surface or total cellular expression of VSV-E1-Q1 expression when compared to the VSV-E1-Q1 control (VSV-E1-Q1 + pcDNA3.1). Similarly, expression of PJ-SAC and Tgn38-FRB had no effect on either the total or cell-surface expression of the VSV-E1-Q1 construct (figure 59). Expression of PJ with Tgn38-FRB did, however, result in a small reduction of the cell-surface expression, reducing the level to approximately 75% of the control level of expression ($p<0.05$) (figure 58).

To recruit the lipid-depleting constructs to the Golgi and study whether $PIP_2$ and/or PI4P depletion here resulted in any change (or further change, in the case of PJ in VSV-E1-Q1 trafficking), HEK293 cells expressing VSV-E1-Q1, Tgn38-FRB and either PJ-DEAD, PJ-SAC or PJ were incubated with rapamycin (5 μM) for 1 or 24 hours.

Incubation of cells expressing PJ-DEAD and Tgn38-FRB with rapamycin for 1 hour prior to the start of the assay had no effect on either the total or cell-surface expression of VSV-E1-Q1 (p=NS), and 1 hour incubation of cells expressing PJ-SAC and Tgn38-FRB with rapamycin also had no effect on the cell-surface or total expression of the VSV-E1-Q1 construct (figure 59) (p=NS).

Incubating cells expressing Tgn38-FRB and either PJ-DEAD, PJ-SAC or PJ with rapamycin for 24 hours had no significant effect on the VSV-E1-Q1 total or cell-surface expression in any of the conditions (figure 58 & 58) (p=NS).

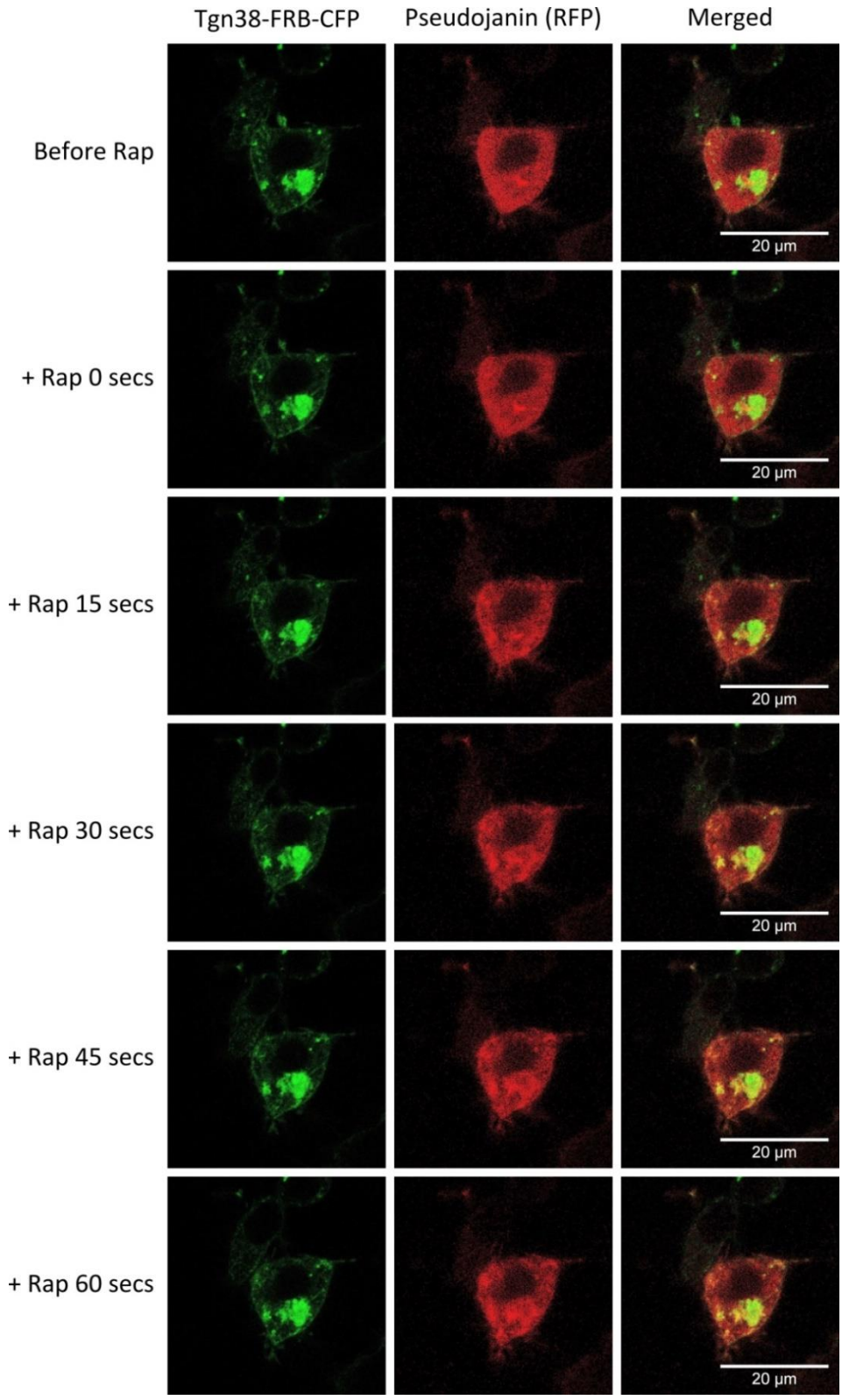


**Figure 57. The rapamycin-induced recruitment of PJ to Tgn38-FRB at the Golgi.** The localisation of PJ and Tgn38-FRB in HEK293 cells, and the rapamycin-induced recruitment of PJ to Tgn38-FRB. The top row shows HEK293 cells transiently expressing PJ and Tgn38-FRB. The 5 centre and bottom rows show the same cell at different time points after the addition of rapamycin (5 µM) to the cell. Images were obtained using confocal microscopy (method described in section 4.2.2). Response from one cell (n=1).

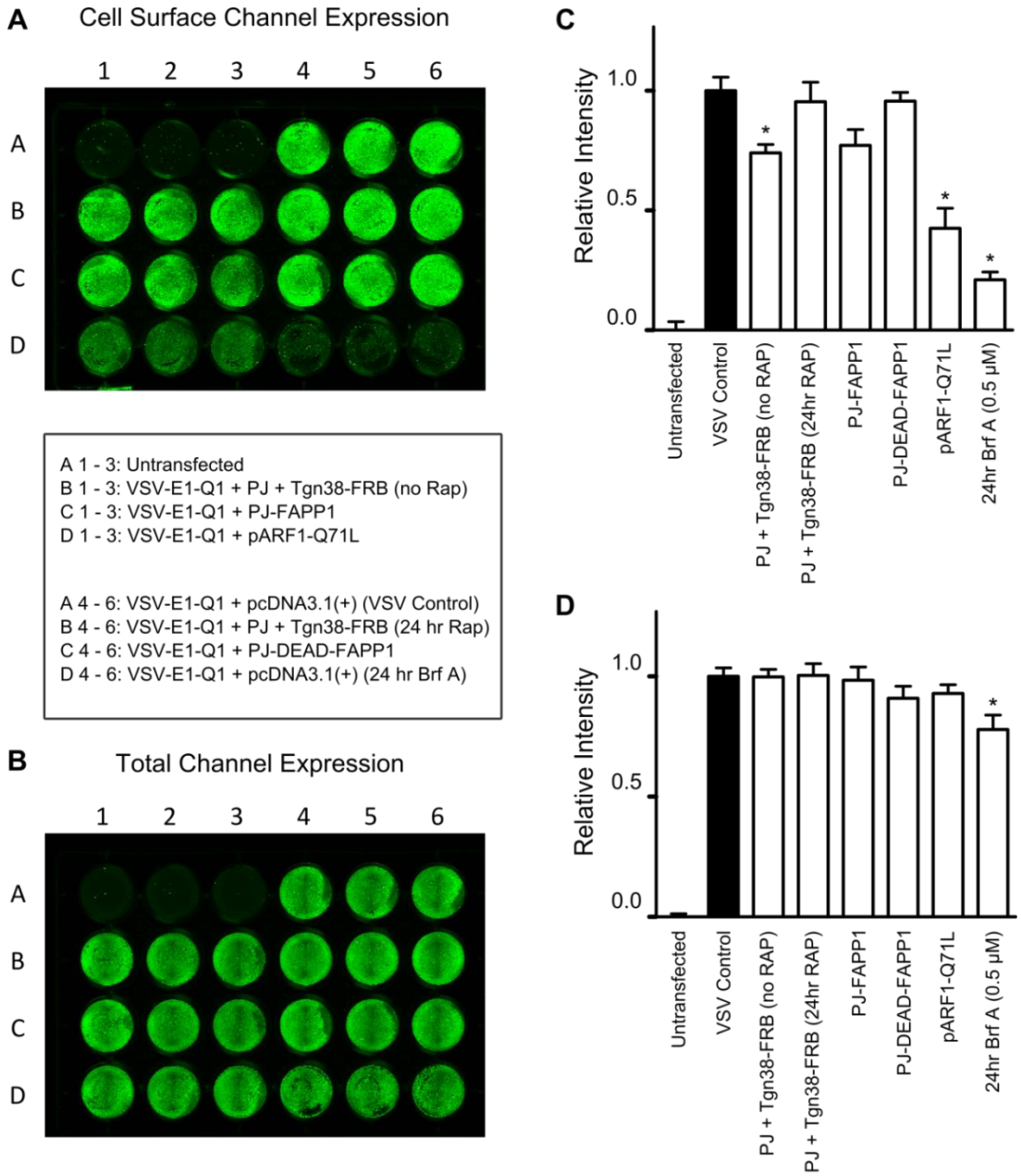


**Figure 58. Manipulating the cell-surface and total expression levels of VSV-KCNE1-KCNQ1 by depleting Golgi $PIP_2$/PI4P. A** and **B** show representative assay plates from the on- and in-cell western assay, enabling quantification of the cell surface and total cellular expression respectively. The VSV-E1-Q1 construct was co-expressed with either pcDNA3.1, PJ + Tgn38-FRB, PJ-FAPP1, PJ-DEAD-FAPP1 or pARF1-Q71L. Cells expressing VSV-E1-Q1 with pcDNA3.1 were incubated with 0.5 µM brefeldin A (Brf A) for 24 hours. Each condition was performed in triplicate within each plate, and a total of 3 independent experiments were performed. Mean data from three independent experiments represented in **A** and **B** are shown in **C** and **D** respectively. Data represented as mean ± SEM. [4°C fixed on-cell western].

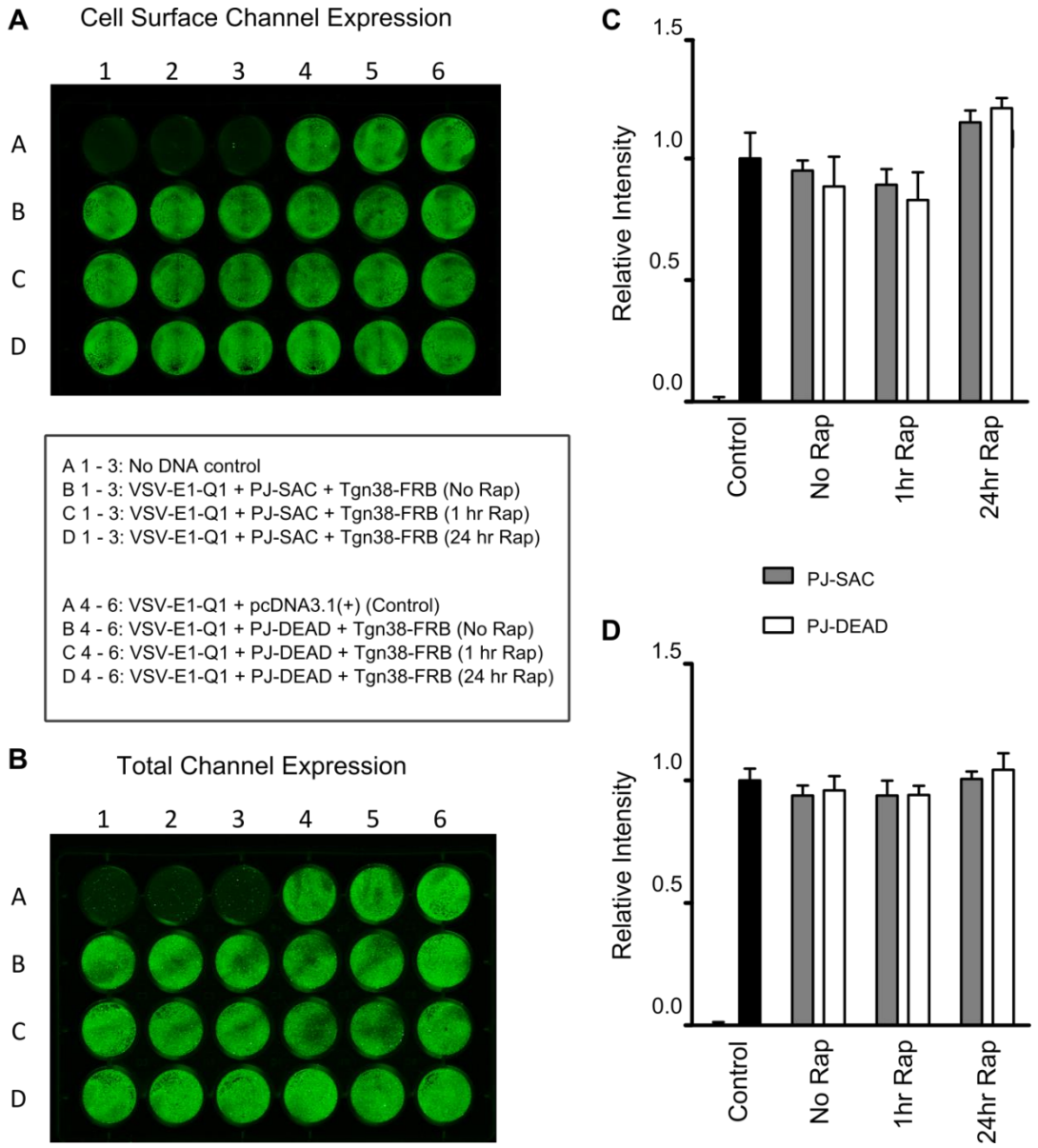


**Figure 59. Depletion of PI4P at the Golgi does not affect the cell-surface or total expression level of VSV KCNE1-KCNQ1. A** and **B** show representative assay plates from the on- and in-cell western assay, enabling quantification of the cell surface and total cellular expression respectively. The VSV-E1-Q1 construct was co-expressed with pcDNA3.1, or with Tgn38-FRB and PJ-SAC) or PJ-DEAD. Cells expressing Tgn38-FRB with either PJ or PJ-DEAD were incubated in the absence of 5 µM rapamycin (Rap), or in the presence of Rap for 1 hour or 24 hours. Each condition was performed in triplicate within each plate, and a total of 3 independent experiments were performed. Mean data from three independent experiments represented in **A** and **B** are shown in **C** and **D** respectively. Data represented as mean ± SEM. [4°C fixed on-cell western].

### 5.3.6 Problems with $I_{Ks}$ current stability in the whole-cell patch clamp configuration

Anterograde trafficking of the $I_{Ks}$ current does not appear to be regulated by $PIP_2$, but the regulation of channel function is still possible. In chapter 3, I successfully recovered the $I_{Ks}$ current using a 40:60 ratio of PJ-INPP5E to PJ-DEAD, which may allow characterisation of the effect of $PIP_2$ depletion on $I_{Ks}$ function by recruiting the lipid-depleting constructs to the PM.

First, HEK293 cells expressing the $I_{Ks}$ channel subunits, KCNQ1 and KCNE1, with PJ-DEAD and LYN11-FRB were subject to repeated I-V protocols in order to assess the stability of the $I_{Ks}$ current in WCPC. Rapamycin (5µM) was perfused over the cells for 2 minutes after completion of the first I-V recording, after which a second I-V protocol was run. Cells expressing PJ-DEAD were first used (as a control) to establish the stability of the $I_{Ks}$ current under the experimental conditions and time-course that would be used for other lipid-depleting constructs.

As can be seen in figure 60, the current density and peak tail current density recorded from the second I-V protocol were significantly reduced compared to those recorded from the first I-V protocol (CD: $p<0.01$; PTCD: <0.01). Over a period of 5 minutes (3 minutes for the I-V protocol and 2 minutes for rapamycin perfusion) there was a 36% reduction in CD and a 44% reduction in PTCD. This effect could not be attributed to activity of the phosphatase domains in the lipid-depleting construct because PJ-DEAD was used. Due to the extensive channel rundown observed it was not possible to test the effects of the recruitment of the active PJ constructs in WCPC.

### 5.3.7 $I_{Ks}$ current stability and the effect of wortmannin in the perforated patch configuration

Based on the previous findings and those of others (Yang *et al*., 2009) it is clear that the $I_{Ks}$ current is susceptible to rundown in WCPC. In order to test whether the preservation of the intracellular environment would prevent channel rundown, the stability of the $I_{Ks}$ current was assessed using the perforated-patch configuration of WCPC.

To test the stability of the $I_{Ks}$ current in P-WCPC, I-V protocols were repeated every 4 minutes, where t=0 denotes sweep 12 of the first I-V (during sweep 12, the PM is clamped at +30 mV before dropping to -20 mV to elicit the tail current, and is where each value of relative CD and relative PTCD is taken from in each I-V recording).

Figure 61A, C, D & E show that after 16 minutes, the CD and PTCD remain similar to the values recorded in the first I-V. The $V_{0.5}$ values, calculated using a Boltzmann function on normalised PTCD densities, did not change between the first I-V (38.0 ± 1.84 mV) and the

I-V protocols run at + 4, 8, 12 or 16 minutes (31.9 ± 1.41 mV, 34.58 ± 1.15 mV, 39.5 ± 1.49 mV and 36.7 ± 1.23 mV respectively) (figure 61F).

Before investigating the effect of recruiting the lipid-depleting constructs to the PM with rapamycin, an alternative, previously published method of $PIP_2$ and PI4P depletion was attempted as a positive control. WTM, an inhibitor of PI 4-K activity when used at micromolar concentrations, was continuously perfused over untransfected HEK-$I_{Ks}$ cells after completion of the first I-V protocol, and I-V protocols were repeated for a period of 15 minutes.

Perfusion of WTM (10 μM) over untransfected HEK-$I_{Ks}$ cells caused a reduction in $I_{Ks}$ CD and PTCD (figure 61 A, C, D & E). In detail, 2 minutes of WTM perfusion caused a noticeable reduction in the $I_{Ks}$ current, and 50% of the current was inhibited after approximately 8 minutes. The voltage-dependence of activation did not significantly change throughout the addition of WTM (figure 61F). Comparison of the $V_{0.5}$ values of normalised tail currents before (44.8 mV ± 1.42) and at + 2, 6 and 10 minutes of WTM addition (37.3 mV ± 1.62, 40.8 mV ± 1.6 and 45.2 mV ± 2.6, respectively) shows only a slight variation between these (which was significant at + 2 mins, $p<0.05$), but no change between the values before WTM addition and after 10 minutes of WTM (10 μM) addition. Analysis of the voltage-dependence of activation at 16 minutes of WTM addition was not possible in some cells because the tail current density was reduced to such an extent that it could not be accurately measured.

### 5.3.8 Effect of recruiting lipid-depleting constructs to the PM on the $I_{Ks}$ current in HEK-$I_{Ks}$ cells

Now that a stable system to record $I_{Ks}$ currents had been established, rundown of the $I_{Ks}$ current would not interfere with the interpretation of any results from patch-clamp experiments spanning >1 I-V recording. P-WCPC was used from here onwards when investigating the effects of lipid depletion on the $I_{Ks}$ current.

First, however, the effect of expressing the PJ constructs on the $I_{Ks}$ current in P-WCPC was assessed. When expressing any of the lipid-depleting constructs with LYN11-FRB in HEK-$I_{Ks}$ cells, there was no significant difference in the CD or PTCD when compared to control at any of the voltages analysed (p=NS) (figure 62A, B & C), which was assessed using a one-way ANOVA with Bonferroni's post hoc test. There was also no difference between the CD or PTCD of PJ-DEAD and any of the active lipid-depleting constructs (p=NS). There appeared to be little change in the $V_{0.5}$ value between control and PJ-DEAD, PJ-SAC, PJ-INPP5E and PJ (37.98 ±1.84, 45.69 ±1.08, 41.65 ±1.35, 47.46 ±1.53 and 44.93 ±1.23, respectively), but a one-way ANOVA with Bonferroni's post hoc test showed that there was a significant difference between control and PJ-DEAD ($p<0.05$), PJ-INPP5E ($p<0.005$) and PJ ($p<0.05$).

There was not, however, a significant different between the $V_{0.5}$ values from PJ-DEAD and any other construct (figure 62D).

As it was evident that expression of the active lipid-depleting constructs had little effect on the $I_{Ks}$ current when recorded in P-WCPC, the effect of recruiting the constructs to the PM using rapamycin was investigated.

First, PJ-DEAD and LYN11-FRB were expressed in HEK-$I_{Ks}$ cells, and after a first I-V protocol, a second was run immediately whilst rapamycin (5 μM) was perfused over the cells for 2 minutes. I-V protocols were repeatedly recorded until the $I_{Ks}$ current had been recorded at +2, 5, 8 and 11 minutes rapamycin addition. T=0 denotes sweep 12 of the first I-V (during sweep 12, the PM is clamped at +30 mV before dropping to -20 mV to elicit the tail current, and is where each value of relative current density and relative peak tail current density is taken from in each I-V recording). At t=11 minutes, the $I_{Ks}$ CD and PTCD were not significantly different from the current measured at t=0, before rapamycin perfusion (p=NS) (figure 62F & G).

After it was established that both perfusion of rapamycin and recruitment of PJ-DEAD to the PM did not affect the $I_{Ks}$ current, the active lipid-depleting constructs were expressed in turn (in the place of PJ-DEAD) in HEK-$I_{Ks}$ cells. The same protocol was followed for recording the $I_{Ks}$ current in P-WCPC, with 2 minutes of rapamycin (5 μM) perfusion commencing after completion of the first I-V recording.

The recruitment of either PJ-SAC, PJ-INPP5E or PJ to the PM with rapamycin did not act to alter $I_{Ks}$ CD or PTCD over the period of the experiment (figure 62F & G) (p=NS), and there was also no difference between values at each time point for control compared to each lipid-depleting construct, or between PJ-DEAD and the active lipid-depleting constructs (p=NS), assessed using a one-way ANOVA with Bonferroni's multiple comparison test.

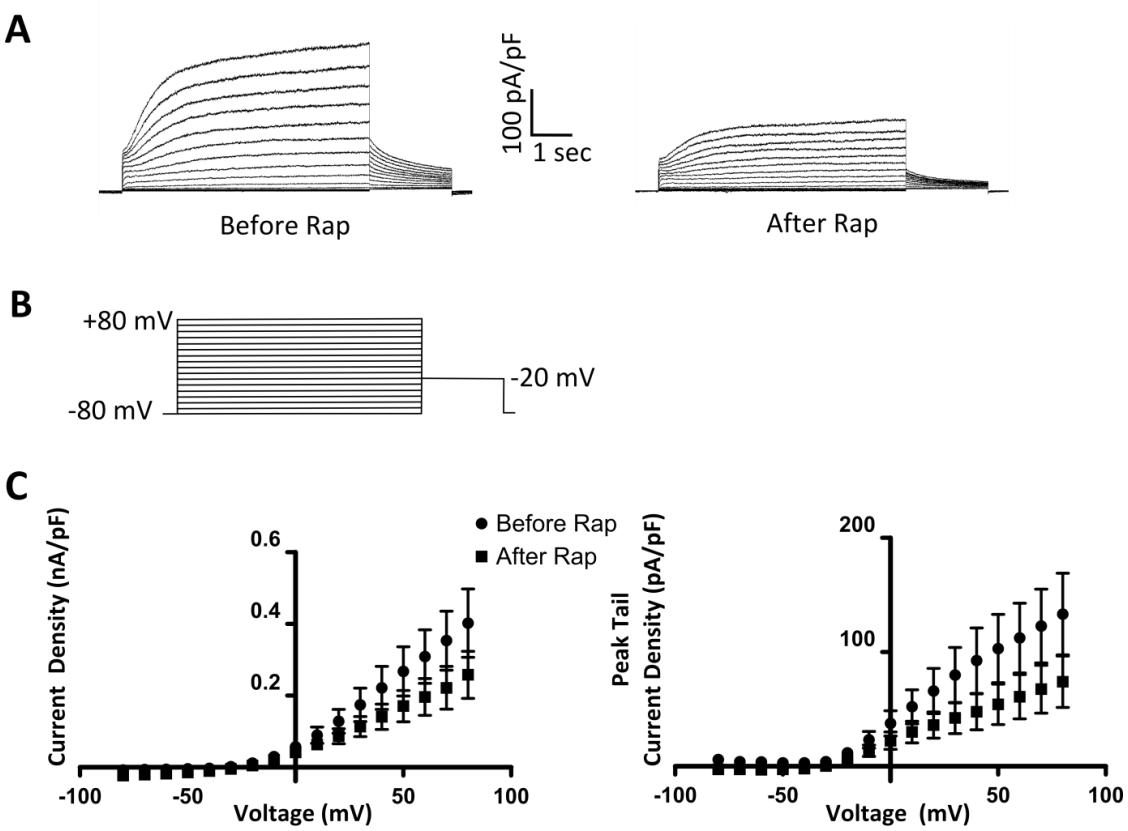


**Figure 60. Stability of the $I_{Ks}$ current in HEK-$I_{Ks}$ cells in the whole-cell patch clamp configuration. A** – Representative current traces recorded in WCPC from HEK-$I_{Ks}$ cells before and after 2 minutes rapamycin (Rap) (5µM) perfusion. **B** – Voltage protocol used to elicit currents recorded in WCPC. **C** – Mean current density (left) and peak tail current density (right) recorded in WCPC from HEK-$I_{Ks}$ cells transiently expressing PJ-DEAD and LYN11-FRB (n=7) before and after approximately 5 minutes from the start of Rap perfusion (2 mins Rap + 3 mins recording). Data are represented as mean ± SE.

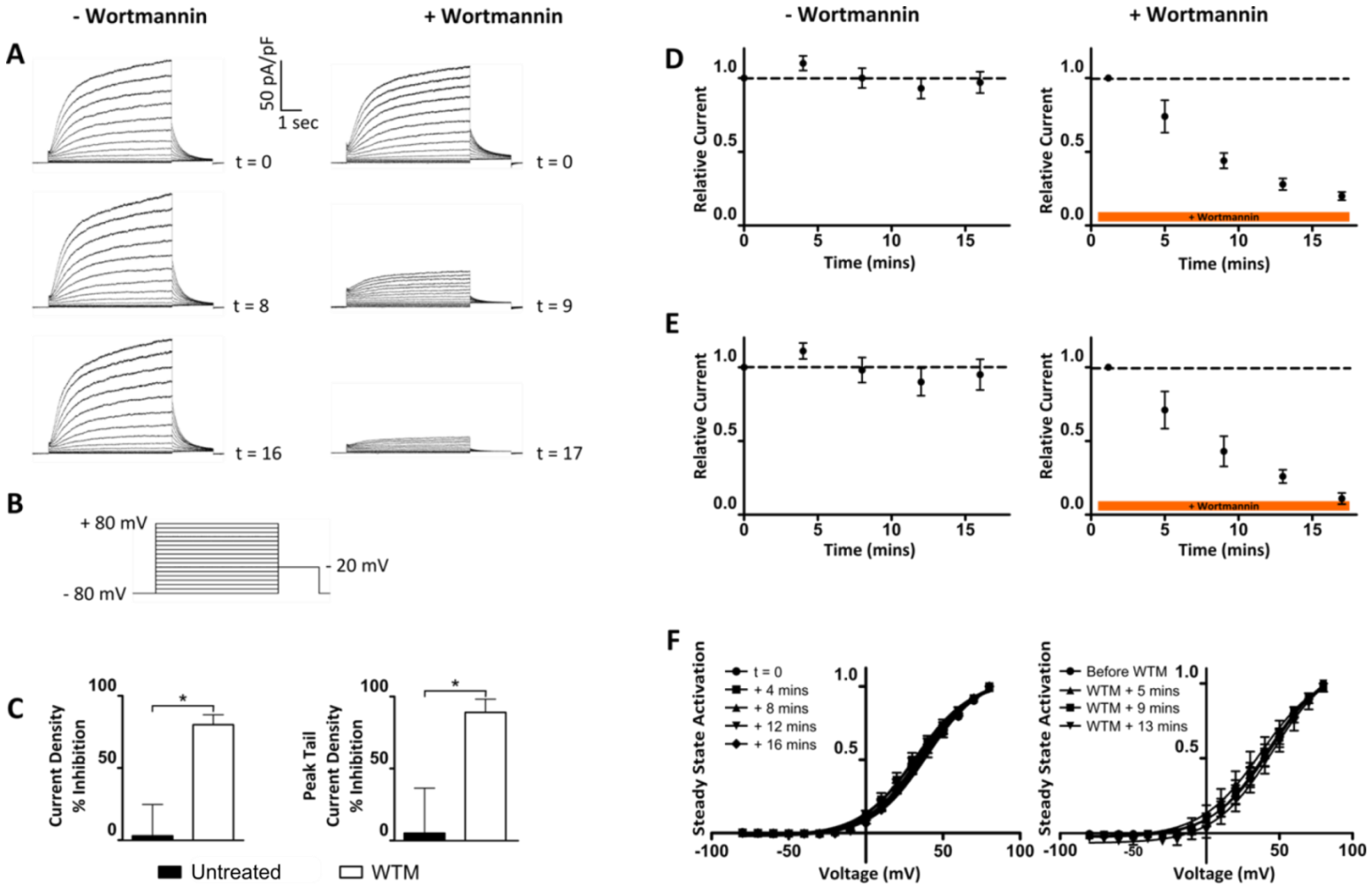
- Wortmannin
+ Wortmannin
A
50 pA/pF
1 sec
t = 0
t = 0
t = 8
t = 9
t = 16
t = 17
B
+ 80 mV
- 80 mV
- 20 mV
C
Current Density % Inhibition
Peak Tail Current Density % Inhibition
100
50
0
*
Untreated
WTM
D
E
Relative Current
Time (mins)
+ Wortmannin
F
Steady State Activation
Voltage (mV)
t = 0
+ 4 mins
+ 8 mins
+ 12 mins
+ 16 mins
Before WTM
WTM + 5 mins
WTM + 9 mins
WTM + 13 mins

**Figure 61. Stability of the $I_{Ks}$ current in the perforated patch configuration, and the effect of wortmannin addition on the $I_{Ks}$ current in HEK-$I_{Ks}$ cells.**
**A** – Representative current traces recorded in P-WCPC from HEK-$I_{Ks}$ cells in the absence (- Wortmannin; control) and presence (+ Wortmannin) of 10 µM wortmannin (WTM). Current traces at t = 0, 8 and 16 for recordings in the absence of wortmannin, and t = 0, 9 and 16 for recordings in the presence of wortmannin. Recordings in HEK-$I_{Ks}$ cells after wortmannin addition were taken 1 minute later than control recordings, due to an additional 1 minute of wortmannin perfusion before recording. **B** – Voltage protocol used to elicit the currents recorded in P-WCPC. **C** – Percentage inhibition from after 16 minutes of WTM exposure of $I_{Ks}$ current density (left) and peak tail current density (right). Normalised ($y/y_{max}$) **D** – current density and **E** – peak tail current density at 30 mV of currents recorded in P-WCPC from HEK-$I_{Ks}$ cells without (- Wortmannin; n=9) and with (+ Wortmannin; n=6) wortmannin (WTM) perfusion (10 µM). **F** – Steady state of activation curves for HEK-$I_{Ks}$ cells and HEK-$I_{Ks}$ cells after WTM perfusion (n=6). Steady-state activation curves were constructed by plotting normalised peak tail current densities ($y/y_{max}$) against test potential with a Boltzmann function (solid lines). Data are presented as mean ± SE. A t-test was used to determine statistical significance between groups in **C**. A Boltzmann function was applied to steady state activation data in **F** to fit sigmoidal curves, and a one-way ANOVA with Dunnett's post hoc test was used to determine statistical significance between $V_{0.5}$ values.

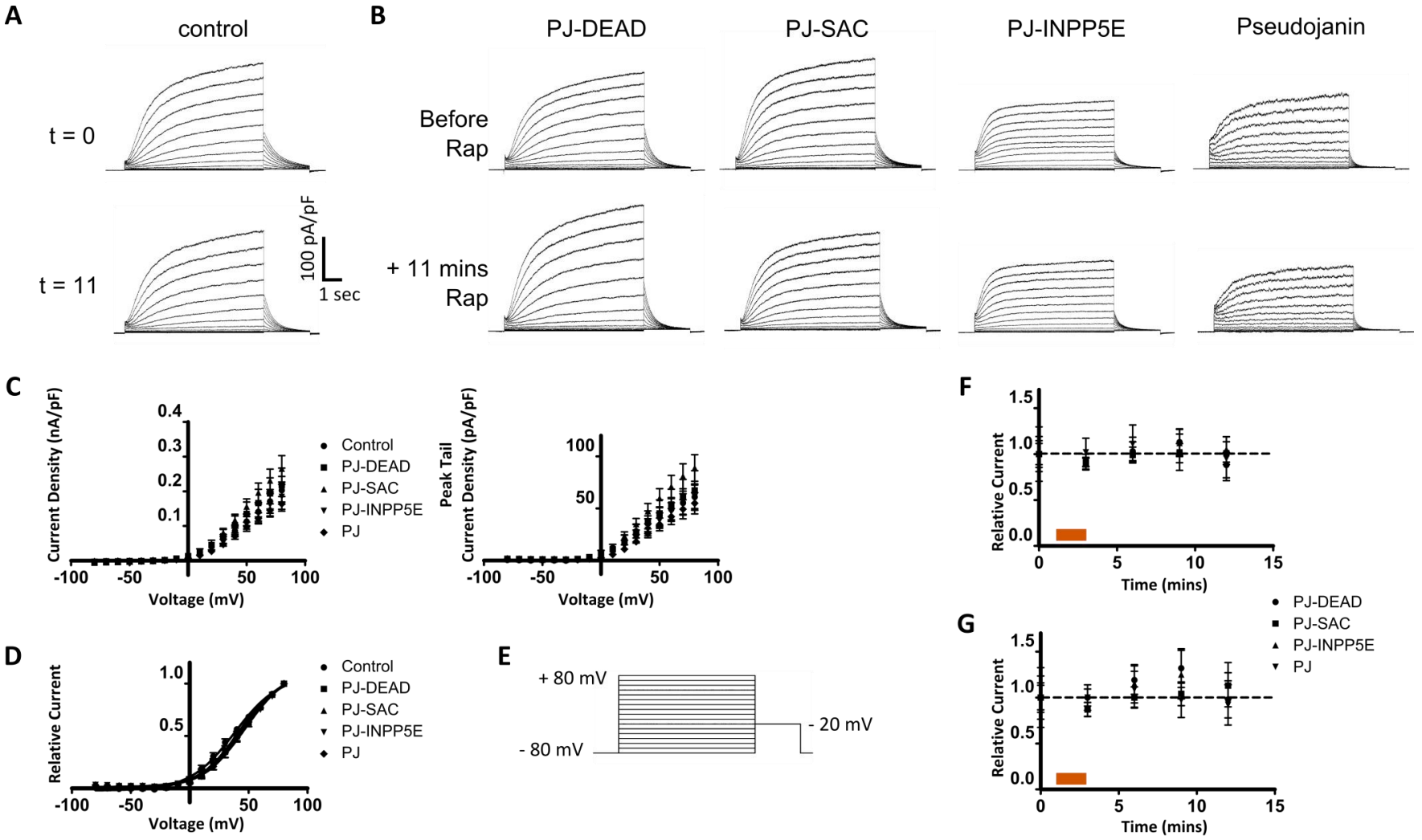
A
control
t = 0
t = 11
100 pA/pF
1 sec
B
PJ-DEAD
PJ-SAC
PJ-INPP5E
Pseudojanin
Before Rap
+ 11 mins Rap
C
Current Density (nA/pF)
Voltage (mV)
Control
PJ-DEAD
PJ-SAC
PJ-INPP5E
PJ
Peak Tail Current Density (pA/pF)
Voltage (mV)
D
Relative Current
Voltage (mV)
Control
PJ-DEAD
PJ-SAC
PJ-INPP5E
PJ
E
+ 80 mV
- 80 mV
- 20 mV
F
Relative Current
Time (mins)
G
Relative Current
Time (mins)
PJ-DEAD
PJ-SAC
PJ-INPP5E
PJ

**Figure 62. The effect of rapamycin-induced recruitment of lipid-depleting constructs to the PM on the $I_{Ks}$ current in HEK-$I_{Ks}$ cells in the perforated whole-cell patch clamp configuration.**

**A** – Representative current traces recorded in P-WCPC from HEK-$I_{Ks}$ cells recorded at t = 0 and 11 minutes (control). **B** – Representative current traces recorded in P-WCPC from HEK-$I_{Ks}$ cells transiently expressing PJ-DEAD, PJ-SAC, PJ-INPP5E or PJ with LYN11-FRB, before and 11 minutes after the start of rapamycin (5µM) addition. **C** – Mean current density (left) and peak tail current density (right) of currents recorded in P-WCPC from untransfected HEK-$I_{Ks}$ cells (control; n=14) and HEK-$I_{Ks}$ cells transiently expressing PJ-DEAD (n=9), PJ-SAC (n=14), PJ-INPP5E (n=14) or PJ (n=9) with LYN11-FRB. **D** – Steady state of activation curve, constructed by plotting normalised peak tail current densities ($y/y_{max}$) against test potential. **E** – Voltage protocol used to elicit the currents recorded in P-WCPC. **F** – Mean current density, and **G** – Mean peak tail current density, over 11 minutes, relative to that at t = 0. Current recorded from HEK-$I_{Ks}$ cells transiently expressing PJ-DEAD (n=9), PJ-SAC (n=14), PJ-INPP5E (n=14) or PJ (n=9) with LYN11-FRB. Rapamycin (5 µM) was perfused over cells after the 1$^{st}$ IV for a period of 2 minutes, and IVs were recorded every 3 minutes. Orange bars represent rapamycin perfusion. Data are presented as mean ± SEM. A one-way ANOVA with Bonferroni's post hoc test was used to determine statistical significance between relative current values at each time point in **F** and **G.** A Boltzmann function was applied to steady state activation data in **D** to fit sigmoidal curves, and a one-way ANOVA with Bonferroni's post hoc test was used to determine statistical significance between $V_{0.5}$ values.

**5.4 Discussion**

A number of LQT1-associated mutations have been characterised in heterologous cell systems and found to be defectively trafficked to the PM (table 6). The identification of a $PIP_2$-binding region in the KCNQ1 subunit and the observation that mutations within this domain caused retention of the channel in the ER, led to the hypothesis that $PIP_2$ binding to the channel could be required for its anterograde trafficking (figure 24).

The discovery in chapter 3 and in this chapter that the rapamycin-inducible dimerisation system was not optimal for investigation of $I_{Ks}$ function does not preclude using it to study the role of $PIP_2$ in $I_{Ks}$ trafficking. PJ-DEAD and LYN11-FRB/Tgn38-FRB expression provide the optimal negative control, and PJ-DEAD with LYN11-FRB have already been shown to have no effect on the $I_{Ks}$ current in WCPC experiments (because the construct contains inactive enzyme domains; chapter 3).

*Overcoming $I_{Ks}$ rundown using the perforated whole-cell patch clamp configuration*

First, the stability of the $I_{Ks}$ channel was assessed, and I observed that the $I_{Ks}$ current was subject to rundown in the WCPC configuration. This occurred when expressing PJ-DEAD in HEK-$I_{Ks}$ cells, and so the loss of $I_{Ks}$ current density over the 5-minute recording period cannot be attributed to phosphatase activity and lipid depletion. Current rundown is known to occur with channels that are particularly sensitive to changes in intracellular signalling molecules, which are lost in WCPC as the pipette solution dialyses the intracellular solution (Dufy *et al*., 1986; Hattori *et al*., 2003; Loussouarn *et al*., 2003).

To overcome the rundown that occurred in WCPC, the P-WCPC was used. Amphotericin B, an antifungal drug, was included in the pipette solution to form ion-permeable pores in the PM. These pores prevent large signalling molecules from being lost over time, which occurs by dilution of the intracellular milieu with the pipette solution in the whole-cell configuration. In P-WCPC, the $I_{Ks}$ current was stable over a period of 15 minutes, enabling the effect of rapamycin perfusion and the consequent recruitment of lipid-depleting construct to the PM to be investigated. First, however, an agent known to cause the gradual loss of $PIP_2$ from the cell was used to provide a positive control in P-WCPC. Wortmannin, a steroid metabolite of the fungi *Penicillium funiculosum*, inhibits PI4K activity at micromolar concentrations (Matavel & Lopes, 2009), and when continuously perfused over HEK-$I_{Ks}$ cells there was a gradual reduction of the $I_{Ks}$ current density with no change in the voltage-dependence of activation. This suggests that the reduction of $PIP_2$, caused by removal of its precursor, PI4P, does inhibit the $I_{Ks}$ current.

When recruiting the lipid-depleting constructs to the PM using rapamycin, there was no change in the current density over the course of 11 minutes after rapamycin addition for any of the constructs. This appears to be in contrast to the observed effect that each construct has when currents were recorded in WCPC, and, most surprisingly, there was a drastic decrease in the inhibition caused by expression of PJ or PJ-INPP5E with LYN11-FRB (without rapamycin).

A possible explanation for this is that the level of $PIP_2$ in the PM before membrane rupture in WCPC is sufficient to allow activation of the $I_{Ks}$ channel, but the turnover of $PIP_2$ in the PM is so rapid that the $PIP_2$ level dips below that required by the channel for activation before the start of a WCPC recording. In P-WCPC the intracellular environment is maintained, retaining the energy requirements of $PIP_2$ synthesis within the cell. This could explain why HEK-$I_{Ks}$ cells expressing PJ or PJ-INPP5E and LYN11-FRB elicit a smaller current in WCPC than the respective currents in P-WCPC. When the lipid-depleting constructs were recruited to the PM in P-WCPC there was no change in the $I_{Ks}$ current, suggesting that the $I_{Ks}$ channel is regulated differently in P-WCPC than in WCPC. The confocal experiments using Tubby-YFP as a marker for $PIP_2$ depletion show that even in intact cells, $PIP_2$ levels are reduced by recruiting PJ to the PM (which means that re-synthesis and maintenance of $PIP_2$ levels during PJ recruitment are not responsible for the lack of response observed in P-WCPC when PJ was recruited to the PM with rapamycin).

In P-WCPC, the $I_{Ks}$ channel may be regulated differently than in WCPC, but in addition, $PIP_2$ may be regulated differently, which may have a knock on effect on channel regulation. $PIP_2$ is synthesised in a number of locations within the cell – including membranes of the trafficking organelles, which are known to easily transfer membrane constituents between one another – and the cell may be able to redirect $PIP_2$ produced at these locations to the PM. On the other hand, the activity of the kinases that are involved in $PIP_2$ production at the PM may be regulated differently in the different patch clamp configurations.

Despite there being no change in the $I_{Ks}$ current after recruitment of the lipid-depleting constructs to the PM and consequent $PIP_2$ depletion, addition of WTM did result in a large inhibition of the $I_{Ks}$ current. Even though WTM is not specific in its inhibition of PI4Ks, it does suggest that if $PIP_2$ depletion occurs to a certain extent, the $I_{Ks}$ current is inhibited, meaning that the $I_{Ks}$ current may bind $PIP_2$ tightly and hence show a low sensitivity to $PIP_2$ depletion when in physiological conditions (i.e. P-WCPC). This could be due to the presence of KCNE1, which increases the channel's sensitivity to $PIP_2$ (Li *et al.,* 2011).

Any of the mechanisms discussed above could negate the effect of $PIP_2$ depletion resulting from rapamycin-induced recruitment of PJ or PJ-INPP5E, explaining not only the P-WCPC results in this chapter, but the lack of effect on trafficking that will be discussed below.

*Establishing the in/on-cell western assay as a tool to investigate the role of $PIP_2$ in $I_{Ks}$ channel trafficking*

To calibrate the in- and on-cell western assays so that the effect of $PIP_2$ and/or PI4P depletion on $I_{Ks}$ channel trafficking could be investigated, a number of positive control experiments were performed. These were known to affect broad trafficking pathways or specifically KCNQ1 surface expression. The expression of the SAR1 mutant, SAR1-H79G, and the KCNQ1 DN mutant, KCNQ1-E2691D, both caused a reduction in the cell-surface expression of the VSV-E1-Q1 construct whilst preserving the total amount of channel expression in the cell. SAR1 is a small GTPase that is involved in ER to Golgi trafficking by regulating the coat assembly and fission of new ER vesicles (Kuge *et al.*, 1994; Long *et al.*, 2010). The SAR1 mutant, SAR1-H79G, is a non-hydrolysable version of SAR1 that remains in the GTP-bound state rendering it constitutively active. This mutant has a DN effect over WT SAR1 and prevents vesicle trafficking between the ER and Golgi (Takida & Wedegaertner, 2004), explaining the reduction of VSV-E1-Q1 cell-surface expression.

The function of another crucial component of protein trafficking, ARF1, was compromised by expression of the constitutively active mutant, ARF1-Q71L. This mutant remains restricted in its GTP-bound form, which causes an accumulation of cargo in pre-Golgi intermediates and prevents transport through Golgi compartments (Dascher & Balch, 1994). Again, disruption of VSV-E1-Q1 trafficking after production in the ER explains the reduction in cell-surface expression whilst there was no change in total channel expression.

The KCNQ1-E261D mutant has a DN effect over the WT channel (Huang *et al*., 2001; Wilson *et al*., 2005). The reduction in VSV-E1-Q1 cell-surface expression recorded here when KCNQ1-E261D was co-expressed complements results published by Wilson and colleagues (2005), who observed with confocal microscopy that in both CHO-K1 cells and a murine myoblast cell line that KCNQ1-E261D increased the colocalisation of WT KCNQ1 with DsRed-ER (a fluorescent ER marker), indicating ER-retention of the WT subunit.

In addition to these cellular manipulations brought about by expressing mutant proteins, 1-hour incubation with WTM reduced the cell-surface expression of VSV-E1-Q1 without altering the total channel expression. These three methods of disrupting channel trafficking interfered at stages after the production of the channel protein in the ER, so it is unsurprising that the total channel

expression was unchanged. However, the effect of WTM on VSV-E1-Q1 cell-surface expression cannot be directly attributed to the inhibition of PI4K (and the resulting reduction of $PIP_2$) because WTM is non-selective in its action on PI4K. At both high and low concentrations, WTM is a potent inhibitor of PI3K (Wymann *et al*., 1996). Depending on the class of PI3K, these enzymes phosphorylate either PI or $PIP_2$ to form PI3P and PI-3,4,5-$P_3$ ($PIP_3$), respectively. PI3P is found in the endocytic pathway, highly concentrated on early endosomes, and is therefore involved in the recycling of membrane proteins. Disruption of the cellular PI3P levels may therefore lead to altered trafficking of the channel.

Supporting this are results from preliminary data obtained from an in-/on-cell western assay in which VSV-E1-Q1-expressing HEK293 cells were exposed to wortmannin for 7.5 and 15 minutes (figure 63). The purpose of this experiment was to investigate the mechanism behind the reduction in $I_{Ks}$ current when $I_{Ks}$-expressing cells are exposed to WTM, i.e. can the reduction in current observed over a period of 15 minutes be explained by a reduction in cell-surface expression?

Despite only performing 1 repeat of this assay, previous results show this assay to be robust and the results highly reproducible.

From the in-/on-cell western assay performed here it is clear that there was no change in VSV-E1-Q1 expression over the range of time points evaluated. These time points run parallel to the recordings in P-WCPC, where a 50% reduction in $I_{Ks}$ current density was observed after 8 minutes. This suggests that short-term WTM exposure, and the inhibition of PI4K that is assumed to lead to $I_{Ks}$ inhibition, inhibits the $I_{Ks}$ current through a purely functional mechanism (i.e. channel closure) rather than a reduction in cell-surface expression.

Kjeken *et al*. (2015) found that WTM treatment of rat liver endothelial cells led to the release of EEA1 from early endosomes and disrupted transport between early endosomes and lysosomes. It was also observed by another laboratory that treatment of CHO-K1 cells expressing the transferrin receptor with WTM led to a 60% increase in receptor internalisation and a 35% decrease in recycling rate due to inhibition of PI 3-kinase activity (Martys *et al*., 1996). These studies, together with the preliminary data that I obtained, suggest that the reduction of VSV-E1-Q1 surface expression after the longer exposure to WTM may be due to inhibition of PI3K activity and not inhibition of PI4K activity.

In contrast to the methods that caused altered cell-surface expression with no accompanying change in total channel expression, incubation of the cells with brefeldin A (5 μM) for 24 hours caused complete loss of the cell-surface channel expression and a severe reduction of total channel expression. Even using a lower concentration of brefeldin A (0.5 μM) led to a small reduction in total

channel expression, and a large reduction of VSV-E1-Q1 cell-surface expression. This is likely due to the fact that brefeldin A prevents COPI-mediated transport from the Golgi to the ER, and previous reports have found that this results in retrograde transport of Golgi lipids and proteins to the ER, which leads to degradation of the Golgi (Sciaky *et al.*, 1997). This process can lead to ER stress and apoptosis – evidenced here by the reduced cell number, which was even apparent by visual inspection using a bright-field microscope. The reduced signal in the in-cell assay could therefore partly be due to the reduction in cell number. Cells were originally incubated with 5 µM brefeldin A because this concentration had previously been used to incubate cells for 24 hours in the study of KCNQ1-KCNE1 assembly, with no cell death being reported (Vanoye *et al.*, 2010). When this concentration was reduced to 0.5 µM, however, there was no visible reduction in cell number, but a change in cell morphology and a reduction in the total expression of VSV-E1-Q1 did occur.

The cellular manipulations that were used to disrupt KCNQ1 trafficking (whether directly or indirectly) showed that the in/on-cell western assays can be used to report changes in VSV-E1-Q1 trafficking to the PM.

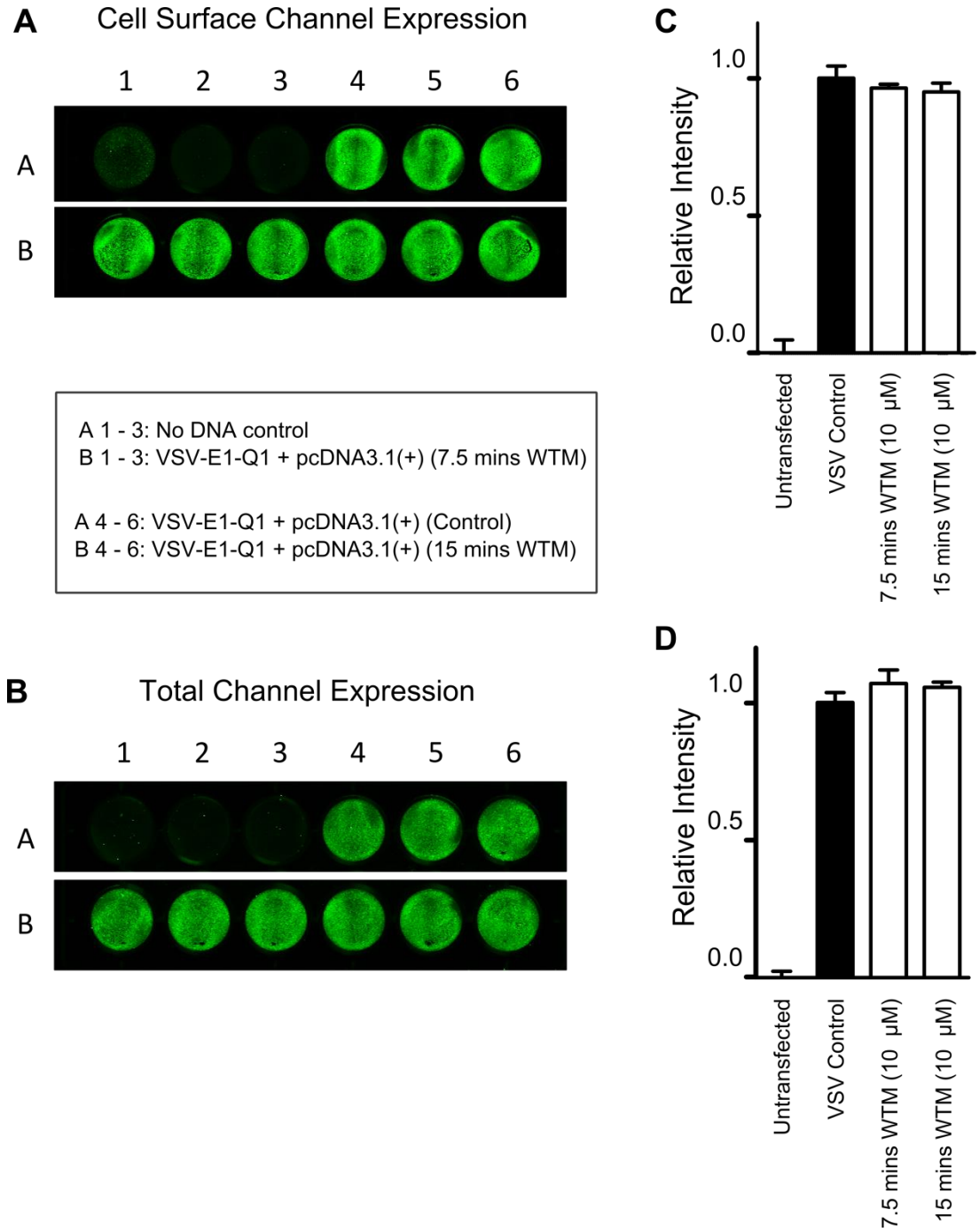


**Figure 63. Short-term inhibition of PI4K using wortmannin does not affect the cell-surface or total expression level of VSV-KCNE1-KCNQ1. A** and **B** show representative assay plates from the on- and in-cell western assay, enabling quantification of the cell surface and total cellular expression, respectively. The VSV-E1-Q1 construct was co-expressed with pcDNA3.1, and cells were incubated in the absence of 10 µM wortmannin (WTM), or in the presence of WTM for 7.5 or 15 mins. Each condition was performed in triplicate within each plate. Mean data from one experiment represented in **A** and **B** are shown in **C** and **D** respectively. Data represented as mean ± SEM. [4°C fixed on-cell western].

*Depletion of $PIP_2$ and PI4P from the PM and PI4P from the Golgi did not affect VSV-E1-Q1 trafficking*

To find out if depletion of $PIP_2$ at the PM affected trafficking of the VSV-E1-Q1 construct, VSV-E1-Q1 was expressed with either pcDNA3.1, or PJ-DEAD/PJ and LYN11-FRB. Cells expressing the lipid-depleting constructs were incubated without rapamycin or with rapamycin for 1 hour or 24 hours, to assess the acute and long-term effects of $PIP_2$ depletion at the PM on trafficking. None of these conditions resulted in any changes in the expression of the VSV-E1-Q1 construct, suggesting that the reduction of $PIP_2$ does not affect the anterograde trafficking and expression of the VSV-E1-Q1 construct, neither does it alter the rate of internalisation of the VSV-E1-Q1 construct.

Thomas and colleagues (2011) found that the cluster of basic residues in the proximal C-terminal of KCNQ1 bound not only to $PIP_2$, but to a range of other PI species. Could the mutations in this binding region have caused increased ER-retention due to the reduction in binding of a different PI? As PI4P is present at the Golgi at higher concentrations than in the rest of the cell, and is suggested to be involved in the forward trafficking of proteins destined for the cell surface, I selectively depleted PI4P and/or $PIP_2$ at the Golgi.

To provide positive controls for the depletion of PIs at the Golgi, a number of Golgi-targeted constructs were used. PJ-FAPP1, which is targeted to the Golgi and depletes PI4P and $PIP_2$, and the PJ-DEAD-FAPP1 control construct were used. It was expected that PJ-FAPP1 would cause a reduction of PI4P and $PIP_2$ at the Golgi, but the extent to which this would occur was unknown. Compared to PJ-DEAD-FAPP1, PJ-FAPP1 caused a slight reduction in cell-surface expression of the VSV-E1-Q1 construct.

The way in which these enzyme domains would act at the Golgi was unknown because they were targeted using the PI4P-binding domain, FAPP1 (for localisation of FAPP1-containing constructs, see figure 46 in chapter 4). The presence of the FAPP1 domain may have a 'protective' effect over PI4P, lowering the pool of PI4P available for dephosphorylation and hence maintaining PI4P levels. Alternatively, these two constructs may sequester PI4P with binding of the FAPP1 domain, effectively causing PI4P depletion. The observations that PJ-FAPP1 resulted in a slight reduction in VSV-E1-Q1 cell-surface expression compared to PJ-DEAD-FAPP1 (p=NS) and that PJ-DEAD-FAPP1 did not significantly alter VSV-E1-Q1 expression compared to control, suggest that these constructs do not sequester PI4P, and PI4P is available to the enzyme domains for dephosphorylation (although the size of the available pool of PI4P remains unknown).

In order to specifically deplete PI4P and/or $PIP_2$ at the Golgi to decipher the individual role of PI4P in KCNQ1 trafficking, PJ or PJ-SAC were expressed with Tgn38-FRB. Dickson *et al.* (2013) showed that

recruitment of PJ-SAC to the Golgi using Tgn38-FRB caused the depletion of PI4P using tandem PH domains of oxysterol-binding protein homolog 2 ($PH_{OSH2\times2}$) as a reporter of PI4P. $PH_{OSH2x2}$ moved from the TGN to the cytoplasm upon recruitment of PJ-SAC to the TGN, indicating that the level of PI4P here had reduced. Szentpetery *et al*. (2014) also recruited PJ-SAC to the Tgn38-FRB at the Golgi using rapamycin to investigate the relevance of PI4P in vesicular trafficking from the Golgi, and reported that depletion of PI4P using this method caused a rapid decline in the trafficking of VSVg from the Golgi to the PM. In contrast to this, I found that there was no change in VSV-E1-Q1 cell-surface expression when PJ-SAC was recruited to the Golgi with either 1 or 24 hours rapamycin incubation. The disparity between the results obtained here and by Szentpetery and colleagues regarding the effect of Golgi PI4P depletion may be due to the different proteins being investigated, different cell type used (HEK293 vs COS-7 cells) and the different methods of quantification (i.e. in- and on-cell western assay used here compared to confocal microscopy where a change in fluorescence intensity of VSVg at the Golgi was measured).

There was a small but significant reduction in the cell-surface expression of VSV-E1-Q1 when PJ was expressed in the cells with Tgn38-FRB (without rapamycin), but not when the cells were incubated in rapamycin for 24 hours.

Of course, there are limitations to this technique that may hinder the detection of subtle changes to VSV-E1-Q1 expression, or parameters that are not optimal for the detection of these changes. An example this may be that after 48 hours of VSV-E1-Q1 expression the PM becomes saturated with the VSV-E1-Q1 construct and small changes may be difficult to detect. In addition, high expression levels may mask the effect that $PIP_2$ or PI4P depletion would produce at physiological $I_{Ks}$ expression levels.

**5.5 Conclusion and Future Directions**

Using the rapamycin-induced dimerisation system to deplete $PIP_2$ and/or PI4P at the PM and Golgi, I was able to investigate whether these phospholipids played a role in regulating the function and anterograde trafficking of the $I_{Ks}$ channel. It emerged that depletion of these lipids did not affect the function of the $I_{Ks}$ channel when tested in physiological conditions (i.e. in P-WCPC), nor did it affect the total cellular expression in any instance, and the cell-surface expression of the channel was only reduced (by approximately 25%) when PJ was expressed with Tgn38-FRB.

Although it appears from these results that $PIP_2$ is not involved in the regulation of $I_{Ks}$ function or trafficking, this may not be the case; it has been suggested that the relatively low levels of $PIP_2$ in the

secretory pathway is important in silencing the channel whilst it is in transit (Hilgemann *et al*., 2001). If this mechanism of silencing is not in place, opening of the $I_{Ks}$ channel (or any other ion channel for that matter) could cause stress to the intracellular environment. The silencing that the channel experiences whilst in transit to the PM is re-established when the channel is recycled back from the PM.

To further the study into KCNQ1 trafficking, other methods can be used in the future. Even though the rapamycin-inducible dimerisation system is specific for particular PI species, the methods of targeting the constructs to particular cellular compartments can interfere with results or confuse the interpretation of these. For example, when expressing FAPP1-containing constructs, which localise to the TGN through binding to ARF1 and PI4P, PI4P levels may be altered in an unknown way. Even though it appears there was no change in VSV-E1-Q1 expression when PJ-DEAD-FAPP1 was expressed in the cells, the actual effect on PI4P levels cannot be explored by this assay.

In chapter 3, expression of PJ with LYN11-FRB resulted in a loss of $I_{Ks}$ function, even in the absence of rapamycin. However, the P-WCPC experiments in this chapter led me to hypothesise that the channel may be regulated differently in a more physiological environment, but the cell could also upregulate certain PI-production pathways to counteract any lipid depletion that may occur by action of the lipid-depleting constructs. In the in/on-cell western assays, the cells remain intact (i.e. the intracellular environment is not tampered with and remains in a physiological state, similar to cells in P-WCPC experiments). The P-WCPC recordings in this chapter would suggest that even upon recruitment of PJ to the PM with rapamycin, there is a regulation of the $I_{Ks}$ channel that maintains channel activity even in the face of $PIP_2$ depletion. The experiments using Tubby-YFP as a marker of $PIP_2$ depletion indicate that $PIP_2$ levels do decrease at the PM. However, this does not mean that trafficking pathways show the same sensitivity, and the chronic effect of rapamycin exposure to trafficking pathways cannot be predicted from such short-term recordings.

One way to overcome this uncertainty would be to knockdown the expression of a phosphatase involved in the production of PI4P or $PIP_2$ and record the effect on cell-surface expression of the VSV-E1-Q1 construct.

As previously mentioned, a possible limitation of the in-/on-cell assay is the overexpression of the VSV-E1-Q1 channel. This may prevent either the increase of VSV-E1-Q1 at the PM (i.e. the PM is saturated) or the sensitivity of the technique is not high enough to detect the % increase in PM expression. To remedy this, the amount of VSV-E1-Q1 construct used in transfections could be

optimised to enable a high enough level of expression for robust detection, but a low enough level to allow increases in expression to be detected.

One surprising observation of these experiments is that the depletion of $PIP_2$ and its precursor, PI4P, at the PM (by recruiting PJ to LYN11-FRB with rapamycin) did not change cell-surface expression levels. As $PIP_2$ is involved in CCV formation it would be expected that a reduction or depletion of $PIP_2$ would affect this process. $PIP_2$ in the PM is required for CCV formation, but subsequent depletion of $PIP_2$ needs to occur for CCV budding to complete the process of membrane internalisation. Even though depletion is required for the final stages of endocytosis, chronic depletion of $PIP_2$ may not allow initial CCV formation, inhibiting the whole internalisation process. If the rate of recycling of VSV-E1-Q1 was reduced by the loss of $PIP_2$ at the PM, an increase in VSV-E1-Q1 expression at the PM could be expected.

To investigate whether depletion of $PIP_2$ and/or PI4P at the PM reduces the rate of channel endocytosis, an assay quantifying the level of channel internalisation could be performed, and this will be discussed further in section 7.3.1.

## CHAPTER 6: Does $PIP_2$ play a role in the β1-adrenergic receptor-mediated augmentation of the $I_{Ks}$ current?

### 6.1 Introduction

In previous chapters, I found that the $I_{Ks}$ current was inhibited by $PIP_2$ depletion under certain experimental conditions. The $I_{Ks}$ inhibition that I observed in WCPC after $PIP_2$ depletion resulting from rapamycin-induced dimerisation supports work previously published by Kruse *et al*. (2012), who used a PI5K to selectively deplete $PIP_2$. This group used PJ to deplete $PIP_2$ (and PI4P) when investigating other channels, but when investigating the effect of $PIP_2$ depletion on the $I_{Ks}$ current it appears that PJ was not suitable (but this was not stated in the published results). Others have also investigated how the $I_{Ks}$ channel responds to $PIP_2$ depletion, including Matavel & Lopes (2009), who induced $PIP_2$ depletion with $G_q$-coupled GPCR activation, and Loussouarn *et al.* (2003), who used the gradual rundown of $PIP_2$ after patch excision in electrophysiological experiments.

In contrast, the P-WCPC experiments performed in Chapter 5 using the rapamycin-induced dimerisation system to cause $PIP_2$ and/or PI4P depletion indicated that when the intracellular environment is maintained, $PIP_2$ depletion may not affect the $I_{Ks}$ channel to the extent previously suggested.

It seems reasonable to suggest, however, that the $I_{Ks}$ channel might still be regulated physiologically by changes in $PIP_2$ levels, as this channel contains a $PIP_2$ binding region in the proximal C-terminus (Thomas *et al*., 2011), the movement of the VSD in the KCNQ1 subunit is coupled to pore opening by $PIP_2$ (Zaydman *et al*., 2013) and this channel does appear to be more sensitive to changes in $PIP_2$ concentration than other cardiac ion channels (Kruse *et al*., 2012).

*β1-adrenergic signalling and the $I_{Ks}$ channel*

During the ventricular action potential, the $I_{Ks}$ current does not contribute greatly to repolarisation. However, in a setting of increased adrenergic drive, various studies have shown that the $I_{Ks}$ current increases in amplitude (Kurokawa, *et al*., 2002; Matavel, *et al.,* 2010; Moline *et al*., 2014; Volders *et al*., 2003) and can hence supply the increased repolarising current needed to counteract the increased inward L-type $Ca^{2+}$ current. This notion is supported by the fact that β-blockers, which prevent signalling through the β-AR, reduce the occurrence of potentially fatal cardiac arrhythmias that can occur during increased adrenergic signalling in patients with KCNQ1 or KCNE1 mutations (LQT1 and LQT5, respectively) (Moss *et al*., 2000).

Physiologically, the $I_{Ks}$ channel associates with AKAP 9, also known as yotiao, which localises proteins involved in the β1-adrenergic response to the $I_{Ks}$ channel (Li *et al*., 2012; Marx *et al*., 2002; Terrenoire *et al*., 2009). The β1-AR primarily binds to the stimulatory Gα subunit, $G_s$, and when this receptor is activated by catecholamines such as epinephrine and norepinephrine, Gα dissociates from Gβγ and activates AC9. This in turn increases the local concentration of cAMP, leading to activation of PKA. AC9 and PKA are both brought into close proximity to the $I_{Ks}$ channel by yotiao. PKA then phosphorylates the $I_{Ks}$ channel at Ser27 (Kurokawa *et al*., 2004) and possibly Ser92 (Lopes *et al*., 2007), which results in conformational changes in the channel that lead to enhanced activation.

*Interaction between $PIP_2$ and β1-AR-dependent mechanisms of $I_{Ks}$ regulation*

The way the $I_{Ks}$ channel is modulated by $PIP_2$ and β1-AR activation is not completely understood, but what is even more complex is whether an interaction is present between these two regulatory mechanisms or whether they overlap. In the $I_{Ks}$ channel complex, the KCNE1 subunit influences channel opening in response to membrane depolarisation, but this subunit also sits in a prime position to impact the regulation of the $I_{Ks}$ channel by $PIP_2$, and increases the sensitivity of the $I_{Ks}$ channel to $PIP_2$ by 100 times compared to the $K_v7.1$ channel (KCNQ1 alone) (Li *et al*., 2011). Furthermore, when the Pro127Thr mutation was introduced to the KCNE1 C-terminus, the yotiao-dependent cAMP-mediated upregulation of the $I_{Ks}$ current was supressed due to a reduced phosphorylation of the KCNQ1 subunit at Ser27 (Dvir *et al*, 2014). Evidently, these two regulatory processes converge at a structural point in the $I_{Ks}$ channel complex, and could consequently be influenced by one another.

The exact mechanism that converts phosphorylation of the KCNQ1 subunit into enhancement of the $I_{Ks}$ current is not known, but considering that $PIP_2$ lies at the interface between the VSD and PD (Zaydman *et al*., 2013), an interaction between the $PIP_2$- and β1-AR-dependent regulation of the $I_{Ks}$ channel could be possible. This could be exhibited in a number of ways, including a change in $PIP_2$ levels altering the effect of β1-AR activation or β1-AR signalling acting through $PIP_2$ to bring about upregulation of the $I_{Ks}$ current.

It is now widely thought that the $I_{Ks}$ channel is dependent on $PIP_2$ for channel opening as this PI stabilises the open state of the channel (Loussouarn *et al*., 2003), and studies have shown that the $I_{Ks}$ channel can be activated by exogenous $PIP_2$ application (Zaydman & Cui, 2014). This is supported by my work presented in chapters 3 and 5.

Liou *et al*. (1999) show that the activation of PKA upregulates the activity of the ROMK1 channel by enhancing the strength of $PIP_2$–channel interaction. Whether this is the case for the $I_{Ks}$ channel will be investigated in this chapter.

**Hypothesis:** That $PIP_2$ plays a role in β1-mediated augmentation of the $I_{Ks}$ current.

**Aim:** To investigate whether $PIP_2$ plays a role in the augmentation of the $I_{Ks}$ current upon β1-AR activation.

## 6.2 Methods

### 6.2.1 Constructs and chemicals

The VSP from *Ciona intestinalis,* Ci-VSP, and the VSP from *Danio rerio,* Dr-VSP, were a gift from Professor Yasushi Okamura (Osaka University, Japan). Both Ci-VSP and Dr-VSP convert $PIP_2$ to PI4P through dephosphorylation. The Ci-VSP and Dr-VSP inserts are contained within the pIRES2-EGFP vector. This vector contains GFP after an IRES element, and the two inserts (Dr-VSP and GFP) are therefore expressed in cells in approximately a 1:1 ratio, enabling identification of cells expressing comparable levels of the VSP.

Isoproterenol (ISO), an agonist of the β1-AR, was used to augment the $I_{Ks}$ current. In all experiments, 100 nM ISO was used. HEK293 cells endogenously express the β1-AR, so exogenous expression of this receptor was not required.

The CF-PIPK construct was obtained from Tobias Meyer (Stanford University, U.S.A; Suh *et al*., 2006). CF-PIPK is PI4P kinase and contains the FKBP domain. As such, this construct can be used in the rapamycin-inducible dimerisation system along with LYN11-FRB. Using CF-PIPK to selectively phosphorylate PI4P to $PIP_2$ will enable the response of the $I_{Ks}$ current to an increase in only $PIP_2$ levels to be recorded.

### 6.2.2 Electrophysiology

WCPC or P-WCPC (where stated) were used to record the $I_{Ks}$ current in HEK-$I_{Ks}$ cells. HEK-$I_{Ks}$ cells for WCPC and P-WCPC were incubated as described in section 3.2.2. WCPC and P-WCPC solutions and recordings were as described in section 3.2.2 and 4.2.3, respectively.

In WCPC, I-V protocols were recorded by holding the $V_m$ at -80mV before a 2 or 6 second activation step (depending on the experiment), from -80 mV to +80 mV (or +120 mV in experiments with Ci-

VSP or Dr-VSP) in 10 mV increments. After the 2 second activation step, a 2 second repolarising step to -20 mV was used to record tail currents, before stepping back to -80 mV.

To assess the ISO-induced change in $I_{Ks}$ at a higher temporal resolution than repeated I-V protocols can offer, a sweep protocol was used. Within one sweep, the $V_m$ was held at -80 mV before a 6-second activation step to +30 mV. After this activation step, the $V_m$ was stepped to -20 mV to elicit a tail current, and then the $V_m$ returned to the holding potential of -80 mV. This one sweep was repeated every 10 seconds, and the current was recorded at the same time point in each to enable the change in current characteristics over time to be visualised.

Data were analysed as described in section 3.2.2.

### 6.2.3 Statistical analysis

Data are expressed as mean ± SE, and Boltzmann functions were generated using GraphPad Prism. A Student's T Test was used to determine statistical significance for single comparisons ($p<0.05$), and a one-way ANOVA with Bonferroni's multiple comparison test ($p<0.05$) or Dunnett's test ($p<0.05$) were used to determine significance when multiple groups were compared.

## 6.3 Results

### 6.3.1 The effect of isoproterenol on the $I_{Ks}$ current in HEK-$I_{Ks}$ cells

To enable the comparison of the $I_{Ks}$ current in the presence and absence of ISO, HEK-$I_{Ks}$ cells were pre-incubated with ISO before recording.

Before performing experiments where cells were pre-incubated with ISO, ISO (100 nM) was perfused whilst HEK-$I_{Ks}$ cells were recorded in P-WCPC. This was done to determine the amount of time it would take for any effect on the $I_{Ks}$ current to plateau. For these recordings, a voltage protocol consisting of 1 sweep was used (figure 64), which was repeated every 10 seconds. This allowed the $I_{Ks}$ current to be recorded over time at the same voltage.

First, HEK-$I_{Ks}$ cells were recorded in P-WCPC in the absence of ISO until a stable baseline was reached. ISO (100 nM) was then perfused onto the cells and the +30 mV sweep protocol was continued until the $I_{Ks}$ current response plateaued. Figure 64 shows a representative current trace and time course data for the same cell, where perfusion of ISO (100 nM) led to an increase in CD and PTCD of approximately 100% over a period of around 8 minutes. Based on this data, cells in the following experiments (utilising I-V protocols in WCPC to record the $I_{Ks}$ current in the presence of

ISO) were subject to ISO (100 nM) perfusion for 10 minutes before the commencement of the WCPC recordings.

When HEK-$I_{Ks}$ cells were pre-incubated with ISO (100 nM) for 10 mins, the $I_{Ks}$ CD increased compared to HEK-$I_{Ks}$ cells in the absence of ISO, between $V_m$ values of 0 mV to +70 mV. At 0 mV, the $I_{Ks}$ current was 2.87 times greater, at 30 mV, 1.19 times greater and at 50 mV, 1.47 times greater than the current at the same respective $V_m$ in HEK-$I_{Ks}$ cells. When the $V_m$ reached +80 mV, however, the current density values were not significantly different. The PTCD showed a similar trend to the values of CD between HEK-$I_{Ks}$ cells in the presence or absence of ISO (100 nM). The steady state of activation for HEK-$I_{Ks}$ cells pre-incubated in ISO (100 nM) was shifted to more hyperpolarised potentials compared to that for untreated HEK-$I_{Ks}$ cells, and the value of $V_{0.5}$ was significantly different, changing from 31.94 ± 0.54 mV to 11.48 ± 0.29 mV ($p<0.005$).

The activation kinetics of the $I_{Ks}$ current when recorded in HEK-$I_{Ks}$ cells pre-incubated with ISO (100 nM) for 10 mins were significantly quicker between +20 mV and +80 mV compared to untreated HEK-$I_{Ks}$ cells ($p<0.01$). Also, the deactivation time constant (measured after a test pulse to +40 mV) significantly reduced (figure 65E and F).

### 6.3.2 The effect of increasing cellular $PIP_2$ levels on the $I_{Ks}$ current in HEK-$I_{Ks}$ cells

To increase the $PIP_2$ concentration within the intact cell during patch-clamp experiments, a construct named CF-PIPK was expressed in cells along with LYN11-FRB. CF-PIPK is similar to the PJ-related constructs used in previous chapters, but contains a PI5K domain in place of the PI phosphatase domains. This construct can also be used in the rapamycin-induced dimerisation system, so can be recruited to the PM upon addition of rapamycin to cells expressing these two constructs.

To enable the direct comparison of the effects of ISO and the increase in $PIP_2$ concentration on the $I_{Ks}$ current, CF-PIPK and LYN11-FRB were expressed in HEK-$I_{Ks}$ cells. Overexpression of the lipid-depleting constructs (i.e. PJ and PJ-related constructs) with LYN11-FRB in HEK-$I_{Ks}$ cells (chapter 3) led to inhibition of the $I_{Ks}$ current without recruitment of the lipid-depleting constructs to the PM with rapamycin, when investigated using WCPC. Due to this observation, it was expected that CF-PIPK would act in a similar fashion, but instead of causing lipid depletion (and hence current inhibition) this construct would lead to an increase in $PIP_2$ at the PM even in the absence of rapamycin.

CF-PIPK and LYN11-FRB were expressed in HEK-$I_{Ks}$ cells and the $I_{Ks}$ current was recorded in WCPC using the voltage protocol shown in figure 65.

Transient expression of CF-PIPK with LYN11-FRB in HEK-$I_{Ks}$ cells caused an increase in the $I_{Ks}$ current at all membrane potentials above those where activation of the $I_{Ks}$ channel occurs compared to untransfected HEK-$I_{Ks}$ cells, which was significant across all voltages analysed ($p<0.01$). In addition, the PTCD increased approximately 2-fold across membrane potentials between 0 mV and 50 mV, and was significantly increased across all voltages analysed ($p<0.05$). The steady state of activation was left-shifted compared to untransfected HEK-$I_{Ks}$ cells, and the $V_{0.5}$ was significantly different, changing from 31.94 ± 0.54 mV to 15.27 ± 0.50 mV ($p<0.005$) (figure 65).

The activation of the $I_{Ks}$ current when CF-PIPK and LYN11-FRB were expressed in HEK-$I_{Ks}$ cells was significantly quicker between +20 mV and +70 mV compared to HEK-$I_{Ks}$ cells ($p<0.05$), and the deactivation was significantly slowed (measured after a test pulse to +40 mV) ($p<0.01$) (figure 65E and F).

Even though CF-PIPK was not recruited to the PM with rapamycin, this PI4P 5-K appeared to increase the $PIP_2$ concentration, causing the changes in $I_{Ks}$ current observed here. Without recruitment of CF-PIPK to the PM, the $I_{Ks}$ current increased dramatically compared to control levels.

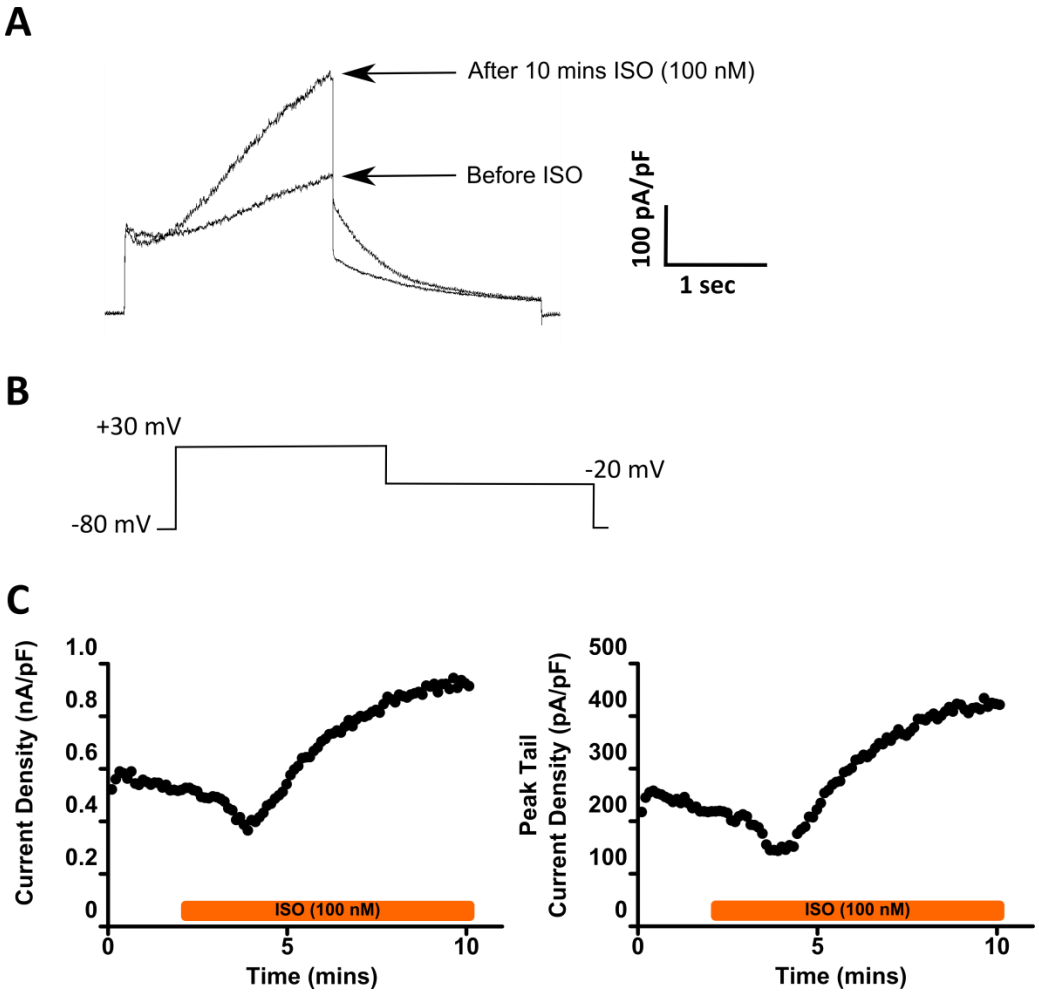


**Figure 64. The time course of the effect of isoproterenol on the $I_{Ks}$ current. A** – Representative current trace recorded in P-WCPC from HEK-$I_{Ks}$ cells perfused with ISO (100 nM) after a stable baseline current had been reached, showing a sweep before ISO addition and when the $I_{Ks}$ current plateaued after approximately 8 minutes of ISO perfusion. **B** – Voltage protocol used to elicit the currents recorded in P-WCPC. **C** – Current density (left) and peak tail current density (right) recorded in P-WCPC from an untransfected HEK-$I_{Ks}$ cell showing the time course of the effect of ISO (100 nM) perfusion (orange bar) on the $I_{Ks}$ current.

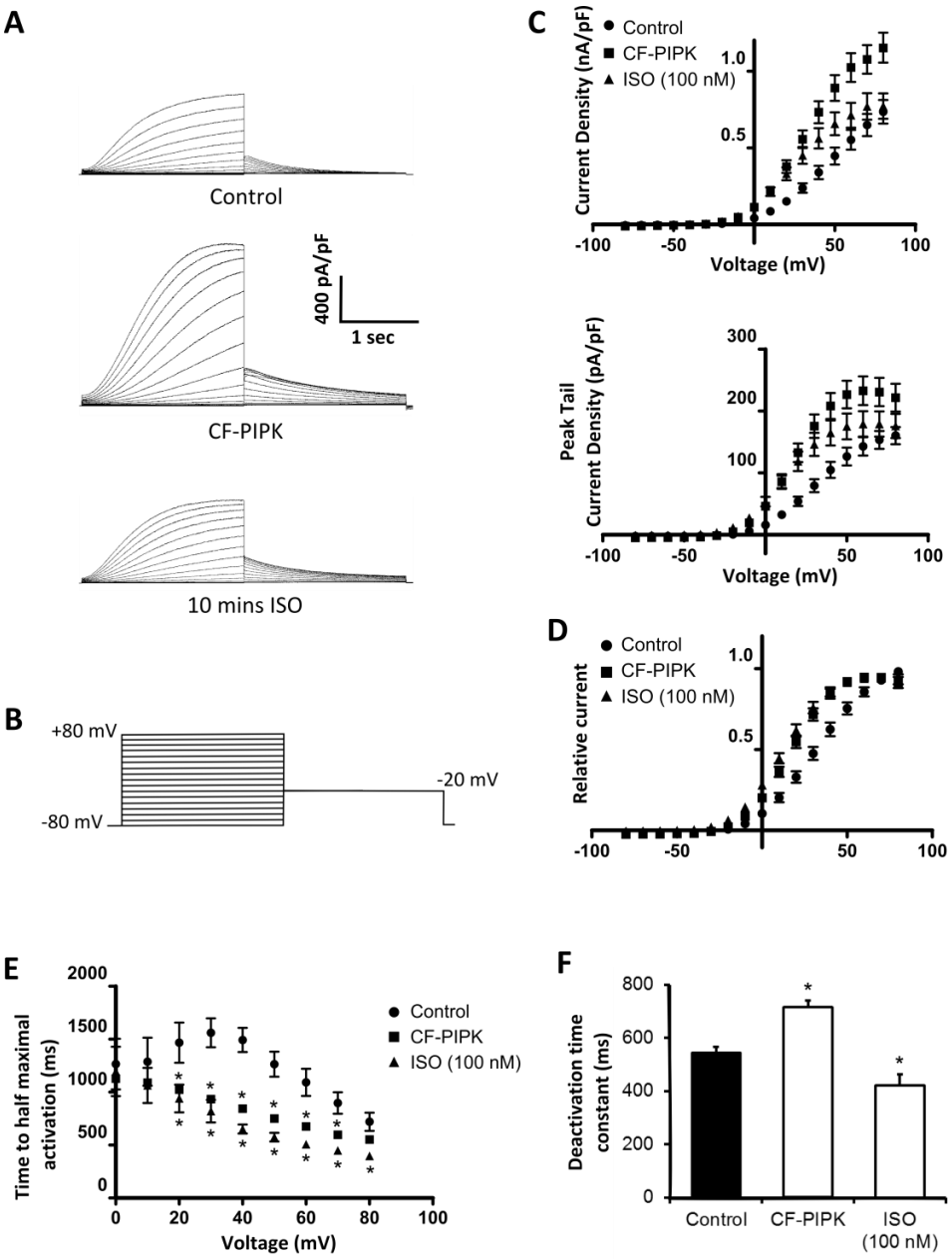


**Figure 65. The effect of increased $PIP_2$ or β1-adrenergic receptor enhancement on the $I_{Ks}$ current in HEK-$I_{Ks}$ cells. A –** Representative traces of currents recorded in WCPC from untransfected HEK-$I_{Ks}$ cells (control), HEK-$I_{Ks}$ transiently expressing CF-PIPK with LYN11-FRB or untransfected HEK-$I_{Ks}$ cells pre-incubated for 10 mins with ISO (100 nM). **B –** Voltage protocol used to elicit currents recorded in WCPC. **C –** Mean current density (top) and peak tail current density (bottom) of currents recorded in WCPC from untransfected HEK-$I_{Ks}$ cells (control), HEK-$I_{Ks}$ cells expressing CF-PIPK with LYN11-FRB (n=15) and untransfected cells pre-incubated with ISO (100 nM) (n=14). **D –** Steady state of activation, constructed by plotting normalised peak tail current densities ($y/y_{max}$) against test potential. **E –** Activation kinetics and **F –** Deactivation time constance (measured following a test pulse to +40 mV) of $I_{Ks}$ currents from untransfected HEK-$I_{Ks}$ cells (control), HEK-$I_{Ks}$ cells expressing CF-PIPK with LYN11-FRB and HEK-$I_{Ks}$ cells pre-incubated with ISO (100 nM). Data are presented as mean ± SE. A one-way ANOVA with Dunnett's post hoc test was used to determine statistical significance between control and all other groups in **C** and **F**, between +30 mV and +80 mV, in **E** across all voltages, and between $V_{0.5}$ values obtained from **D**. A Boltzmann function was applied to data in **D** to fit a sigmoidal curve.

### 6.3.3 The effect of voltage-sensitive phosphatase activation on the $I_{Ks}$ current in HEK-$I_{Ks}$ cells

To investigate how $PIP_2$ concentration affects the response of the $I_{Ks}$ channel to β1-AR activation (using ISO), a VSP was used to progressively deplete $PIP_2$ with increasing depolarisation of the PM. This strategy was chosen because it has previously been used by others to 'titrate' the levels of $PIP_2$ in the PM whilst recording channel function (Falkenburger *et al*., 2010; Rjasanow *et al*., 2015). Furthermore, the VSPs dephosphorylate $PIP_2$ and not PI4P, and the VSPs exist in an inactive state until activated by increasing voltage. This provides a selective, inducible and reversible method of titrating $PIP_2$ on a timescale of seconds. Before performing this, however, the VSP that is most suitable to use with the $I_{Ks}$ current was determined.

Dr-VSP and Ci-VSP both activate in response to membrane depolarisation, and 50% Dr-VSP activation occurs at approximately +100 mV (Okamura *et al*., 2009). Each VSP was transiently expressed in HEK-$I_{Ks}$ cells and the $I_{Ks}$ current was recorded using the voltage protocol shown in figure 66.

When Ci-VSP was expressed in HEK-$I_{Ks}$ cells, there was an inhibition of the $I_{Ks}$ current compared to untransfected HEK-$I_{Ks}$ cells, and it appeared that even at the lower membrane potentials, $PIP_2$ became depleted to an extent that severely impacted the $I_{Ks}$ current (figure 66). Because of the drastic inhibition caused by Ci-VSP, only n=3 were recorded, therefore only representative traces are shown in figure 66.

In contrast, when Dr-VSP was expressed in HEK-$I_{Ks}$ cells, the lower membrane potentials that activate the $I_{Ks}$ channel (approximately >0 mV) did give rise to sizable $I_{Ks}$ current, but this was still reduced ($p<0.05$) compared to untransfected HEK-$I_{Ks}$ cells (figure 66).

It appears that Ci-VSP activates across a very similar voltage range to the $I_{Ks}$ channel, and so Dr-VSP should be used with the $I_{Ks}$ channel to allow recording of $I_{Ks}$ current before $PIP_2$ depletion from VSP activation. The effects seen with these two VSPs clearly reinforces that the $I_{Ks}$ channel is dependent on $PIP_2$ for its function. The effect of ISO perfusion or CF-PIPK expression on the $I_{Ks}$ current was investigated in the setting of $PIP_2$ depletion by Dr-VSP activation from here onwards.

### 6.3.4 The effect of PI4P 5-K expression on the $I_{Ks}$ current in HEK-$I_{Ks}$ cells that also express a voltage-sensitive phosphatase

After establishing that Dr-VSP was optimal for use with the $I_{Ks}$ channel, manipulations to regulatory mechanisms of the $I_{Ks}$ channel could then be performed and the effect of gradual $PIP_2$ depletion by VSP activation could be observed.

CF-PIPK, LYN11-FRB and Dr-VSP were transiently expressed in HEK-$I_{Ks}$ cells and the $I_{Ks}$ current was recorded using the voltage protocol shown in figure 67B.

When compared to HEK-$I_{Ks}$ cells only expressing Dr-VSP, the $I_{Ks}$ CD and PTCD recorded in HEK-$I_{Ks}$ cells expressing CF-PIPK, LYN11-FRB and Dr-VSP significantly increased across all $I_{Ks}$ channel-activating membrane potentials ($p<0.05$). This can be explained by the fact that CF-PIPK may show a basal level of activity and Dr-VSP may act to sequester $PIP_2$ prior to activation, but that the increased production of $PIP_2$ by overexpression of CF-PIPK can override the effective $PIP_2$ depletion brought about by Dr-VSP activation.

Figure 67 shows the normalised PTCD values, and curves were fitted using a Boltzmann function. $V_{0.5}$ values were analysed with a one-way ANOVA with Bonferroni's post hoc test, which showed that there was a significant difference between the values for CF-PIPK (2.41 ± 0.67 mV) and Dr-VSP (7.71 ± 0.67 mV; $p<0.001$), and between CF-PIPK and control (6.95 ± 1.05 mV; $p<0.01$). Comparing relative CD and PTCD showed that Dr-VSP expression with CF-PIPK and LYN11-FRB was significantly different to Dr-VSP cells ($p<0.05$), but not significantly different from control cells across all voltages compared (p=NS).

### 6.3.5 The interaction between PKA- and $PIP_2$-dependent mechanisms of $I_{Ks}$ regulation

In a similar fashion to the experiments looking into the effect of PI4P 5-K activity on the $I_{Ks}$ current whilst activating Dr-VSP, the effect of ISO was also investigated so the two could be compared. This comparison allowed investigation into whether $PIP_2$ is involved in the β1-AR-activation-induced increase in the $I_{Ks}$ current.

As before, ISO (100 nM) was perfused over cells for 10 mins prior to WCPC recordings, but this time the HEK-$I_{KS}$ cells transiently expressed Dr-VSP. $I_{Ks}$ currents were recorded in HEK-$I_{Ks}$ cells using the voltage protocol shown in figure 67B.

After 10 mins of ISO (100 nM) perfusion in HEK-$I_{Ks}$ cells expressing Dr-VSP, the $I_{Ks}$ current was significantly increased compared to HEK-$I_{Ks}$ cells expressing Dr-VSP in the absence of ISO across all voltages analysed ($p<0.5$). The $I_{Ks}$ CD and PTCD were very similar to those elicited when CF-PIPK and LYN11-FRB were expressed with Dr-VSP in HEK-$I_{Ks}$ cells, and to control cells. The pre-incubation with ISO appeared to reverse the effect of $PIP_2$ depletion resulting from Dr-VSP activation, up to 80 mV. The $V_{0.5}$ value, however, changed significantly between control cells and those expressing Dr-VSP also pre-incubated with ISO (6.95 ± 1.05 mV vs. 0.00 ± 0.71 mV; $p<0.0001$) (figure 67D). When the

membrane potential reached +80 mV, the CD values diverged and began to increase when compared to cells expressing CF-PIPK, but this trend did not reach significance (p=NS) (figure 67C).

Figure 67 also shows the normalised PTCD values of $I_{Ks}$ cells expressing Dr-VSP that were pre-incubated for 10 mins with ISO (100 nM), and curves were fit using a Boltzmann function. $V_{0.5}$ values were analysed with a one-way ANOVA with Bonferroni's post hoc test, which showed that there was no significant difference between the values for control (4.72 ± 0.81 mV), Dr-VSP (3.92 ± 3.2 mV; p=NS) or Dr-VSP also incubated with ISO (100 nM) for 10 mins (-4.20 ± 1.76 mV; p=NS). Comparing relative CD and PTCD values showed that Dr-VSP expression with 10 mins ISO (100 nM) pre-incubation was significantly different to control cells ($p<0.05$) (figure 68). In addition, the relative CD was significantly different from that of HEK-$I_{Ks}$ cells expressing Dr-VSP from 70 mV–90 mV ($p<0.05$), and the relative PTCD was significantly different from that of HEK-$I_{Ks}$ cells from 80 mV–110 mV ($p<0.05$). The relative CD and PTCD values were significantly different between HEK-$I_{Ks}$ cells expressing Dr-VSP with CF-PIPK and LYN11-FRB and HEK-$I_{Ks}$ cells expressing Dr-VSP pre-incubated with ISO (100 nM) for 10 mins from 90 mV–120 mV ($p<0.05$).

### 6.3.6 The effect of isoproterenol on the $I_{Ks}$ current in HEK-$I_{Ks}$ cells that also express PJ

As pre-incubation with ISO (100 nM) was able to overcome Dr-VSP-induced $PIP_2$ depletion, the ability to overcome $PIP_2$ depletion caused by PJ expression was studied.

As performed for previous pre-incubation experiments, ISO (100 nM) was perfused over cells for 10 mins prior to WCPC recordings, but this time the HEK-$I_{Ks}$ cells transiently expressed PJ and LYN11-FRB. $I_{Ks}$ currents were recorded in HEK-$I_{Ks}$ cells using the voltage protocol shown in figure 69.

Figure 69 shows currents recorded from HEK-$I_{Ks}$ cells, HEK-$I_{Ks}$ cells pre-incubated with ISO and HEK-$I_{Ks}$ cells expressing PJ with LYN11-FRB, previously shown in this chapter and chapter 3. When cells expressing PJ with LYN11-FRB were pre-incubated with ISO (100 nM) for 10 mins prior to recording, there was a recovery of the $I_{Ks}$ current when compared to the current recorded from cells expressing PJ and LYN11-FRB without ISO pre-incubation. This recovery was significant between +30 mV and +50 mV ($p<0.05$). This current, however, was reduced compared to control cells at the more positive voltages used, but this was not a significant difference when comparing CD (p=NS) and PTCD values (p=NS) between +30 mV and +50 mV.

$V_{0.5}$ values were determined by fitting a Boltzmann function to the normalised PTCD, which showed that compared to control (9.33 ± 0.53 mV), pre-incubation of cells expressing PJ and LYN11-FRB with ISO (100 nM) caused a hyperpolarising shift (2.23 ± 0.46 mV), which was significant ($p<0.001$). The

shift in $V_{0.5}$ was not to the extent of untransfected cells pre-incubated with ISO (-11.55 ± 0.99 mV), and there was a significant difference between this and cells pre-incubated with ISO also expressing PJ with LYN11-FRB ($p<0.001$).

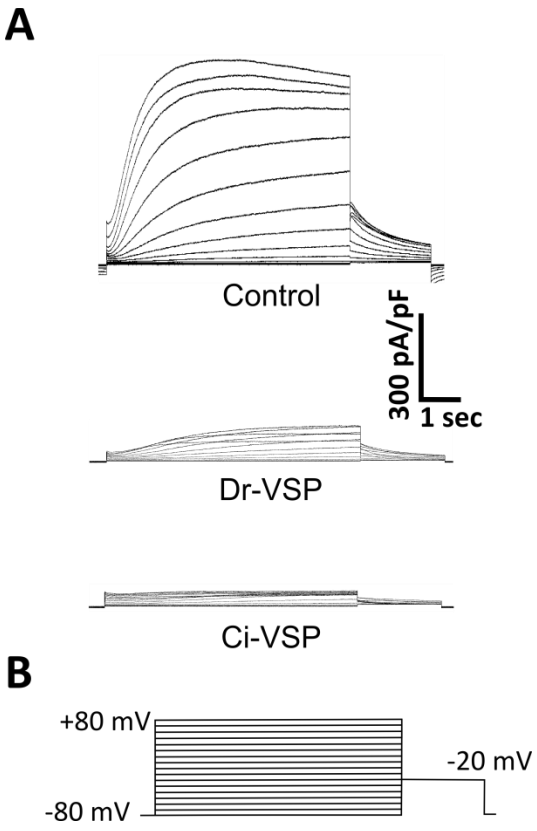


**Figure 66. Comparison of the effect of different voltage-sensitive phosphatases on the $I_{Ks}$ current in HEK-$I_{Ks}$ cells. A** – Representative current traces recorded in WCPC from untransfected HEK-$I_{Ks}$ cells (control) and HEK-$I_{Ks}$ cells expressing Dr-VSP or Ci-VSP. **B** – Voltage protocol used to elicit the currents recorded in WCPC. Mean data are not shown here due to the low number of recordings obtained for Ci-VSP-transfected cells.

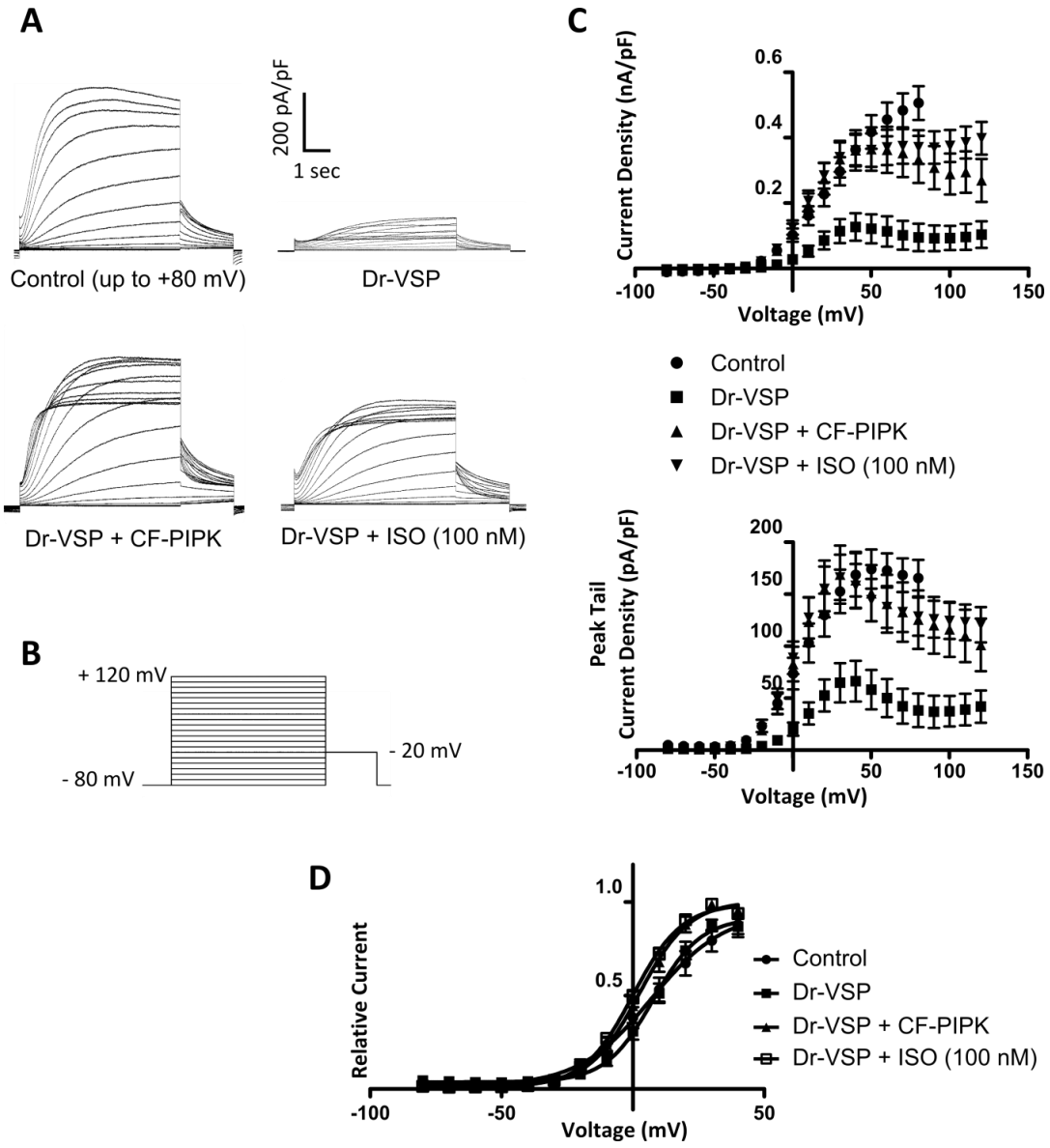


**Figure 67. The effect of gradual $PIP_2$ depletion using a voltage-sensitive phosphatase in the setting of increased $PIP_2$ or β1-adrenergic receptor activation on the $I_{Ks}$ current in HEK-$I_{Ks}$ cells. A –** Representative traces of currents recorded in WCPC from HEK-$I_{Ks}$ cells (control) and HEK-$I_{Ks}$ cells expressing Dr-VSP, Dr-VSP with CF-PIPK and LYN11-FRB or Dr-VSP whilst being pre-incubated for 10 mins with ISO (100 nM). **B –** Voltage protocol used to elicit currents recorded in WCPC. **C** – Mean current density (top) and peak tail current density (bottom) of currents recorded in WCPC from HEK-$I_{Ks}$ cells (control) and HEK-$I_{Ks}$ expressing Dr-VSP (n=12), Dr-VSP with CF-PIPK and LYN11-FRB (n=16) or Dr-VSP whilst being pre-incubated for 10 mins with ISO (100 nM) (n=14). **D –** Steady state of activation curves, constructed by plotting normalised peak tail current densities ($y/y_{max}$) against test potential. Data are presented as mean ± SE. A one-way ANOVA with Bonferroni's post hoc test was used to determine statistical significance across all groups in **C**, between +30 mV and +120 mV (+80 mV in the case of control cells), and between $V_{0.5}$ values obtained from **D**. A Boltzmann function was applied to data in **D** to fit sigmoidal curves.

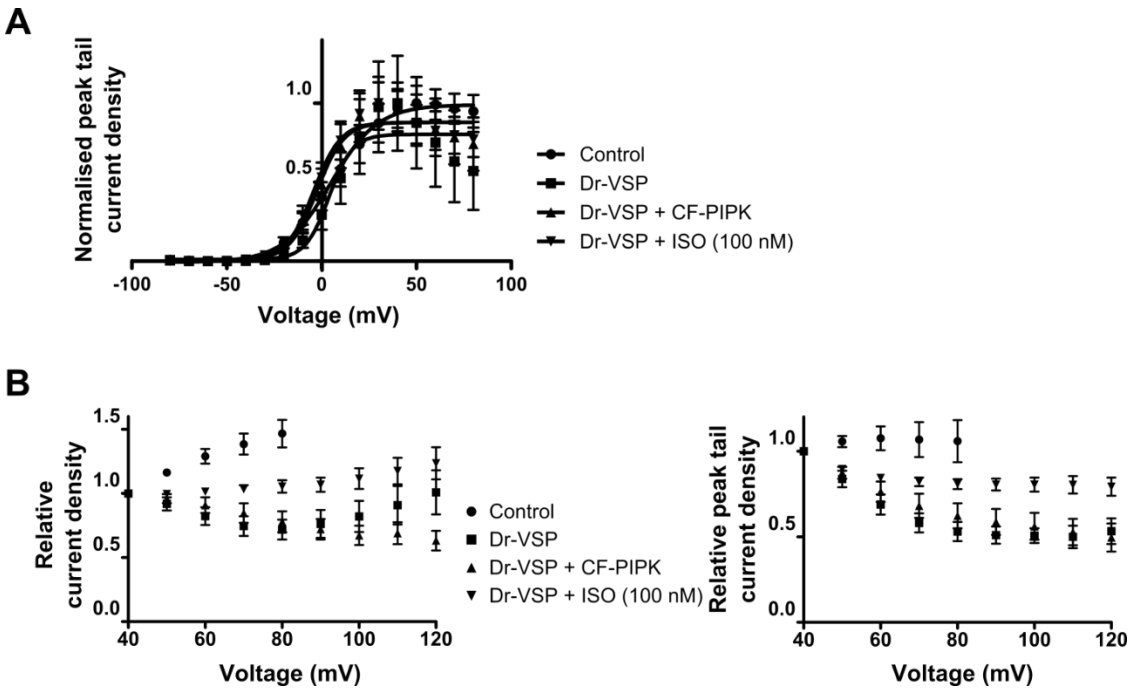


**Figure 68. Comparison of the relative effects of gradual $PIP_2$ depletion using a voltage-sensitive phosphatase in the setting of increased $PIP_2$ or β1-adrenergic receptor activation on the $I_{Ks}$ current in HEK-$I_{Ks}$ cells. A –** Normalised current recorded in WCPC from untransfected HEK-$I_{Ks}$ cells (control) (n=9), HEK-$I_{Ks}$ cells transiently expressing Dr-VSP (n=12), Dr-VSP with CF-PIPK and LYN11-FRB (n=16) or Dr-VSP whilst being pre-incubated for 10 mins with ISO (100 nM) (n=14). Peak tail current density was normalised to the maximum and minimum mean peak tail current density values. **B –** Relative current density (left) and relative peak tail current density (right) of currents recorded in WCPC, constructed by plotting $y/y_{max}$ against test potential. Data are presented as mean ± SE. A Boltzmann function was applied to data in **A** to fit sigmoidal curves. A one-way ANOVA with Bonferroni's post hoc test was used to determine statistical significance between $V_{0.5}$ values from **A**, and all group pairs in **B** across all voltages.

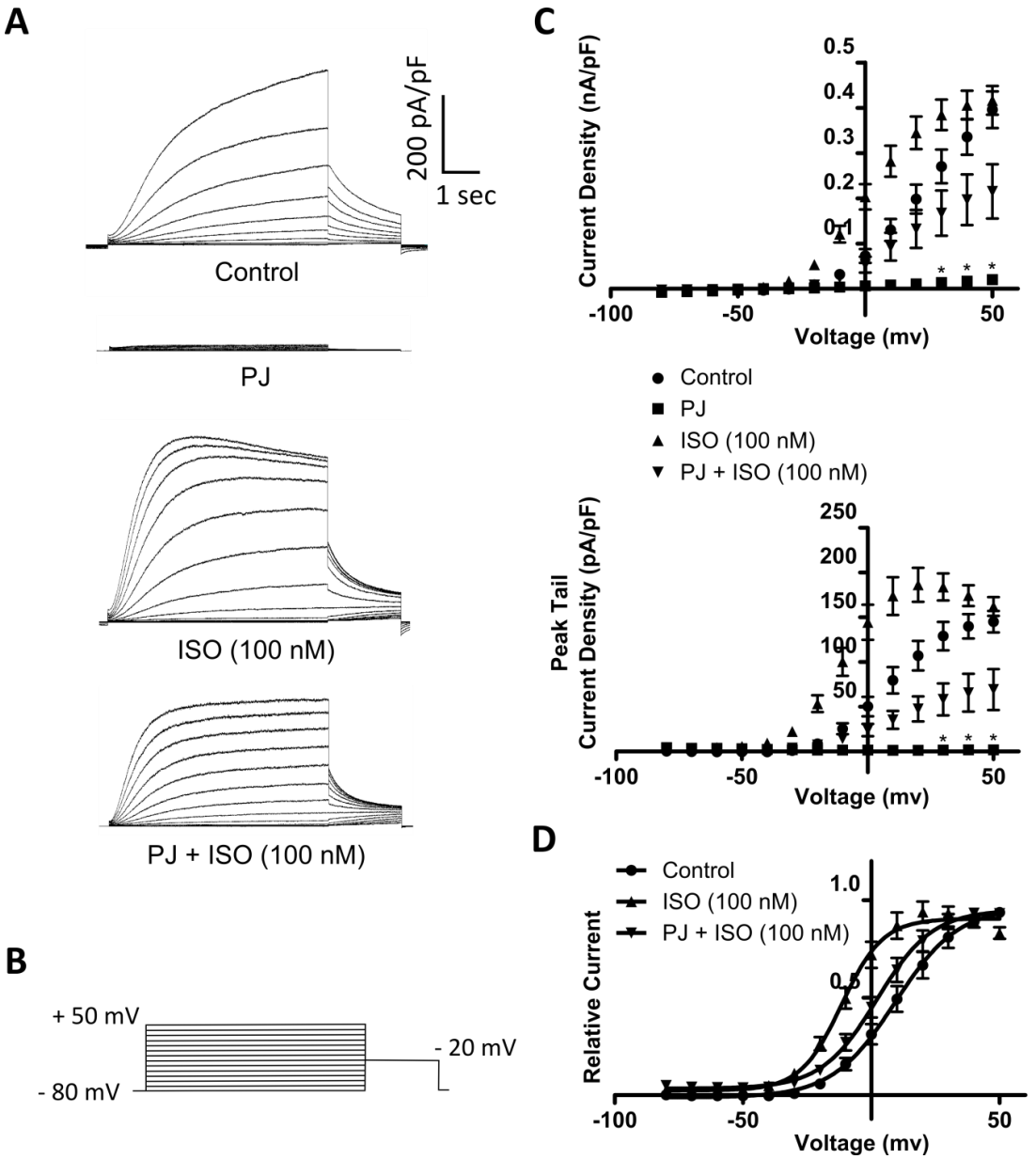


**Figure 69. Effect of β1-adrenergic receptor activation on the $I_{Ks}$ inhibition caused by expression of lipid-depleting constructs in HEK-$I_{Ks}$ cells. A –** Representative traces of currents recorded in WCPC from untransfected HEK-$I_{Ks}$ cell (control), HEK-$I_{Ks}$ cells expressing PJ, untransfected HEK-$I_{Ks}$ cells pre-incubated for 10 mins with ISO (100 nM) and HEK-$I_{Ks}$ cells expressing PJ also pre-incubated with ISO (100 nM) for 10 mins. **B –** Voltage protocol used to elicit currents recorded in WCPC. **C** – Mean current density (top) and peak tail current density (bottom) of currents from HEK-$I_{Ks}$ cell (n=12), HEK-$I_{Ks}$ cells expressing PJ with LYN11-FRB (n=11), untransfected HEK-$I_{Ks}$ cells pre-incubated for 10 mins with ISO (100 nM) (n=7) and HEK-$I_{Ks}$ cells expressing PJ with LYN11-FRB also pre-incubated with ISO (100 nM) for 10 mins (n=14). **D –** Steady state of activation curves, constructed by plotting normalised peak tail current densities ($y/y_{max}$) against test potential. Data are presented as mean ± SE. A one-way ANOVA with Dunnett's post hoc test was used to determine statistical significance between control and all other groups in **C**, between +30 mV and +50 mV, and between $V_{0.5}$ values obtained from **D**. A Boltzmann function was applied to data in **D** to fit sigmoidal curves.

## 6.4 Discussion

$PIP_2$ lies in an optimal position within the $I_{Ks}$ channel complex to be involved in different regulatory processes, including the effect that KCNE1 has on the homomeric KCNQ1 channel (Li *et al*., 2011). Due to the sensitivity of the $I_{Ks}$ channel to $PIP_2$ depletion that others have previously found (Kruse *et al*., 2012; Loussouarn *et al*., 2003; Matavel & Lopes, 2009), it is thought that this channel might be regulated physiologically by depletion of $PIP_2$ from the PM (addressed in chapter 3 and 5).

$PIP_2$ is known to stabilise the open state of the $I_{Ks}$ channel (Loussouarn *et al*., 2003), and Zaydman *et al.* (2013) suggested that $PIP_2$ couples voltage-sensor movement to pore opening. Supporting these findings, the experiments I performed in chapter 3 suggest that $PIP_2$ is critical for $I_{Ks}$ channel function.

One aspect of the $I_{Ks}$ channel's regulation that has not been studied extensively is how phosphorylation of the KCNQ1 subunit at Ser27 and Ser92 by PKA, downstream of β1-AR activation, leads to enhancement of the $I_{Ks}$ current. An increase in the macroscopic current could suggest that the channel remains in the open state for a longer period of time, indicating that $PIP_2$ may be involved. Drawing on evidence from others regarding the role of $PIP_2$ in coupling voltage-sensor movement to pore opening (Zaydman *et al*., 2013), I hypothesised that $PIP_2$ is involved in the enhancement of the $I_{Ks}$ current resulting from PKA-dependent phosphorylation.

*Increasing $PIP_2$ at the PM enhances the $I_{Ks}$ current*

To decipher whether a change in $PIP_2$ alone is responsible for this augmentation in $I_{Ks}$ current, the PI4P 5-K, CF-PIPK, was used to increase the $PIP_2$ concentration within the cell. Despite not recruiting PJ to LYN11-FRB at the PM with rapamycin, experiments with the lipid-depleting constructs in chapter 3 revealed that the enzyme activity of the lipid-depleting constructs could bring about changes in $PIP_2$ concentration that were sufficient to completely abolish $I_{Ks}$ function. As such, CF-PIPK was initially overexpressed with LYN11-FRB to assess whether the $I_{Ks}$ current was affected prior to rapamycin addition. Indeed, the $I_{Ks}$ current was significantly increased compared to untransfected HEK-$I_{Ks}$ cells, reflecting the increase in $PIP_2$ caused by overexpression of the CF-PIPK construct. Others have reported that overexpression of a PIP 5-K increased the $PIP_2$ concentration in rat atrial myocytes (Bender *et al*., 2002) or sympathetic neurons (Winks *et al*., 2005).

In addition to establishing that CF-PIPK can increase $PIP_2$ in the PM, and that this can be detected as an increase in the $I_{Ks}$ current, this experiment revealed that the $I_{Ks}$ channel does not reside in a $PIP_2$-saturated state (at least in the HEK293 stably-expressing cell line used here), as increased $PIP_2$ concentrations led to changes in the channel's biophysics. This strengthens the possibility that β1-AR

activation could lead to a change in how $PIP_2$ influences the function of the $I_{Ks}$ channel, as there exists scope for channel augmentation to occur.

*Activating the β1-adrenergic receptor enhances the $I_{Ks}$ current*

The effect of β1-AR activation on the $I_{Ks}$ current resulting from pre-incubating HEK-$I_{Ks}$ cells with ISO (100 nM) is different in some ways to the effect of overexpressing CF-PIPK in these cells. Up to a voltage of approximately +30 mV, the $I_{Ks}$ current behaves in a similar manner, but after this the responses diverge; pre-incubation with ISO (100 nM) does not result in a significant change in $I_{Ks}$ CD at voltages ≥50 mV when compared to control cells.

This data is largely in accordance with previously published studies, which have shown an increase in $I_{Ks}$ CD in the presence of ISO, and a hyperpolarising shift in the voltage-dependence of activation (Imredy *et al*., 2008; Severi *et al*., 2009). This group did observe a larger increase in $I_{Ks}$ current compared to the results I obtained, but this may be due to the difference in cell types studied (a HEK293 cell line compared to guinea-pig ventricular myocytes).

ISO pre-incubation increased activation kinetics of the $I_{Ks}$ channel, resulting in larger currents at more negative membrane potentials, but also decreased the time taken for deactivation. This is in contrast to the effect that CF-PIPK had, which was to speed up activation whilst increasing the time taken for deactivation. β1-AR activation in the heart acts to increase the force of contraction, but also to increase heart rate. The increase in both activation and deactivation kinetics observed here when pre-incubating HEK-$I_{Ks}$ cells with ISO fits with the need for an increase in repolarising current paired with the capacity for rapid reactivation.

The fact that the effect on $I_{Ks}$ channel deactivation differs between these two conditions suggests that in addition to the possibility that $PIP_2$ may be involved in transmitting β1-AR activation to the $I_{Ks}$ channel, other cellular processes are likely to be involved in the overall process, in particular deactivation of the channel.

*Voltage-sensitive phosphatase activation and the $I_{Ks}$ current*

As another means of deciphering how $PIP_2$ is involved in regulating the function of the $I_{Ks}$ channel, VSPs were expressed in HEK-$I_{Ks}$ cells. Unfortunately, the expression of both Ci-VSP and Dr-VSP decreased the $I_{Ks}$ current prior to when activation of the respective VSP is thought to occur, which is detailed in Okamura *et al.* (2009) and here in Chapter 2. The extent to which the $I_{Ks}$ current was inhibited was more severe with Ci-VSP than Dr-VSP, and so Dr-VSP was then used for all further experiments.

The reason behind why the $I_{Ks}$ current is inhibited by overexpression of the VSPs (even before activation) could lie in the VSPs' mechanism of $PIP_2$ dephosphorylation. The VSPs may exist in a $PIP_2$-bound state at membrane potentials negative to those that activate the VSP, which could sequester $PIP_2$ and consequently reduce the available pool. Alternatively, there may be activation of these VSPs at more hyperpolarised potentials than previously reported. Falkenburger and colleagues (2010) suggested that the number of VSP molecules in the PM may far surpass the number of $PIP_2$ molecules, effectively causing rapid $PIP_2$ 'depletion' by binding $PIP_2$ before a full cycle of enzymatic activity.

*Rescue of $PIP_2$-depletion-induced $I_{Ks}$ inhibition with β1-AR activation*

To further probe whether the increase in $I_{Ks}$ current resulting from β1-AR activation involves $PIP_2$, the response of the $I_{Ks}$ current to CF-PIPK expression and ISO pre-incubation was assessed in the presence of $PIP_2$ depletion via Dr-VSP activation. Expression of CF-PIPK with LYN11-FRB (and hence an increase in the PM $PIP_2$ concentration) was able to overcome the $PIP_2$ loss brought about by activation of Dr-VSP.

If the PKA-dependent increase in $I_{Ks}$ requires the presence of $PIP_2$ in the PM, then perhaps activation of β1-AR with ISO would lead to minimal enhancement of the $I_{Ks}$ current when $PIP_2$ is depleted from the PM using Dr-VSP. On the other hand, if PKA phosphorylation of the $I_{Ks}$ channel leads to an increase in $PIP_2$ sensitivity or $PIP_2$ concentration, then the $I_{Ks}$ current density may increase compared to when expressing Dr-VSP alone. Indeed, the $I_{Ks}$ current density did increase in the setting of $PIP_2$ depletion. This could suggest that PKA-dependent increases in the $I_{Ks}$ current act through $PIP_2$. However, combined with the previous results showing differing effects on activation and deactivation kinetics, it is probable that $PIP_2$ is one of a number of signalling molecules involved in how the current is augmented.

If PKA-mediated phosphorylation of the channel enhanced the sensitivity or strength of interaction with $PIP_2$, then a depolarising shift in the inhibition caused by activation of Dr-VSP should be observed. From figure 67 it is evident that this did not change, and $V_{0.5}$ values were not significantly different (p=NS). This is in contrast to Rjasanow *et al*. (2015), who showed that KCNQ2/3 mutants that reduce $PIP_2$ binding alter the voltage at which Ci-VSP reduces the current (i.e. they shift the voltage at which inhibition occurs to more hyperpolarised potentials). Following the logic that a weaker channel-$PIP_2$ interaction had this effect, an increase in the channel-$PIP_2$ interaction would cause inhibition at membrane potentials that cause a greater $PIP_2$ depletion by the activation of Dr-VSP. On the other hand, signalling through the β1-AR may reduce the $I_{Ks}$ channel's need for $PIP_2$ to

function, and this would be expected to have the same effect on the Dr-VSP-induced inhibition described above.

Although the voltage at which the initial plateau or maximum current before inhibition (depending on the condition) was reached did not change, the effect on the current after that point was different between groups. Dr-VSP and Dr-VSP with CF-PIPK and LYN11-FRB caused an inhibition of the current after ~40 mV, although the current began to increase after 90 mV when CF-PIPK and LYN11-FRB were co-expressed. However, when cells were pre-incubated with ISO (100 nM) for 10 mins the current was not inhibited, but actually increased. The same effect was not seen for PTCD, where there was inhibition across all groups compared to control, but to a lesser extent when cells were pre-incubated with ISO (100 nM) for 10 mins. This effect could imply that physiologically, $G_q$-coupled GPCR activation is not effective at regulating the $I_{Ks}$ current through $PIP_2$ depletion during β1-AR signalling due to the channel requiring less $PIP_2$ in the PM to function. This, however, was not investigated during this project, but these results imply that β1-AR can largely override $PIP_2$-dependent regulation.

The mechanism behind how PKA-dependent phosphorylation of the channel leads to $I_{Ks}$ channel augmentation is still unknown. Liou and colleagues investigated whether PKA activates the ROMK1 channel through manipulation of $PIP_2$, and concluded that PKA does so by enhancing the channel's interaction with $PIP_2$ (Liou *et al*., 1999). Considering the results obtained in this chapter that are discussed above, it seems unlikely that $PIP_2$ is the only signalling molecule involved in the PKA-dependent augmentation of the $I_{Ks}$ current. However, activation of the β1-AR did manage to partially overcome $I_{Ks}$ inhibition caused by $PIP_2$ depletion arising from PJ expression, arguing that the relationship between the $I_{Ks}$ channel and $PIP_2$ is altered during this signalling event, suggesting that the $I_{Ks}$ channel could be regulated in a similar way to the ROMK1 channel.

The experiments I conducted in this chapter were different to those of Liou and colleagues – I performed $PIP_2$ depletion by dephosphorylation (Dr-VSP activation and PJ expression), and recorded the effect of β1-AR activation on the inhibition of the $I_{Ks}$ current caused by these $PIP_2$ depletion methods, which uses channel function as a surrogate marker for the interaction of the channel with $PIP_2$. On the other hand, Liou *et al*. (1999) directly studied phosphorylation of the $I_{Ks}$ channel and $PIP_2$ affinity of the channel using biochemical methods.

Given that β1-AR activation with ISO provided the channel with a means to overcome Dr-VSP-activation-induced inhibition, the ability of ISO pre-incubation to overcome PJ-induced inhibition was investigated. Despite ISO pre-incubation being unable to rescue the $I_{Ks}$ current to the level of control

cells, it did significantly hyperpolarise the $V_{0.5}$ value compared to control. This provides further evidence to suggest that β1-AR activation and the following PKA-dependent phosphorylation of the $I_{Ks}$ channel do not solely transduce the signal via manipulation of $PIP_2$.

Interestingly, β1-AR activation was able to partially recover the $I_{Ks}$ inhibition caused by overexpression of PJ with LYN11-FRB. This could suggest that $PIP_2$ is directly involved with $I_{Ks}$ enhancement here. However, it is important to note that when pre-incubating PJ-expressing cells with ISO (100 nM) the 2 minutes of intracellular dialysis that are routinely performed in WCPC experiments before recording were omitted. This reduced level of dialysis may have led to a higher initial CD. Therefore, in the future this experiment should be repeated to incorporate the 2 minutes of dialysis before recording so that a direct comparison can be made.

### 6.5 Conclusions and future directions

By manipulating the levels of $PIP_2$ in the PM using VSPs, the mechanism of $I_{Ks}$ enhancement upon β1-AR activation was investigated.

The $I_{Ks}$ channel is known to require $PIP_2$ for function (Loussouarn *et al*, 2003), and I have presented results in this chapter that show that an increase in the $PIP_2$ level in the PM (brought about by overexpression of a PIP 5-K in this instance) enhances the amplitude of the $I_{Ks}$ current whilst shifting the voltage-dependence of activation to more hyperpolarised potentials. Work by others has shown that activation of the β1-AR causes enhancement of the $I_{Ks}$ current (Kurokawa, *et al*., 2002; Matavel, *et al.,* 2010; Moline *et al*., 2014; Volders *et al*., 2003), and I demonstrated here that this enhancement is accompanied by a hyperpolarising shift in the voltage dependence of activation.

By comparing the effects of the PIP 5-K with the effects of β1-AR activation on the $I_{Ks}$ current, and by looking at how the current responded when $PIP_2$ was depleted by Dr-VSP activation, I concluded that the PKA-dependent alterations in the $I_{Ks}$ current do not solely act through a mechanism involving $PIP_2$. I have not obtained enough evidence to completely accept or reject the hypothesis that $PIP_2$ plays a role in the β1-mediated augmentation of the $I_{Ks}$ current, and have not elucidated the mechanism underlying augmentation of the $I_{Ks}$ current downstream of β1-AR activation. To elucidate whether any changes to the channel occur independent of PKA-dependent phosphorylation, PKA inhibitors could also be used.

To further investigate the roles of $PIP_2$ and β1-AR in the regulation of the $I_{Ks}$ channel, experiments mimicking those used in Liou *et al* (1999) could be performed, and experiments that follow β1-AR

activation with $G_q$-GPCR activation would provide valuable insights into the physiological reasons behind this regulation.

## CHAPTER 7: Discussion, conclusions and future directions

### 7.1 Discussion

The $I_{Ks}$ current constitutes part of the repolarisation reserve in the human myocardium, and whilst it does not play a major role at resting heart rates, this current becomes a crucial component of repolarisation in the setting of increased sympathetic tone and high heart rates (Jost *et al*., 2005; Silva & Rudy, 2005). The formation of the $I_{Ks}$ current requires the presence of the KCNE1 β-subunit (Barhanin *et al*., 1996; Sanguinetti *et al*., 1996), but also the minor membrane PI, $PIP_2$ (Loussouarn *et al.*, 2003; Zaydman *et al.*, 2013). Several studies helped to reach the conclusion that the $I_{Ks}$ channel requires $PIP_2$ for its function, and $PIP_2$ is believed to stabilise the open conformation of the channel. $PIP_2$ binding regions have been identified in different areas of the channel, but it has been asserted that $PIP_2$ interacts with the channel in a prime position to influence how KCNE1 affects the $I_{Ks}$ channel and how the channel converts voltage sensor movement to pore opening (Li *et al.,* 2011; Zaydman *et al*., 2013).

Mutations in the KCNQ1 or KCNE1 subunits can lead to LQTS (Dvir *et al*, 2014; Kapplinger *et al*., 2009), and different mechanisms – including trafficking and functional defects (Aizawa *et al*., 2004; Bianchi *et al*., 2000) – have been shown to be responsible for the decrease in $I_{Ks}$ current available during cardiac repolarisation. Previously in this laboratory, mutations within a PI binding region in the proximal C-terminus of KCNQ1 led to retention of the channel in the ER (unpublished data, Thomas *et al*., 2011).

This project aimed to investigate how $PIP_2$ is involved in the regulation of function and trafficking of the $I_{Ks}$ channel, in order to better understand the possible mechanisms underlying the generation of LQTS caused by mutations in KCNQ1. A summary of this project can be seen in figure 70, while the major findings of this project are summarised and discussed below.

*Sensitivity of the $I_{Ks}$ current to $PIP_2$ depletion*

Using the rapamycin-inducible dimerisation system to deplete $PIP_2$ from the PM in HEK-$I_{Ks}$ cells, it was immediately apparent that the $I_{Ks}$ channel requires $PIP_2$ for channel opening, as when $PIP_2$ was selectively depleted from the PM the $I_{Ks}$ current was inhibited. This supports the notion that $PIP_2$ stabilises the open state of the $I_{Ks}$ channel. In addition, I found that this channel is more sensitive to $PIP_2$ depletion than the hERG and Kir2.1 channels, both also present in the heart and involved in cardiac repolarisation. This supports data from Kruse *et al.* (2012), who used the rapamycin-inducible dimerisation system to investigate the $PIP_2$ sensitivity of a number of ion channels.

However, by comparing the effect of lipid-depleting construct expression on the $I_{Ks}$ current elicited in both WCPC and P-WCPC, it was clear that the cellular environment during patch-clamp recordings affected the amplitude of the $I_{Ks}$ current when the lipid-depleting constructs were expressed: WCPC recording of HEK-$I_{Ks}$ cells expressing PJ with LYN11-FRB led to a complete loss of $I_{Ks}$ current, whereas P-WCPC recording of HEK-$I_{Ks}$ cells expressing PJ with LYN11-FRB caused no change in the $I_{Ks}$ current when compared to control. The maintenance of the $I_{Ks}$ current in P-WCPC suggests that in a physiological environment, i.e. in the cardiac myocyte, the $I_{Ks}$ current may not be as sensitive to $PIP_2$ depletion as some *in vitro* studies may suggest (i.e. those performed in WCPC).

Given these results that were obtained in P-WCPC, the configuration of patch clamp that mimics a physiological environment closer than any other, it is of great interest now to decipher just how $PIP_2$ regulates the channel physiologically. In order to further investigate the physiological regulation of the $I_{Ks}$ channel by $PIP_2$ depletion, studies involving the activation of cardiac Gq-coupled GPCRs should be performed. The $I_{Ks}$ current in these studies should be recorded in P-WCPC to ensure the cell retains many of the intracellular cofactors required by the cell to undergo normal $PIP_2$ turnover, as the $I_{Ks}$ channel runs down with the gradual loss of $PIP_2$ from the PM (Matavel & Lopes, 2009).

*The effect of $PIP_2$ and/or PI4P depletion on $I_{Ks}$ channel trafficking*

I found that $PIP_2$ is not involved in $I_{Ks}$ channel anterograde trafficking to the PM, despite $PIP_2$ binding region mutations causing retention of the channel in the ER. This was demonstrated by using the rapamycin-induced dimerisation system in HEK cells expressing the VSV-E1-Q1 construct and visualising the expression of this construct at the PM or within the whole cell.

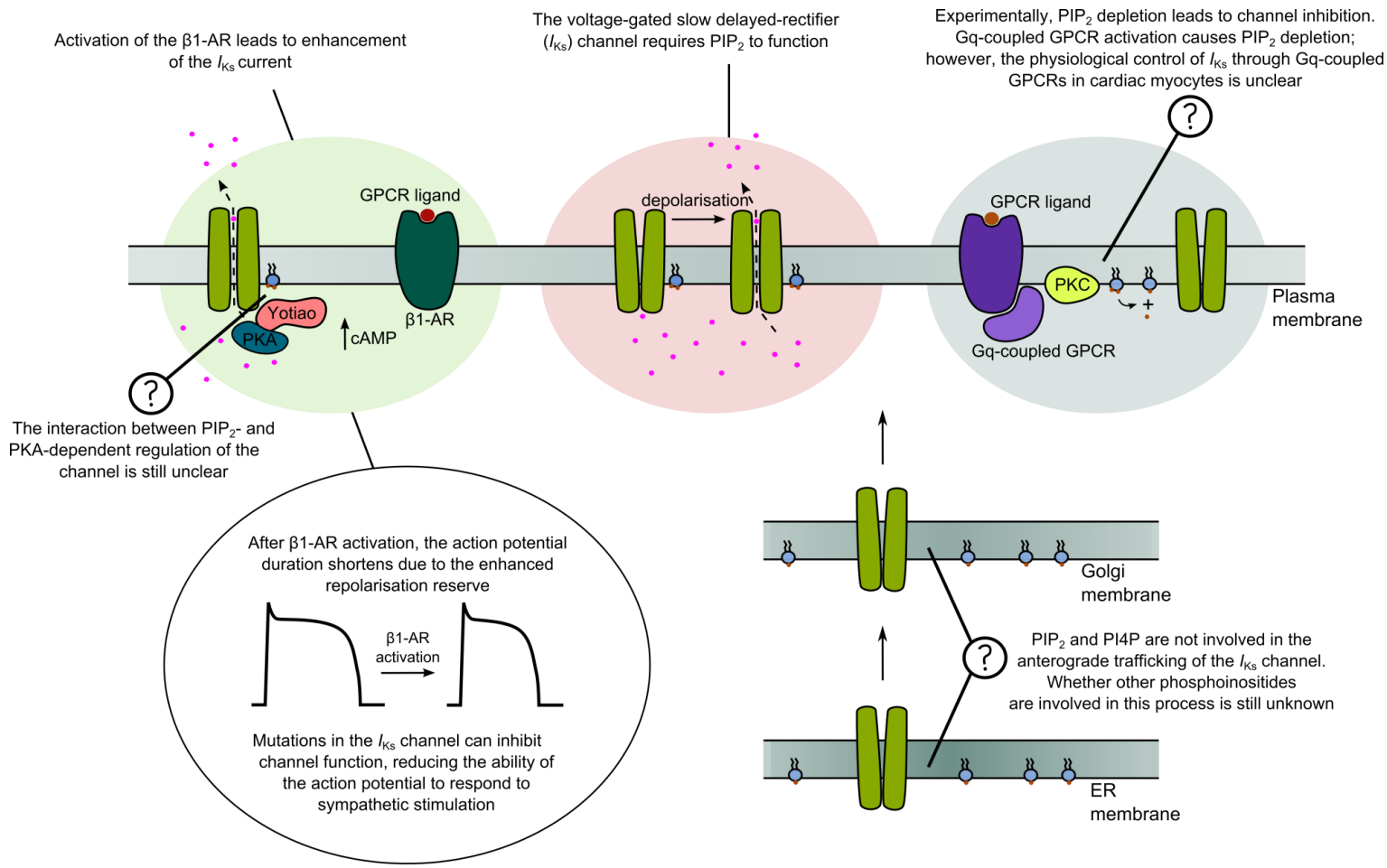


**Figure 70. A summary of the findings of this project.**

$PIP_2$ is not involved in anterograde trafficking of the $I_{Ks}$ channel, but may be involved in the $G_q$-coupled GPCR regulation and β1-AR regulation of the channel, although these findings require further investigation

.

This suggests that the $PIP_2$ binding-region mutations that were introduced into the proximal C terminus by Thomas and colleagues (2011; unpublished data), which I have since repeated, did not cause ER-retention of the channel through a reduced capacity to bind $PIP_2$. Rather, disrupted anterograde trafficking was more likely caused by KCNQ1 protein misfolding independent of effects on $PIP_2$ binding.

Thomas *et al*. (2011) found that the region that binds $PIP_2$ also binds a number of other PIs. It is possible that $PIP_2$ is required for activation of the channel, and other PIs are involved in regulating $I_{Ks}$ channel trafficking.

*Using the rapamycin-inducible dimerisation system*

Throughout this project, the rapamycin-inducible dimerisation system was used with the knowledge that it was not optimal for investigating the $I_{Ks}$ channel. However, it did selectively deplete PI4P and/or $PIP_2$. Even though in chapter 4 I tried to optimise the system by targeting the lipid-depleting constructs to intracellular organelles and mutating residues in the FRB domain to attempt to reduce potential FRB-FKBP interactions, I was not able to produce an improved system that would enable the lipid-depleting constructs to be expressed in cells also expressing the $I_{Ks}$ channel without affecting the functional properties of the $I_{Ks}$ channel.

Another inducible dimerisation system was developed by Miyamoto and colleagues (2012), using the plant hormone gibberellin to dimerise two proteins (which can be engineered to be tethered to phosphatase domains as in the FRB- and FKBP-containing constructs used throughout the project). In chapter 4 I tried to customise the components of the gibberellin-induced dimerisation system to incorporate the phosphatase domains used in the rapamycin-induced dimerisation system. Unfortunately, the cloned construct, PJ-GID1, did not recruit to the PM upon exposure of the cells to the dimerising agent, GA3-AM.

For further investigation into the role of $PIP_2$ in the regulation of the $I_{Ks}$ channel careful consideration should be given when using these dimerisation systems, as depletion of $PIP_2$ may occur and affect the channel's function before dimerisation of the recruitable domains during baseline recordings.

*The effect of β1-AR activation on the $I_{Ks}$ current*

Recent research has reported that the effects of $PIP_2$ and β1-AR-dependent augmentation of the $I_{Ks}$ channel to converge (Dvir *et al*., 2014), and PKA-dependent phosphorylation of the ROMK1 channel has been shown to act through $PIP_2$ (Liou *et al.,* 1999). However, evidence that this occurs with the $I_{Ks}$ channel has not yet been provided, nor has a mechanism been proposed. By activating the β1-AR

whilst manipulating the levels of $PIP_2$ in the PM, I began to probe how $PIP_2$ may or may not be involved in the adrenergic regulation of the $I_{Ks}$ channel. I could not provide definitive evidence to conclude that $PIP_2$ is or is not involved. However, the results presented in chapter 6 do provide preliminary data suggesting that $PIP_2$ may be involved, but the β1-AR-induced augmentation of the $I_{Ks}$ current does not solely rely on $PIP_2$ to convey this signal to the channel.

In addition to this, it appears that under adrenergic stimulation the $I_{Ks}$ channel may be less sensitive to $PIP_2$ depletion, which could provide evidence to suggest the β1-AR and $G_q$-coupled GPCR pathways of $I_{Ks}$ regulation interact. The overriding of $PIP_2$ regulation by β1-AR signalling may occur due to the channel's sensitivity to phosphorylation, which may be conserved in the P-WCPC configuration. In a state of increased adrenergic drive, which requires increased repolarisation reserve to counteract the increase in $Ca^{2+}$ current through the L-type $Ca^{2+}$ channel and contribute to the increased force of contraction, the $I_{Ks}$ current may become less sensitive to $PIP_2$ depletion (and hence closure) to increase the proportion of channels available for activation.

## 7.2 Conclusions

In conclusion, the results presented in the previous chapters confirm that $PIP_2$ in the PM is crucial for $I_{Ks}$ channel opening. $PIP_2$ is not, however, required for $I_{Ks}$ anterograde channel trafficking, but these experiments do not rule out a role for many other PIs in the regulation of this process. Regarding the physiological role of β1-AR-induced augmentation of the $I_{Ks}$ channel, my results suggest that $PIP_2$ could be in part involved in this process, but also that the channel may become less sensitive to $PIP_2$ depletion when under sympathetic stimulation, increasing the availability of the $I_{Ks}$ channel during periods which require a larger repolarisation current.

## 7.3 Future directions

### 7.3.1 Future direction of chapter 4

<u>An assay to investigate the role of $PIP_2$ in internalisation of the $I_{Ks}$ channel</u>

In chapter 4, I found that depleting $PIP_2$ and PI4P from the PM did not change the total or cell-surface expression of the VSV-E1-Q1 construct, which was investigated using the in- and on-cell western assays, respectively. The way this assay was performed, however, did not enable the investigation into whether the depletion of $PIP_2$ and PI4P at the PM affects the rate of channel internalisation.

*Mechanisms of endocytosis*

CME is one process by which ion channels can be internalised for recycling or degradation. The clathrin lattice that forms on the intracellular side of the PM recruits a number of clathrin-associated proteins, which promote membrane curvature and vesicle formation. One of these recruited proteins is the adaptor protein 2 (AP-2), which is crucial in the formation of CCVs. There is evidence to suggest that $PIP_2$ is crucial for recruitment of the AP-2 complex (Gaidarov & Keen, 1999). Further supporting this, the inositol 5-phosphatase synaptojanin, whose substrates are $PIP_2$ and $PIP_3$, was discovered due to its role in synaptic vesicle endocytosis (Cremona *et al*., 1999).

A number of TM proteins have been found to be internalised by CME, including RTKs (Goh & Sorkin, 2013) and Kir3.x channels (Nagi *et al*., 2015). Others, including the TGF-β type 1 receptor (Zhao *et al*., 2012), are internalised via a caveolin-dependent mechanism, and O'Kelly (2015) found that the two-pore domain $K^+$ channels can be internalised via clathrin-dependent or clathrin-independent mechanisms depending on the external cue. In addition, there are little-studied mechanisms of endocytosis, such as the clathrin- and calveolin-independent pathway utilised by the interleukin-2 receptor (Basquin *et al*., 2015).

*Assay design*

In order to enable quantification of the rate of internalisation, a similar assay to that used in chapter 4 would be used. In this internalisation assay, cells expressing VSV-E1-Q1 with lipid-depleting constructs and LYN11-FRB would be incubated with primary Ab (α-VSV) at 4°C for 1 hour, and then incubated at 37°C for either 2, 5, 10, 20 or 30 minutes. For each time point, all experimental conditions would be performed in 2 plates: one for the in-cell western and one for the on-cell western. After incubation at 37°C, the cells would be washed and the secondary Ab would be added, then the assay would proceed as described in chapter 4. By assessing the VSV-E1-Q1 expression at a number of time points, internalisation of the labelled VSV-E1-Q1 can be followed.

If VSV-E1-Q1 is internalised via CME, I predict that internalisation would occur in control and PJ-DEAD-expressing cells, but not in cells where $PIP_2$ and PI4P depletion occurred. If this process is not CME-dependent, however, I would not expect the rate of internalisation to differ between control cells and cells in which $PIP_2$ had been depleted.

### 7.3.2 Future direction of chapter 6

Using Gq-coupled GPCR activation to investigate the physiological role of $PIP_2$ depletion in regulation of the $I_{Ks}$ channel

In this project I have used the rapamycin-induced dimerisation system to induce $PIP_2$ and/or PI4P depletion upon addition of rapamycin, used VSPs to deplete $PIP_2$ through activation of the phosphatase domain, and applied WTM to cells to deplete $PIP_2$ via inhibition of PI4K activity. Whilst these methods are helpful in pushing $PIP_2$ depletion as far as possible and investigating the role of $PIP_2$ in $I_{Ks}$ regulation without other interfering cellular processes (with the exception of WTM exposure), these systems are not physiological.

To complement the experiments performed with these non-physiological methods, I would express different $G_q$-coupled GPCRs in HEK-$I_{Ks}$ cells and activate the receptors by applying their respective agonists. Experiments would be performed in P-WCPC to enable recording of the $I_{Ks}$ current over multiple subsequent IV protocols without risk of current run down, so that observation of the effect of receptor activation would be possible.

PLC is activated upon activation of $G_q$-coupled GPCRs, which causes hydrolysis of $PIP_2$ at the PM, resulting in its depletion and the concomitant production of $IP_3$ and DAG. This release of second messengers was purposefully avoided in the rapamycin-induced depletion system and when using VSPs because the effect of solely depleting $PIP_2$ was under question. Taking into consideration the results obtained in chapter 5, where the use of P-WCPC prevented the inhibition of $I_{Ks}$ current that was previously seen in WCPC when expressing the same lipid-depleting constructs, the physiological environment evidently plays a huge role in the *in vitro* response of the $I_{Ks}$ channel. Maintaining a cellular environment that is as close to physiological as possible will greatly benefit the understanding of how $PIP_2$ regulates the $I_{Ks}$ channel.

The $G_q$-GPCRs that would be used in these experiments are the AT1, ET1 and α1-AR, as these are present in cardiac myocytes and can therefore provide valuable information on how the $I_{Ks}$ channel is regulated in the heart. This work could be extended to investigate how LQTS-associated mutations affect the channel's response to β1-AR and $G_q$-coupled GPCR activation, separately and together (as described previously in this section).

## References


Abe, N., Inoue, T., Galvez, T., Klein, L., & Meyer, T. (2008). Dissecting the role of PtdIns(4,5)P2 in endocytosis and recycling of the transferrin receptor. *Journal of Cell Science,* 121(Pt 9), 1488–1494

Agilent Technologies Inc. (2015). PfuUltra High-Fidelity DNA Polymeras Instruction Manual. Accessed at: http://www.agilent.com/cs/library/usermanuals/public/600380.pdf

Aizawa, Y., Ueda, K., Wu, L. M., Inagaki, N., Hayashi, T., Takahashi, M., Ohta, M., Kawano, S., Hirano, Y., Yasunami, M., Aizawa, Y., Kimura, A. & Hiraoka, M. (2004). Truncated KCNQ1 mutant, A178fs/105, forms hetero-multimer channel with wild-type causing a dominant-negative suppression due to trafficking defect. *FEBBS Letters*, 574 (1–3) 145–150

Alaimo, A., Gómez-Posada, J. C., Aivar, P., Etxeberría, A., Rodriguez-Alfaro, J. A., Areso, P. & Villarroel, A. (2009). Calmodulin activation limits the rate of KCNQ2 K+ channel exit from the endoplasmic reticulum, *The Journal of Biological Chemistry*, 284 (31) 20668–20675

Amoasii, L., Hnia, K., Chicanne, G., Brech, A., Cowling, B. S., Müller, M. M., Schwab, Y., Koebel, P., Ferry, A., Payrastre, B. & Laporte, J. (2013). Myotubularin and PtdIns3P remodel the sarcoplasmic reticulum in muscle in vivo. *Journal of Cell Science*, 126 (Pt 8) 1806–1819

Anderson, C. L., Delisle, B. P., Anson, B. D., Kilby, J. A., Will, M. L., Tester, D. J., Gong, Q., Zhou, Z., Ackerman, M. J. & January, C. T. (2006). Most LQT2 mutations reduce Kv11.1 (hERG) current by a class 2 (trafficking-deficient) mechanism. *Circulation*, 113 (3) 365–373

Anderson, C. L., Kuzmicki, C. E., Childs, R. R., Hintz, C. J., Delisle, B. P. & January, C. T. (2014). Large-scale mutational analysis of Kv11.1 reveals molecular insights into type 2 long QT syndrome. *Nature Communications*, 5; 5535

Angelo, K., Jespersen, T., Grunnet, M., Nielsen, M. S., Klaerke, D. A. & Olesen, S. P. (2002). KCNE5 induces time- and voltage-dependent modulation of the KCNQ1 current. *Biophysical Journal*, 83 (4) 1997–2006

Antzelevitch, C. (2005) Role of transmural dispersion of repolarization in the genesis of drug-induced torsades de pointes. *Heart Rhythm,* 2 (2 Suppl) S9–15

Antzelevitch, C. (2007). Ionic, molecular, and cellular bases of QT-interval prolongation and torsade de pointes. *Europace : European Pacing, Arrhythmias, and Cardiac Electrophysiology : Journal of the Working Groups on Cardiac Pacing, Arrhythmias, and Cardiac Cellular Electrophysiology of the European Society of Cardiology*, 9 (Suppl 4) iv4–i15

Arcaro, A., Volinia, S., Zvelebil, M. J., Stein, R., Watton, S. J., Layton, M. J., Gout, I., Ahmadi, K., Downward, J. & Waterfield, M. D. (1998). Human phosphoinositide 3-kinase C2beta, the role of calcium and the C2 domain in enzyme activity. *The Journal of Biological Chemistry*, 273 (49) 33082–33090

Aromolaran, A. S., Subramanyam, P., Chang, D. D., Kobertz, W. R., & Colecraft, H. M. (2014). LQT1 mutations in KCNQ1 C-terminus assembly domain suppress $I_{Ks}$ using different mechanisms. *Cardiovascular Research*, 104 (3) 501–511

Audhya, A., Foti, M. & Emr, S. D. (2000). Distinct roles for the yeast phosphatidylinositol 4-kinases, Stt4p and Pik1p, in secretion, cell growth, and organelle membrane dynamics. *Molecular Biology of the Cell*, 11 (8( 2673–2689

Aziz, Q., Thomas, A. M., Khambra, T. & Tinker, A. (2012). Regulation of the ATP-sensitive potassium channel subunit, Kir6.2, by a $Ca^{2+}$-dependent protein kinase C, *The Journal of Biological Chemistry,* 287 (9) 6196–6207

Backer, J. M. (2008). The regulation and function of Class III PI3Ks: novel roles for Vps34. *The Biochemical Journal*, 410 (1) 1–17

Bai, C. X., Namekata, I., Kurokawa, J., Tanaka, H., Shigenobu, K. & Furukawa, T. (2005) Role of nitric oxide in $Ca^{2+}$ sensitivity of the slowly activating delayed rectifier $K^+$ current in cardiac myocytes. *Circulation Research,* 96 (1) 64–72

Balla, T. (2013). Phosphoinositides: Tiny Lipids With Giant Impact on Cell Regulation, *Physiological Reviews*, 93 (3) 1019–1137

Balla, A., Tuymetova, G., Barshishat, M., Geiszt, M. & Balla, T. (2002). Characterization of type II phosphatidylinositol 4-kinase isoforms reveals association of the enzymes with endosomal vesicular compartments. *The Journal of Biological Chemistry*, 277(22) 20041–20050

Balla, A., Tuymetova, G., Tsiomenko, A., Várnai, P. & Balla, T. (2005). A plasma membrane pool of phosphatidylinositol 4-phosphate is generated by phosphatidylinositol 4-kinase type-III alpha: studies with the PH domains of the oxysterol binding protein and FAPP1. *Molecular Biology of the Cell*, 16 (3) 1282–1295

Ballou, L. M., & Lin, R. Z. (2008). Rapamycin and mTOR kinase inhibitors. *The Journal of Chemical Biology,* 1 (1-4) 27–36

Banaszynski, L. A., Liu, C. W. & Wandless, T. J. (2005) Characterization of the FKBP.rapamycin.FRB ternary complex. *Journal of the American Chemical Society,* 127 (13) 4715–4721

Barbour, B. (2011). Electronics for electrophysiologists. from http://www.biologie.ens.fr/~barbour/

Barhanin, J., Lesage, F., Guillemare, E., Fink, M., Lazdunski, M. & Romey, G. (1996) K(V)LQT1 and lsK (minK) proteins associate to form the I(Ks) cardiac potassium current. *Nature*, 384 (6604) 78–80

Barik, S. (2006). Imunophilins: for the love of proteins. *Cellular and Molecular Life Sciences*, 63 (24) 2889–2900

Baroudi, G., Acharfi, S., Larouche, C. & Chahine, M. (2002) Expression and intracellular localization of an SCN5A double mutant R1232W/T1620M implicated in Brugada syndrome. *Circulation Research*, 90 (1) E11–16

Barro-Soria, R., Rebolledo, S., Liin, S. I., Perez, M. E., Sampson, K. J., Kass, R. S., & Larsson, H. P. (2014). KCNE1 divides the voltage sensor movement in KCNQ1/KCNE1 channels into two steps. *Nature Communications,* 5, 3750

Bartos, D. C., Grandi, E. & Ripplinger, C. M. (2015). Ion Channels in the Heart. *Comprehensive Physiology,* 5 (3) 1423–1464

Basquin, C., Trichet, M., Vihinen, H., Malardé, V., Lagache, T., Ripoll, L., Jokitalo, E., Olivo-Marin, J. C. Gautreau, A. & Sauvonnet, N. (2015). Membrane protrusion powers clathrin-independent endocytosis of interleukin-2 receptor, *The EMBO Journal,* 34 (16) 2147–2161

Bastidas, R. J., Shertz, C. A., Lee, S. C., Heitman, J. & Cardenas, M. E. (2012). Rapamycin exerts antifungal activity in vitro and in vivo against Mucor circinelloides via FKBP12-dependent inhibition of Tor. *Eukaryotic Cell*, 11 (3) 270–281

Behere, S. P. & Weindling, S. N. (2015). Pause induced early afterdepolarizations in the long QT syndrome: a simulation study. *Annals of Pediatric Cardiology*, 8 (3) 210–220

Behnia, R. & Munro, S. (2011). Organelle identity and the signposts for membrane traffic. *Nature*, 438 (7068) 597–604

Bellin, M., Casini, S., Davis, R. P., D'Aniello, C., Haas, J., Ward-van Oostwaard, D., Tertoolen, L. G., Jung, C. B., Elliott, D. A., Welling, A., Laugwitz, K. L., Moretti, A. & Mummery, C. L. (2013). Isogenic human pluripotent stem cell pairs reveal the role of a KCNH2 mutation in long-QT syndrome. *EMBO Journal*, 32 (24) 3161–3175

Bender, K., Wellner-Kienitz, M. C. & Pott, L. (2002). Transfection of a phosphatidyl-4-phosphate 5-kinase gene into rat atrial myocytes removes inhibition of GIRK current by endothelin and alpha-adrenergic agonists. *FEBBS Letters,* 529 (2–3) 356–360

Bennett, P. B., Yazawa, K., Makita, N. & George, A. L. Jr. (1995). Molecular mechanism for an inherited cardiac arrhythmia. *Nature,* 376 (6542) 683–685

Bers, D. M. (2002). Cardiac excitation-contraction coupling. *Nature Insight*, 415, 198–205

Berstein, G., Blank, J. L., Jhon, D-Y., Exton, J. H., Rhee, S. G. & Ross, E. M. (1992) Phospholipase C-β1 is a GTPase-activating protein for $G_{q/11}$, its physiologic regulator. *Cell,* 70, 411–18

Béthune, J., Wieland, F. & Moelleken, J. (2006). COPI-mediated transport. *The Journal of Membrane Biology*, 211 (2) 65–79

Bezanilla, F. (2000). The voltage sensor in voltage-dependent ion channels. *Physiological Reviews,* 80 (2) 555–592

Bianchi, L., Priori, S. G., Napolitano, C., Surewicz, K. A., Dennis, A. T., Memmi, M., Schwartz, P. J. & Brown, A. M. (2000). Mechanisms of I(Ks) suppression in LQT1 mutants. *American Journal of Physiology*. *Heart and Circulatory Physiology,* 279 (6) H3003–3011

Bichet, D., Haass, F. A. & Jan, L. Y. (2003). Merging functional studies with structures of inward-rectifier K(+) channels. *Nature Reviews Neuroscience*, 4 (12) 957–967

Bocksteins, E., Labro, A. J., Snyders, D. J., & Mohapatra, D. P. (2012). The electrically silent Kv6.4 subunit confers hyperpolarized gating charge movement in Kv2.1/Kv6.4 heterotetrameric channels. *PLoS One,* 7 (5) e37143

Bojjireddy, N., Botyanszki, J., Hammond, G., Creech, D., Peterson, R., Kemp, D. C., Snead, M., Brown, R., Morrison, A., Wilson, S., Harrison, S., Moore, C. & Balla, T. (2014). Pharmacological and genetic targeting of the PI4KA enzyme reveals its important role in maintaining plasma membrane phosphatidylinositol 4-phosphate and phosphatidylinositol 4,5-bisphosphate levels. *The Journal of Biological Chemistry*, 289 (9) 6120–6132

Bos, K., Wraight, C. & Stanley, K. K. (1993). TGN38 is maintained in the trans-Golgi network by a tyrosine-containing motif in the cytoplasmic domain. *The EMBO Journal*, 12 (5) 2219–2228

Boulet, I. R., Raes, A. L., Ottschytsch, N. & Snyders, D. J. (2006). Functional effects of a KCNQ1 mutation associated with the long QT syndrome. *Cardiovascular Research*, 70 (3) 466–474

Bristow, M. R. (2000). beta-adrenergic receptor blockade in chronic heart failure. *Circulation*, 101 (5) 558–569

Brown, D. A., Hughes, S. A., Marsh, S. J., & Tinker, A. (2007). Regulation of M(Kv7.2/7.3) channels in neurons by PIP(2) and products of PIP(2) hydrolysis: significance for receptor-mediated inhibition. *The Journal of Physiology,* 582 (Pt 3) 917–925

Brown, D. A., & Passmore, G. M. (2009). Neural KCNQ (Kv7) channels. *British Journal of Pharmacology*, 156 (8) 1185–1195

Brownfield, J. & Herbert, M. (2008). EKG Criteria for Fibrinolysis: What's Up with the J Point? *Western Journal of Emergency Medicine*, 9 (1) 40–42

Burashnikov, A. & Antzelevitch, C. (2000). Block of I(Ks) does not induce early afterdepolarization activity but promotes beta-adrenergic agonist-induced delayed afterdepolarization activity. *Journal of Cardiovascular Electrophysiology*, 11 (4) 458–465

Burgess, D. E., Bartos, D. C., Reloj, A. R., Campbell, K. S., Johnson, J. N., Tester, D. J., Ackerman, M. J., Fressart, V., Denjoy, I., Guicheney, P., Moss, A. J., Ohno, S., Horie, M. & Delisle, B. P. (2012). High-risk long QT syndrome mutations in the Kv7.1 (KCNQ1) pore disrupt the molecular basis for rapid K(+) permeation. *Biochemistry*, 51 (45) 9076–9085

Cabantous, S., Nguyen, H. B., Pedelacq, J.-D., Koraïchi, F., Chaudhary, A., Ganguly, K., Lockard, M. A., Favre, G., Terwilliger, T. C. & Waldo, G. S. (2013). A New Protein-Protein Interaction Sensor Based on Tripartite Split-GFP Association. *Scientific Reports*, *3*;2854

Calvillo, L., Spazzolini, C., Vullo, E., Insolia, R., Crotti, L. & Schwartz, P. J. (2014). Propranolol prevents life-threatening arrhythmias in LQT3 transgenic mice: implications for the clinical management of LQT3 patients. *Heart Rhythm*, 11(1) 126–132

Campa, F., Yoon, H.-Y., Ha, V. L., Szentpetery, Z., Balla, T. & Randazzo, P. A. (2009). A PH Domain in the Arf GTPase-activating Protein (GAP) ARAP1 Binds Phosphatidylinositol 3,4,5-Trisphosphate and Regulates Arf GAP Activity Independently of Recruitment to the Plasma Membranes. *The Journal of Biological Chemistry*, *284* (41) 28069–28083

Campbell, R. E., Tour, O., Palmer, A. E., Steinbach, P. A., Baird, G. S., Zacharias, D. A., & Tsien, R. Y. (2002). A monomeric red fluorescent protein. *Proceedings of the National Academy of Sciences of the United States of America 99* (12) 7877–7882

Carmeliet, E. (2006) Repolarization reserve in cardiac cells. *Journal of Medical and Biological Engineering*, 26 (3) 97–105

Charman, W. N. (1998). Imaging in the 21st century. *Ophthalmic and Physiological Optics, 18* (2) 210–223

Chen, H., Kim, L. A., Rajan, S., Xu, S., & Goldstein, S. A. (2003). Charybdotoxin binding in the I(Ks) pore demonstrates two MinK subunits in each channel complex. *Neuron,* 40 (1) 15–23

Chen, J., Zou, A., Splawski, I., Keating, M. T. & Sanguinetti, M. C. (1999). Long QT syndrome-associated mutations in the Per-Arnt-Sim (PAS) domain of HERG potassium channels accelerate channel deactivation. *The Journal of Biological Chemistry*, 274 (15) 10113–10118

Cheng, S. H., Gregory, R. J., Marshall, J., Paul, S., Souza, D. W., White, G. A., O'Riordan, C. R. & Smith, A. E. (1990) Defective intracellular transport and processing of CFTR is the molecular basis of most cystic fibrosis. *Cell,* 63 (4) 827–834

Choi, J., Chen, J., Schreiber, S. L., & Clardy, J. (1996). Structure of the FKBP12-rapamycin complex interacting with the binding domain of human FRAP. *Science,* 273(5272) 239–242

Choi, S., Thapa, N., Tan, X., Hedman, A. C. & Anderson, R. A. (2015). PIP kinases define PI4,5$P_2$signaling specificity by association with effectors. *Biochimica et Biophysica Acta*, 1851 (6) 711–723

Ciampa, E. J., Welch, R. C., Vanoye, C. G. & George, A. L. (2011). KCNE4 Juxtamembrane Region Is Required for Interaction with Calmodulin and for Functional Suppression of KCNQ1. *The Journal of Biological Chemistry*, 286 (6) 4141–4149

Chouabe, C., Neyroud, N., Richard, P., Denjoy, I., Hainque, B., Romey, G., Drici, M. D., Guicheney, P., & Barhanin, J. (2000). Novel mutations in KvLQT1 that affect $I_{Ks}$ activation through interactions with Isk. *Cardiovascular Research*, 45 (4) 971–980

Cody, C. W., Prasher, D. C., Westler, W. M., Prendergast, F. G. & Ward W. W. (1993). Chemical structure of the hexapeptide chromophore of the Aequorea green-fluorescent protein. *Biochemistry*, 32 (5) 1212–1218

Cohn, J. N. & Tognoni, G. (2001). A randomized trial of the angiotensin-receptor blocker valsartan in chronic heart failure. *The New England Journal of Medicine*, 354 (23) 1667–1675

Colilla, S., Crow, A., Petkun, W., Singer, D. E., Simon, T. & Liu, X. (2013). Estimates of current and future incidence and prevalence of atrial fibrillation in the U.S. adult population. *American Journal of Cardiology*, 112 (8) 1142–1147

Compton, S. J., Lux, R. L., Ramsey, M. R., Strelich, K. R., Sanguinetti, M. C., Green, L. S., Keating, M. T. & Mason, J. W. (1996). Genetically defined therapy of inherited long-QT syndrome. Correction of abnormal repolarization by potassium. *Circulation*, 94 (5) 1018–1022

Conti, E. & Kuriyan, J. (2000). Crystallographic analysis of the specific yet versatile recognition of distinct nuclear localization signals by karyopherin alpha. *Structure*, 8 (3) 329–338

Cremona, O., Di Paolo, G., Wenk, M. R., Lüthi, A., Kim, W. T., Takei, K., Daniell, L., Nemoto, Y., Shears, S. B., Flavell, R. A., McCormick, D. A. & De Camilli, P. (1999). Essential role of phosphoinositide metabolism in synaptic vesicle recycling. *Cell*, 99 (2) 179–188

Cui, J., Melman, Y., Palma, E., Fishman, G. I. & McDonald, T. V. (2000). Cyclic AMP regulates the HERG K(+) channel by dual pathways. *Current Biology*, 10 (11) 671–674

Cutler, M. J., Jeyaraj, D. & Rosenbaum, D. S. (2011). Cardiac electrical remodeling in health and disease. *Trends in Pharmacological Sciences*, 32 (3) 174–180

Cutting, G. R. (2015) Cystic fibrosis genetics: from molecular understanding to clinical application. *Nature Reviews Genetics*, 16 (1) 45–56

Czech, M. C. (2000). PIP2 and PIP3: Complex Roles at the Cell Surface. *Cell*, 100 (6) 603–606

Dahimène, S., Alcoléa, S., Naud, P., Jourdon, P., Escande, D., Brasseur, R., Thomas, A., Baró, I. & Mérot, J. (2006). The N-terminal juxtamembranous domain of KCNQ1 is critical for channel surface expression: implications in the Romano-Ward LQT1 syndrome. *Circulation Research,* 99 (10) 1076–1083

Daleau, P. & Turgeon, J. (1994). Angiotensin II modulates the delayed rectifier potassium current of guinea pig ventricular myocytes. *Pflugers Archiv: European Journal of Physiology*, 427 (5-6) 553–555

Danna, K. & Nathans, D. (1971). Specific Cleavage of Simian Virus 40 DNA by Restriction Endonuclease of Hemophilus Influenzae. P*roceedings of the National Academy of Sciences of the United States of America,* 68 (12) 2913–2917

Dascher, C. & Balch, W. E. (1994). Dominant inhibitory mutatnts of ARF1 block endoplasmic reticulum to Golgi transport and trigger disassembly of the Golgi apparatus, *The Journal of Biological Chemistry* 269 (2) 1437–1448

Davare, M. A., Avdonin, V., Hall, D. D., Peden, E. M., Burette, A., Weinberg, R. J., Horne, M. C., Hoshi, T. & Hell, J. W. (2001). A beta2 adrenergic receptor signaling complex assembled with the Ca2+ channel Cav1.2. *Science*, 293 (5527) 98–101

Day, R. N., & Davidson, M. W. (2012). Fluorescent proteins for FRET microscopy: monitoring protein interactions in living cells. *Bioessays, 34* (5) 341–350

De Graaf, P., Zwart, W. T., van Dijken, R. A., Deneka, M., Schulz, T. K., Geijsen, N., Coffer, P. J., Gadella, B. M., Verkleij, A. J., van der Sluijs, P. & van Bergen en Henegouwen, P. M. (2004) Phosphatidylinositol 4-kinasebeta is critical for functional association of rab11 with the Golgi complex. *Molecular Biology of the Cell*, 15 (4) 2038–2047

Debonneville, C., Flores, S. Y., Kamynina, E., Plant, P. J., Tauxe, C., Thomas, M. A., Münster, C., Chraïbi, A., Pratt, J. H., Horisberger, J. D., Pearce, D., Loffing, J., & Staub, O. (2001). Phosphorylation of Nedd4-2 by Sgk1 regulates epithelial Na(+) channel cell surface expression. *The EMBO Journal*, 20 (24) 7052–7059

Delisle, B. P., Underkofler, H. A., Moungey, B. M., Slind, J. K., Kilby, J. A., Best, J. M., Foell, J. D., Balijepalli, R. C., Kamp, T. J. & January, C. T. (2009). Small GTPase determinants for the Golgi processing and plasmalemmal expression of human ether-a-go-go related (hERG) K+ channels. *The Journal of Biological Chemistry*, 284 (5) 2844–2853

DeRose, R., Miyamoto, T. & Inoue, T. (2013). Manipulating signaling at will: chemically-inducible zation (CID) techniques resolve problems in cell biology. *Pflugers Archiv: European Journal of Physiology*, 465 (3) 409–417

Dhein, S., Seidel, T., Salameh, A., Jozwiak, J., Hagen, A., Kostelka, M., Hindricks, G., Mohr, F. W. (2014) Remodeling of cardiac passive electrical properties and susceptibility to ventricular and atrial arrhythmias. F*rontiers in Physiology*, 5 (424) e-collection.

Di Paolo, G. & De Camilli, P. (2006). Phosphoinositides in cell regulation and membrane dynamics, *Nature*, 443 (7112) 651–657

Dickson, E. J., Jensen, J. B. & Hille, B. (2014) Golgi and plasma membrane pools of PI(4)P contribute to plasma membrane PI(4,5)$P_2$ and maintenance of KCNQ2/3 ion channel current. *Proceedings of the National Academy of Sciences of the United States of America*, 111 (22) E2281–2290

Digby, G. C., Pérez Riera, A. R., Barbosa Barros, R., Simpson, C. S., Redfearn, D. P., Methot, M., Femenía, F. & Baranchuk, A. (2011). Acquired long QT interval: a case series of multifactorial QT prolongation. *Clinical Cardiology*, 34 (9) 577–582

Domin, J., Pages, F., Volinia, S., Rittenhouse, S. E., Zvelebil, M. J., Stein, R. C. & Waterfield, M. D. (1997). Cloning of a human phosphoinositide 3-kinase with a C2 domain that displays reduced sensitivity to the inhibitor wortmannin. *Biochemical Journal*, 326 (Pt 1) 139–147

Donger, C., Denjoy, I., Berthet, M., Neyroud, N., Cruaud, C., Bennaceur, M., Chivoret, G., Schwartz, K., Coumel, P. & Guicheney, P. (1997). KVLQT1 C-terminal missense mutation causes a forme fruste long-QT syndrome. *Circulation, 96* (9) 2778–2781

Doyle, D. A. (1998). The structure of the potassium channel: Molecular Basis of K+ Conduction and Selectivity. *Science,* 280 (5360) 69–77

Drew, B. J., Ackerman, M. J., Funk, M., Gibler, W. B., Kligfield, P., Menon, V., Philippides, G. J., Roden, D. M. & Zareba W. (2010). Prevention of Torsade de Pointes in Hospital Settings: A Scientific Statement From the American Heart Association and the American College of Cardiology FoundationEndorsed by the American Association of Critical-Care Nurses and the International Society for Computerized Electrocardiology. *Circulation*, 121 (8) 1047–1060

Dufy, B., MacDermott, A. & Barker, J. L. (1986). Rundown of GH3 cell K+ conductance response to TRH following patch recording can be obviated with GH3 cell extract. *Biochemical and Biophysical Research and Communications*, 137 (1) 388–396

Dvir, M., Strulovich, R., Sachyani, D., Ben-Tal Cohen, I., Haitin, Y., Dessauer, C., Pongs, O., Kass, R., Hirsch, J. A. & Attali, B. (2014). **L**ong QT mutations at the interface between KCNQ1 helix C and KCNE1 disrupt I(KS) regulation by PKA and $PIP_2$. *Journal of Cell Science*, 127 (Pt 18) 3943–3955

Eberhard, D. A., Cooper, C. L., Low, M. G. & Holz, R. W. (1990) Evidence that the inositol phospholipids are necessary for exocytosis. Loss of inositol phospholipids and inhibition of secretion in permeabilized cells caused by a bacterial phospholipase C and removal of ATP. *Biochemical Journal*, 268;15–25

Eckardt, N. A. (2007). GA Signaling: Direct Targets of DELLA Proteins. *The Plant Cell*, 19 (10) 2970

Eckey, K., Wrobel, E., Strutz-Seebohm, N., Pott, L., Schmitt, N. & Seebohm, G. (2014). Novel Kv7.1-phosphatidylinositol 4,5-bisphosphate interaction sites uncovered by charge neutralization scanning. *The Journal of Biological Chemistry,* 289 (33) 22749–22758

Edwards, S. R. & Wandless, T. J. (2007). The rapamycin-binding domain of the protein kinase mammalian target of rapamycin is a destabilizing domain. *The Journal of Biological Chemistry*, 282 (18) 13395–13401

Efstratiadis, G., Sarigianni, M. & Gougourelas, I. (2006). Hypomagnesemia and cardiovascular system. *Hippokratia*, 10 (4) 147–152

Eldar, M., Griffin, J. C., Abbott, J. A., Benditt, D., Bhandari, A., Herre, J. M., Benson, D. W. & Scheinman, M. M. (1987). Permanent cardiac pacing in patients with the long QT syndrome. *Journal of the American College of Cardiology*, 10 (3) 600–607

Eldstrom, J., Xu, H., Werry, D., Kang, C., Loewen, M. E., Degenhardt, A., Sanatani, S., Tibbits, G. F., Sanders, C. & Fedida, D. (2010). *The Journal of General Physiology,* 135 (5) 433-438

Enyedi, P., & Czirják, G. (2010). Molecular background of leak K+ currents: two-pore domain potassium channels. *Physiological Reviews*, 90 (2), 559–605

Falasca, M. & Maffucci, T. (2012). Regulation and cellular functions of class II phosphoinositide 3-kinases. *The Biochemical Journal,* 443 (3) 587–601

Falkenburger, B. H., Jensen, J. B. & Hille, B. (2010). Kinetics of PIP2 metabolism and KCNQ2/3 channel regulation studied with a voltage-sensitive phosphatase in living cells. *Journal of General Physiology,* 135 (2) 99–114

Fan, Z. & Makielski, J. C. (1997). Anionic phospholipids activate ATP-sensitive potassium channels. *The Journal of Biological Chemistry,* 272 (9) 5388–5395

Fernandez, D., Ghanta, A., Kauffman, G. W. & Sanguinetti, M. C. (2003). Physicochemical features of the HERG channel drug binding site. *The Journal of Biological Chemistry*, 279 (11) 10120–10127

Ferrer, T., Rupp, J., Piper, D. R., & Tristani-Firouzi, M. (2006). The S4-S5 linker directly couples voltage sensor movement to the activation gate in the human ether-a'-go-go-related gene (hERG) K+ channel. *The Journal of Biological Chemistry,* 281 (18) 12858–12864

Fili, N., Calleja, V., Woscholski, R., Parker, P. J. & Larijani, B. (2006). Compartmental signal modulation: Endosomal phosphatidylinositol 3-phosphate controls endosome morphology and selective cargo sorting. *Proceedings of the National Academy of Sciences of the United States of America,* 103 (42) 15473–15478

Flanagan, C. A. & Thorner, J. (1992) Purification and characterization of a soluble phosphatidylinositol 4-kinase from the yeast Saccharomyces cerevisiae. *The Journal of Biological Chemistry*, 267 (33) 24117–24125

Franqueza, L., Lin, M., Shen, J., Splawski, I., Keating, M. T. & Sanguinetti, M. C. (1999). Long QT syndrome-associated mutations in the S4-S5 linker of KvLQT1 potassium channels modify gating and interaction with minK subunits. *The Journal of Biological Chemistry*, 274 (30) 21063–21070

Fredriksson, R., Lagerström, M. C., Lundin, L. G. & Schiöth, H. B. (2003). The G-protein-coupled receptors in the human genome form five main families. Phylogenetic analysis, paralogon groups, and fingerprints. *Molecular Pharmacology*, 63 (6) 1256–1272

Gaidarov, I. & Keen, J. H. (1999). Phosphoinositide-AP-2 interactions required for targeting to plasma membrane clathrin-coated pits. *The Journal of Cell Biology*, 146 (4) 755–764

Garcia, P., Gupta, R., Shah, S., Morris, A. J., Rudge, S. A., Scarlata, S., Petrova, V., McLaughlin, S. & Rebecchi, M. J. (1995). The pleckstrin homology domain of phospholipase C-delta 1 binds with high affinity to phosphatidylinositol 4,5-bisphosphate in bilayer membranes. *Biochemistry*, 34 (49) 16228–16234

Gaztañaga, L., Marchlinski, F. E., Betensky, B. P. (2012). Mechanisms of cardiac arrhythmias. *Revista Española de Cardiología (English edition)*, 65 (2) 174–185

Ghosh, S., Nunziato, D. A., & Pitt, G. S. (2006). KCNQ1 assembly and function is blocked by long-QT syndrome mutations that disrupt interaction with calmodulin. *Circulation Research*, 98 (8) 1048–1054

Gillooly, D. J., Morrow, I. C., Lindsay, M., Gould, R., Bryant, N. J., Gaullier, J. M., Parton, R. G., & Stenmark, H. (2000). Localization of phosphatidylinositol 3-phosphate in yeast and mammalian cells. *The EMBO Journal,* 19 (17) 4577–4588

Godi, A., Pertile, P., Meyers, R., Marra, P., Di Tullio, G., Iurisci, C., Luini, A., Corda, D. & De Matteis, M. A. (1999) ARF mediates recruitment of PtdIns-4-OH kinase-beta and stimulates synthesis of PtdIns(4,5)P2 on the Golgi complex. *Nature Cell Biology*, 1 (5) 280–287

Godi, A., Di Campi, A., Konstantakopoulos, A., Di Tullio, G., Alessi, D. R., Kular, G. S., Daniele, T., Marra, P., Lucocq, J. M. & De Matteis, M. A. (2004). FAPPs control Golgi-to-cell-surface membrane traffic by binding to ARF and PtdIns(4)P. *Nature Cell Biology*, 6 (5) 393–404

Godinho, R. O., Duarte, T. & Pacini, E. S. A. (2015). New perspectives in signaling mediated by receptors coupled to stimulatory G protein: the emerging significance of cAMP efflux and extracellular cAMP-adenosine pathway. *Frontiers in Pharmacology*, 6, 58

Goh, L. K. & Sorkin, L. (2013). Endocytosis of receptor tyrosine kinases. *Cold Spring Harbour Perspectives in Biology*, 5 (5) a017459

Gouas, L., Bellocq, C., Berthet, M., Potet, F., Demolombe, S., Forhan, A., Lescasse, R., Simon, F., Balkau, B., Denjoy, I., Hainque, B., Baró, I. & Guicheney, P. (2004). New KCNQ1 mutations leading to haploinsufficiency in a general population; Defective trafficking of a KvLQT1 mutant. *Cardiovascular Research*, 63 (1) 60–68

Grant, A. O. (2009). Cardiac ion channels. *Circulation: Arrhythmia Electrophysiology*, 2 (2) 185–194

Grant, B. D. & Donaldson, J. G. (2009). Pathways and mechanisms of endocytic recycling. *Nature Reviews. Molecular Cell Biology*, 10 (9) 597–608

Griffiths, A. J. F., Miller, J. H., Suzuki, D. T., Lewontin, R. C. & Gelbart, W. M. (2000). An Introduction to Genetic Analysis. 7th edition, New York: W. H. Freeman

Grunnet, M., Jespersen, T., Rasmussen, H. B., Ljungstrøm, T., Jorgensen, N. K., Olesen, S. P. & Klaerke, D. A. (2002). KCNE4 is an inhibitory subunit to the KCNQ1 channel. *The Journal of Physiology*, 542 (Pt 1) 119–130

Guo, J., Massaeli, H., Xu, J., Jia, Z., Wigle, J. T., Mesaeli, N. & Zhang, S. (2009). Extracellular K+ concentration controls cell surface density of IKr in rabbit hearts and of the HERG channel in human cell lines. *The Journal of Clinical Investigation*, 119 (9) 2745–2757

Guo, X., Gao, X., Wang, Y., Peng, L., Zhu, Y. & Wang, S. (2012). $I_{Ks}$ protects from ventricular arrhythmia during cardiac ischemia and reperfusion in rabbits by preserving the repolarization reserve. *PLoS One*, 7 (2) e31545

Hammond, G. R. V., Schiavo, G. & Irvine, R. F. (2009). Immunocytochemical techniques reveal multiple, distinct cellular pools of PtdIns4*P* and PtdIns(4,5)$P_2$. *Biochemical Journal*, 422 (Pt 1) 23–35

Hammond, G. R. V., Fischer, M. J., Anderson, K. E., Holdich, J., Koteci, A., Balla, T. & Irvine, R. F. (2012). PI4P And PI(4,5)$P_2$ Are Essential But Independent Lipid Determinants Of Membrane Identity. *Science (New York, N.Y.)*, *337* (6095) 727–730

Hammond, G. R. & Balla, T. (2015) Polyphosphoinositide binding domains: Key to inositol lipid biology. *Biochimica et Biophysica Acta*, 1851 (6) 746–758

Hansen, S. H., Olsson, A. & Casanova, J. E. (1995). Wortmannin, an inhibitor of phosphoinositide 3-kinase, inhibits transcytosis in polarized epithelial cells. *The Journal of Biological Chemistry*, 270 (47) 28425–28432

Hao, J. J., Liu, Y., Kruhlak, M., Debell, K. E., Rellahan, B. L., & Shaw, S. (2009). Phospholipase C–mediated hydrolysis of PIP2 releases ERM proteins from lymphocyte membrane. *The Journal of Cell Biology*, *184* (3) 451–462

Harmati, G., Bányász, T., Bárándi, L., Szentandrássy, N., Horváth, B., Szabó, G., Szentmiklósi, J. A., Szénási, G., Nánási, P. P. & Magyar, J. (2011). Effects of β-adrenoceptor stimulation on delayed rectifier $K^+$ currents in canine ventricular cardiomyocytes. *British Journal of Pharmacology*, 162 (4) 890–896

Harmer, S. C., Mohal, J. S., Royal, A. A., McKenna, W. J., Lambiase, P. D. & Tinker, A. (2014). Cellular mechanisms underlying the increased disease severity seen for patients with long QT syndrome caused by compound mutations in KCNQ1. *The Biochemical Journal*, 462 (1) 133–142

Hattori, S., Murakami, F. & Song, W. J. (2003). Rundown of a transient potassium current is attributable to changes in channel voltage dependence. *Synapse*, 48 (2) 57–65

Hay, J. C. & Martin, T. F. (1993). Phosphatidylinositol transfer protein required for ATP-dependent priming of Ca(2+)-activated secretion. *Nature,* 366 (6455) 572–575

Hayashi, K., Sasai, M. & Iwasaki, A. (2015). Toll-like receptor 9 trafficking and signaling for type I interferons requires PIKfyve activity. *International Immunonology*, 27 (9) 435–445

He, S., Ni, D., Ma, B., Lee, J.-H., Zhang, T., Ghozalli, I., Pirooz, S. D., Zhao, Z., Bharatham, N., Li, B., Oh, S., Lee, W. H., Takahashi, Y., Wang, H. G., Minassian, A., Feng, P., Deretic, V., Pepperkok, R., Tagaya, M., Yoon, H. S. & Liang, C. (2013). PI(3)P-bound UVRAG coordinates Golgi-ER retrograde and Atg9 transport by differential interactions with the ER tether and the Beclin1 complex. *Nature Cell Biology*, 15 (10) 1206–1219

He, J., Scott, J. L., Heroux, A., Roy, S., Lenoir, M., Overduin, M., Stahelin, R. V., & Kutateladze, T. G. (2011). Molecular basis of phosphatidylinositol 4-phosphate and ARF1 GTPase recognition by the FAPP1 pleckstrin homology (PH) domain. *Journal of Biological Chemistry*, 286 (21) 18650–18657

Heginbotham, L., Lu, Z., Abramson, T., & MacKinnon, R. (1994). Mutations in the K+ channel signature sequence. *Biophysical Journal*, 66 (4) 1061–1067

Heitzmann, D., Koren, V., Wagner, M., Sterner, C., Reichold, M., Tegtmeier, I., Volk, T. & Warth, R. (2007) KCNE beta subunits determine pH sensitivity of KCNQ1 potassium channels. *Cellular Physiology and Biochemistry*, 19 (1-4) 21–32

Herbert, E., Trusz-Gluza, M., Moric, E., Smiłowska-Dzielicka, E., Mazurek, U. & Wilczok, T. (2002). KCNQ1 gene mutations and the respective genotype-phenotype correlations in the long QT syndrome. *Medical Science Monitor: International Medical Journal of Experimental and Clinical Research*, 8 (10) RA240–248

Hernandez, C. C., Falkenburger, B. & Shapiro, M. S. (2009). Affinity for phosphatidylinositol 4,5-bisphosphate determines muscarinic agonist sensitivity of Kv7 K+ channels. *The Journal of General Physiology*, 134 (5) 437–448

Hibino, H., Nin, F., Tsuzuki, C. & Kurachi, Y. (2009) How is the highly positive endocochlear potential formed? The specific architecture of the stria vascularis and the roles of the ion-transport apparatus. *Pflugers Archiv: European Journal of Physiology*, 459 (4) 521–533

Hilgemann, D. W. & Ball, R. (1996). Regulation of cardiac Na+,Ca2+ exchange and KATP potassium channels by PIP2. *Science*, 273 (5277) 956–959

Hilgemann, D. W., Feng, S., & Nasuhoglu, C. (2001). The complex and intriguing lives of PIP2 with ion channels and transporters. *Science STKE, 2001*(111), re19

Ho, K., Nichols, C. G., Lederer, W. J., Lytton, J., Vassilev, P. M., Kanazirska, M. V., & Hebert, S. C. (1993). Cloning and expression of an inwardly rectifying ATP-regulated potassium channel. *Nature*, 362 (6415) 31–38

Hodgkin, A. L. & Huxley, A. F. (1939). Action Potentials recorded from inside a nerve fibre. *Nature*, 144; 710–711

Hodgkin, A. L., Huxley, A. F., & Katz, B. (1952). Measurement of current-voltage relations in the membrane of the giant axon of *Loligo*. *The Journal of Physiology*, 116 (4) 424–448.

Hoffman, B. F. (1959). Electrophysiology of single cardiac cells. *Bulletin of the New York Academy of Medicine,* 35, 689–706

Hong, .K, Piper, D. R., Diaz-Valdecantos, A., Brugada, J., Oliva, A., Burashnikov, E., Santos-de-Soto, J., Grueso-Montero, J., Diaz-Enfante, E., Brugada, P., Sachse, F., Sanguinetti, M. C. & Brugada, R. (2005). De novo KCNQ1 mutation responsible for atrial fibrillation and short QT syndrome in utero. *Cardiovascular Research*, 68 (3) 433–440

Hossain, M. I., Iwasaki, H., Okochi, Y., Chahine, M., Higashijima, S., Nagayama, K. & Okamura, Y. (2008). Enzyme domain affects the movement of the voltage sensor in ascidian and zebrafish voltage-sensing phosphatases. *The Journal of Biological Chemistry*, 283 (26) 18248–18259

Huang, L., Bitner-Glindzicz, M., Tranebjaerg, L., & Tinker, A. (2001). A spectrum of functional effects for disease causing mutations in the Jervell and Lange-Nielsen syndrome. *Cardiovascular Research*, 51 (4) 670–680

Huang, C. L. & Kuo, E. (2007). Mechanism of hypokalemia in magnesium deficiency. *Journal of the American Society of Nephrology*, 18 (10) 2649–2653

Hurowitz, E. H., Melnyk, J. M., Chen, Y. J., Kouros-Mehr, H., Simon, M. I. & Shizuya, H. (2000) Genomic characterization of the human heterotrimeric G protein alpha, beta, and gamma subunit genes. *DNA Research*, 7 (2) 111–120

Hurst, J. W. (1998). Naming of the waves in the ECG, with a brief account of their genesis. *Circulation,* 98 (18) 1937–1942

Ikonomov, O. C., Sbrissa, D., Venkatareddy, M., Tisdale, E., Garg, P. & Shisheva, A. (2015). Class III PI 3-kinase is the main source of PtdIns3P substrate and membrane recruitment signal for PIKfyve constitutive function in podocyte endomembrane homeostasis. *Biochimica et Biophysica Acta*, 1853 (5) 1240–1250

Imredy, J. P., Penniman, J. R., Dech, S. J., Irving, W. D. & Salata, J. J. (2008). Modeling of the adrenergic response of the human $I_{Ks}$ current (hKCNQ1/hKCNE1) stably expressed in HEK-293 cells. *American Journal of Physiology. Heart and Circulatory Physiology*, 295 (5) H1867–1881

Inoue, T., Heo, W. D., Grimley, J. S., Wandless, T. J., & Meyer, T. (2005). An inducible translocation strategy to rapidly activate and inhibit small GTPase signaling pathways. *Nature Methods,* 2 (6) 415–418

Inoue, T. & Meyer, T. (2008). Synthetic Activation of Endogenous PI3K and Rac Identifies an AND-Gate Switch for Cell Polarization and Migration. *PLoS ONE,* 3 (8) e3068

Ishihara, H., Shibasaki, Y., Kizuki, N., Katagiri, H., Yazaki, Y., Asano, T. & Oka, Y. (1996). Cloning of cDNAs encoding two isoforms of 68-kDa type I phosphatidylinositol-4-phosphate 5-kinase. *The Journal of Biological Chemistry*, 271 (39) 23611–23614

Itoh, H., Shimizu, W., Hayashi, K., Yamagata, K., Sakaguchi, T., Ohno, S., Makiyama, T., Akao, M., Ai, T., Noda, T., Miyazaki, A., Miyamoto, Y., Yamagishi, M., Kamakura, S. & Horie, M. (2010). Long QT syndrome with compound mutations is associated with a more severe phenotype: a Japanese multicenter study. *Heart Rhythm*, 7 (10) 1411–1418

Jervell, A. & Lange-Nielson, F. (1957). Congenital deaf-mutism, functional heart disease with prolongation of the Q-T interval and sudden death. *American Heart Journal*, 54 (1) 59-68

Jespersen, T., Membrez, M., Nicolas, C. S., Pitard, B., Staub, O., Olesen, S. P., Baró, I. & Abriel, H. (2007) The KCNQ1 potassium channel is down-regulated by ubiquitylating enzymes of the Nedd4/Nedd4-like family. *Cardiovascular Research*, 74 (1) 64–74

John Innes Centre (2012). Confocal Microscopy. Accessed at https://www.jic.ac.uk

Johnson, J. N., & Ackerman, M. J. (2009). QTc: how long is too long? *British Journal of Sports Medicine*, 43 (9) 657–662

Jones, D. H., Sakamoto, K., Vorce, R. L. & Howard, B. H. (1990). DNA mutagenesis and recombination. *Nature*, 344 (6268) 783–794

Jones, S. M. & Howell, K. E. (1997). Phosphatidylinositol 3-kinase is required for the formation of constitutive transport vesicles from the TGN. *Journal of Cell Biology*, 139 (2) 339–349

Jones, D. H., Morris, J. B., Morgan, C. P., Kondo, H., Irvine, R. F. & Cockcroft, S. (2000). Type I phosphatidylinositol 4-phosphate 5-kinase directly interacts with ADP-ribosylation factor 1 and is responsible for phosphatidylinositol 4,5-bisphosphate synthesis in the golgi compartment. *The Journal of Biological Chemistry*, 275 (18) 13962–13966

Jost, M., Simpson, F., Kavran, J. M., Lemmon, M. A. & Schmid, S. L. (1998). Phosphatidylinositol-4,5-bisphosphate is required for endocytic coated vesicle formation. *Current Biology: CB*, 8 (25) 1399–1402

Jost, N., Virág, L., Bitay, M., Takács, J., Lengyel, C., Biliczki, P., Nagy, Z., Bogáts, G., Lathrop, D. A., Papp, J.G. & Varró, A. (2005) Restricting excessive cardiac action potential and QT prolongation: a vital role for $I_{Ks}$ in human ventricular muscle. *Circulation,* 112 (10) 1392–1399

Jovic, M., Bojjireddy, N., Kean, M., Gingras, A. C., Brill, J. & Balla, T. (2012) Regulation of PI4KIIα distribution between the Golgi and endosomal compartments. *FASEB Journal: Official Publication of the Federation of American Societies for Experimental Biology*, 28 (988.9)

Jurevicius, J., & Fischmeister, R. (1996). cAMP compartmentation is responsible for a local activation of cardiac Ca2+ channels by beta-adrenergic agonists. *Proceedings of the National Academy of Sciences of the United States of America*, *93* (1) 295–299

Kallergis, E. M., Goudis, C. A., Simantirakis, E. N., Kochiadakis, G. E. & Vardas, P. E. (2012). Mechanisms, risk factors, and management of acquired long QT syndrome: a comprehensive review. *The Scientific World Journal*, 2012: 212178

Kanda, V. A., Purtell, K. & Abbott, G. W. (2011). Protein Kinase C downregulates $I_{Ks}$ by stimulating KCNQ1-KCNE1 potassium channel endocytosis. *Heart Rhythm*, 8 (10) 1641–1647

Kang, M., Chung, K. Y. & Walker, J. W. (2007). G-protein coupled receptor signaling in myocardium: not for the faint of heart. *Physiology (Bethesda, Md.),* 22;174–184

Kapplinger, J. D., Tester, D. J., Salisbury, B. A., Carr, J. L., Harris-Kerr, C., Pollevick, G. D., Wilde, A. A. & Ackerman, M. J. (2009). Spectrum and prevalence of mutations from the first 2,500 consecutive unrelated patients referred for the FAMILION long QT syndrome genetic test. *Heart Rhythm*, 6; 1297–1303.

Keith, A., & Flack, M. (1907). The form and nature of the muscular connections between the primary divisions of the vertebrate heart. *Journal of Anatomy and Physiology,* 41 (pt 3) 172–189

Kim, T. K., & Eberwine, J. H. (2010). Mammalian cell transfection: the present and the future. *Analytical and Bioanalytical Chemistry*, 397 (8) 3173–3178

Kim ,Y. J., Guzman-Hernandez, M. L. & Balla, T. (2011). A highly dynamic ER-derived phosphatidylinositol-synthesizing organelle supplies phosphoinositides to cellular membranes. *Developmental Cell*, 21 (5) 812–824

Kinoshita, K., Komatsu, T., Nishide, K., Hata, Y., Hisajima, N., Takahashi, H., Kimoto, K., Aonuma, K., Tsushima, E., Tabata, T., Yoshida, T., Mori, H., Nishida, K., Yamaguchi, Y., Ichida, F., Fukurotani, K., Inoue, H. & Nishida, N. (2014). A590T mutation in KCNQ1 C-terminal helix D decreases $I_{Ks}$ channel trafficking and function but not Yotiao interaction. *Journal of Molecular and Cellular Pharmacology*, 72; 272–280

Kjeken, R., Mousavi, S. A., Brech, A., Griffiths, G. & Berg, T. (2001). Wortmannin-sensitive trafficking steps in the endocytic pathway in rat liver endothelial cells. *Biochemical Journal*, 357 (Pt 2) 497–503

Kléber, A. G. & Rudy, Y. (2004) Basic mechanisms of cardiac impulse propagation and associated arrhythmias. Physiological Reviews, 84 (2) 431–488

Koch, M. & Holt, M. (2012). Coupling exo- and endocytosis: an essential role for $PIP_2$ at the synapse. *Biochimica et Biophysica Acta*, 1821 (8) 1114–1132

Kosenko, A., & Hoshi, N. (2013). A Change in Configuration of the Calmodulin-KCNQ Channel Complex Underlies Ca(2+)-Dependent Modulation of KCNQ Channel Activity. *PLoS One*, 8 (12) e82290

Kozasa, T., Jiang, X., Hart, M. J., Sternweis, P. M., Singer, W. D., Gilman, A. G., Bollag, G. & Sternweis, P. C. (1998) p115 RhoGEF, a GTPase activating protein for Galpha12 and Galpha13. *Science*, 280 (5372) 2109–2111

Krauter, T., Ruppersberg, J. P. & Baukrowitz, T. (2001). Phospholipids as modulators of K(ATP) channels: distinct mechanisms for control of sensitivity to sulphonylureas, K(+) channel openers, and ATP. *Molecular Pharmacology*, 59 (5) 1086–1093

Kruse, M., Hammond, G. R., & Hille, B. (2012). Regulation of voltage-gated potassium channels by PI(4,5)P2. *Journal of General Physiology,* 140 (2) 189–205

Kubisch, C., Schroeder, B. C., Friedrich, T., Lütjohann, B., El-Amraoui, A., Marlin, S., Petit, C., & Jentsch, T. J. (1999). KCNQ4, a novel potassium channel expressed in sensory outer hair cells, is mutated in dominant deafness. *Cell*, 96 (3) 437–446

Kubo, Y., Baldwin, T. J., Jan, Y. N., & Jan, L. Y. (1993). Primary structure and functional expression of a mouse inward rectifier potassium channel. *Nature*, 362 (6416) 127–13

Kubo, Y., Murata, Y. (2001) Control of rectification and permeation by two distinct sites after the second transmembrane region in Kir2.1 $K^+$ channel. *The Journal of Physiology*, 531 (Pt 3) 645–660

Kubota, T., Shimizu, W., Kamakura, S. & Horie, M. (2000). Hypokalemia-induced long QT syndrome with an underlying novel missense mutation in S4-S5 linker of KCNQ1. *Journal of Cardiovascular Electrophysiology*, 11 (9) 1048–1054

Kuge, O., Dascher, C., Orci, L., Rowe, T., Amherdt, M., Plutner, H., Ravazzola, M., Tanigawa, G., Rothman, J. E., & Balch, W. E. (1994). Sar1 promotes vesicle budding from the endoplasmic reticulum but not Golgi compartments. *The Journal of Cell Biology,* 125 (1) 51–65

Kurachi, Y., Nakajima, T., & Sugimoto, T. (1986). Acetylcholine activation of K+ channels in cell-free membrane of atrial cells. *The American Journal of Physiology*, 251(3 Pt 2), H681–684

Kurokawa, J., Chen, L. & Kass, R. S. (2003). Requirement of subunit expression for cAMP-mediated regulation of a heart potassium channel. *Proceedings of the National Academy of Sciences of the United States of America,* 100 (4) 2122–2127

Kurokawa, J., Motoike, H. K., Rao, J. & Kass, R. S. (2004). Regulatory actions of the A-kinase anchoring protein Yotiao on a heart potassium channel downstream of PKA phosphorylation. *Proceedings of the National Academy of Sciences of the United States of America,* 101 (46) 16374–16378

Kwon, Y., Hofmann, T., & Montell, C. (2007). Integration of phosphoinositide- and calmodulin-mediated regulation of TRPC6. *Molecular Cell,* 25 (4) 491–503

Lambert, N. A. (2008). Dissociation of heterotrimeric g proteins in cells. *Science Signalling,* 1 (25) re5

Lange, A., Mills, R. E., Lange, C. J., Stewart, M., Devine, S. E. & Corbett, A. H. (2007) Classical nuclear localization signals: definition, function, and interaction with importin alpha. *The Journal of Biological Chemistry*, 282 (8) 5101–5105

Law, B. K. (2005). Rapamycin: an anti-cancer immunosuppressant? *Critical Reviews in Oncology/Hematology*, 56 (1) 47–60

Lawyer, F. C., Stoffel, S., Saiki, R. K., Myambo, K., Drummond, R., & Gelfand, D. H. (1989). Isolation, characterization, and expression in Escherichia coli of the DNA polymerase gene from Thermus aquaticus. *Journal of Biological Chemistry*, 264 (11) 6427–6437

Lee, S. B., & Rhee, S. G. (1995). Significance of PIP2 hydrolysis and regulation of phospholipase C isozymes. *Current Opinion in Cell Biology,* 7 (2) 183–189

Lee, K. W., Webb, S. E., & Miller, A. L. (2003). Ca2+ released via IP3 receptors is required for furrow deepening during cytokinesis in zebrafish embryos. *The International Journal of Developmental Biology*, 47 (6) 411–421

Lee, P. Y., Costumbrado, J., Hsu, C. Y. & Kim, Y. H. (2012). Agarose Gel Electrophoresis for the Separation of DNA Fragments. *Journal of Visualised Experiments*, (62) e3923

Lemmon, M. A. (2008). Membrane recognition by phospholipid-binding domains. *Nature Reviews Molecular Cell Biology, 9* (2) 99–111

Lesage, F. & Lazdunski, M. (2000). Molecular and functional properties of two-pore-domain potassium channels. *American Journal of Physiology. Renal Physiology,* 279 (5) F793–801

Li, G. R., Feng, J., Yue, L., Carrier, M. & Nattel, S. (1996). Evidence for two components of delayed rectifier K+ current in human ventricular myocytes. *Circulation Research*, 78 (4) 689–696

Li, Y., Gamper, N., Hilgemann, D. W. & Shapiro, M. S. (2005). Regulation of Kv7 (KCNQ) K+ channel open probability by phosphatidylinositol 4,5-bisphosphate. *The Journal of Neuroscience*, 25 (43) 9825–9835

Li, Y., Sroubek, J., Krishnan, Y. & McDonald, T. V. (2008). A-kinase anchoring protein targeting of protein kinase A and regulation of HERG channels. *The Journal of Membrane Biology*, 223 (2) 107–116

Li, W., Du, R., Wang, Q. F., Tian, L., Yang, J. G. & Song, Z. F. (2009). The G314S KCNQ1 mutation exerts a dominant-negative effect on expression of KCNQ1 channels in oocytes, *Biochemical and biophysical research communications*,383 (2) 206–209

Li, Y., Chen, L., Kass, R. S. & Dessauer, C. W. (2012). The A-kinase anchoring protein Yotiao facilitates complex formation between adenylyl cyclase type 9 and the $I_{Ks}$ potassium channel in heart. *The Journal of Biological Chemistry*, 287 (35) 29815–29824

Li, Y., Zaydman, M. A., Wu, D., Shi, J., Guan, M., Virgin-Downey, B. & Cui, J. (2011). KCNE1 enhances phosphatidylinositol 4,5-bisphosphate (PIP2) sensitivity of $I_{Ks}$ to modulate channel activity. *Proceedings of the National Academy of Sciences of the United States of America*, 108 (22) 9095–9100

Li, P., Liu, H., Lai, C., Sun, P., Zeng, W., Wu, F., Zhang, L., Wang, S., Tian, C. & Ding, J. (2014). Differential modulations of KCNQ1 by auxiliary proteins KCNE1 and KCNE2. *Scientific Reports,* 4 (4973)

Liang, J., Choi, J. & Clardy, J. (1999) Refined structure of the FKBP12-rapamycin-FRB ternary complex at 2.2 A resolution. *Acta Crystallographica. Section D, Biolological Crystallography*, 55 (pt 4) 736–744

Liang, T., Xie, L., Chao, C., Kang, Y., Lin, X., Qin, T., Xie, H., Feng, Z. P. & Gaisano, H. Y. (2014). Phosphatidylinositol 4,5-Biphosphate ($PIP_2$) Modulates Interaction of Syntaxin-1A with Sulfonylurea Receptor 1 to Regulate Pancreatic β-Cell ATP-sensitive Potassium Channels. *The Journal of Biological Chemistry*, 289 (9) 6028–6040

Lin, C., Cvetanovic, I., Ke, X., Ranade, V. & Somberg, J. (2005). A mechanism for the potential proarrhythmic effect of acidosis, bradycardia, and hypokalemia on the blockade of human ether-a-go-go-related gene (HERG) channels. *American Journal of Therapeutics*, 12 (4) 328–336

Lindholm, L. H., Ibsen, H., Dahlöf, B., Devereux, R. B., Beevers, G., de Faire, U., Fyhrquist, F., Julius, S., Kjeldsen, S. E., Kristiansson, K., Lederballe-Pedersen, O., Nieminen, M. S., Omvik, P., Oparil, S., Wedel, H., Aurup, P., Edelman, J. & Snapinn, S. (2002). Cardiovascular morbidity and mortality in patients with diabetes in the Losartan Intervention For Endpoint reduction in hypertension study (LIFE): a randomised trial against atenolol. *Lancet*, 359 (9311) 1004–1010

Liou, H. H., Zhou, S. S. & Huang, C. L. (1999). Regulation of ROMK1 channel by protein kinase A via a phosphatidylinositol 4,5-bisphosphate-dependent mechanism. *Proceedings of the National Academy of Sciences for the United States of America*, 96 (10) 5820–5825

Lippiat, J. D. (2008) Whole-cell recording using the perforated patch clamp technique. *Methods in Molecular Biology (Clifton, N.J.)*, 491, 141–149

Liu, Y., Kahn, R. A. & Prestegard, J. H. (2014). Interaction of Fapp1 with Arf1 and PI4P at a membrane surface: an example of coincidence detection. *Structure (London, England: 1993)*, 22 (3) 421–430

Liu, B., Liang, H., Liu, L. & Zhang, H. (2008). Phosphatidylinositol 4,5-bisphosphate hydrolysis mediates histamine-induced KCNQ/M current inhibition. *American Journal of Physiology. Cell Physiology*, 295 (1) C81–91

Lo, C. W. (2000). Role of gap junctions in cardiac conduction and development: insights from the connexin knockout mice. *Circulation Research*, 187 (5) 346–348

Logothetis, D. E., Lupyan, D. & Rosenhouse-Dantsker, A. (2007). Diverse Kir modulators act in close proximity to residues implicated in phosphoinositide binding. *The Journal of Physiology*, 582 (Pt 3) 953–965

Lohse, M. J., Engelhardt, S. & Eschenhagen, T. (2003). What is the role of beta-adrenergic signaling in heart failure? *Circulation Research*, 93 (10) 896–906

Long, S. B., Campbell, E. B. & Mackinnon, R. (2005). Crystal structure of a mammalian voltage-dependent Shaker family K+ channel. *Science*, 309 (5736) 897–903

Long, K. R., Yamamoto, Y., Baker, A. L., Watkins, S. C., Coyne, C. B., Conway, J. F., & Aridor, M. (2010). Sar1 assembly regulates membrane constriction and ER export. *Journal of Cell Biology,* 190 (1) 115–128

Lopatin, A. N., Makhina, E. N., & Nichols, C. G. (1994). Potassium channel block by cytoplasmic polyamines as the mechanism of intrinsic rectification. *Nature,* 372 (6504) 366–369

Lopes, C. M., Zhang, H., Rohacs, T., Jin, T., Yang, J. & Logothetis, D. E. (2002). Alterations in conserved Kir channel-PIP2 interactions underlie channelopathies. *Neuron*, 34 (6) 933–944

Lopes, C. M. B., Remon, J. I., Matavel, A., Sui, J. L., Keselman, I., Medei, E., Shen, Y., Rosenhouse-Dantsker, A., Rohacs, T. & Logothetis, D.E. (2007). Protein Kinase A modulates PLC-dependent regulation and PIP2-sensitivity of K+ channels. *Channels,* 1 (2) 124–34

Loussouarn, G., Park, K. H., Bellocq, C., Baró, I., Charpentier, F., & Escande, D. (2003). Phosphatidylinositol-4,5-bisphosphate, PIP2, controls KCNQ1/KCNE1 voltage-gated potassium channels: a functional homology between voltage-gated and inward rectifier K+ channels. *The EMBO Journal,* 22 (20) 5412–5421

Lukacs, V., Thyagarajan, B., Varnai, P., Balla, A., Balla, T. & Rohacs, T. (2007). Dual regulation of TRPV1 by phosphoinositides. *The Journal of Neuroscience*, 27 (26) 7070–7080

Ma, D., Zerangue, N., Lin, Y. F., Collins, A., Yu, M., Jan, Y. N., & Jan, L. Y. (2001). Role of ER export signals in controlling surface potassium channel numbers. *Science*, 291 (5502) 316–319

Madamanchi, A. (2007). β-Adrenergic receptor signaling in cardiac function and heart failure. *McGill Journal of Medicine : MJM*, *10* (2) 99–104

Makkar, R. R., Fromm, B. S., Steinman, R. T., Meissner, M. D. & Lehmann, M. H. (1993). Female gender as a risk factor for torsades de pointes associated with cardiovascular drugs. *The Journal of the American Medical Association*, 270 (21) 2590–2597

Le Maout, S., Brejon, M., Olsen, O., Merot, J. & Welling, P. A. (1997). Basolateral membrane targeting of a renal-epithelial inwardly rectifying potassium channel from the cortical collecting duct, CCD-IRK3, in MDCK cells. *Proceedings of the National Academy of Sciences of the United States of America*, 94 (24) 13329–13334.

Marban, E., Robinson, S. W. & Wier, W. G. (1986). Mechanisms of arrhythmogenic delayed and early afterdepolarizations in ferret ventricular muscle. *The Journal of Clinical Investigation*, 78 (5) 1185–1192

Martin, T. F. (2001). PI(4,5)P(2) regulation of surface membrane traffic. *Current Opinions in Cell Biology*, 13 (4) 493–499

Martin, T. F. J. (2012). Role of PI(4,5)$P_2$ in Vesicle Exocytosis and Membrane Fusion. *Sub-Cellular Biochemistry*, *59*, 111–130

Martys, J. L., Wjasow, C., Gangi, D. M., Kielian, M. C., McGraw, T. E. & Backer, J. M. (1996). Wortmannin-sensitive trafficking pathways in Chinese hamster ovary cells. Differential effects on endocytosis and lysosomal sorting. *The Journal of Biological Chemistry*, 271 (18) 10953–10962

Marx, S. O., Kurokawa, J., Reiken, S., Motoike, H., D'Armiento, J., Marks, A. R. & Kass, R. S. (2002). Requirement of a macromolecular signaling complex for beta adrenergic receptor modulation of the KCNQ1-KCNE1 potassium channel. *Science*, 295 (5554) 496–499

Matavel, A., & Lopes, C. M. (2009). PKC activation and PIP(2) depletion underlie biphasic regulation of $I_{Ks}$ by Gq-coupled receptors. *Journal of Molecular and Cellular Cardiology*, 46 (5) 704–712

Matavel, A., Medei, E. & Lopes, C. M. (2010). PKA and PKC partially rescue long QT type 1 phenotype by restoring channel-PIP2 interactions. *Channels (Austin, Tex.)*, 4 (1) 3–11

Matsuda, H., Saigusa, A., & Irisawa, H. (1987). Ohmic conductance through the inwardly rectifying K channel and blocking by internal Mg2+. *Nature,* 3325 (7000) 156–159

McCartney, A. J., Zhang, Y. & Weisman, L. S. (2014a). Phosphatidylinositol 3,5-bisphosphate: low abundance, high significance. *Bioessays*, 36 (1) 52–64

McCartney, A. J., Zolov, S. N., Kauffman, E. J., Zhang, Y., Strunk, B. S., Weisman, L. S., Sutton, M. A. (2014b). Activity-dependent PI(3,5)P2 synthesis controls AMPA receptor trafficking during synaptic depression. *Proceedings of the National Academy of Sciences of the United States of America*, 111 (45) E4896–4905

Mesmin, B., Bigay, J., Moser von Filseck, J., Lacas-Gervais, S., Drin, G. & Antonny, B. (2013). A four-step cycle driven by PI(4)P hydrolysis directs sterol/PI(4)P exchange by the ER-Golgi tether OSBP. *Cell*, 155 (4) 830–843

Meyers, R., & Cantley, L. C. (1997). Cloning and characterization of a wortmannin-sensitive human phosphatidylinositol 4-kinase. *Journal of Biological Chemistry*, 272 (7) 4384–4390

Minsky, M. (1988). Memoir on inventing the confocal scanning microscope. *Scanning, 10* (4) 128–138

Mitcheson, J. S., Chen, J., Lin, M., Culberson, C. & Sanguinetti, M. C. (2000). A structural basis for drug-induced long QT syndrome. *Proceedings of the National Academy of Sciences of the United States of America,* 97 (22) 12329–12333

Miyamoto, T., DeRose, R., Suarez, A., Ueno, T., Chen, M., Sun, T. P., Wolfgang, M. J., Mukherjee, C., Meyers, D. J. & Inoue, T. (2012) Rapid and orthogonal logic gating with a gibberellin-induced dimerization system. *Nature Chemical Biology*, 8 (5) 465–470

Molina, C. E., Johnson, D. M., Mehel, H., Spätjens, R. L. H. M. G., Mika, D., Algalarrondo, V., Slimane, Z. H., Lechêne, P., Abi-Gerges, N., van der Linde, H. J., Leroy, J., Volders, P. G., Fischmeister, R. & Vandecasteele, G. (2014). Interventricular Differences in β-Adrenergic Responses in the Canine Heart: Role of Phosphodiesterases.*Journal of the American Heart Association: Cardiovascular and Cerebrovascular Disease*, *3* (3) e000858

Moretti, A., Bellin, M., Welling, A., Jung, C. B., Lam, J. T., Bott-Flügel, L., Dorn, T., Goedel, A., Höhnke, C., Hofmann, F., Seyfarth, M., Sinnecker, D., Schömig, A. & Laugwitz, K. L. (2010). Patient-specific induced pluripotent stem-cell models for long-QT syndrome. *New England Journal of Medicine*, 363 (15) 1397–1409

Morise, H., Shimomura, O., Johnson, F. H. & Winant, J. (1974). Intermolecular energy transfer in the bioluminescent system of Aequorea. *Biochemistry*, 13 (12) 2656–2662

Moss, A. J., Zareba, W., Hall, W. J., Schwartz, P. J., Crampton, R. S., Benhorin, J., Vincent, G. M., Locati, E. H., Priori, S. G., Napolitano, C., Medina, A., Zhang, L., Robinson, J. L., Timothy, K., Towbin, J. A. & Andrews, M. L. (2000). Effectiveness and limitations of beta-blocker therapy in congenital long-QT syndrome. *Circulation*, 101 (6) 616–623

Murata, Y., Iwasaki, H., Sasaki, M., Inaba, K. & Okamura, Y. (2005). Phosphoinositide phosphatase activity coupled to an intrinsic voltage sensor. *Nature*, 435 (7046) 1239–1243

Murata, Y. & Okamura, Y. (2007). Depolarization activates the phosphoinositide phosphatase Ci-VSP, as detected in Xenopus oocytes coexpressing sensors of PIP2. *The Journal of Physiology*, 583 (Pt 3) 875–889

Murray, C. I., Westhoff, M., Eldstrom, J., Thompson, E., Emes, R. & Fedida, D. (2016). Unnatural amino acid photo-crosslinking of the $I_{Ks}$ channel complex demonstrates a KCNE1:KCNQ1 stoichiometry of up to 4:4. *eLife,* 5. pii: e11815

Näbauer, M., Beuckelmann, D. J., Uberfuhr, P. & Steinbeck, G. (1996) Regional differences in current density and rate-dependent properties of the transient outward current in subepicardial and subendocardial myocytes of human left ventricle. *Circulation,* 93 (1) 168–177

Nakagawa, T., Goto, K. & Kondo, H. (1996) Cloning, expression, and localization of 230-kDa phosphatidylinositol 4-kinase. *The Journal of Biological Chemistry*, 271 (20) 12088–12094

Nakajima, T., Furukawa, T., Tanaka, T., Katayama, Y., Nagai, R., Nakamura, Y. & Hiraoka, M. (1998). Novel mechanism of HERG current suppression in LQT2: shift in voltage dependence of HERG inactivation. *Circulation Research*, 83 (4) 415–422

Nakajo, K., & Kubo, Y. (2007). KCNE1 and KCNE3 Stabilize and/or Slow Voltage Sensing S4 Segment of KCNQ1 Channel. *The Journal of General Physiology*, 130 (3) 269–281

Nakanishi, S., Catt, K. J., & Balla, T. (1995). A wortmannin-sensitive phosphatidylinositol 4-kinase that regulates hormone-sensitive pools of inositolphospholipids. *Proceedings of the National Academy of Sciences of the United States of America,* 92 (12) 5317–5321

National Heart, Lung & Blood Institute (2011). Heart Interior. Accessed at http://www.nhlbi.nih.gov

Nattel, S., Maguy, A., Le Bouter, S., Yeh, Y. H. (2007). Arrhythmogenic ion-channel remodeling in the heart: heart failure, myocardial infarction, and atrial fibrillation. *Physiological Reviews*, 87 (2) 425–456

Nagi, K., Charfi, I. & Pineyro ,G. (2015) Kir3 channels undergo arrestin-dependant internalization following delta opioid receptor activation. *Cellular and Molecular Life Sciences,* 72 (18) 3543–3557

Neher, E., & Sakmann, B. (1976). Single-channel currents recorded from membrane of denervated frog muscle fibres. N*ature*, 260 (5554) 799–802

Neyroud, N., Richard, P., Vignier, N., Donger, C., Denjoy, I., Demay, L., Shkolnikova, M., Pesce, R., Chevalier, P., Hainque, B., Coumel, P., Schwartz, K. & Guicheney, P. (1999). Genomic organization of the KCNQ1 K+ channel gene and identification of C-terminal mutations in the long-QT syndrome. *Circulation Research*, 84 (3) 290–297

Niwa, N., & Nerbonne, J. M. (2010). Molecular determinants of cardiac transient outward potassium current (I(to)) expression and regulation. *The Journal and Molecular and Cellular Cardiology,* 48(1), 12–25

O'Connell, T. D., Jensen, B. C., Baker, A. J. & Simpson, P. C. (2014). Cardiac Alpha1-Adrenergic Receptors: Novel Aspects of Expression, Signaling Mechanisms, Physiologic Function, and Clinical Importance. *Pharmacological Reviews*, 66 (1) 308–333

O'Kelly, I. (2015). Endocytosis as a mode to regulate functional expression of two-pore domain potassium ($K_2p$) channels. *Pflugers Archiv: European Journal of Physiology,* 467 (5) 1133–1142

Ogden, D., & Standifeld, P. (1994). Patch clamp techniques for single channel and whole-cell recording. In D. Ogden (Ed.), Microelectrode Techniques: The Plymouth Workshop Handbook (Vol. 2). England: The Company of Biologists.

Okamura, Y., Murata, Y. & Iwasaki, H. (2009). Voltage-sensing phosphatase: actions and potentials. *The Journal of Physiology*, 587 (Pt 3) 513–520

Panaghie, G. & Abbott, G. W. (2007). The Role of S4 Charges in Voltage-dependent and Voltage-independent KCNQ1 Potassium Channel Complexes. J*ournal of General Physiology*, 129 (2) 121–133

Panja, S., Aich, P., Jana, B. & Basu, T. (2008). How does plasmid DNA penetrate cell membranes in artificial transformation process of Escherichia coli? *Molecular Membrane Biology*, 25 (5) 411–422

Park, K. H., Piron, J., Dahimene, S., Merot, J., Baro, I., Escande, D., & Loussouarn, G. (2005). Impaired KCNQ1-KCNE1 and phosphatidylinositol-4,5-bisphosphate interaction underlies the long QT syndrome. *Circulation Research,* 96 (7) 730–739

Patel, S. P., Campbell, D. L. & Strauss, H. C. (2002). Elucidating KChIP effects on Kv4.3 inactivation and recovery kinetics with a minimal KChIP2 isoform. *The Journal of Physiology,* 545(Pt 1) 5–11

Patel, C., Yan, G. X. & Antzelevitch, C. (2010). Short QT syndrome: from bench to bedside. *Circulation. Arrhythmia and Electrophysiology*, 3 (4) 401–408

Paulussen, A. D., Gilissen, R. A., Armstrong, M., Doevendans, P. A., Verhasselt, P., Smeets, H. J., Schulze-Bahr, E., Haverkamp, W., Breithardt, G., Cohen, N. & Aerssens, J. (2004). Genetic variations of KCNQ1, KCNH2, SCN5A, KCNE1, and KCNE2 in drug-induced long QT syndrome patients. *Journal of Molecular Medicine (Berlin, Germany)*, 82 (3) 182–188

Pearse, B. M. (1975) Coated vesicles from pig brain: purification and biochemical characterization. *Journal of Molecular Biology*, 91 (1) 93–98

Perkins, K. L. (2006). Cell-attached voltage-clamp and current-clamp recording and stimulation techniques in brain slices. *Journal of Neuroscience Methods,* 154 (1-2) 1–18

Pfeffer, M. A., Braunwald, E., Moyé, L. A., Basta, L., Brown, E. J. Jr., Cuddy, T. E., Davis, B. R., Geltman, E. M., Goldman, S. & Flaker, G. C. (1992). Effect of captopril on mortality and morbidity in patients with left ventricular dysfunction after myocardial infarction. Results of the survival and ventricular enlargement trial. The SAVE Investigators. *The New England Journal of Medicine*, 327 (10) 669–677

Phua, S. C., Pohlmeyer, C. & Inoue, T. (2012). Rapidly relocating molecules between organelles to manipulate small GTPase activity. *ACS Chemical Biology*, *7* (12) 1950–1955

Pingoud, A. & Jeltsch, A. (2001) Structure and function of type II restriction endonucleases. *Nucleic Acids Research*, 29 (18) 3705–3727

Plant, L. D., Xiong, D., Dai, H., & Goldstein, S. A. (2014). Individual $I_{Ks}$ channels at the surface of mammalian cells contain two KCNE1 accessory subunits. *Proceedings of the National Academy of Sciences of the United States of America,* 111 (14) E1438–1446

Porta, C., Paglino, C., & Mosca, A. (2014). Targeting PI3K/Akt/mTOR Signaling in Cancer. *Frontiers in Oncology*, 4; 64

Posor, Y., Eichhorn-Gruenig, M., Puchkov, D., Schöneberg, J., Ullrich, A., Lampe, A., Müller, R., Zarbakhsh, S., Gulluni, F., Hirsch, E., Krauss, M., Schultz, C., Schmoranzer, J., Noé, F. & Haucke, V. (2013). Spatiotemporal control of endocytosis by phosphatidylinositol-3,4-bisphosphate. *Nature*, 499 (7457) 233–237

Posor, Y., Eichhorn-Grünig, M. &, Haucke, V. (2015). Phosphoinositides in endocytosis. *Biochimica et Biophysica Acta*, 6; 794–804

Postema, P. G. & Wilde, A. A. M. (2014). The measurement of the QT interval. *Current Cardiology Reviews,* 10 (3) 287–294

Preston, P., Wartosch, L., Günzel, D., Fromm, M., Kongsuphol, P., Ousingsawat, J., Kunzelmann, K., Barhanin, J., Warth, R. & Jentsch, T. J. (2010). Disruption of the K+ channel beta-subunit KCNE3 reveals an important role in intestinal and tracheal Cl- transport. *The Journal of Biological Chemistry*, 285 (10) 7165–7175

Priori, S. G., Schwartz, P. J., Napolitano, C., Bianchi, L., Dennis, A., De Fusco, M., Brown, A. M. & Casari, G. (1998). A recessive variant of the Romano-Ward long-QT syndrome? *Circulation*, 97 (24) 2420–2425

Priori, S. G., Schwartz, P. J., Napolitano, C., Bloise, R., Ronchetti, E., Grillo, M., Vicentini, A., Spazzolini, C., Nastoli, J., Bottelli, G., Folli, R. & Cappelletti, D. (2003). Risk stratification in the long-QT syndrome. *The New England Journal of Medicine,* 348 (19) 1866–1874

Purves, D., Augustine, G. J., Fitzpatrick, D., Katz, L. C., LaMantia, A. S., McNamara, J. O., & Williams, S. M. (2001) Neuroscience, 2nd Edition. Sunderland (MA): Sinauer Associates

Pusch, M., Magrassi, R., Wollnik, B., & Conti, F. (1998). Activation and inactivation of homomeric KvLQT1 potassium channels. *Biophysical Journal,* 75(2), 785–792

Rameh, L. E., Tolias, K. F., Duckworth, B. C. & Cantley, L. C. (1997). A new pathway for synthesis of phosphatidylinositol-4,5-bisphosphate. *Nature*, 390 (6656) 192–196

Rampe, D., Roy, M. L., Dennis, A. & Brown, A. M. (1997). A mechanism for the proarrhythmic effects of cisapride (Propulsid): high affinity blockade of the human cardiac potassium channel HERG. *FEBS Letters*, 417 (1) 28–32

Rautaharju, P. M., Zhou, S. H., Wong, S., Calhoun, H. P., Berenson, G. S., Prineas, R. & Davignon, A. (1992). Sex differences in the evolution of the electrocardiographic QT interval with age. *The Canadian Journal of Cardiology*, 8 (7) 690–695

Ravens, U., & Cerbai, E. (2008). Role of potassium currents in cardiac arrhythmias. *Europace,* 10 (10) 1133–1137

Redfern, W. S., Carlsson, L., Davis, A. S., Lynch, W. G., MacKenzie, I., Palethorpe, S., Siegl, P. K., Strang, I., Sullivan, A. T., Wallis, R., Camm, A. J. & Hammond, T. G. (2003). Relationships between preclinical cardiac electrophysiology, clinical QT interval prolongation and torsade de pointes for a broad range of drugs: evidence for a provisional safety margin in drug development. *Cardiovascular Research*, 58 (1) 32–45

Remedios, C. G. & Nosworthy, N. J. (2008). The role of $PIP_2$ in actin, actin-binding proteins and disease. In: Remedios, C. G. & Chhabra, D. ed. *Actin Binding Proteins and Disease*. New York: Springer

Ritsema van Eck, H. J., Kors, J. A., & van Herpen, G. (2005). The U wave in the electrocardiogram: a solution for a 100-year-old riddle. *Cardiovascular Research*, 67(2) 256–262

Rhee, S. G. & Choi, K. D. (1992). Regulation of inositol phospholipid-specific phospholipase C isozymes. *The Journal of Biological Chemistry*, 267 (18) 12393–12396

Rjasanow, A., Leitner, M. G., Thallmair, V., Halaszovich, C. R. & Oliver, D. (2015). Ion channel regulation by phosphoinositides analyzed with VSPs—PI(4,5)P2 affinity, phosphoinositide selectivity, and PI(4,5)P2 pool accessibility. *Frontiers in Pharmacology,* 6; 127

Robbins, J., Dilworth, S. M., Laskey, R. A. & Dingwall, C. (1991). Two interdependent basic domains in nucleoplasmin nuclear targeting sequence: identification of a class of bipartite nuclear targeting sequence. *Cell*, 64 (3) 615–623

Rocheleau, J. M., & Kobertz, W. R. (2008). KCNE Peptides Differently Affect Voltage Sensor Equilibrium and Equilibration Rates in KCNQ1 $K^+$ Channels. *The Journal of General Physiology*, 131 (1) 59–68

Roden, D. M. (1998). Taking the "idio" out of "idiosyncratic": predicting torsades de pointes. *Pacing and Clinical Electrophysiology: PACE,* 21 (5) 1029–1034

Roden, D. M. & Viswanathan, P. C. (2005). Genetics of acquired long QT syndrome. *Journal of Clinical Investigation*, *115* (8), 2025–2032

Rodriguez-Menchaca, A. A., Adney, S. K., Tang, Q. Y., Meng, X. Y., Rosenhouse-Dantsker, A., Cui, M., & Logothetis, D. E. (2012). PIP2 controls voltage-sensor movement and pore opening of Kv channels through the S4-S5 linker. *Proceedings of the National Academy of Sciences of the United States of America,* 109 (36) E2399–2408

Rohács, T., Chen, J., Prestwich, G. D. & Logothetis, D. E. (1999). Distinct specificities of inwardly rectifying K(+) channels for phosphoinositides. *The Journal of Biological Chemistry*, 274 (51) 36065–36072

Rohács, T., Lopes, C. M., Jin, T., Ramdya, P. P., Molnár, Z. & Logothetis, D. E. (2003). Specificity of activation by phosphoinositides determines lipid regulation of Kir channels. *Proceedings of the National Academy of Sciences of the United States of America,* 100 (2) 745–750

Rohr, S. (2004). Role of gap junctions in the propagation of the cardiac action potential. *Cardiovascular Research*, 62 (2) 308–322

Romano, C., Gemme, G. & Pongiglione, R. (1963). Rare cardiac arrhythmias of the pediatric age. II. Syncopal attacks due to paroxysmal ventricular fibrillation. (Presentation of 1st case in Italian pediatric literature). *La Clinica Pediatrica*, 45; 656–683

Rosati, B., Pan, Z., Lypen, S., Wang, H.-S., Cohen, I., Dixon, J. E., & McKinnon, D. (2001). Regulation of KChIP2 potassium channel β subunit gene expression underlies the gradient of transient outward current in canine and human ventricle. *The Journal of Physiology,* 533(Pt 1) 119–125

Rossi, R., Montecucco, A., Ciarrocchi, G. & Biamonti, G. (1997). Functional characterization of the T4 DNA ligase: a new insight into the mechanism of action. *Nucleic Acids Research*, 25 (11) 2106–2113

Roy, A. & Levine, T. P. (2004). Multiple pools of phosphatidylinositol 4-phosphate detected using the pleckstrin homology domain of Osh2p. *The Journal of Biological Chemistry*, 279 (43) 44683–44689

Ruscic, K. J., Miceli, F., Villalba-Galea, C. A., Dai, H., Mishina, Y., Bezanilla, F., & Goldstein, S. A. N. (2013). $I_{Ks}$ channels open slowly because KCNE1 accessory subunits slow the movement of S4 voltage sensors in KCNQ1 pore-forming subunits. *Proceedings of the National Academy of Sciences of the United States of America,* 110 (7) E559–E566.

Rutherford, A. C., Traer, C., Wassmer, T., Pattni, K., Bujny, M. V., Carlton, J. G., Stenmark, H. & Cullen, P. J. (2006). The mammalian phosphatidylinositol 3-phosphate 5-kinase (PIKfyve) regulates endosome-to-TGN retrograde transport. *Journal of Cell Science*, 119 (Pt 19) 3944–3957

Ryan, S. (2014). ECG. Accessed at www.a-fib.com

Rycroft, B., Halliday, F. C., & Gibb, A. (2006). Patch Clamping Cell Biology (pp. 395-403). USA: Elsevier

Saiki, R. K., Gelfand, D. H., Stoffel, S., Scharf, S. J., Higuchi, R., Horn, G. T., Mullis, K. B., & Erlich, H. A. (1988). Primer-directed enzymatic amplification of DNA with a thermostable DNA polymerase. *Science*, 239 (4839) 487–491

Saiki, R. K., Scharf, S., Faloona, F., Mullis, K. B., Horn, G. T., Erlich, H. A., & Arnheim, N. (1985). Enzymatic amplification of beta-globin genomic sequences and restriction site analysis for diagnosis of sickle cell anemia. *Science*, 230 (4732) 1350–1354

Sandow, A. (1952). Excitation-contraction coupling in muscular response. *Yale Journal of Biology and Medicine*, 25 (3) 176–201

Sanguinetti, M. C. & Jurkiewicz, N. K. (1992). Role of external Ca2+ and K+ in gating of cardiac delayed rectifier K+ currents. *Pflugers Archiv: Europoean Journal of Physiology*, 420 (2) 180–186

Sanguinetti, M. C., Jiang, C., Curran, M. E. & Keating, M. T. (1995). A mechanistic link between an inherited and an acquired cardiac arrhythmia: HERG encodes the IKr potassium channel. *Cell*, 81 (2) 299–307

Sanguinetti, M. C., Curran, M. E., Zou, A., Shen, J., Spector, P. S., Atkinson, D. L. & Keating, M. T. (1996). Coassembly of K(V)LQT1 and minK (IsK) proteins to form cardiac I(Ks) potassium channel. *Nature,* 384 (6604) 80–83

Sanguinetti, M. C. & Bennett, P. B. (2003). Antiarrhythmic drug target choices and screening. *Circulation Research*, 93 (6) 491–499

Sarkes, D., & Rameh, L. E. (2010). A Novel HPLC-Based Approach Makes Possible the Spatial Characterization of Cellular PtdIns5*P* and Other Phosphoinositides. *The Biochemical Journal*, 428 (3) 375–384

Sasaki, M., Takagi, M. & Okamura, Y. (2006). A voltage sensor-domain protein is a voltage-gated proton channel. *Science*, 312 (5773) 589–592

Sasaki, T., Sasaki, J., Kaneyasu, Y. & Suzuki, S. (2006). Compartmentalization of phosphatidylinositol 4, 5-bisphosphate. *The Japanese Journal of Clinical Pathology,* 54 (1) 45–50

Sato, A., Arimura, T., Makita, N., Ishikawa, T., Aizawa, Y., Ushinohama, H., Aizawa, Y. & Kimura, A. (2009). Novel Mechanisms of Trafficking Defect Caused by *KCNQ1* Mutations Found in Long QT Syndrome. *The Journal of Biological Chemistry*, *284* (50) 35122–35133

Schmitt, N., Schwarz, M., Peretz, A., Abitbol, I., Attali, B. & Pongs, O. (2000). A recessive C-terminal Jervell and Lange-Nielsen mutation of the KCNQ1 channel impairs subunit assembly. *The EMBO Journal,* 19 (3) 332–340.

Schmitt, N., Calloe, K., Nielsen, N. H., Buschmann, M., Speckmann, E. J., Schulze-Bahr, E. & Schwarz, M. (2007). The novel C-terminal KCNQ1 mutation M520R alters protein trafficking. *Biochemical and Biophysical Research Communications*, 358 (1) 304–310

Schoebel, S., Blankenfeldt, W., Goody, R. S., & Itzen, A. (2010). High-affinity binding of phosphatidylinositol 4-phosphate by *Legionella pneumophila* DrrA. *EMBO Reports*, 11 (8) 598–604

Schroeder, B. C., Hechenberger, M., Weinreich, F., Kubisch, C., & Jentsch, T. J. (2000a). KCNQ5, a novel potassium channel broadly expressed in brain, mediates M-type currents. *Journal of Biological Chemistry*, 275(31) 24089–24095

Schroeder, B. C., Waldegger, S., Fehr, S., Bleich, M., Warth, R., Greger, R. & Jentsch, T. J. (2000b). A constitutively open potassium channel formed by KCNQ1 and KCNE3. *Nature*, 403 (6766) 196–199

Schwartz, P. J., Priori, S. G., Spazzolini, C., Moss, A. J., Vincent, G. M., Napolitano, C., Denjoy, I., Guicheney, P., Breithardt, G., Keating, M. T., Towbin, J. A., Beggs, A. H., Brink, P., Wilde, A. A., Toivonen, L., Zareba , W., Robinson, J. L., Timothy, K. W., Corfield, V., Wattanasirichaigoon, D., Corbett, C., Haverkamp , W., Schulze-Bahr, E., Lehmann, M. H., Schwartz, K., Coumel, P. & Bloise, R. (2001). Genotype-phenotype correlation in the long-QT syndrome: gene-specific triggers for life-threatening arrhythmias. *Circulation*, 103 (1) 89–95

Schwartz, P. J., Priori, S. G. & Napolitano, C. (2002). How really rare are rare diseases?: the intriguing case of independent compound mutations in the long QT syndrome. *Journal of Cardiovascular Electrophysiology*, 14 (10) 1120–1121

Schwartz, P. J., Stramba-Badiale, M., Crotti, L., Pedrazzini, M., Besana, A., Bosi, G., Gabbarini, F., Goulene, K., Insolia, R., Mannarino, S., Mosca, F., Nespoli, L., Rimini, A., Rosati, E., Salice, P. & Spazzolini, C. (2009). Prevalence of the congenital long-QT syndrome. *Circulation*, 120 (18) 1761–1767

Schwartz, P. J., Spazzolini, C., Priori, S. G., Crotti, L., Vicentini, A., Landolina, M., Gasparini, M., Wilde, A. A., Knops, R. E., Denjoy, I., Toivonen, L., Mönnig, G., Al-Fayyadh, M., Jordaens, L., Borggrefe, M., Holmgren, C., Brugada, P., De Roy, L., Hohnloser, S. H. & Brink, P. A. (2010). Who are the long-QT syndrome patients who receive an implantable cardioverter-defibrillator and what happens to them?: data from the European Long-QT Syndrome Implantable Cardioverter-Defibrillator (LQTS ICD) Registry. *Circulation*, 122 (13) 1272–1282

Sciaky, N., Presley, J., Smith, C., Zaal, K. J., Cole, N., Moreira, J. E., Terasaki, M., Siggia, E. & Lippincott-Schwartz J. (1997). Golgi tubule traffic and the effects of brefeldin A visualized in living cells. *The Journal of Cell Biology*, 139 (5) 1137–1155

Seebohm, G., Strutz-Seebohm, N., Birkin, R., Dell, G., Bucci, C., Spinosa, M. R., Baltaev, R., Mack, A. F., Korniychuk, G., Choudhury, A., Marks, D., Pagano, R. E., Attali, B., Pfeufer, A., Kass, R. S., Sanguinetti, M. C., Tavare, J. M., & Lang, F. (2007). Regulation of endocytic recycling of KCNQ1/KCNE1 potassium channels. *Circulation Research,* 100 (5) 686–692

Selzer, A. & Wray, H. W. (1964). Quinidine syncope. Paroxysmal ventricular fibrillation occurring during treatment of chronic atrial arrhythmias. *Circulation*, 30; 17–26

Sepúlveda, F. V., Pablo Cid, L., Teulon, J. & Niemeyer, M. I. (2015). Molecular aspects of structure, gating, and physiology of pH-sensitive background K2P and Kir K+-transport channels. *Physiological Reviews*, 95 (1) 179–217

Sesti, F. & Goldstein, S. A. N. (1998). Single-Channel Characteristics of Wild-Type $I_{Ks}$ Channels and Channels formed with Two MinK Mutants that Cause Long QT Syndrome. *Journal of General Physiology,* 112 (6) 651–663

Severi, S., Corsi, C., Rocchetti, M. & Zaza, A. (2009). Mechanisms of β-Adrenergic Modulation of $I_{Ks}$ in the Guinea-Pig Ventricle: Insights from Experimental and Model-Based Analysis. *Biophysical Journal,* 96 (9) 3862–3872

Shamgar, L., Ma, L., Schmitt, N., Haitin, Y., Peretz, A., Wiener, R., Hirsch, J., Pongs, O., & Attali, B. (2006). Calmodulin is essential for cardiac $I_{Ks}$ channel gating and assembly: impaired function in long-QT mutations. *Circulation Research,* 98(8), 1055–1063

Shils, M. E. (1964). Experimental human magnesium depletion. I. Clinical observations and blood chemistry alterations. *The American Journal of Clinical Nutrition*, 15; 133–143

Shimizu, W., Ohe, T., Kurita, T., Takaki, H., Aihara, N., Kamakura, S., Matsuhisa, M. & Shimomura, K. (1991). Early afterdepolarizations induced by isoproterenol in patients with congenital long QT syndrome. *Circulation*, 84 (5) 1915–1923

Shyng, S. L. & Nichols, C. G. (1998). Membrane phospholipid control of nucleotide sensitivity of KATP channels. *Science*, 282 (5391) 1138–1141

Shyng, S. L., Cukras, C. A., Harwood, J., & Nichols, C. G. (2000). Structural Determinants of $PIP_2$ Regulation of Inward Rectifier $K_{ATP}$ Channels. *The Journal of General Physiology*, 116 (5) 599–608

Siehler, S. (2009) Regulation of RhoGEF proteins by G12/13-coupled receptors. *British Journal of Pharmacology*, 158 (1) 41–49

Sigworth, F. (2014). Patch and whole-cell recording. Warner instruments technical references. from https://www.warneronline.com

Silva, J. & Rudy, Y. (2005). Subunit Interaction Determines $I_{Ks}$ Participation in Cardiac Repolarization and Repolarization Reserve. *Circulation*, 112 (10) 1384–1391

Smith, J., Vanoye, C. G., George, A. L., Meiler, J. & Sanders, C. R. (2007). Structural Models for the KCNQ1 Voltage-Gated Potassium Channel. *Biochemistry*, 46 (49) 14141–14152

Snyders, D. J. (1999) Structure and function of cardiac potassium channels. C*ardiovascular Research*, 42 (2) 377–390

Splawski, I., Shen, J., Timothy, K. W., Lehmann, M. H., Priori, S., Robinson, J. L., Moss, A. J., Schwartz, P. J., Towbin, J. A., Vincent, G. M. & Keating, M. T. (2000). Spectrum of Mutations in Long-QT Syndrome Genes: KVLQT1, HERG, SCN5A, KCNE1, and KCNE2. *Circulation, 102* (10) 1178–1185

Stanfield, P. R., Davies, N. W., Shelton, P. A., Sutcliffe, M. J., Khan, I. A., Brammar, W. J., & Conley, E. C. (1994). A single aspartate residue is involved in both intrinsic gating and blockage by Mg2+ of the inward rectifier, IRK1. *The Journal of Physiology*, 478(Pt 1), 1–6

Stockklausner, C., Ludwig, J., Ruppersberg, J. P., & Klöcker, N. (2001). A sequence motif responsible for ER export and surface expression of Kir2.0 inward rectifier K(+) channels. *FEBS Letters,* 493(2-3), 129–133

Su, S., Gao, Y. G., Robinson, H., Liaw, Y. C., Edmondson, S. P., Shriver, J. W., & Wang, A. H. (2000). Crystal structures of the chromosomal proteins Sso7d/Sac7d bound to DNA containing T-G mismatched base-pairs. *Journal of Molecular Biology,* 303(3), 395–403

Suh, B.C. & Hille, B. (2002). Recovery from muscarinic modulation of M current channels requires phosphatidylinositol 4,5-bisphosphate synthesis. *Neuron*, 35 (3) 507–520.

Suh, B. C., & Hille, B. (2008). PIP2 is a necessary cofactor for ion channel function: how and why? *Annual Review of Biophysics, 37*, 175–195

Suh, B. C., Inoue, T., Meyer, T., & Hille, B. (2006). Rapid chemically induced changes of PtdIns(4,5)P2 gate KCNQ ion channels. *Science,* 314(5804), 1454–1457

Sun, Y., Carroll, S., Kaksonen, M., Toshima, J. Y. & Drubin, D. G. (2007). PtdIns(4,5)P2 turnover is required for multiple stages during clathrin- and actin-dependent endocytic internalization. *The Journal of Cell Biology*, 177 (2) 355–367

Sun, T. (2010). Gibberellin-GID1-DELLA: A Pivotal Regulatory Module for Plant Growth and Development. *Plant Physiology*, 154 (2) 567–570

Surawicz, B. (1989). Is hypomagnesemia or magnesium deficiency arrhythmogenic? *Journal of the American College of Pharmacology*, 14 (4) 1093–1096

Szentpetery, Z., Várnai, P. & Balla, T. (2014) Acute manipulation of Golgi phosphoinositides to assess their importance in cellular trafficking and signaling. *Proceedings of the National Academy of Sciences of the United States of America*, 107 (18) 8225–8230

Tabassum, N. & Feroz, A. (2011) Ion channels and their modulation. *The Journal of Applied Pharmaceutical Science*, 1 (1) 20–25

Takida, S., & Wedegaertner, P. B. (2004). Exocytic pathway-independent plasma membrane targeting of heterotrimeric G proteins. *FEBS Letters*, 567 (2-3) 209–213

Takumi, T., Ohkubo, H. & Nakanishi, S. (1988) Cloning of a membrane protein that induces a slow voltage-gated potassium current. *Science,* 242 (4881) 1042–1045

Tang, X. L., Wang, Y., Li, D. L., Luo, J. & Liu, M. Y. (2012). Orphan G protein-coupled receptors (GPCRs): biological functions and potential drug targets. *Acta Pharmalogica Sinica*, 33 (3) 363–371

Taylor, J. J., D'Agrosa, L. S., & Burns, E. M. (1978). The pacemaker cell of the sinoatrial node of the rabbit. *The American Journal of Physiology*, 235(4), H407–412

Tempel, B. L., Papazian, D. M., Schwarz, T. L., Jan, Y. N., & Jan, L. Y. (1987). Sequence of a probable potassium channel component encoded at Shaker locus of Drosophila. *Science,* 237(4816), 770–775

Temple, I. P., Inada, S., Dobrzynski, H., & Boyett, M. R. (2013). Connexins and the atrioventricular node. *Heart Rhythm,* 10(2), 297–304

Terrenoire, C., Houslay, M. D., Baillie, G. S. & Kass, R. S. (2009). The Cardiac $I_{Ks}$ Potassium Channel Macromolecular Complex Includes the Phosphodiesterase PDE4D3. *The Journal of Biological Chemistry*, 284 (14) 9140–9146

Tester, D. J., & Ackerman, M. J. (2012). The Molecular Autopsy: Should the Evaluation Continue After the Funeral? *Pediatric Cardiology*, *33* (3) 461–470

Tewson, P., Westenberg, M., Zhao, Y., Campbell, R. E., Quinn, A. M., & Hughes, T. E. (2012). Simultaneous detection of Ca2+ and diacylglycerol signaling in living cells. *PLoS One*, 7 (8) e42791

Thomas, D., Wimmer, A. B., Karle, C. A., Licka, M., Alter, M., Khalil, M., Ulmer, H. E., Kathöfer, S., Kiehn, J., Katus, H. A., Schoels, W., Koenen, M. & Zehelein, J. (2005). Dominant-negative I(Ks) suppression by KCNQ1-deltaF339 potassium channels linked to Romano-Ward syndrome. *Cardiovascular Research*, 67 (3) 487–497

Thomas, A. M., Brown, S. G., Leaney, J. L. & Tinker, A. (2006). Differential phosphoinositide binding to components of the G protein-gated K+ channel. *The Journal of Membrane Biology,* 211 (1) 43–53

Thomas, A. M., Harmer, S. C., Khambra, T., & Tinker, A. (2011). Characterization of a Binding Site for Anionic Phospholipids on KCNQ1. *Journal of Biological Chemistry*, 286(3), 2088–2100

Thompson, Q. W. (1956). Quinidine as a cause of sudden death. *Circulation*, 14; 757–765

Tinel, N., Diochot, S., Borsotto, M., Lazdunski, M. & Barhanin, J. (2000) KCNE2 confers background current characteristics to the cardiac KCNQ1 potassium channel. *The EMBO Journal,* 19 (23) 6326–6330

Townsend, J. A., Wright, D. A., Winfrey, R. J., Fu, F., Maeder, M. L., Joung, J. K. & Voytas, D. F. (2009) High-frequency modification of plant genes using engineered zinc-finger nucleases. *Nature,* 459 (7245) 442–445

Tristani-Firouzi, M. & Sanguinetti, M. C. (1998) Voltage-dependent inactivation of the human K+ channel KvLQT1 is eliminated by association with minimal K+ channel (minK) subunits. *The Journal of Physiology*, 510 (pt 1) 37–45

Van der Heyden, M. A., Wijnhoven, T. J. & Opthof, T. (2005). Molecular aspects of adrenergic modulation of cardiac L-type Ca2+ channels. *Cardiovascular Research*, 65 (1) 28–39

Vanoye, C. G., Welch, R. C., Tian, C., Sanders, C. R., & George, A. L. J. (2010). KCNQ1/KCNE1 assembly, co-translation not required. *Channels (Austin, Tex.)*, 4 (2) 108–114

Várnai, P. & Balla, T. (1998). Visualization of phosphoinositides that bind pleckstrin homology domains: calcium- and agonist-induced dynamic changes and relationship to myo-[3H]inositol-labeled phosphoinositide pools. *The Journal of Cell Biology*, 143 (2) 501–510

Várnai, P., Thyagarajan, B., Rohacs, T. & Balla T. (2006). Rapidly inducible changes in phosphatidylinositol 4,5-bisphosphate levels influence multiple regulatory functions of the lipid in intact living cells. *The Journal of Cell Biology*, 175 (3) 377–382

Varnum, M. D., Busch, A. E., Bond, C. T., Maylie, J. & Adelman, J. P. (1993). The min K channel underlies the cardiac potassium current $I_{Ks}$ and mediates species-specific responses to protein kinase C. *Proceedings of the National Academy of Sciences of the United States of America*, 90 (24) 11528–11532

Varró, A., & Baczkó, I. (2011). Cardiac ventricular repolarization reserve: a principle for understanding drug-related proarrhythmic risk. British Journal of Pharmacology, 164 (1) 14–36

Vincent, G. M. (2002). The long QT syndrome. *Indian Pacing Electrophysiology Journal*, 2 (4) 127–142

Vincent, G. M., Schwartz, P. J., Denjoy, I., Swan, H., Bithell, C., Spazzolini, C., Crotti, L., Piippo, K., Lupoglazoff, J. M., Villain, E., Priori, S. G., Napolitano, C. & Zhang, L (2009). High efficacy of beta-blockers in long-QT syndrome type 1: contribution of noncompliance and QT-prolonging drugs to the occurrence of beta-blocker treatment "failures". *Circulation*, 119 (2) 215–221

Viskin, S., Rosovski, U., Sands, A. J., Chen, E., Kistler, P. M., Kalman, J. M., Rodriguez Chavez, L., Iturralde Torres, P., Cruz, F. F. E., Centurión, O. A., Fujiki, A., Maury, P., Chen, X., Krahn, A. D., Roithinger, F., Zhang, L., Vincent, G. M. & Zeltser, D. (2005) Inaccurate electrocardiographic interpretation of long QT: the majority of physicians cannot recognize a long QT when they see one. *Heart Rhythm*, 2 (6) 569–574

Viskin, S. (2000). Cardiac Pacing in the Long QT Syndrome. *Journal of Cardiovascular Electrophysiology*, 11 (5) 593–599

Viswanathan, P. C. & Rudy, Y. (1999). Pause induced early afterdepolarizations in the long QT syndrome: a simulation study, *Cardiovascular Research*, 42 (2) 530–542

Volders, P. G., Vos, M. A., Szabo, B., Sipido, K. R., de Groot, S. H., Gorgels, A. P., Wellens, H. J., & Lazzara, R. (2000). Progress in the understanding of cardiac early afterdepolarizations and torsades de pointes: time to revise current concepts. *Cardiovascular Research*, 46(3), 376–392

Volders, P. G., Stengl, M., van Opstal, J. M., Gerlach, U., Spätjens, R. L., Beekman, J. D., Sipido, K. R. & Vos, M. A. (2003). Probing the contribution of $I_{Ks}$ to canine ventricular repolarization: key role for beta-adrenergic receptor stimulation. *Circulation*, 107 (21) 2753–2760

Wang, W. (1998). MinK-KvLQT1 Fusion Proteins, Evidence for Multiple Stoichiometries of the Assembled IsK Channel. *Journal of Biological Chemistry*, 273(51), 34069–34074

Wang, Z., Fermini, B. & Nattel, S. (1993) Sustained depolarization-induced outward current in human atrial myocytes. Evidence for a novel delayed rectifier K+ current similar to Kv1.5 cloned channel currents. *Circulation Research*, 73 (6) 1061–1076

Wang, Z., Fermini. B. & Nattel, S. (1994) Rapid and slow components of delayed rectifier current in human atrial myocytes. *Cardiovascular Research,* 28 (10) 1540–1546

Wang, Q., Shen, J., Splawski, I., Atkinson, D., Li, Z., Robinson, J. L., Moss, A. J., Towbin, J. A. & Keating, M. T. (1995). SCN5A mutations associated with an inherited cardiac arrhythmia, long QT syndrome. *Cell*, 80 (5) 805–811

Wang, Y. J., Wang, J., Sun, H. Q., Martinez, M., Sun, Y. X., Macia, E., Kirchhausen, T., Albanesi, J. P., Roth, M. G. & Yin, H. L. (2003). Phosphatidylinositol 4 phosphate regulates targeting of clathrin adaptor AP-1 complexes to the Golgi. *Cell*, 114 (3) 299–310

Wang, S., Xu, D., Wu, T. T., Guo, Y., Chen, Y. H. & Zou, J. G. (2014). β1-adrenergic regulation of rapid component of delayed rectifier K+ currents in guinea-pig cardiac myocytes, *Molecular Medicine Reports*, 9 (5) 1923–1928

Ward, O. C. (1964). A new familial cardiac syndrome in children. *Journal of the Irish Medical Association,* 54; 103–106

Washizuka, T., Horie, M., Watanuki, M. & Sasayama, S. (1997). Endothelin-1 inhibits the slow component of cardiac delayed rectifier K+ currents via a pertussis toxin-sensitive mechanism. *Circulation Research,* 81 (2) 211–218

Watt, S. A., Kular, G., Fleming, I. N., Downes, C. P. & Lucocq, J. M. (2002). Subcellular localization of phosphatidylinositol 4,5-bisphosphate using the pleckstrin homology domain of phospholipase C delta1. *Biochemical Journal*, *363*(Pt 3) 657–666.

Wegener, A. D., Simmerman, H. K., Lindemann, J. P. & Jones, L. R. (1989). Phospholamban phosphorylation in intact ventricles. Phosphorylation of serine 16 and threonine 17 in response to beta-adrenergic stimulation. *The Journal of Biological Chemistry*, 264 (19) 11468–11474

Wei, Y. J., Sun, H. Q., Yamamoto, M., Wlodarski, P., Kunii, K., Martinez, M., Barylko, B., Albanesi, J. P. & Yin, H. L. (2002). Type II phosphatidylinositol 4-kinase beta is a cytosolic and peripheral membrane protein that is recruited to the plasma membrane and activated by Rac-GTP. *The Journal of Biological Chemistry*, 277 (48) 46586–46593

Whang, R. (1997). Clinical disorders of magnesium metabolism. *Comprehensive Therapy*, 23 (3) 168–173

Whorton, M. R. & MacKinnon, R. (2011). Crystal Structure of the Mammalian GIRK2 K+ Channel and Gating Regulation by G-Proteins, PIP2 and Sodium. *Cell,* 147 (1) 199–208

Wible, B. A., Taglialatela, M., Ficker, E., & Brown, A. M. (1994). Gating of inwardly rectifying K+ channels localized to a single negatively charged residue. *Nature*, 371(6494), 246–249

Widimsky, P. (2008). Hypokalemia and the heart. *E-Journal of Cargiology Practice*, 7 (9)

Wilson, A. J., Quinn, K. V., Graves, F. M., Bitner-Glindzicz, M., & Tinker, A. (2005). Abnormal KCNQ1 trafficking influences disease pathogenesis in hereditary long QT syndromes (LQT1). *Cardiovascular Research*, 67 (3) 476–486

Winks, J. S., Hughes, S., Filippov, A. K., Tatulian, L., Abogadie, F. C., Brown, D. A. & Marsh, S. J. (2005). Relationship between membrane phosphatidylinositol-4,5-bisphosphate and receptor-mediated inhibition of native neuronal M channels. *The Journal of Neuroscience*, 25 (13) 3400–3413

Wirth, M., Joachim. J. & Tooze, S. A. (2013). Autophagosome formation--the role of ULK1 and Beclin1-PI3KC3 complexes in setting the stage. *Seminars in Cancer Biology*, 23 (5) 301–309

Woosley, R. L., Chen, Y., Freiman, J. P. & Gillis, R. A. (1993). Mechanism of the cardiotoxic actions of terfenadine. *The Journal of the American Medical Association*, 269 (12) 1532–1536

Wu, D., Pan, H., Delaloye, K. & Cui, J. (2010). KCNE1 Remodels the Voltage Sensor of Kv7.1 to Modulate Channel Function. *Biophysical Journal*, 99 (11) 3599–3608

Wymann, M. P., Bulgarelli-Leva, G., Zvelebil, M. J., Pirola, L., Vanhaesebroeck, B., Waterfield, M. D., & Panayotou, G. (1996). Wortmannin inactivates phosphoinositide 3-kinase by covalent modification of Lys-802, a residue involved in the phosphate transfer reaction. *Molecular and Cellular Biology*, 16 (4) 1722–1733

Xiao, R. P. & Lakatta, E. G. (1993). Beta 1-adrenoceptor stimulation and beta 2-adrenoceptor stimulation differ in their effects on contraction, cytosolic Ca2+, and Ca2+ current in single rat ventricular cells. *Circulation Research*, 73 (2) 286–300

Xiao, R. P., Zhu, W., Zheng, M., Cao, C., Zhang, Y., Lakatta, E. G. & Han, Q. (2006). Subtype-specific $\alpha_1$- and β-adrenoceptor signaling in the heart. *Trends in Pharmacological Sciences,* 27 (6) 330–337

Xie, L. H., John, S. A., Ribalet, B. & Weiss, J. N. (2005). Long polyamines act as cofactors in PIP2 activation of inward rectifier potassium (Kir2.1) channels. *The Journal of General Physiology*, 126 (6) 541–549

Xie, L. H., John, S. A., Ribalet, B. & Weiss, J. N. (2008). Phosphatidylinositol-4,5-bisphosphate ($PIP_2$) regulation of strong inward rectifier Kir2.1 channels: multilevel positive cooperativity. *The Journal of Physiology*, 586 (Pt 7) 1833–1848

Xie, Y., Sato, D., Garfinkel, A., Qu, Z., Weiss, J. N. (2010). So little source, so much sink: requirements for afterdepolarizations to propagate in tissue. *Biophysical Journal,* 99 (5) 1408–1415

Yang, J., Jan, Y. N., Jan, L. Y. (1995) Control of rectification and permeation by residues in two distinct domains in an inward rectifier $K^+$ channel. *Neuron*, 14 (5) 1047–1054

Yang, T. & Roden, D. M. (1996). Extracellular potassium modulation of drug block of IKr. Implications for torsade de pointes and reverse use-dependence. *Circulation*, 93 (3) 407–411

Yang, P., Kanki, H., Drolet, B., Yang, T., Wei, J., Viswanathan, P. C., Hohnloser, S. H., Shimizu, W., Schwartz, P. J., Stanton, M., Murray, K. T., Norris, K., George, A. L. Jr. & Roden, D. M. (2002). Allelic variants in long-QT disease genes in patients with drug-associated torsades de pointes. *Circulation*, 105 (16) 1943–1948

Yano, H., Nakanishi, S., Kimura, K., Hanai, N., Saitoh, Y., Fukui, Y., Nonomura, Y. & Matsuda, Y. (1993). Inhibition of histamine secretion by wortmannin through the blockade of phosphatidylinositol 3-kinase in RBL-2H3 cells. *The Journal of Biological Chemistry,* 268 (34) 25946-25856

Yap, Y. G. & Camm, A. J. (2003). Drug induced QT prolongation and torsades de pointes. *Heart,* 89 (11) 1363–1372

Yarov-Yarovoy, V., Baker, D. & Catterall, W. A. (2006). Voltage sensor conformations in the open and closed states in rosetta structural models of K+ channels. *Proceedings of the National Academy of Sciences of the United States of America*, 103 (19) 7292–7297

Yu, J. W., Mendrola, J. M., Audhya, A., Singh, S., Keleti, D., DeWald, D. B., Murray, D., Emr, S. D. & Lemmon, M. A. (2004). Genome-wide analysis of membrane targeting by S. cerevisiae pleckstrin homology domains. *Molecular Cell*, 13 (5) 677–688

Yus-Najera, E., Santana-Castro, I., & Villarroel, A. (2002). The identification and characterization of a noncontinuous calmodulin-binding site in noninactivating voltage-dependent KCNQ potassium channels. *Journal of Biological Chemistry,* 277(32), 28545–28553

Zankov, D. P., Omatsu-Kanbe, M., Isono, T., Toyoda, F., Ding, W. G., Matsuura, H. & Horie, M. (2006). Angiotensin II potentiates the slow component of delayed rectifier K+ current via the AT1 receptor in guinea pig atrial myocytes. *Circulation*, 113 (10) 1278–1286

Zankov, D. P., Toyoda, F., Omatsu-Kanbe, M., Matsuura, H. & Horie, M. (2009). Angiotensin II type 1 receptor mediates partially hyposmotic-induced increase of I (Ks) current in guinea pig atrium. *Pflugers Archiv: European Journal of Physiology*, 458 (5) 837–849

Zaydman, M. A., Silva, J. R., Delaloye, K., Li, Y., Liang, H., Larsson, H. P., Shi, J., & Cui, J. (2013). Kv7.1 ion channels require a lipid to couple voltage sensing to pore opening. *Proceedings of the National Academy of Sciences of the United States of America,* 110 (32) 13180–13185

Zaydman, M. A. & Cui, J. (2014). PIP2 regulation of KCNQ channels: biophysical and molecular mechanisms for lipid modulation of voltage-dependent gating. *Frontiers in Physiology*, 5 (195); eCollection 2014

Zhang, H., Craciun, L. C., Mirshahi, T., Rohács, T., Lopes, C. M., Jin, T. & Logothetis, D. E. (2003). PIP(2) activates KCNQ channels, and its hydrolysis underlies receptor-mediated inhibition of M currents. *Neuron,* 37 (6) 963–975

Zhang, P., Kofron, C. M. & Mende, U. (2015) Heterotrimeric G protein-mediated signaling and its non-canonical regulation in the heart. *Life Sciences,* 129, 35–41

Zhang, R., Zhao, J., Mandveno, A. & Potter, J. D. (1995). Cardiac troponin I phosphorylation increases the rate of cardiac muscle relaxation. *Circulation Research*, 76 (6) 1028–1035

Zhao, Y., Inayat, S., Dikin, D. A., Singer, J. H., Ruoff, R. S., & Troy, J. B. (2008). Patch clamp technique: review of the current state of the art and potential contributions from nanoengineering. *Proceedings of the Institution of Mechanical Engineers, Part N: Journal of Nanoengineering and Nanosystems*, 222 (1) 1–11

Zhao, L. & Vogt, P. K. (2008). Class I PI3K in oncogenic cellular transformation. *Oncogene*, 27 (41) 5486–5496

Zhao, B., Wang, Q., Du, J., Luo, S., Xia, J., Chen, Y. G. (2012). PICK1 promotes caveolin-dependent degradation of TGF-β type I receptor. *Cell Research,* 22 (10)1467–1478

Zhou, Z., Gong, Q., Epstein, M. L. & January, C. T. (1998) HERG channel dysfunction in human long QT syndrome. Intracellular transport and functional defects. *The Journal of Biological Chemistry,* 273 (33) 21061–21066

Zoncu, R., Perera, R. M., Sebastian, R., Nakatsu, F., Chen, H., Balla, T., Ayala, G., Toomre, D., & De Camilli, P. V. (2007). Loss of endocytic clathrin-coated pits upon acute depletion of phosphatidylinositol 4,5-bisphosphate. *Proceedings of the National Academy of Sciences of the United States of America,* 104 (10) 3793–3798